Plasma assisted deposition of thin films using molecular titanium alkoxide and amido precursors

Ratcliffe, Peter John

University of Durham

A thesis entitled

Plasma Assisted Deposition of Thin Films using Molecular Titanium Alkoxide and Amido Precursors

Submitted by Peter John Ratcliffe

BSc (Hons) Dunelm

A candidate for the degree of Doctor of Philosophy

Hatfield College September 1995

The work described in this thesis was carried out at the University of Durham between October 1991 and September 1994. Except where acknowledged by reference, it is the original work of the author and has not been submitted in whole or part for any other degree.

Work in this thesis has formed the whole, or part of the following publications:

1) Plasma Assisted Decomposition of Titanium Tetraisopropoxide, P.J. Ratcliffe, J. Hopkins, A.D. Fitzpatrick, C.P. Barker, J.P.S. Badyal, Proceedings of the 11th International Symposium on Plasma Chemistry, Loughborough, Vol. 3, Aug. 1993, 1154.

2) Plasma Enhanced Chemical Vapour Deposition of TiO_2/Polymer Composite Layers, P.J. Ratcliffe, J. Hopkins, A.D. Fitzpatrick, C.P. Barker, J.P.S. Badyal, *J. Mater. Chem.*, **4**, 1994, 1055.

This work is dedicated to

Jane and Mum and Dad

with love

ACKNOWLEDGEMENTS

I would initially like to thank my supervisor Dr. Jas Pal Badyal for giving me the opportunity to carry out this PhD and for his guidance and support throughout the duration of my work. I am also very grateful to other academic staff for their advice and information. To Courtaulds Coatings I am grateful for their Case funding.

My colleagues in lab CG 98 both past and present have provided tremendous support, advice and many laughs! Keep in touch! Many thanks go to the technical staff for their wonderful expertise (including Brenda's tea!): in particular I must name Kelvin Appleby, George Rowe and Barry Barker in the Electrical Workshop, Jim Hodgson, Mel Higham and Neil Holmes in the Mechanical Workshop, Gordon Haswell and Ray Hart for their artistic skills with glass, Jimmy Lincoln in Stores (for providing me with a long stand!) and Tony Royston for his computing advice.

My housemates in Sutton Street: Rorie, Rob and Don have been great when their patience should have wavered and have provided good company, hot meals and many a beer! Penny and Ash made me feel welcome in their home after bailing me out of my pending homelessness and have recently provided me a familiar base for those necessary trips back to Durham.

Michael and Pauline Duffy have been fantastic hosts, particularly when I have fled Durham to retain my sanity! Michael's proof reading has also been invaluable.

Thanks go to my parents for their continuous love and support over the duration of this work. Their additional handouts helped ease the financial burden!

Finally I have to thank Jane-one of my triumphs of my PhD! Your encouragement, love and limitless patience have been unreal!! I owe you so much.

ABSTRACT

Metal-containing polymer thin films are known to possess interesting electrical, magnetic, optical or barrier properties. Such coatings can be deposited by plasma assisted chemical vapour deposition (PACVD). This technique comprises the fragmentation and rearrangement of metallorganic precursors within a low pressure non-equilibrium electrical discharge. In this work, the deposition of titanium containing species embedded into a polymeric network from titanium tetraisopropoxide (TiTP), $Ti[OCH(CH_3)_2]_4$, and tetrakis (dimethylamido) titanium (TMT), $Ti[N(CH_3)_2]_4$, precursors has been investigated as a function of glow discharge power and substrate location. In addition these precursors have been mixed with hydrogen and ammonia gases during PACVD. These metal-containing plasma polymers layers have been characterized by X-ray photoelectron spectroscopy (XPS), attenuated total reflection Fourier transform infrared spectroscopy (ATR-FTIR) and atomic force microscopy (AFM).

It has been demonstrated that TiO_2/polymer composite layers can be produced using the TiTP precursor with a wide range of stoichiometries. The mixing of hydrogen gas with TiTP create films which are stable towards oxidation and aging. TiTP/ammonia mixtures produced Ti(O,N)/polymer films which contained Ti-N bonds.

Injection of TMT into a glow discharge has been found to result in a non-thermally assisted intramolecular alkyl β-hydrogen activation mechanism to produce Ti(O,C,N)/polymer composite films. The film composition is found to be independent of glow discharge power beyond 5 W. Mixing with hydrogen gas lowers the carbon content due to recombination reactions competing with plasma polymerization. TMT/ammonia mixtures result in a gas phase transamination reaction prior to and during plasma activation causing a drop in the total carbon content due to replacement of the $-N(CH_3)_2$ ligand by $-NH_x$.

CONTENTS

CHAPTER 1: INTRODUCTION

1.0 SCOPE OF THESIS

In the production of many so-called high-tech products, subtle manipulation or coating of surfaces is often required. Low pressure glow discharge plasmas have recently become a powerful technique catering for such requirements which in many instances cannot be achieved by any other means. Chemical disposal problems associated with 'wet' processes are almost eliminated, though the small effluent gases must be handled with care. The ability to create a uniform flux of energetic species and the formation of uniformly coated three-dimensional shapes, deposited at lower temperatures than techniques previously used, are just some of the advantages of plasma processing.

At the same time there has been much interest from chemists, physicists and material scientists in the manufacture of novel composite materials possessing useful mechanical, electrical, magnetic, optical, catalytic and barrier properties. Therefore an opportunity exists to combine the deposition process of plasmas with that of the formation of novel composite materials. The aim of this project was to deposit such composite layers from titanium-organic precursors by plasma assisted chemical vapour deposition (PACVD).

Chapter 1 gives an introduction to the fields of composites, 'cold' plasma chemistry and thin film deposition. Chapter 2 describes the basic principles of the surface analytical techniques that were used throughout this project to provide film compositional and morphological information.

Chapters 3 to 5 discuss the experimental set-up and results for the films deposited from the titanium tetraisopropoxide (TiTP) [$Ti(OCH(CH_3)_2)_4$] precursor. Chapter 3 provides a full study of TiTP and the deposition of TiO_2/polymer composite films. Chapters 4 and 5 respectively describe the addition of H_2 and NH_3 gases to TiTP plasmas with the aim of producing titanium suboxide/polymer and TiN/polymer composite films.

Chapters 6 and 7 give the corresponding results for films deposited from the tetrakis (dimethylamido) titanium (TMT) ($Ti[N(CH_3)_2]_4$) precursor. Chapter 6 describes the deposition of Ti(O,C,N)/polymer composite films from TMT, and mixed with H_2 gas. Characterization of coatings deposited from TMT mixed with NH_3 gas is described in Chapter 7. Finally Chapter 8 provides the conclusions of this project and outlines its possible extension.

1.1 COMPOSITES - DEFINITION

A composite is generally defined as a material created when two or more distinct components are combined and take advantage of certain desirable properties of each component.[1] Such materials exist in nature, for example in wood, teeth and bones,[2] and the components can be metallic, organic and inorganic.[1,3] The matrix is the body constituent and serves to enclose the composite and give it its bulk form. The enclosed components can be rods, fibres, lamina, flakes, or may be microscopic or particulate in form. The enhanced properties include those of weight saving, strength, stiffness, corrosion resistance, weatherability, insulation, conductivity, friction and wear.[2]

Initially fibre-reinforced composites were of particular interest to the aerospace industry but with rapid advances in technology and processing such composites are now becoming more widely used, for example in the automobile and leisure industries. Composites where the microscopic particles are the randomly dispersed component[4] also have important applications. If the dispersed components are in the nanometre range, typically 1-20 nm, such materials are said to be nanocomposites.[5]

1.1.1 NANOCOMPOSITES

Nanocomposites are found in the biological world.[2,5] For example bones, teeth, and shells consist of nanocomposites of inorganic and organic materials. Man-made nanocomposites have important properties, however: five major classes of man-made nanocomposites have been identified based on their material function, physical and chemical differences, temperature of formation etc.[5] These are summarized in Table 1.

Sol-gel nanocomposites have been shown to lower crystallization temperatures and generally enhance densification of ceramic materials. Intercalation nanocomposites potentially lead to novel microporous materials and may find applications in catalysis and laser materials. Tailoring of electroceramics has led for example, to improved dielectric, optical, optoelectronic and magnetic properties. Improved mechanical properties such as hardness, strength, creep and fatigue are found in structural ceramic nanocomposites.

Generally manufacture of such materials requires either wet chemical methods and/or high temperatures. To avoid such conditions and to form thin films, PACVD is proposed as an alternative. This work examines the feasibility of this proposition.

Table 1 Summary of Komarneni's nanocomposite classes.[5]

Group	Preparation Summary	Example
Sol-gel	Made at low temperatures (<100 °C); these nanocomposite precursors can lead to homogeneous single-crystalline phase or multiphase crystalline ceramics upon high-temperature heating	Ni/SiO_2, Cu/SiO_2
Intercalation	Can be prepared at low temperatures (<200 °C) and lead to useful materials upon heating to modest temperatures (<500 °C)	Cu/silicate
Entrapment	Prepared from three-dimensional linked network structures such as zeolites	Ni/zeolite (see ref. 6)
Electroceramic	Prepared from mixing of ferroelectric, dielectric, superconducting or ferroic nanophases in a polymer matrix at low temperatures (<200 °C)	Silica/polydimethyl-siloxane
Structural ceramic	Prepared by traditional high temperature ceramic processing (100-1800 °C)	Al_2O_3/SiC, Si_3N_4/SiC

1.1.1.1 Properties of Nanocomposites

The small components, termed 'clusters' or 'inclusions',[7] that are dispersed within the matrix behave as intermediates between isolated atoms and long range ordered solids. Since these clusters possess such small dimensions and large surface areas, a large percentage of the clusters lie near or at the surface.[7,8] For example, a 50 Å CdS cluster in a polymer matrix has ~15% of the atoms on the surface.[7] As a result, the interface between the cluster and the surrounding medium can have a large effect on the physico-chemical behaviour of the clusters. A major goal in the field of nanocomposite research is therefore to obtain total control of the cluster in terms of its size, interface with its medium and its composition in order to achieve or enhance the desired properties. Such properties include conduction, enhanced catalytic effects, non-linear optics and increased absorption coefficients.[7]

For example, if the clusters are semiconducting or metallic, the electrical conductivity of the nanocomposite is predominantly governed by the cluster concentration and their microstructural arrangement. Three structural regimes can be considered to explain this (see Fig. 1):

(a) Dielectric regime

At low cluster concentration, isolated clusters are dispersed in the dielectric medium and conductivity is predominately via electrons tunnelling from cluster to cluster.[7,9] This results in very low conducting or insulating systems.

(b) Transition regime

With increasing cluster concentration, agglomeration of clusters occurs until eventually they begin to touch one another to form a network of conducting phases contained within the dielectric medium.[7,9] At this point the conductivity begins to show a dramatic increase (by orders of magnitude). This is called the 'percolation effect'. It occurs where electron tunnelling is accompanied by conduction through a continuous three-dimensional network.

(c) Metallic regime

Above the percolation threshold, only a small increase in conductivity is observed with further increase in cluster concentration due to an enhancement of the conductive network.[7,9] As a result of the reduction in the electron mean free path arising from the electron scattering at the cluster/medium boundaries, the DC conductivity is usually orders of magnitude lower than the values associated with the respective bulk metal/semiconductor.

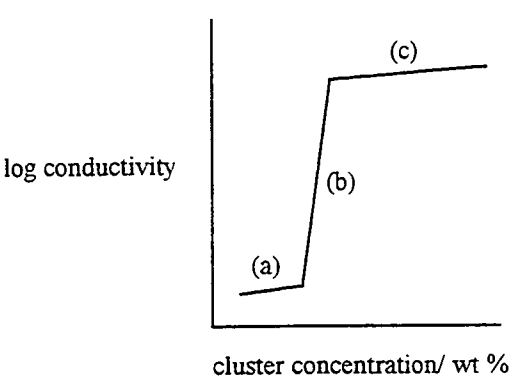

Fig. 1 Schematic diagram of the conductivity of a binary mixture made up from an insulating matrix and conducting clusters.[9]

1.1.2 TITANIUM OXIDE AND NITRIDE CERAMICS

Titanium oxide and titanium nitride both have interesting electrical properties. Therefore they are potential candidates for the conducting component of a polymer/ceramic nanocomposite material.

1.1.2.1 Titanium Oxide

The oxidation state of titanium varies between 0 and +IV, though the +IV oxidation state is the most stable.[10] Therefore titanium dioxide, TiO_2, is the most commonly occurring oxide of titanium. Three stable crystalline forms of TiO_2 exist: rutile, anatase and brookite. Rutile occurs as one of the natural ores of titanium, along with ilmenite ($FeTiO_3$), although anatase is 8 to 12 $kJmol^{-1}$ more stable than rutile. At high temperatures (>900 K), only rutile is stable.[11]

TiO_2 is a well studied and widely used compound. It is used as a versatile whitening pigment[12] for paints, plastics, printing inks and paper and is chemically inert to common solvents and acids.[11] It can act as a catalyst for various organic reactions such as the cyclotrimerization[13] of ethene to form benzene at 300 K and as a heterogeneous catalytic support and promotor.[14] TiO_2 possesses a high dielectric constant (up to ε=110),[15] and has therefore found use as a thin film capacitor.[11] Its high refractive index (2.5-2.7)[12] makes it a suitable anti-reflection coating, whilst its optical transparency in the visible and near infrared regions means it is suitable as an optical waveguide.[11]

Pure stoichiometric TiO_2 is highly insulating with a room temperature resistivity of 10^{13} Ωcm.[16] A reduction of oxygen from the lattice results from annealing in either a low oxygen pressure or in the presence of hydrogen.[11,17] The reduced TiO_2 then behaves as an 'n'-type semiconductor with properties dependent on the extent of oxygen loss. Non-stoichiometric TiO_{2-x}, Ti_nO_{2n-1} Magnéli series of homologous compounds, Ti_3O_5 and Ti_2O_3 can be formed by reduction.[17] TiO is known to be conducting.[18] Lower resistive 'n'-type films can be achieved by doping reduced TiO_2 with for example niobium, tantalum, vanadium, fluorine and hydrogen.[11]

1.1.2.2 Titanium Nitride

Titanium nitride, TiN, possesses various interesting properties and has been extensively studied because of its many potential technological applications. For instance, the

optical properties of TiN resemble those of gold,[19] yet it is harder than most elements (Moh's value of 9) and almost as hard as diamond (Moh's value of 10).[20] Its melting point[20] is 2930 °C which is higher than that of most materials, and it is inert to most chemicals and solvents except HF and aqua regia, in which it dissolves slowly.[19] Although TiN is thermodynamically stable, it is oxidized when exposed to oxygen or air and a surface oxide layer is formed.[21] The reaction:[22]

$$TiN + O_2 \rightarrow TiO_2 + \frac{1}{2}N_2$$

is thermodynamically favourable, with a ΔG° value of -582 $kJmol^{-1}$. The formation of TiO_xN_y type transition layer at the TiO_2/TiN interface has also been proposed.[23,24] The oxidation behaviour of TiN has important effects on corrosion stability and surface properties such as conductivity and friction.[25] Bulk TiN has an electrical resistivity of 21.7 $\mu\Omega$ cm at room temperature[20] which is lower than Ti metal.[19]

As a result of such properties, TiN thin films are widely used as wear-resistant coatings on machine tools and as gold coloured decorative coatings on watches and jewellery.[19,25] More recent applications of TiN films include their use as diffusion barriers in various semiconductor metallization schemes, as contact layers for silicon, as gate electrodes in metal/oxide/semiconductor integrated circuits and, because of TiN's optical transparency in the visible and near infrared regions, as solar energy absorbers and transparent heat mirrors.[26]

1.2 PLASMAS

1 2.1 INTRODUCTION

Partially ionized plasmas have extensive use in many areas of modern technology[27] such as in the microelectronics, aerospace, automotive and biomedical industries.[28] They are also used in waste management for the decomposition of organic waste[29] and for the treatment of flue gases[30,31] in order to reduce NO_x and SO_2 emissions, both major contributors to acid rain. Plasma processing is used for deposition of thin films, etching of the actual surfaces and modification of existing surfaces by oxidation, nitriding or texturing. Often the results obtained are unique to plasma processes and cannot be achieved by other means.

Compared with wet chemical methods, low-pressure plasma technology is safe and environmentally friendly,[32] producing very low volumes of toxic waste. However development and optimization are difficult because of the complexity of both the plasma volume chemistry and the surface chemistry in the reactive gas plasma environment.[27]

1.2.2 DEFINITION AND CLASSIFICATION

A plasma is an assembly or collection of ions, electrons, photons, neutral atoms and molecules[33-35] and is often referred to as the 'fourth state of matter'.[20,36] A plasma can be produced through the action of either very high temperatures, or strong electric or magnetic fields.[33] This account will only refer to those 'cold' plasmas (see below) that are partially ionized (i.e. the total number density of charged particles is much less than the total number density of the neutral particles) and produced by gaseous electric discharges. In a discharge, free electrons gain energy from an imposed electric field and lose this energy through collisions with neutral gas molecules.[33] The transfer of energy to the molecules leads to the formation of the listed species. To be deemed a plasma, the ionized gas produced in the discharge must be quasi-neutral, that is the total number of positively charged particles is virtually equal to the total number of negatively charged particles.[33,34] This can be satisfied only if the dimensions of the discharged gas volume, L, are significantly larger than the Debye length,[33] λ_D, which defines the distance over which a charge imbalance can exist:

$$\lambda_D = (\varepsilon_0 kT_e/ne^2)^{1/2}$$

where ε_0 is the permittivity of free space, k is the Boltzmann constant, T_e is the electron temperature, n is the electron density and e is the electronic charge.

Plasmas can be characterized[33] by average electron temperature (T_e), average electron energy (kT_e), or by electron density, n. For instance, as shown in Fig. 2, a range exists from very 'hot' plasmas used to induce thermonuclear fusion processes, to 'cold' plasmas which are used to deposit thin films or to modify surfaces.[37] Low temperature or 'cold' plasmas are generated by low-pressure (10^{-2}-10^{-1} Torr) glow electrical discharges where the electron temperature, T_e, is not equal to the gas temperature, T_g. Typically, T_e is two to three orders of magnitude greater than T_g (T_g ~100-200 °C) and this type of 'cold' plasma is therefore also known as a 'non-equilibrium' plasma. The reactive species in these plasma have an increased internal energy, permitting a reaction to proceed at near ambient temperatures. This is beneficial for thermally sensitive materials such as organic materials e.g. polymer films.

A 'hot' plasma[34] is found at high pressures and temperatures where many collisions occur between charged particles and neutrals resulting in an equal energy distribution amongst all the particles; hence the plasma is termed an 'equilibrium' plasma. The disadvantage of using an equilibrium plasma is that it is very difficult to control the creation of individual species with a defined energy.

1.2.3 LOW PRESSURE NON-EQUILIBRIUM PLASMAS

Low pressure non-equilibrium plasmas can be generated in a number of ways. The three major parameters which control the plasma are the source of electrical power to sustain the plasma, the coupling mechanism and the plasma environment.[34,36] Most of the early plasma work involved AC and DC electrode discharges, but with greater flexibility and control over the operating parameters there has been a shift towards the use of inductively or capacitively coupled RF and microwave plasmas.

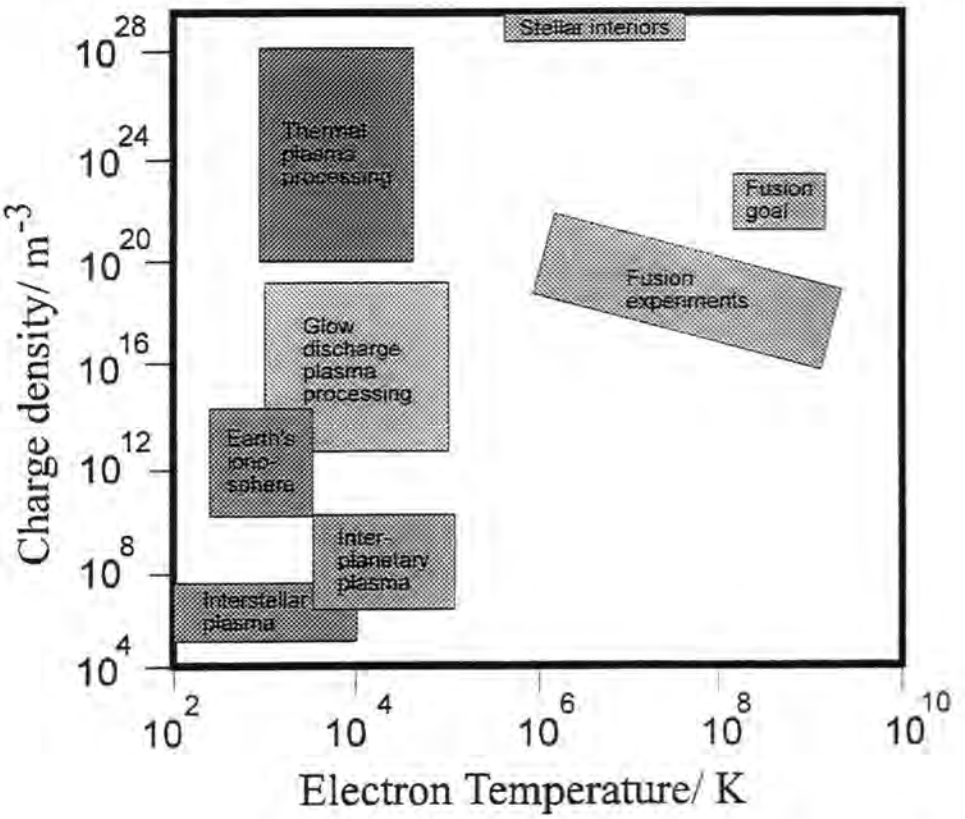

Fig. 2 Typical plasmas characterized by their electron energy and density.[28]

1.2.3.1 DC Discharge

The basic low pressure glow discharge is sustained between two parallel-plate metal electrodes[34,38-40] encased in a gas filled tube at pressures typically lower than 10 mbar as illustrated in Fig. 3. Such plasmas are commonly used in fluorescent tubes and neon signs because light is emitted in the visible region.[40]

The basic design can be slightly modified to allow plasma polymerization, for example by adding an inlet and outlet to the system.[38] The belljar configuration uses a feed tube to allow monomer in and a port in its base plate allows the removal of unconsumed

monomer and gaseous products. The lower electrode can serve as the substrate holder and may be heated or cooled. One disadvantage of this configuration is that monomer flow is not limited to passing through the plasma between the electrodes. A way round this is to use a rectangular flow reactor to give constant monomer flow over the entire electrode area. A major disadvantage of these two reactors is the contamination of the electrodes[33,38] with plasma polymer deposit.

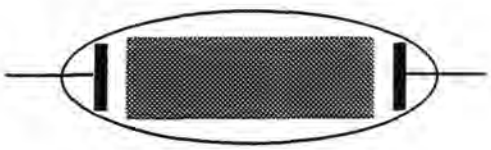

Fig. 3 A typical DC discharge.[33]

1.2.3.2 RF (High Frequency) Discharge

Direct contact between electrodes[33] and plasma is avoided using an electrodeless method where the electrodes are outside the reactor. The energy is provided to the plasma by inductive and/or capacative coupling methods. Thus contamination of the electrodes or contamination of the plasma with metal vapour from electrode erosion does not occur.[34,38] Reasonably homogenous plasmas can be generated if the wavelength of the electric field is much larger than the reactor dimensions.[34] If the collision frequency is higher than the applied field frequency, the discharge is very similar to a DC discharge. Three basic configurations are used as illustrated in Fig. 4. In capacitive coupling the electrodes enclose the plasma tube and are mainly used at low pressure (see Fig. 4 (a), (b)). For inductive coupling the tube lies on the axis of the coil (Fig. 4 (c)). RF plasmas work well at low pressure (10^{-2}-10^{-1} Torr) but can work at atmospheric pressure. Power generators with fixed frequency and variable power are preferred.[33] The most common frequency used is the industrial frequency of 13.56 MHz.[41] Efficient coupling of the power to the discharge and protection of the power generator requires the use of a matching network. A Faraday cage may be required to isolate the external environment (such as radio and other equipment) which can otherwise suffer from interference in the absence of shielding.

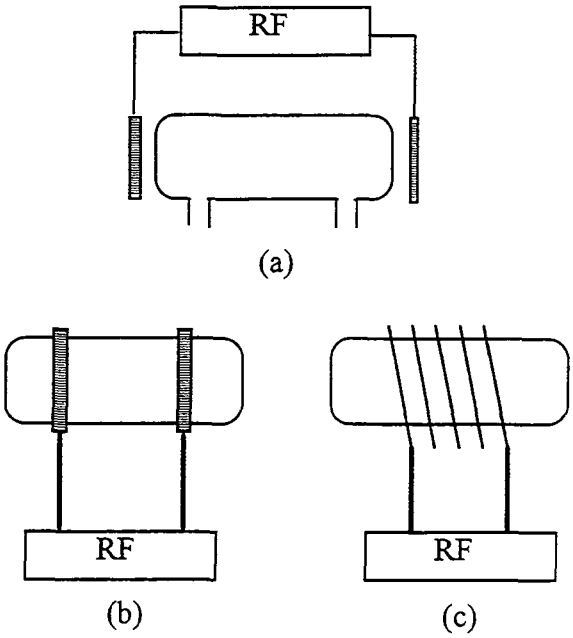

Fig. 4 Schematic diagram of typical arrangements for RF discharges; (a) and (b) capacitively coupled, (c) inductively coupled.[33]

1.2.3.3 Microwave Discharge

The microwave region (0.3-10 GHz) has wavelengths of electromagnetic radiation comparable to the dimensions of the discharge reactor[34,39] which causes an uneven distribution of energy and power. Therefore other coupling mechanisms are required. Microwave power is led by coaxial cable or wave guide from the generator to a resonant cavity which encloses the reactor. A commonly used frequency is 2.45 GHz which is also the frequency used in microwave ovens.[34] Microwave discharges are more difficult to initiate and to sustain at low pressures ($\leq$ 1 Torr) than DC or RF discharges.[33] Therefore pressures of several Torr[33] and even atmospheric pressure have been used.[34] However at higher pressure, the gas temperature can rise substantially leading to the pyrolytic decomposition of reactants.[33]

1.2.4 BASIC CONCEPTS OF LOW PRESSURE NON-EQUILIBRIUM PLASMA PHYSICS

1.2.4.1 Average Electron Energy

The electrons in a plasma are the dominant charge species and are generally more energetic than the ions due to their lower mass.[42] It is primarily the electrical field that provides the energy to the electrons which initiate the chemical reactions.[34] At low

pressure electrons do not collide frequently enough with the neutral gas species and so do not come into equilibrium with the heavy particles. The steady state is governed by energy losses of electrons and ions on recombination on the container walls. This is the case for glow, RF and microwave discharges.

The electrons span a range of energies governed by the electron energy distribution function (EEDF). Often, the energy distribution is Maxwellian:[34]

$$f(E) = 2(E)^{1/2}/[(\pi)^{1/2}(kT_e)^{3/2}]\exp(-E/kT_e)$$

where E is the electron energy, k is the Boltzmann constant and T_e is the electron temperature. The plasma electron energy is often described in terms of the average electron energy of the Maxwellian distribution; typically 1-10 eV rather than 0.02-0.1 eV for the ions.

1.2.4.2 Plasma Potential

Following ignition of the plasma, electrons rapidly leave the plasma volume resulting in the build up of a positive potential in the plasma volume and negatively charged surfaces in contact with the plasma.[42] The plasma potential is finally achieved when an equal rate of loss of electrons and ions occurs to give the plasma overall quasineutrality.

1.2.4.3 Sheaths

A dark space or sheath is usually observed adjacent to all surfaces in contact with the plasma.[42] This is because the surfaces in contact with the plasmas are negatively charged and a positive space-charge layer is formed in front of these surfaces. There are few electrons in the space-charge layer or sheath and so fewer species are excited by electron collisions. Consequently fewer species relax and give off radiation.

1.2.4.4 The Origin of a Glow Discharge

For the simplest glow discharge case, the gas filling the space between the two electrodes will break down and a self-sustained discharge as illustrated in Fig. 5 will be established if a sufficiently high DC potential is applied across the electrodes.[35]

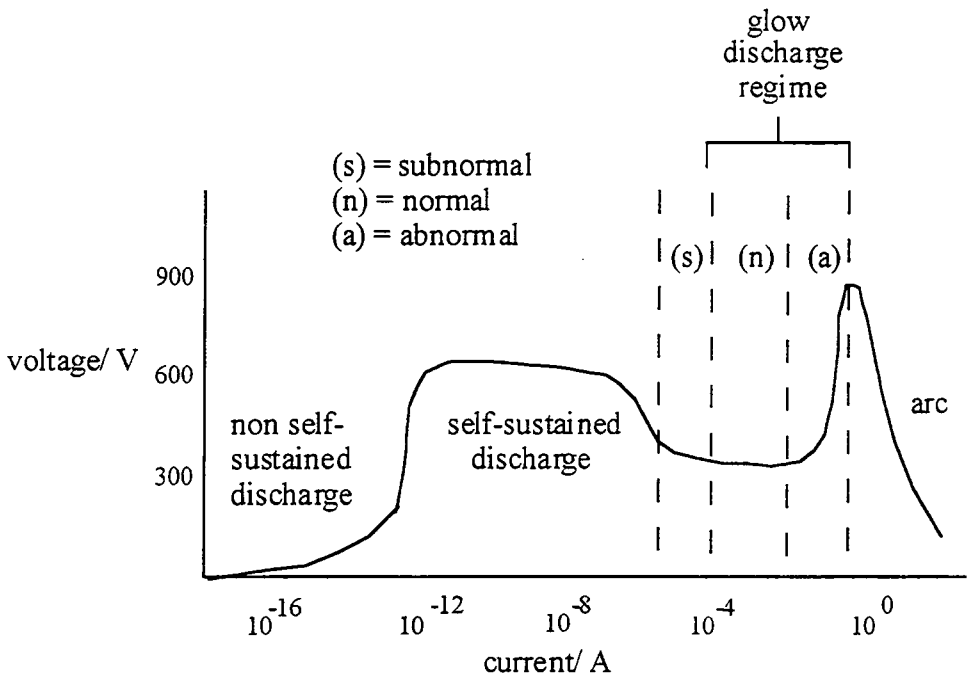

Fig. 5 Electric breakdown of a gas at a low pressure.[35]

The voltage at which the gas begins to breakdown is known as the breakdown potential, which is dependent on the inter-electrode distance and the gas pressure. The relationship between these two variables and the applied voltage is governed by Pashen's Law, see Fig. 6. On increasing the current between the electrodes, the subnormal and normal regions are passed through (see Fig. 5), finally reaching the abnormal region at large current values. At very large current values, the electrodes are excessively heated causing thermoemission. This results in the abnormal region turning into an arc. The normal and abnormal regions are of importance for thin film deposition processes.

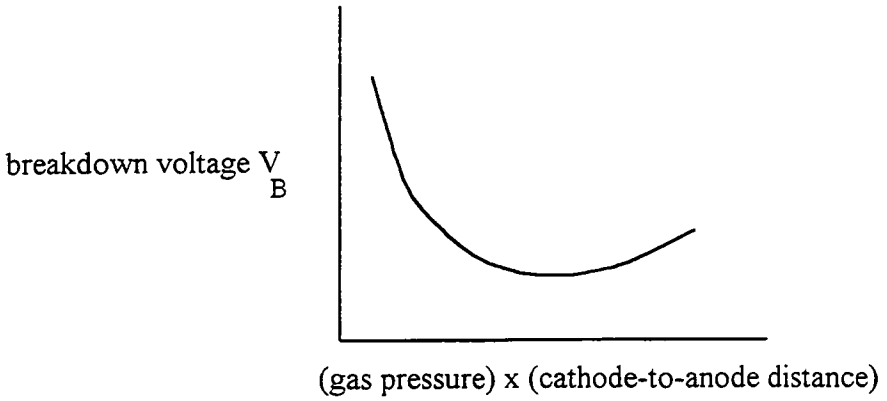

Fig. 6 Pashen's Law.[35]

In an AC set-up, each electrode acts as a cathode and anode alternately[35] and no significant displacement of electrons or positive ions occurs if the frequency is increased to the MHz region i.e. RF discharge. Losses of charged species by diffusion or recombination are replaced by electron-impact ionization of neutral gas molecules in the discharge volume.

1.2.5 THE CHEMISTRY OF LOW PRESSURE NON-EQUILIBRIUM PLASMAS

The electrons created in the discharge typically initiate chemical reactions.[34] If the electron energy is relatively low, elastic collisions take place.[43] Inelastic collisions take place at higher electron energies where atomic or molecular excitation to higher energy levels can occur with the equivalent loss of energy from the colliding electrons, and at very high electron energies ionization can occur. This last process is essential for maintaining an electric discharge in the presence of an electric field. The electrons can replenish their lost energy from the electric field.[34] Excited molecules can now, due to their high internal energy, either dissociate or initiate other reactions.

The main types of chemical reactions occurring in the plasma volume are listed in Tables 2-5. The most important reactions are electron losses by attachment and recombination which have to be balanced by ionization and detachment processes.[34]

Table 2 Electron/molecular plasma reactions.[34]

Reaction	Reactants	Products
Excitation	$e^- + A_2$	$A_2^* + e^-$
Dissociation	$e^- + A_2$	$2A + e^-$
Attachment	$e^- + A_2$	A_2^-
Ionization	$e^- + A_2$	$A_2^+ + 2e^-$
Dissociative Ionization	$e^- + A_2$	$A^+ + A + e^-$
Recombination	$e^- + A_2^+$	A_2
Detachment	$e^- + A_2^-$	$A_2 + 2e^-$

Table 3 Atomic/molecular plasma reactions.[34]

Reaction	Reactants	Products
Penning Dissociation	$M^* + A_2$	$2A + M$
Charge Transfer	$A^\pm + B$	$B^\pm + A$
Ion Recombination	$A^- + B^+$	AB
Neutral Recombination	$A + B + M$	$AB + M$

Table 4 Decomposition plasma reactions.[34]

Reaction	Reactants	Products
Electronic	$e^- + AB$	$A + B + e^-$
Atomic	$A^* + B_2$	$AB + B$

Table 5 Synthesis plasma reactions.[34]

Reaction	Reactants	Products
Electronic	$e^- + A$	$A^* + e^-$
	$A^* + B$	AB
Atomic	$A + B$	AB

1.2.6 PLASMA APPLICATIONS

Partially ionized plasmas are used extensively to process surfaces in many areas of technology, including deposition of thin films, etching of surfaces and modification of existing surfaces by oxidation, nitriding or texturing.[27] Often results are obtained with partially ionized plasmas which cannot be obtained by other methods. Though the plasma environment is vastly complex, great potential lies ahead for process development, optimization, discovery and invention. After surveying plasma assisted etching and plasma assisted surface modification, this account concentrates on plasma assisted deposition processes.

1.2.6.1 Plasma Assisted Etching

A molecular gas is chosen such that when it is activated in a glow discharge, the ions and/or radicals that are formed (by excitation, dissociation or ionization) will react with the substrate to produce volatile products that ablate from the surface.[27] These products are then be pumped out of the system.

Etching has been used in the microelectronics industry in a variety of ways for example in removing photoresists and plasma cleaning of surfaces (i.e. removal of adventitious contamination such as adsorbed gas) prior to subsequent thin film deposition. The advantages of plasma assisted etching over wet etching include a higher degree of anisotropic etching and lower costs due to higher efficiency and reduced waste disposal.

1.2.6.2 Surface Modification

The optical, reflection and adhesion characteristics, friction coefficient, surface energy (wettability and water repellancy), permeability and biocompatability of conventional polymers can all be controlled by the application of an appropriate plasma treatment.[35] Such treatments include:

1) The use of O_2, air, H_2O and N_2O to act as oxidizing gases removing organics and leave oxygenated species on polymer surfaces.[44]
2) The use of H_2 gas to replace fluorine or oxygen atoms on the surface and remove organics that are sensitive to oxidation.[44] The organics are converted to volatile molecular weight species that are not polymerized or redeposited.
3) The use of noble gas plasmas such as Ar or He which have been shown to cause crosslinking in polymer surfaces.[44] Excited atoms and vacuum UV (VUV) light

break C-C and C-H bonds leaving free radicals in the surface. Recombination, unsaturation, branching and crosslinking may then occur.

4) The use of NH_3 plasmas to graft amino groups to the surface of polymers.[44]

Modification of metallic and semiconductor surfaces can also be performed using plasmas.[27] Oxide films on metals and semiconductors can be produced at low temperatures in the oxidation of Si, GaAs and InP and in the growth of tunnelling junctions (e.g. Josephson junctions) on Nb, Pb and related alloys. Plasma nitriding of metals is carried out using a N_2 or NH_3 plasma; this is usually best accomplished as a cathodic process with relatively high energetic positive ion bombardment. One of the most used commercial applications of plasma nitriding is the case-hardening of machine tools and a H_2 plasma has also been used to reduce silver oxide to silver metal.[44]

1.2.6.3 Plasma Assisted Deposition Processes

Current and future applications in high-technology areas require the deposition of simple and multiple layers of various materials in a thin film form which can be consistently reproduced.[45] Plasma assisted or plasma enhanced deposition processes use a plasma in the space between the source and the substrate. Most applications make use of low pressure (glow discharges) plasmas where the most energetic species are the electrons since they gain energy much faster than the ions from the electric field.[46,47] The electrons accumulate sufficient energy to undergo inelastic collisions with the gas molecules to sustain ionization while the heavy particle temperature remains low. A unique mixture of species including ions, metastables and radicals can be generated in the plasma which can react to form thin films.

The processes used to deposit films can be classified into physical (PVD) and chemical (CVD) vapour deposition processes, as indicated in Table 6. CVD can be defined as a reaction of volatile components at the surface of a substrate with the formation of a solid layer and volatile reaction products.[48] The reaction is controlled by the thermodynamic equilibrium which depends on the vapour pressure and the temperature. PVD may be defined as the condensation of a flux of atoms or clusters of atoms in a vacuum.[48] The atoms may either be neutral or ionized. There are three basic PVD processes: evaporation, sputtering and ion plating. Deposition of compounds in a PVD process can be carried out by using either a 'direct' or a 'reactive' method.[45] 'Direct' means that the target is the same compound as the film, whilst 'reactive' infers that a metal/alloy is evaporated in the presence of a reactive gas to deposit a compound. A well documented example of the latter case is the sputter deposition of TiN using a Ti cathode in the presence of nitrogen gas where the properties of the deposited TiN are strongly

influenced by the stoichiometry.[49-51] The stoichiometry itself therefore needs to be controlled and this depends on the process and plasma variables.[45]

Table 6 Classification of PVD and CVD processes.[45]

PVD		CVD	
PVD Process	PAPVD Process	CVD Process	PACVD Process
Evaporation	Activated reactive evaporation	Thermal	DC excitation
Sputtering	Reactive sputtering		AC excitation
Ion plating	Reactive ion plating		RF excitation
			Microwave excitation
			Photon excitation

Some of the plasma assisted deposition techniques used are discussed in the following sections.

1.2.6.3.(a) Plasma Assisted Physical Vapour Deposition (PAPVD) Techniques

(i) Sputter Deposition

Atoms are ejected from a target electrode due to momentum exchange associated with bombardment of inert gas ions from a plasma.[45-47] These atoms will then condense onto a substrate. Usually low pressure (0.1-10 Pa) inert gas plasmas (typically Ar) are used.[47] Often reactive gases are added to the inert gas in the sputter deposition process to provide a component of a multicomponent coating.[27,45-47] This is known as reactive sputter deposition.

(ii) Ion Plating

Ion plating[46,47] is a process in which ion bombardment of substrates for substrate cleaning prior to deposition, and to modify surface properties during the deposition, is achieved by making the substrate the cathode electrode (usually DC) of a low pressure plasma discharge (V =2000-5000 V) in a mixture of coating flux and inert working gas (usually Ar at ~4 Pa). The coating flux is usually provided by evaporation or sputtering. The working gas may contain reactive gas species as before and the process is then known as reactive ion plating (RIP). Plasma assisted ion plating is commonly used for

metal films, oxides, nitrides, carbides, carbonitrides, alloy films, and multicomponent materials.

(iii) Activated Reactive Evaporation (ARE)

In ARE, the plasma discharge is sustained in a flux of evaporated material and reactive gas.[46,47] Dissociation and ionization are induced in a low pressure (1-35 mbar) reactive gas which enhances the reactivity on the surface. The plasma may be driven by a DC or RF potential and is commonly used for depositing metal oxides, carbides and nitrides.

1.2.6.3.(b) Plasma Assisted/Enhanced Chemical Vapour Deposition (PACVD/PECVD) Techniques

(i) Introduction

Reactant gas or gases are passed through a low pressure plasma discharge (typically 0.01-0.2 Torr). Dissociation, ionization and gas phase reactions are induced permitting coatings to be deposited at relatively low temperatures.[46] The substrate can be heated to improve film quality, but the temperature will still be lower than those used in thermal CVD.[1] Reactor configurations include all those mentioned in section 1.2.3.2, but the parallel-plate is most commonly used.[46,47] The discharges are usually driven between 300 Hz to GHz (microwave), though 13.56 MHz is the most commonly used frequency.

PACVD is probably the most complex of all plasma based surface processing techniques and there is little understanding of the chemical and physical mechanisms that determine the characteristics of the deposited films.[27] Important parameters controlling film growth include reactant partial pressure, flow rate, RF power, substrate temperature and bias[45] all of which affect both the process parameters, such as deposition rate, and the plasma parameters, such as electron density, electron energy and its distribution function. The reactant gas partial pressure together with the RF power determine the dissociation rate of the reactive gas and hence the deposition rate. These variables also determine the electron energy and electron density. Also the substrate floating potential depends on the average electron energy, so therefore the pressure and RF power control substrate bombardment. The consequent interdependence of plasma and processing parameters clearly illustrates the difficulties associated with PACVD.

With all CVD processes, the existence of volatile precursors is a prerequisite[52,53] with vapour pressures ≥10 Pa at room temperature.[52] The precursors should also be stable to heating until such a pressure is reached. Other requirements include ease of preparation in significant quantities of high purity, reasonable safety, thermal stability at handling temperatures, and the ability to fragment in a desired manner.[53]

It should be noted here that among CVD users the term 'organometallic' is often inappropriately used to describe any compound where a metal is bonded to an organic containing group or fragment and does not necessarily possess a direct metal-carbon bond as required by definition.[54] Typical examples of films deposited from organometallic, metallorganic and inorganic precursors are summarized below. Further examples can be found in Table 7.

PACVD is widely used in the microelectronics industry. One of the most important applications is the deposition of amorphous hydrogenated silicon photovoltaic films by the plasma decomposition of silane.[27] Also silicon oxide,[46] silicon nitride[55] and silicon oxy-nitride[46] films have been deposited using this technique.

A few metallic elements form volatile halides and hydrides and have been used in PACVD.[52] In the case of carbonyls, $Ni(CO)_4$ and $Co_2(CO)_8$ resulted in carbon contaminated metallic films whilst those of Cr, Mo, W and Mn were also contaminated with oxygen.

Alkyl compounds of In and Sn have been used as precursors for oxide films, whilst aluminium alkyls such as $Al(^iBu)_3$ need to be handled with care as they are very moisture and oxygen sensitive.[52] Aluminium nitride has been formed from $Al(Me)_3$[56] and $Al(^iBu)_3$[57] in the presence of N_2 or N_2/H_2 and N_2 respectively, whilst β-Sn can be deposited from $Sn(Me)_4$.[58]

Metal π-complexes, such as ferrocene $(\pi\text{-}C_5H_5)_2Fe$, $(\pi\text{-}C_3H_6)Pd(\pi\text{-}C_5H_5)$ and $(\pi\text{-}C_5H_5)_2Pd$ have been used to deposit films, in the former case the ferrocene structure is primarily retained,[59] whilst in the latter case the Pd compounds gave Pd films.[60]

Oxide films have been of interest and the use of metal chelates[61,62] or alkoxides[62] have been considered as precursors. Further discussion on titanium alkoxides is reviewed in Chapter 3. The potential to produce superconducting thin films of Ba,Y,Cu,O from the respective β-diketonates is now attracting much attention.[63,64]

Hard tribological coatings[65] such as TiN and ZrN have been extensively studied using metal organic amido $M(NR_2)_4$ precursors; in the case of TiN low substrate

temperatures (~100 °C) have been achieved using an electron cyclotron resonance plasma technique.[66] Chapters 6 and 7 review the work using the titanium precursors. BN films, useful as chemically and thermally inert hard coatings, have been produced using diborane (B_2H_6) and either N_2[67] or NH_3.[68]

New interest in the deposition of diamond films has been launched recently.[35,42] The reviews of PACVD by Reif and Kern and Lucovsky and Tsu give more details on the types of materials that are being deposited.[42]

PACVD will probably become the most important method in the future for thin film deposition since greater adhesion, excellent step coverage and awkward geometrical coverage can be achieved compared with conventional techniques such as painting, spraying or dip coatings.[35]

(ii) Plasma Polymerization

The introduction of a suitable organic or metallorganic precursor into a low temperature non-equilibrium plasma results in the deposition of a polymeric material by plasma polymerization.[35] All the surfaces in contact with the plasma are coated with a thin film or powder[4] which can be highly crosslinked, strongly bonded to the surface and contain a large quantity of free radicals trapped in the polymer.[43] Formation of free radicals has been ascribed to the bombardment of energetic particles on the surface and to the UV radiation generated in the plasma.

Yasuda has proposed a rapid step-growth polymerization mechanism involving two major routes as depicted in Fig. 7.[43] Monofunctional activated species capable of participating in chemical bond forming reactions are given by M·, whilst difunctional activated species are shown by ·M·. The subscripts i, j, k indicate different sized species. Cycle I in Fig. 7 involves repeated activation of products from monofunctional activated species whilst Cycle II is via difunctional activated species. The active species may be radicals, ions or both. Unsaturated monomers such as benzene and ethylene polymerize mainly through difunctional intermediates, while saturated monomers such as methane polymerize via monofunctional species giving rise to fewer radicals in the polymer.

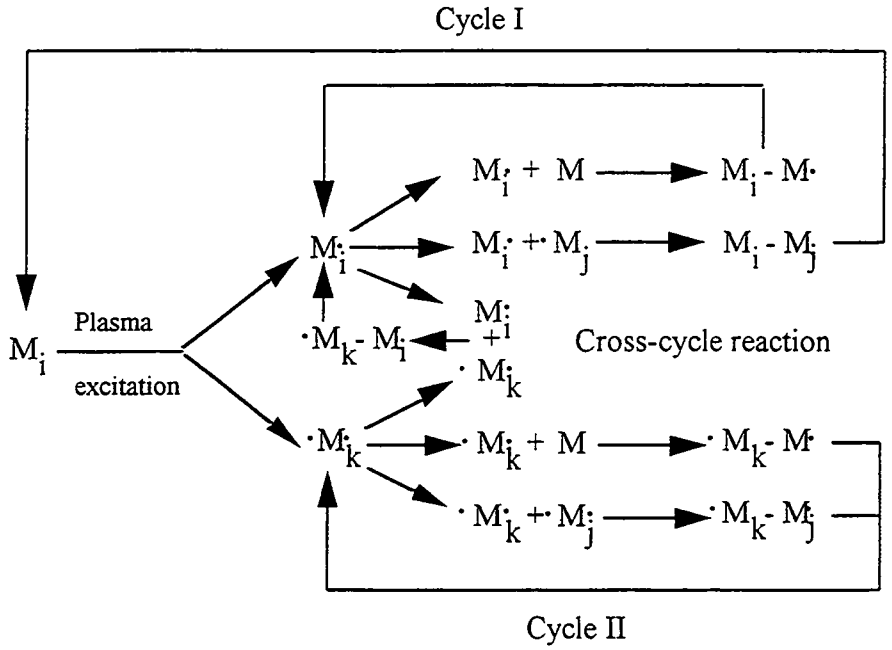

Fig. 7 Schematic of bicyclic step-growth mechanism of plasma polymerization.[43]

Once a plasma is created, the gas phase is no longer the original monomer vapour, but becomes a complex mixture of the original monomer, ionized species, excited monomer species, excited species of monomer fragments and gas products such as H_2 gas. The plasma also interacts with the walls of the vacuum vessel, substrates and any deposited material. As a result, anything that comes into plasma contact can take part in the plasma polymerization process. The net polymerization therefore will be a result of the balance between polymerization and ablation of species on the surfaces, the so called competitive ablation polymerization (CAP) model as illustrated in Fig. 8.[43] Ablation is a key feature of fluorocarbon plasmas due to the presence of highly reactive fluorine species which can etch the surface.[4] Alternatively, physical sputtering typically occurs in the presence of inert gases such as Ar. The balance between polymer formation and ablation, depends not only on the chemical nature of the monomer and all the surfaces that come into contact with the plasma, but also on the operational parameters of the plasma.[43]

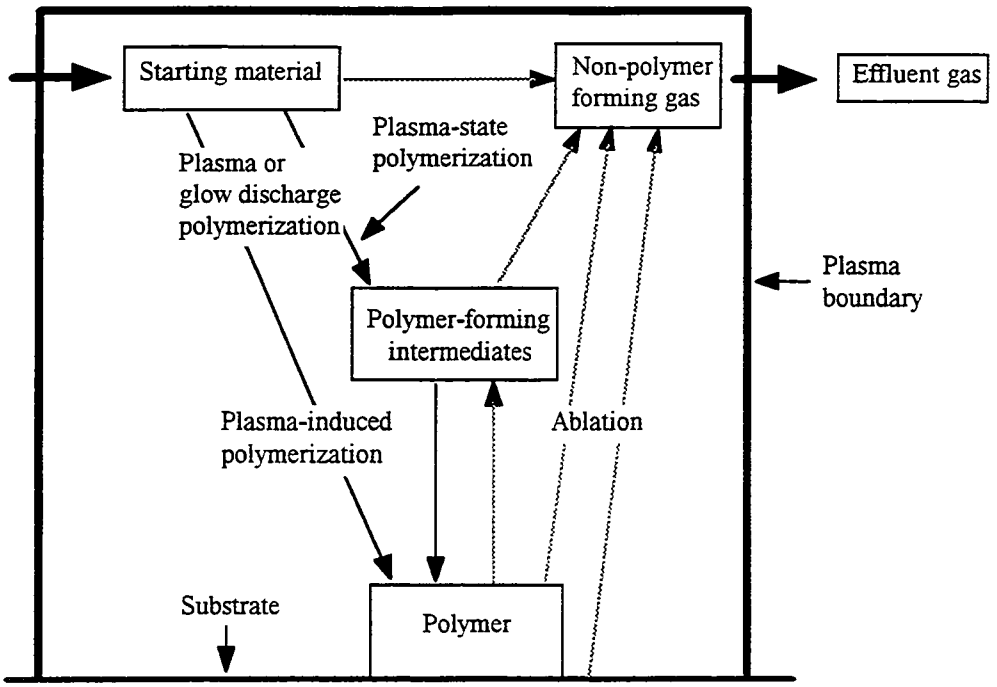

Fig. 8 Competitive Ablation Polymerization (CAP) Mechanism.[43]

Plasma-induced polymerization can be considered to be similar to conventional molecular polymerization with the plasma acting as an initiator.[43] Initiation of the polymerization process, such as formation of free radical chain ends, can be created in the plasma. Plasma-state polymerization however can only occur under plasma conditions. For example saturated monomers (i.e. monomers that cannot undergo conventional addition polymerization) can be polymerized and the rates of polymerization are on the whole found to be similar regardless of monomer structure.

It is important to recognise that the discharge power level described for plasma polymerization is a system-dependent parameter. Once the monomer is broken up in the plasma, it is said that plasma polymerization follows an atomic rule, rather than a molecular one.[69-72] Therefore for a steady-state flow system, it is more appropriate to work with mass flow rates than with molecular ones. For a fixed geometry and pressure, use of the composite parameter, W/F_m, where F_m is the mass flow rate and W is the discharge power, is a useful way to characterise the behaviour of a plasma in relation to power. The composite parameter, W/F_m, represents the energy input per unit mass of monomer.

The value of F_m can be estimated by assuming ideal gas behaviour.[73] For an ideal gas:

$$m = \left(\frac{MV}{RT}\right)p$$

where m is the mass of gas inside the reactor, M is the molecular weight of the gas, V is the volume of the reactor, R is the universal gas constant, T the gas temperature and p the gas pressure.

If the reactor is continually fed monomer with a mass flow rate, F_m, and the outlet of the reactor is closed off to the pump at time t = 0 s, then the value of F_m can be calculated according to:

$$F_m = \frac{dm}{dt} = \left(\frac{MV}{RT}\right)\left.\frac{dp}{dt}\right|_{t=0}$$

Estimating the value of $\left.\frac{dp}{dt}\right|_{t=0}$ as $\frac{\Delta p}{\Delta t}$, then:

$$F_m = \left(\frac{MV}{RT}\right)\frac{\Delta p}{\Delta t}$$

Similarly the leak rates can be calculated using this method. This assumption has been used throughout the experimental work.

1.2.7 METAL/CERAMIC CONTAINING ORGANIC THIN FILMS

Formation of polymer composites or 'hydrid' films[74] containing metal or ceramic (refractory, inorganic solid-state material)[54] species or clusters in an organic matrix can give rise to interesting physical, chemical, medical and electrical properties.[75] The dielectric polymer matrix can also serve to isolate the clusters from one another and so facilitate the study of such clusters.

Kay introduced the principal methods of metal incorporation into organic matrices:

1.2.7.1 Simultaneous plasma polymerization of an organic gas and sputtering or etching of a metal from a target electrode

The simplest method involves a RF parallel-plate arrangement[4,35] where the metal target is sputtered, usualy by Ar or halocarbon gases e.g. CF_4, C_2F_6. Metal emission into the plasma volume occurs at the same time as the monomer gas or vapour undergoes plasma polymerization. The coated substrate is usually located on the opposing grounded parallel elelctrode or on the floating insulating substrate. Increased metal emission, as a result of higher plasma density, can be achieved by using magnetron

excitation electrodes. Carbide or silica layers on the metal target are found to suppress metal emission if hydrocarbon or organosilicon monomers are used.

1.2.7.2 Simultaneous plasma polymerization of an organic gas and metal produced by evaporation

Metal emission suppression can be overcome using a metal containing resistively heated boat in the above mentioned RF parallel-plate arrangement where the substrate is located on the grounded electrode.[4,35] Hard polymeric films can be achieved by positioning the substrate on a negatively biased RF powered electrode. RF coils outside the reactor have also been used though silica incorporation has resulted from sputter-etching of the silica glass walls.

1.2.7.3 Sputtering from a composite metal/polymer target

Ar is often used as the working gas which can sufficiently decompose the polymer in the plasma.[4,35] As a result, the Ar supply can be closed off after the initial period and the discharge can continue with sputtering in the polymer decomposition gases alone. Sputtered polymers however tend to give different coatings from those obtained by plasma polymerization.

PTFE/metal composites have been deposited from PTFE/Pt-Rh, Au, Cu and Ekonol (trade name)/Pt-Rh targets in Ar.[4,35] Target, substrate geometry and input power have been used to control the metal/polymer ratio.

1.2.7.4 Simultaneous evaporation of metal and polymer

Co-evaporation of two resisitively heated sources has been carried out with metals such as Al, Au, Ag, Cu and Cr and polyvinylidenefluoride, polyethylene, polycarbonate and melinex (PET).[4,35] Pressure increases during film growth has been observed due to the thermal degradation of the polymer resulting in a high concentration of low molecular weight fragments in the deposit.

1.2.7.5 Plasma polymerization of metallorganic compounds

Organosilicon and metallorganic compounds, like almost all volatile organic molecules, can be converted into thin films on injection to a plasma. It is this method that has been used in this work. By variation of plasma and process parameters, it is possible to deposit either metallic/ceramic films or composite metal/ceramic/polymer films.[4,35] As a result of the wide varying compositions, film optical and electrical properties will be affected. For example, plasma polymerization of copper acetylacetonate was carried out under various conditions and it was found that the colour and appearance of the films were determined by the sum of plasma and thermal energies.[76,77] Even though the films were found to have alternating organic and metallic layers, the electrical conductivity went through the percolation threshold to give metallic conduction. With metallic/ceramic films, the composite host is then the metal/ceramic component and the dispersed component is the dielectric. It should be noted that plasma polymers derived from organic and organosilicon precursors tend to be insulating and interest in such films lies with their potential as dielectric media.[43]

Due to the interdependency of the plasma and process parameters on film composition, simple comparisons between the literature values of the electrical properties of deposited films may not be appropriate. For instance, geometry of reactors and substrate position have been shown to be important as observed in the case of tetramethyltin[58] and the thin nature of the deposited films means that surface effects can become competitive with the bulk phenomena with regards to electrical properties.[78] Measurement conditions also play an important role on the values obtained. For example, Bradley and Hammes[79] obtained their experimental data at temperatures greater than room temperature; extrapolation to room temperature should give values at least one order of magnitude lower.[43]

From this evidence, the best conductive films are those with metallic appearance[58,77,80,81] and little carbon content. Higher conductivity values have been achieved with[82] and without[81] the presence of a depolymerization gas such as O_2. Such a gas forms the volatile carbon oxide gases which are pumped away resulting in lower carbon content. However oxide films can be formed in the presence of oxygen,[60,83] which can subsequently be reduced to the pure metal after H_2 plasma treatment. Alternatively raising the substrate temperature to about 100 °C in the absence of a depolymerization gas is thought to supply enough thermal energy to cause desorption of organic fragments.[81]

Table 7 summarizes the electrical properties of some films deposited by the plasma polymerization of organometallic or metallorganic precursors. Films with conductivities

greater than 10^4 Scm^{-1} (resistivities less than 100 μΩcm) are generally considered as metallic, films with conductivities between 10^3-10^4 Scm^{-1} (resistivities between 100-1000 μΩcm) are regarded as semiconductors, while those films with conductivities less than 10^3 Scm^{-1} (resistivities above 1000 μΩcm) are considered as insulators.[81] Metallic films in Table 7 are indicated by the bold print.

Table 7 Electrical properties of films deposited from the plasma polymerization of metal organic precursors (continued on the two following pages).

Monomer/Gases	Reactor Configuration	Comments & Conductivities (σ)	Ref.
Ferrocene	Parallel electrodes, ultra-audio (10-50 kc)	$\sigma = 2.7 \times 10^{-13}$ Scm^{-1} (150 °C) $\sigma = 4.5 \times 10^{-12}$ Scm^{-1} (250 °C)	79
Diphenylmercury	Parallel electrodes, ultra-audio (10-50 kc)	$\sigma = 2.8 \times 10^{-15}$ Scm^{-1} (150 °C) $\sigma = 2.7 \times 10^{-13}$ Scm^{-1} (250 °C)	79
Hexa-n-butyltin	Parallel electrodes, ultra-audio (10-50 kc)	$\sigma = 1.5 \times 10^{-15}$ Scm^{-1} (150 °C) $\sigma = 7 \times 10^{-13}$ Scm^{-1} (250 °C)	79
Tetramethylsilane	Parallel electrodes, RF 13.56 MHz	$\sigma = 10^{-15}$-10^{-16} Scm^{-1} in M/PP/Si structure	84
Hexamethyl-disiloxane	Glow discharge	$\sigma = 1.4 \times 10^{-15}$ Scm^{-1}	85
Tetramethyltin (TMT)	RF inductively coupled, 3.9 MHz	Metallic films with C/Sn ratios 1-2.5 have σ 10^{-1}-10^{-2} Scm^{-1} (position dependent) and insulating transparent films at other positions	80
TMT, O_2	RF inductively coupled, 3.9 MHz	Position dependent reflective films with $\sigma \sim 10^{2}$-10^{4} Scm^{-1}, C/Sn<2 for conduction, transparent films insulating, evidence of a threshold value of C/Sn below which structure changed to β-Sn with C in interstices	58
TMT, O_2	DC glow discharge, parallel plate	For optimum TMT/O_2 σ =333 Scm^{-1}, σ increases as T_s increased; addition of $SbCl_5$ increases σ to as much as 588 Scm^{-1}	86
Tributyltin methacrylate	RF inductively coupled, 13.56 MHz	$\sigma = 8 \times 10^{-2}$ Scm^{-1}, 32% Sn (T_s=150 °C, power=5W)	87
TMT, Ar	Parallel electrodes, RF 13.56 MHz	$\sigma \sim 3.3 \times 10^{-4}$-10 Scm^{-1}, 80-95% Sn (T_s=150 °C, power=50W)	87
Allyl cyclopentadienyl palladium II, Ar	Parallel electrodes, DC 300V	$\sigma \leq 1.7 \times 10^{4}$ Scm^{-1}, 80-100% Pd (T_s=100 °C, power=30W)	87
Allyl cyclopentadienyl palladium II, Ar	Parallel electrodes, DC 400V	σ =5.5 Scm^{-1}, 67% Pd; further O_2 plasma $\sigma = 1.2 \times 10^{4}$ Scm^{-1}, 96% Pd; further H_2 plasma $\sigma = 2.0 \times 10^{4}$ Scm^{-1}, 97% Pd	60
Allyl cyclopentadienyl palladium II, O_2	Parallel electrodes, DC 400V	$\sigma = 1.1 \times 10^{2}$ Scm^{-1}, 85% Pd, PdO films; reduction in H_2 plasma $\sigma = 4.5 \times 10^{4}$ Scm^{-1}, 100% Pd (bulk Pd, $\sigma = 9.26 \times 10^{4}$ Scm^{-1})	60
Hexamethylditin (HMDT)	RF inductively coupled, 3.9 MHz	$\sigma \sim 10^{-4}$ Scm^{-1}, presence of O_2 enhances σ because of CO/CO_2 formation with reduction of C in film, $\sigma \sim 0.8$-2.2×10^{1} Scm^{-1}	82
Tetraethyltin (TET)	RF inductively coupled, 3.9 MHz	Behave as an insulator, presence of O_2 enhances σ because of CO/CO_2 formation with reduction of C in film, $\sigma \sim 0.12$-7.9×10^{1} Scm^{-1}	82

Monomer/Gases	Reactor Configuration	Comments & Conductivities (σ)	Ref.
Tetramethyl-germanium (TMG)	RF inductively coupled, 3.9 MHz	Behave as an insulator, presence of O_2 enhances σ because of CO/CO_2 formation with reduction of C in film	82
Tetravinyltin (TVT)	RF inductively coupled, 3.9 MHz	Behave as an insulator, presence of O_2 enhances σ because of CO/CO_2 formation with reduction of C in film	82
Cu-hexafluoro-acetylacetonate, Ar/H_2	Parallel electrodes, RF 13.56 MHz	σ >$2x10^5$ Scm^{-1} for 95~100% Cu films, presence of H_2 increases metal content and σ increases, presence of O_2/Ar decreases σ to give oxidised films	83
Dimethyl(2,4-pentane-dionato)gold III (Au), Ar	Parallel electrodes, RF 13.56 MHz	σ increases as Au content increased (Au content increases as power increased), best films with σ only 2x higher than bulk gold (2.44 Scm^{-1})	88
Dimethyl(2,4-pentane-dionato)gold III (Au), O_2	Parallel electrodes, RF 13.56 MHz	Au_2O_3 films with presence of elemental Au, σ ~0.1 Scm^{-1}	88
Dimethyl(2,4-pentane-dionato)gold III (Au), O_2, H_2	Parallel electrodes, RF 13.56 MHz	σ ~$1.4x10^5$ Scm^{-1}	88
Dimethyl(2,4-pentane-dionato)gold III (Au), O_2, Ar	Parallel electrodes, RF 13.56 MHz	σ ~$2.2x10^5$ Scm^{-1}	88
Dimethyl(2,4-pentane-dionato)gold III (Au), propene copolymerization	Parallel electrodes, RF 13.56 MHz	σ ~0.1-1 Scm^{-1}, 74-93% Au	88, 89
TMT, Ar, propene	Parallel electrodes, RF 13.56 MHz	σ ~0.01→$1.1x10^4$ Scm^{-1}, 47-95% Sn	89
Dicobalto-octacarbonyl, Ar, propene	Parallel electrodes, RF 13.56 MHz	σ ~0.01→1000 Scm^{-1}, 43-78% Co	89
Nickel tetracarbonyl, Ar, propene	Parallel electrodes, RF 13.56 MHz	σ ~0.01→100 Scm^{-1}, 33-89% Ni	89
Cu, Mg, Zn, Ni phthalocyanines	Parallel electrodes, RF 13.56 MHz	σ ~10^{-10}-10^4 Scm^{-1}, dependent on process conditions especially T_S	76, 77
Diethyl zinc	RF inductively coupled, 3.9 MHz	Bluish-grey metallic films σ ~10^4 Scm^{-1}, brown-transparent films (C rich) σ ~10^0 Scm^{-1}, σ decreases as C/Zn increased	90
Tetramethyl germanium, O_2	RF inductively coupled, 13.56 MHz	Best σ =1.8 x10^{-6} Scm^{-1} (semiconducting) when C/Ge=0.2, position dependent; absence of O_2 gives insulating films	91

Monomer/Gases	Reactor Configuration	Comments & Conductivities (σ)	Ref.
$Fe(CO)_5$	RF inductively coupled, 3.9 MHz	σ position dependent, if C/Fe>15, films become insulating, $\sigma \sim 10^{-6}$-10^{-1} Scm^{-1}	92
TMT, Ar	Parallel electrodes, RF 13.56 MHz	Metallic Sn films produced by varying process parameters, $\sigma > 100$ Scm^{-1}; no depolmerization gas (eg O_2) is necessary for conduction cf ref. 82	81
Tetraethyl germanium, Ar	Parallel electrodes, RF 13.56 MHz	$\sigma \sim 10^{-7}$-10^{-4} Scm^{-1} dependent on conditions, σ increases as C/Ge decreased	93
$Cu(acac)_2$	Parallel electrodes, RF 13.56 MHz	$\sigma = 9.2 \times 10^{3}$ Scm^{-1} (100W, 10 min, T_S=200 °C)	75
$Co(acac)_2$	Parallel electrodes, RF 13.56 MHz	$\sigma = 7.5 \times 10^{0}$ Scm^{-1} (100W, 10 min, T_S=200 °C)	75
$Co(acac)_3$	Parallel electrodes, RF 13.56 MHz	$\sigma = 4.1 \times 10^{0}$ Scm^{-1} (100W, 10 min, T_S=200 °C)	75
$Fe(acac)_3$	Parallel electrodes, RF 13.56 MHz	$\sigma = 3.2 \times 10^{-2}$ Scm^{-1} (100W, 10 min, T_S=200 °C)	75
$Zn(acac)_2$	Parallel electrodes, RF 13.56 MHz	$\sigma = 1.1 \times 10^{-2}$ Scm^{-1} (100W, 10 min, T_S=200 °C)	75
$Al(acac)_3$	Parallel electrodes, RF 13.56 MHz	$\sigma = 8.2 \times 10^{-8}$ Scm^{-1} (100W, 10 min, T_S=200 °C)	75
Titanium tetraisopropoxide (TiTP)	Parallel electrodes, RF 13.56 MHz	n-type semiconductor, $\sigma \sim 10^{-8}$-10^{2} Scm^{-1} depending on deposition power	75
$Al(Me)_3$, N_2	RPECVD, microwave, 2.45 GHz	AlN films, $\sigma \sim 10^{-12}$ Scm^{-1} (porous film)	56
$Al(Me)_3$, H_2, N_2 (2:1)	RPECVD, microwave, 2.45 GHz	AlN films, $\sigma = 1.1 \times 10^{-16}$ Scm^{-1} (Ohmic-like conductor)	56
Triisobutyl aluminium, N_2, Ar	RPECVD, microwave, 2.45 GHz	σ varied from 8.7×10^{-15}-2.5×10^{-14} Scm^{-1} as T_S varied from 300-500 °C	65
$Zr(NEt_2)_4$, H_2	Parallel electrodes, RF 13.56 MHz	Insulating, $\sigma < 10^{-2}$ Scm^{-1} for T_S 573-673 K; application of self bias to substrate electrode $\sigma \sim 10^{3}$ Scm^{-1}	65
$Mo(CO)_6$, Ar, H_2	Parallel electrodes, RF 13.56 MHz	σ decreases as power decreased, best value $\sigma = 10^{4}$ Scm^{-1} at 448 K, 125W	94
$Mo(CO)_6$, Ar, O_2	Parallel electrodes, RF 13.56 MHz	Showed no conductivity	94
$Mo(CO)_6$, Ar, H_2S (2:1)	Parallel electrodes, RF 13.56 MHz	σ varied from 7×10^{-3}-3×10^{-2} Scm^{-1} (higher power gavelower σ values)	94
$Mo(CO)_6$, Ar, H_2, H_2S (10:4:1)	Parallel electrodes, RF 13.56 MHz	σ varied from 0.3-3.7 Scm^{-1}; possible formation of MoS_x	94
$Mo(CO)_6$, Ar, H_2, H_2S (20:8:1)	Parallel electrodes, RF 13.56 MHz	σ varied from 0.2-5 Scm^{-1}; possible formation of MoS_x	94
$W(CO)_6$, Ar, H_2	Parallel electrodes, RF 13.56 MHz	σ increases as power increased (metal content increases with increasing power), best value $\sigma \sim 3.3 \times 10^{4}$ Scm^{-1} (T_S=448 K); high T_S (523 K) and high power (200W) $\sigma \sim 4 \times 10^{4}$-$1 \times 10^{5}$ Scm^{-1}- possible α-W formation	94
$W(CO)_6$, Ar, O_2	Parallel electrodes, RF 13.56 MHz	Showed no conductivity	94

1.3 SUMMARY OF PROJECT AIMS

This project set out to produce novel composite films from titanium-organic precursors using a unique gaseous plasma medium, created in a glow discharge by the PACVD technique. The incorporation of titanium ceramic species embedded in a polymeric matrix may lead to films possessing useful electrical properties.

Two titanium-organic precursors were chosen because they could potentially provide the conducting ceramic phase and the organic component for the polymeric matrix. Titanium tetraisopropoxide (TiTP) was initially examined because it contains the Ti-O bond, is cheap and commercially available, is the most volatile titanium alkoxide and has already been successfully used to deposit TiO_2 films (see Chapter 3). The second precursor studied was tetrakis(dimethylamido) titanium (TMT), the simplest titanium dialkylamino precursor. This possesses an intrinsic Ti-N bond and has been the centre of much interest for depositing conducting TiN (see Chapters 6 and 7).

1.4 REFERENCES

1. Kirk-Othmer, Encylopedia of Chemical Technology, 3rd Edn., Vol. 6, John Wiley, New York, 1979.
2. T.J. Reinhart, Composites, Engineering Materials Handbook, Vol. 1, ASM International, Metals Park, Ohio, 1987.
3. M.M. Schwartz, Composite Materials Handbook, McGraw-Hill, New York, 1984.
4. R. d'Agostino, Ed., Plasma Deposition, Treatment, and Etching of Polymers, Academic Press, San Diego, 1990.
5. S. Komarneni, *J. Mater. Chem.*, **2**, 1992, 1219.
6. G.A. Ozin, *Adv. Mater.*, **4**, 1992, 612.
7. Y. Wang, N. Herron, *J. Phys. Chem.*, **95**, 1991, 525.
8. A.M. Lyons, S. Nakahara, M.A. Marcus, E.M. Pearce, J.V. Waszczak, *J. Phys. Chem.*, **95**, 1991, 1098.
9. F. Lux, *J. Mater. Sci.*, **28**, 1993, 285.
10. F.A. Cotton, G. Wilkinson, Advanced Inorganic Chemistry, 5th Edn., Wiley, New York, 1988.
11. S.R. Kurtz, R.G. Gordon, *Thin Solid Films*, **147**, 1987, 167.
12. V.P.S. Judin, *Chem. Brit.*, **29**, 1993, 503.
13. Y. Sakata, Z. Liu, H. Imamura, S. Tsuchiya, *J. Chem. Soc., Chem. Commun.*, 1991, 1392.
14. G.L Haller, D.E. Resasco, *Adv. Cat.*, **36**, 1989, 36.
15. H. Döring, K. Hashimoto, A. Fujishima, *Ber. Bunsenges. Phys. Chem.*, **96**, 1992, 620.
16. R.G. Breckenridge, W.R. Hosler, *Phys. Rev.*, **91**, 1953, 793.
17. A. Ohmori, K.-C. Park, M. Inuzuka, Y. Arata, K. Inoue, N. Iwamoto, *Thin Solid Films*, **201**, 1991, 1.
18. J.B. Torrance, P. Lacorre, C. Asavaroengchai, R.M. Metzger, *Physica C*, **182**, 1991, 610.
19. R.M. Fix, R.G. Gordon, D.M. Hoffman, *Chem. Mater.*, **2** , 1990, 235.
20. CRC Handbook of Chemistry and Physics, CRC Press, Inc., 63rd Ed., 1982-1983.
21. N.C. Saha, H.G. Tompkins, *J. Appl. Phys.*, **72**, 1992, 3072.
22. M. Wittmer, J. Noser, H. Melchoir, *J. Appl. Phys.*, **52**, 1981, 6659.
23. I. Montero, C. Jimenez, J. Perriere, *Surf. Sci.*, **251**, 1991, 1038.
24. H.Z. Wu, T.C. Chou, A. Misra, D.R. Anderson, J.K. Lambert, *Thin Solid Films*, **191**, 1990, 55.
25. B. Siemensmeyer, K. Bade, J.W. Schultze, *Ber. Bunsenges. Phys. Chem.*, **95**, 1991, 1461.

26. S.R. Kurtz, R.G. Gordon, *Thin Solid Films*, **140**, 1986, 277.
27. J.W. Coburn, *IEEE Trans Plasma Sci.*, **19**, 1991, 1048.
28. Plasma Processing of Materials-Scientific Opportunities and Technological Challenges, National Academy Press, Washington, 1991.
29. J. Thörnblom, K.-J. Roihert, *Pure Appl. Chem.*, **64**, 1992, 671.
30. S. Masuda, *Pure Appl. Chem.*, **60**, 1988, 727.
31. I. Gallimberti, *Pure Appl. Chem.*, **60**, 1988, 663.
32. W. Mohl, *Adv. Mater.*, **2**, 1990, 424.
33. J.R. Hollahan, A.T. Bell, Eds., Techniques and Applications of Plasma Chemistry, Wiley, New York, 1974.
34. B. Eliasson, U. Kogelschatz, *IEEE Trans. Plasma Sci.*, **19**, 1991, 1063.
35. H. Biederman, Y. Osada, *Adv. Polym. Sci.*, **95**, 1990, 57.
36. D.T. Clark, W.J. Feast, Eds., Polymer Surfaces, Wiley, Bath, 1978.
37. H.F. Winters, *Topics in Current Chemistry*, **94**, 1980, 71.
38. A.T. Bell, *Topics in Current Chemistry,* **94**, 1980, 44.
39. H. Suhr, *Plasma Chem. Plasma Proc.*, **9**, 1989 (Suppl), 8S.
40. J.T. Dakin, *IEEE Trans. Plasma Sci.*, **19**, 1991, 991.
41. B. Chapman, Glow Discharge Processes, John Wiley, New York, 1980.
42. J.L. Vossen, W. Kern, Eds., Thin Film Processes II, Academic Press, London, 1991.
43. H. Yasuda, Plasma Polymerization, Academic Press, London, 1985.
44. E.M. Liston, *J. Adhesion*, **30**, 1989, 199.
45. R.F. Bunshah, *IEEE Trans. Plasma Sci.*, **18**, 1991, 846.
46. H. Randhawa, *Thin Solid Films*, **196**, 1991, 329.
47. J.A. Thornton, *Thin Solid Films*, **107**, 1983, 3.
48. K.-H. Habig, *J. Vac. Sci. Technol.*, **A4**, 1986, 2832.
49. J.M. Poitevin, G. Lemperiere, J. Tardy, *Thin Solid Films*, **97**, 1982, 69.
50. G. Lemperiere, J.M. Poitevin, *Thin Solid Films*, **111**, 1984, 339.
51. Y. Igasaki, H. Mitsahashi, *Thin Solid Films*, **70,** 1980, 17.
52. H. Suhr, *New J. Chem.*, **14**, 1990, 523.
53. K.D. Karlin, Ed., Progress in Inorganic Chemistry, Vol. 41, John Wiley, New York, 1994.
54. T.P. Fehlner, Inorganometallic Chemistry, Plenum Press, New York, 1992.
55. M. Gupta, V.K. Rathi, R. Thangaraj, O.P. Agnihotri, K.S. Chari, *Thin Solid Films*, **204**, 1991, 77.
56. H. Nomura, S. Meikle, Y. Nakanishi, Y. Hatanaka, *J. Appl. Phys.*, **69**, 1991, 990.
57. A. Matsumoto, S. Meikle, Y. Nakanishi, Y. Hatanaka, *Jpn. J. Appl. Phys.*, **31**, 1992, L423.
58. R.K. Sadhir, W.J. James, R.A. Auerbach, *Thin Solid Films*, **97**, 1982, 17.
59. J.G. Eaves, PhD Thesis, University of Durham, 1986.

60. E. Feurer, H. Suhr, *Thin Solid Films*, **157**, 1988, 81.
61. Y.-W. Zhao, H. Suhr, *Appl. Phys.*, **A55**, 1992, 176.
62. E.-T. Kim, S.-G. Yoon, *Thin Solid Films*, **227**, 1993, 7.
63. K. Ebihara, S. Kanazawa, T. Ikegami, M. Shiga, *J. Appl. Phys.*, **68**, 1990, 1151.
64. W.N. Kang, Y.S. Yoon, S.S. Yom, *Supercond. Sci. Technol.*, 7, 1994, 334.
65. H. Wendel, H. Suhr, *Appl. Phys.*, **A54**, 1992, 389.
66. A. Weber, R. Nikulski, C.-P. Klages, M.E. Gross, W.L. Brown, E. Dons, R.M. Charatan, *J. Electrochem. Soc.*, **141**, 1994, 849.
67. Y. Osaka, A. Chayahara, H. Yokoyama, M. Okamoto, T. Hamada, T. Imura, M. Fujisawa, *Mater. Sci. Forum*, **54/55**, 1990, 277.
68. J. Smeets, V. Van De Bergh, J. Meneve, E. Dekenpeneer, L. De Wilde, *Thin Solid Films*, **228**, 1993, 272.
69. H. Yasuda, T. Hirotsu, *J. Appl. Polym. Sci.*, **22**, 1978, 1195.
70. A.R. Westwood, *Eur. Polym. J.*, 7, 1971, 363.
71. H. Yasuda, T. Hirotsu, *J. Appl. Polym. Sci., Polym. Chem. Ed.*, **16**, 1978, 743.
72. H. Yasuda, *Macromol. Rev.*, **16**, 1981, 199.
73. C.D. Ehrlich, J.A. Basford, *J. Vac. Sci. Technol.*, **A10**, 1992, 1.
74. E. Kay, M. Hecq, *J. Appl. Phys.*, **55**, 1984, 370.
75. Y. Kagami, K. Yamada, T. Yamauchi, J. Gong, Y. Osada, *J. Appl. Polym. Sci.: Appl. Polym. Symp.*, **46**, 1990, 289.
76. Y. Osada, A. Mizumoto, *J. Appl. Phys.*, **59**, 1986, 1776.
77. Y. Osada, A. Mizumoto, H. Tsuruta, *J. Macromol. Sci.-Chem.*, **A 24**, 1987, 403.
78. M. Gazicki, H. Yasuda, *Plasma Chem. Plasma Proc.*, **3**, 1983, 279.
79. A. Bradley, J.P. Hammes, *J. Electrochem. Soc.*, **111**, 1963, 15.
80. E. Kny, L.L. Levenson, R.A. Auerbach, *Thin Solid Films*, **85**, 1981, 23.
81. C. Oehr, H. Suhr, *Thin Solid Films*, **155**, 1987, 65.
82. R.K. Sadhir, H.E. Saunders, W.J. James, *Polymers in Electronics, ACS Symp. Ser.*, 242, 1984, 555.
83. C. Oehr, H. Suhr, *Appl. Phys.*, **A45**, 1988, 151.
84. R. Szeto, D.W. Hess, *Thin Solid Films*, **78**, 1981, 125.
85. D. Brosset, B. Ai, Y. Segui, *Appl. Phys. Lett.*, **33**, 1978, 87.
86. D.E. Carlson, *J. Electrochem. Soc.*, **122**, 1975, 1334.
87. H. Suhr, A. Etspüler, E. Feurer, H. Grünwald, C. Haag, C. Oehr, *IUPAC 7th Inter. Symp. Plasma Chem.*, Eindhoven, July 1985, A-1-5, 53.
88. E. Feurer, H. Suhr, *Appl. Phys.*, **A44**, 1987, 171.
89. H. Suhr, A. Etspüler, E. Feurer, C. Oehr, *Plasma Chem. Plasma Proc.*, **8**, 1988, 9.
90. W.J. James, P.-L. Tseng, *J. Vac. Sci. Technol.*, **A3**, 1985, 2634.
91. R.K. Sadhir, W.J. James, R.A. Auerbach, *J. Appl. Polym. Sci.: Appl. Polym. Symp.*, **38**, 1984, 99.

CHAPTER 2:
EXPERIMENTAL TECHNIQUES

2.1 INTRODUCTION

Analytical techniques used to follow PACVD can be subdivided into two categories; plasma diagnostics and surface or bulk characterization methods. Plasma diagnostic studies are useful tools for understanding plasma polymerization mechanisms because they enable monomer fragmentation processes to be determined.[1] Techniques which have been most useful for analyzing the plasma phase have been mass spectroscopy combined with gas chromatography and emission spectroscopy e.g. for organosilicon plasmas.

The amount of solid plasma polymer deposited is usually small, highly crosslinked, and insoluble in common organic solvents. Therefore sophisticated techniques are required in comparison to those needed for conventional polymers. Some of the classical and modern methods that have been used to examine plasma deposited films include, infrared (IR) and ultraviolet (UV) absorption spectroscopies, Auger electron spectroscopy (AES), X-ray photoelectron spectroscopy (XPS), secondary ion mass spectroscopy (SIMS), ion scattering spectroscopy (ISS), solid-state magic angle spinning nuclear magnetic resonance spectroscopy (MASNMR), combined pyrolysis/gas chromatography/mass spectroscopy, atomic absorption spectroscopy (AAS), elemental analysis (EA), X-ray diffraction (XRD), transmission electron microscopy (TEM), scanning electron microscopy (SEM) and atomic force microscopy (AFM).

In this work, the following techniques were used to examine the deposited film surfaces:

a) X-ray photoelectron spectroscopy (XPS)

b) Attenuated total reflection Fourier transform infrared spectroscopy (ATR-FTIR)

c) Atomic force microscopy (AFM)

The main principle of these methods and the experimental set-up used in each case throughout this work are discussed in the next sections.

2.2 X-RAY PHOTOELECTRON SPECTROSCOPY (XPS)

2.2.1 INTRODUCTION

The principle behind X-ray photoelectron spectroscopy is basically an extension of the photoelectric effect.[2] Radiation is shone onto the sample surface and on sufficient penetration into the sample, core electrons as well as valence electrons of the atoms can be ejected with certain kinetic energies (KE). If a soft (low energy) X-ray source is used, core electrons can be ejected as illustrated in Fig. 1 and the technique is known as X-ray photoelectron spectroscopy (XPS). When ultraviolet radiation is used, there is only sufficient energy to remove valence electrons; this technique is known as ultraviolet photoelectron spectroscopy (UPS). The kinetic energies, E_{kin} of the ejected electrons can be detected and can be given by the expression:[3-5]

$$E_{kin} = h\upsilon - E_b - \Phi_{sp}$$

where $h\upsilon$ is the energy of the photons, E_b is the binding energy from the atomic orbital from which the electron originated and Φ_{sp} is the spectrometer workfunction. The workfunction of a metal (in this case the spectrometer) is defined as the difference in energy between an electron at rest in the vacuum just outside the metal and an electron at the Fermi energy or level.

A singly charged atom or molecule (M) results from the ejection of a photoelectron on interaction with a photon:

$$M + h\upsilon \rightarrow M^+ + e^-$$

Conservation of linear momentum means that the much lighter electron is ejected rather than the heavier singly charged atom or molecule.

The identification of the ionization energy of a molecule with an electron in a particular molecular orbital can be approximated by Koopman's theorem: 'For a closed shell molecule the ionization energy of an electron in a particular orbital is approximately equal to the negative of the orbital energy'.[2] This ignores the fact that electrons reorganise on ionization and that they do not move independently, but rather their movements are correlated. Relativity effects on orbital energies are also overlooked.

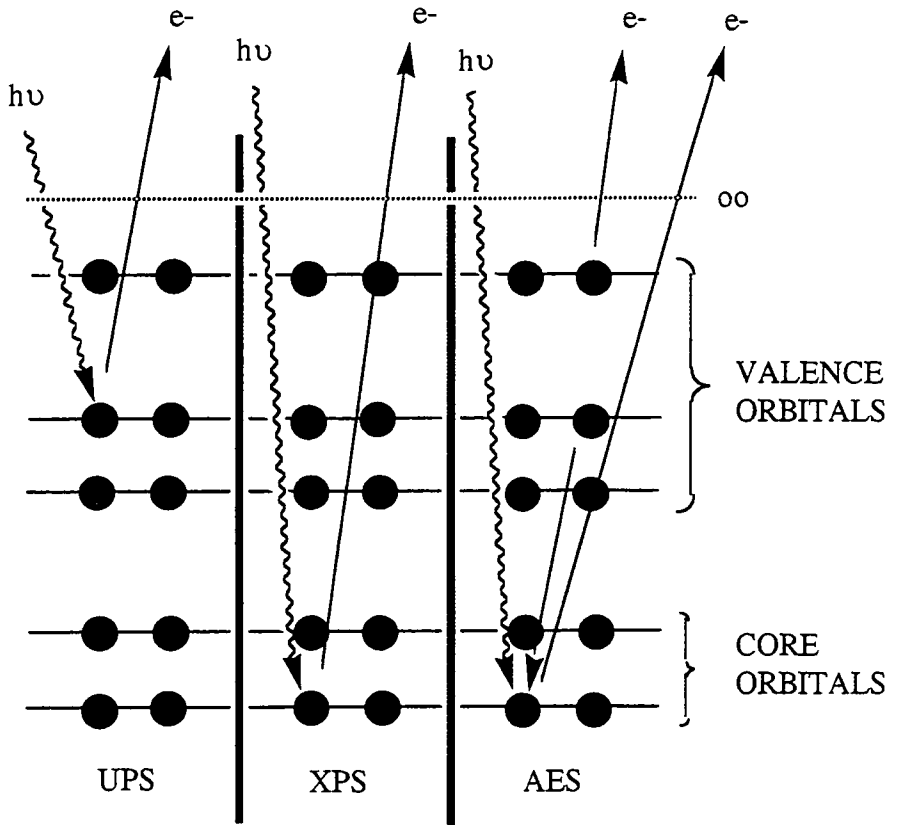

Fig. 1 Schematic of the photoelectron processes.

2.2.2 SAMPLING DEPTH

The surface sensitivity depends upon the probability that the photoelectron can escape to the surface without loss of kinetic energy.[6] The depth from which electrons emerge having undergone no inelastic collisions therefore determines the sampling depth.

Inelastic loss processes for electrons include the excitation of lattice vibrations (phonons with ~10^{-2} eV), electron-electron interactions to give collective oscillations of the electron gas (plasmons ~5-25 eV) and electron interband transitions or ionizations.

The mean free path, λ, prior to inelastic scattering will vary with its kinetic energy.[6] At low energies, the electrons are unable to excite any of the above quantised losses and their mean free paths are long, whilst at high kinetic energies the cross-sections for such processes fall and again the mean free paths are large as illustrated in Fig. 2.

In the intermediate energy range (100-1000 eV), that used in XPS, the electron escape depth is approximately linear with kinetic energy. Consequently, there is a tendency for electrons with high binding energy to be released from the shallow, near surface region (1 nm at ~100 eV to 3 nm at ~1000 eV i.e. 10 atomic monolayers).

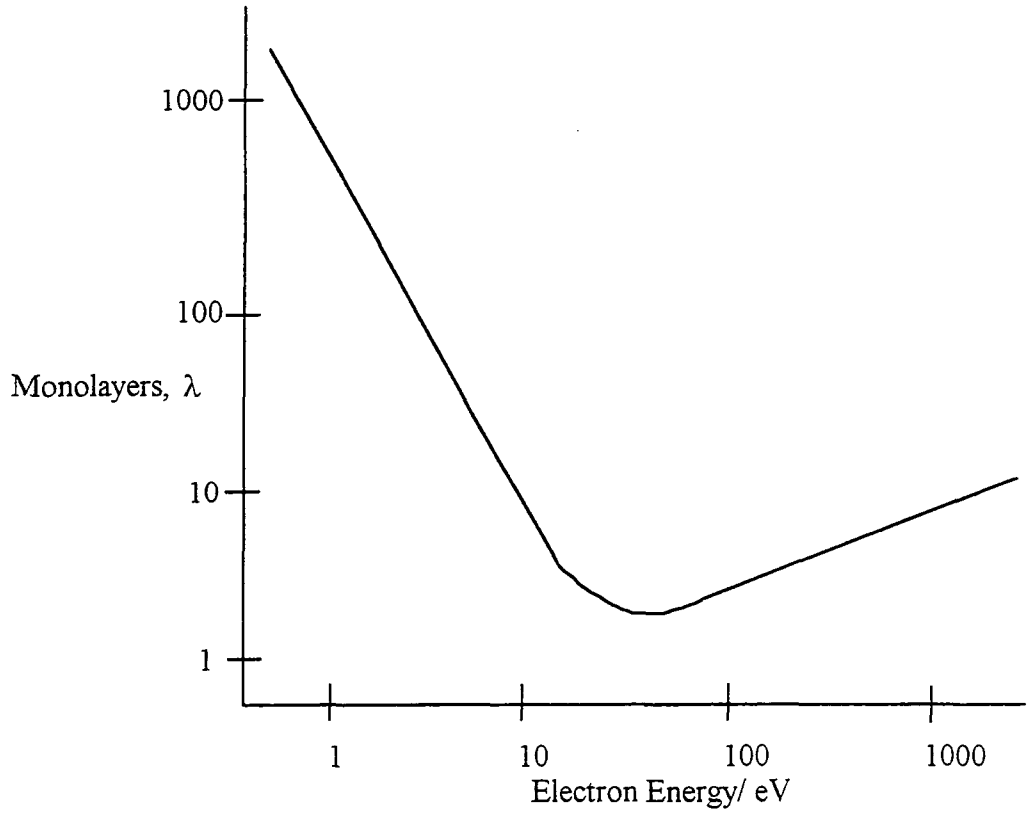

Fig. 2 Schematic of the variation of electron mean free path with kinetic energy.[3]

With reference to Fig. 3, the escape depth, d, of an electron of inelastic mean free path, λ, at a take-off angle, α, to the substrate is given by:[3]

$$d = 3\lambda\sin\alpha$$

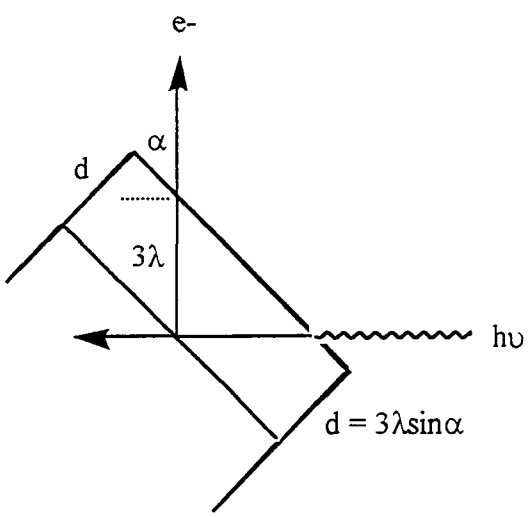

Fig. 3 Surface sensitivity enhancement by variation of the electron take-off angle.[3]

Therefore a non-destructive depth profiling method can be performed by varying the electron take-off angle.

2.2.3 INSTRUMENTATION

An excitation source is needed to irradiate the sample in order to release electrons which can then be collected by an electron energy analyser.

2.2.3.1 X-Ray Excitation Sources

A source of soft (low energy) X-rays can be used to remove core electrons and Auger and/or valence electrons may also be emitted simultaneously (see Fig. 1).[2-4] The choice of the material for the X-ray source is very important for two reasons:

(i) The line width must not limit the energy resolution required
(ii) The characteristic X-ray energy must be high enough that a sufficient range of core electrons can be ejected.

The line width will depend on the line width of hυ, since the line width of the core level is narrow and the workfunction is virtually constant. Materials with line widths less than 1.0 eV have been found to avoid the resolution limitations. Therefore commonly used sources of X-ray radiation are $MgK\alpha_{1,2}$ (1253.6 eV) and $AlK\alpha_{1,2}$ (1486.6 eV) which have line widths of 0.7eV and 0.85eV respectively. The $K\alpha_{1,2}$ indicates that an electron has been ejected, by electron impact on the Mg or Al surface, from the K (n=1, 1s) shell and the radiation is due to the energy emitted when an electron falls down from the next highest energy shell (n=2, $2p_{3/2,1/2}$) to fill the vacancy, giving an unresolved doublet.

Unmonochromatized X-ray sources not only have the principal unresolved $K\alpha_{1,2}$ doublet, but are also accompanied by lower intensity satellite lines.[2-4] Satellites arise from less likely transitions e.g. in multiply ionized atoms ($K\alpha_3$, $K\alpha_4$) and from valence band to 1s transitions ($K\beta$). As a result, weak peaks are observed to lower binding energies of the main peaks. In addition, there is also continuous background radiation called Bremsstrahlung upon which the characteristic X-ray lines are superimposed. Monochromatized X-ray sources are therefore used to cut out X-ray satellites and Bremsstrahlung.

2.2.3.2 Electron Energy Analysers

Electron analysers are of two main types: retarding potential and dispersive analysers.[3] The former relies on retarding electrons (of different energies) by application of a retarding potential prior to electron detection. A commonly used dispersive analyser used for XPS is the concentric hemispherical analyser, as illustrated in Fig. 4, where the electrons follow the median equipotential surface between two concentric hemispheres when an electric potential is applied between them. Such an analyser has been used in this work. The electron energy, E_0, is given by:

$$E_0 = e\Delta V/[(R_2/R_1)-(R_1/R_2)]$$

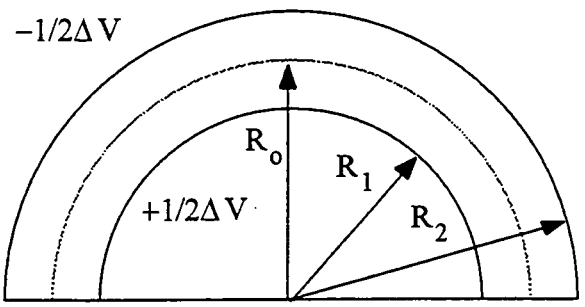

Fig. 4 The concentric hemispherical analyser.[3]

The electron output from the electron energy analysers is typically in the range between 10^{-13}-10^{-19} A. Magnification of the electron signal and detection is carried out by an electron multiplier, either a conventional dynode or a continuous channeltron.[3] The latter electron multiplier has been used in this work. The multiplier output is normally taken through an amplifier/discriminator/rate meter system and the spectrum recorded is the number of electrons per unit time as a function of either the kinetic energy or binding energy. For weak signals the spectra can be time averaged using repeated scans fed into a multichannel analyser.

2.2.4 SPECTRAL INTERPRETATION FOR XPS

2.2.4.1 Core Level

Non equivalent atoms of the same element in a solid, for example different oxidation states or molecular environments, give rise to peaks with measurable binding energy differences or chemical shifts.[3] These chemical shifts can be used for functional group identification and semiquantitative elemental analysis. Core level peaks can also be split

if photoionization occurs from an orbital which has an orbital angular momentum quantum number (l) greater than zero (i.e. p, d and f), for example the titanium Ti(2p) peak is split into two peaks, $Ti(2p_{3/2})$ and $Ti(2p_{1/2})$. The relative peak intensities are determined by the ratio of their respective degeneracies (2j+1).

2.2.4.2 Valence Level

The binding energies of the valence electrons lie typically in the range of 0-20 eV and are therefore also emitted when samples are irradiated with X-rays.[3] UPS studies are typically used to study the valence band structure.

Valence electrons are subjected to an increase in nuclear charge on loss of a photoelectron from the core.[3,5] This will give rise to substantial reorganisation of valence electrons known as relaxation which can involve the excitation of one of them to a higher unfilled level i.e. shake-up. The energy required for this transition is not available for the primary photoelectron and so a shake-up satellite is observed on the low KE side of the photoelectron peak. This can occur, for example, in unsaturated compounds for a π-π^* transition.

Instead of excitation of a valence electron to a higher unfilled level during a shake-up, a valence electron can be excited to the vacuum level i.e. ionization occurs. This gives rise to a shake-off satellite.

2.2.5 CHARACTERIZATION OF PLASMA POLYMERS BY XPS

XPS has become a routine technique for examining plasma polymer films because it gives information on the top surface of the deposited layer (~20-50 Å).[7] This means that the elimination of signal contributions from the substrate which can otherwise greatly hinder many other physical analytical methods when applied to ultrathin films can be achieved.[1,7] The information available from this technique provides semiquantative elemental analysis, functional group identification (depending on electronegativity of the nearest neighbouring atoms), and depth profiling.[1] The use of correction or sensitivity factors provides the elemental ratio or composition at the surface.

The elemental compositions of the deposited plasma polymer films in this work have been determined by XPS, though functional group identification has not always been possible due to overlapping chemical environments.

2.2.6 EXPERIMENTAL XPS CONFIGURATION

X-ray photoelectron spectra were accumulated on a Kratos ES300 surface analysis instrument operating in the fixed retarding ratio (FRR, 22:1) analyser mode. The base pressure was maintained at $1x10^{-9}$ Torr by an Alcatel turbomolecular pump backed by an Edwards mechanical rotary pump, and a Varian ion pump. Magnesium Kα X-rays were used as the photoexcitation source operating at an anode voltage of 12 kV and an emission current of 10 mA. Photoelectrons were collected at a take-off angle of 30° to the surface normal and analysed using a concentric hemispherical analyser. Sample insertion was performed by means of a ball valve pumped by an Edwards mechanical rotary pump (base pressure $5x10^{-2}$ Torr). Instrument performance was calibrated with respect to the gold $4f_{7/2}$ level at 83.8 eV with a full width at half maximum (FWHM) of 1.2 eV. No radiation damage was observed during the typical time scale involved in these experiments. An IBM PC computer was used for data accumulation and component peak analysis (assuming linear background subtraction and Gaussian fits with fixed FWHM). All binding energies are referenced to the hydrocarbon ($\underline{C}_xH_y$) component at 285.0 eV.[8] Instrumentally determined sensitivity factors for unit stoichiometry of C(1s) : O(1s) : N(1s) : Si(2p) : Ti(2p) were taken as equaling 1.00 : 0.55 : 0.74 : 1.02 : 0.36 respectively. The Ti(2p) value above was calculated using the total area under both the $Ti(2p_{3/2})$ and $Ti(2p_{1/2})$ peaks.

2.2.7 CHARACTERIZATION OF PLASMA POLYMERS BY ARGON ION SPUTTER DEPTH PROFILING

Determination of a compositional depth profile can be achieved by angle resolved XPS studies.[3] An alternative method involves the destructive argon ion sputter method where the surface is bombarded by argon ions to remove the outer surface. However chemical environments and elemental compositions in the bulk of the sputtered films need to be interpreted with caution since ion-induced effects, for example preferential sputtering, sample charging etc., are more than likely to take place with this technique.

2.2.8 EXPERIMENTAL ARGON ION SPUTTER DEPTH PROFILES

Argon ion sputter depth profiles were performed on a Vacuum Generators CLAM 100 surface analysis instrument. The base pressure of $5x10^{-9}$ Torr was maintained by an oil diffusion pump backed by an Edwards mechanical rotary pump. Magnesium Kα X-rays were used as the photoexcitation source operating at an anode voltage of 12 kV and an emission current of 20 mA. The concentric hemispherical analyser was operated in the

constant analyser energy mode (CAE) at a pass energy of 50 eV and an electron take-off angle of 20 ° to the surface normal. Sample insertion was performed by means of a modified gate valve pumped by an Edwards mechanical rotary pump (base pressure $1x10^{-3}$ Torr). Argon ion sputtering was carried out using a cold cathode ion gun (Vacumm Generators AG21) operating at a pressure of $2x10^{-6}$ mbar of argon (BOC, research grade), 3 keV beam energy and a constant ion current of 1 μA. An IBM PC computer was used for data accumulation and component peak analysis. All binding energies are referenced to the hydrocarbon ($\underline{C}_xH_y$) component at 285.0 eV.[8]

2.3 ATTENUATED TOTAL REFLECTION FOURIER TRANSFORM INFRARED SPECTROSCOPY (ATR-FTIR)

2.3.1 INTRODUCTION

Infrared (IR) spectroscopy is based upon the excitation of molecular vibrations by absorption of photons in the spectral region of 0.75-2.5 μm (near-IR), 2.5-50 μm (medium-IR) and 50-1000 μm (far-IR).[9] Of greatest practical use for the chemist is the limited portion between 4000-400 cm^{-1} (medium-IR), though there has been some interest in both the near- and far-IR regions.[10]

The most important selection rule for molecular vibration is the change in the dipole moment during excitation. The alternating electric field, produced by the changing charge distribution accompanying a vibration, couples the molecule vibration with the oscillating electric field of the electromagnetic radiation. Totally symmetric vibrations, e.g. the symmetrical vibration of linear CO_2, are IR inactive since this vibration produces no change in the dipole moment of the molecule. Strong IR absorptions are displayed by polar groups which have a large dipole moment in the ground state such as a carbonyl group.

2.3.2 THE BASIC THEORY OF ATR-FTIR

The ATR technique is commonly used for obtaining absorption spectra of thin films and opaque materials.[2] A sample[9,11-13] of refractive index, n_2, is placed in direct contact with a material of refractive index, n_1, where $n_1 > n_2$ (see Fig. 5). This material of n_1 is usually known as the internal reflection element (IRE) and typically comes in the form of a block and/or crystal. The IRE needs to be transparent to infrared (IR) radiation.

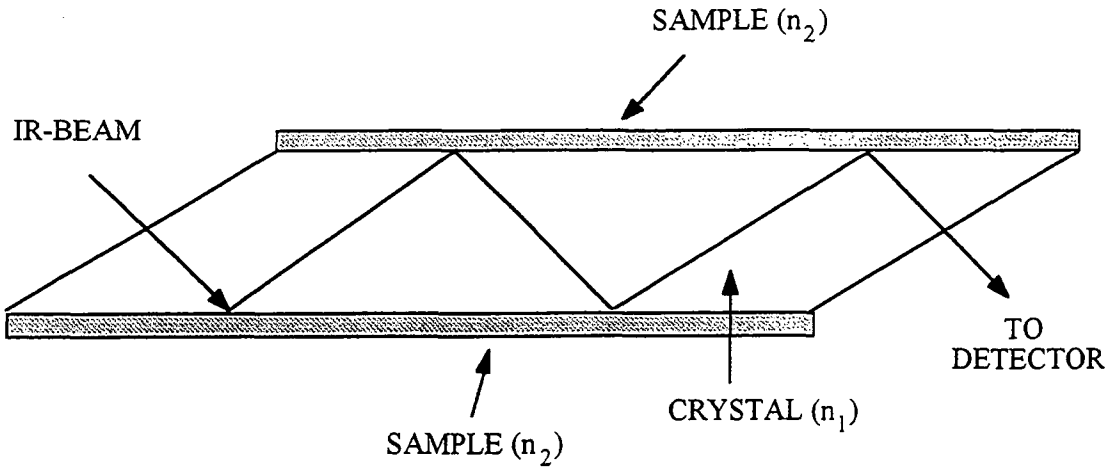

Fig. 5 Multiple internal reflections.

When IR radiation propagates through the optically more dense crystal (n_1), internal reflection occurs at the interface with the optically more rare sample (n_2), when the angle of incidence, Θ, exceeds a certain critical angle,[13] Θ_c, as illustrated in Fig. 6. The critical angle may be defined by:

$$\Theta_c = \sin^{-1} n_{21}$$

where $n_{21} = n_2/n_1$.

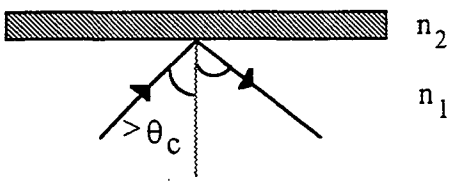

Fig. 6 Total reflection of radiation in a medium of refractive index n_1 by a thin film of refractive index n_2, where $n_1 > n_2$.

The incident and reflected beams coherently interfere at the interface and form a standing wave normal to the totally reflecting interface. The standing wave does not extend into the sample, but a non-propagating evanescent wave will be present in the sample.[9,13] As a result, absorption spectra can be recorded.

2.3.3 DEPTH OF PENETRATION

The depth of penetration, d_p,[9,13] is defined as the distance required for the electric field strength of the evanescent wave to reach 1/e of its initial value at the interface and can be expressed by:

$$d_p = \frac{\lambda}{2\pi\sqrt{\sin^2\Theta - \frac{n_2}{n_1}}}$$

where λ is the wavelength and Θ is the angle of reflection. An estimate[12] for the order of magnitude for the depth of penetration is $\lambda/10$ (10^{-6} to 10^{-5} m), shown in Fig. 7, which is about 1000 to 10000 times greater than the value estimated in XPS. It should be pointed out that this assumes the sample is non-absorbing, though in reality the sample is absorbing otherwise no measurements can be made (i.e. the evanescent field interacts with the sample and energy will be lost on total reflection).[13]

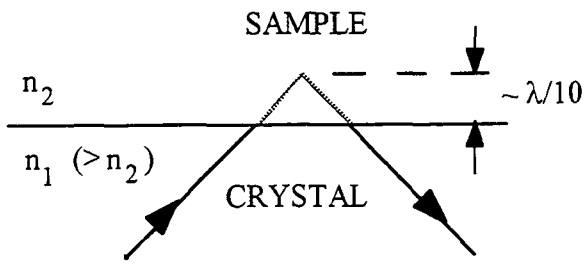

Fig. 7 Single pass internal reflection and depth of penetration.

2.3.4 SUMMARY

ATR has been used for three main types of surface studies: surface identification, surface modification and surface adsorption.[13] Many different systems have been examined from polymers, biological materials, Langmuir-Blodgett films and semiconductors. Depth profiling and orientation studies have been quite common areas of interest amongst the above systems.

To conclude, the following points summarize the practical considerations in ATR:

1) To obtain high quality spectra, good and reproducible contact between the sample and the IRE is a necessity, which might require careful cleaning of the IRE. Precise alignment of the system is also required for good spectra.

2) Multiple reflections enhance the spectral contrast by increasing the pathlength.

3) The angle of incidence and the type of IRE used are the major controlling operating factors:

   a) As Θ approaches Θ_c, d_p increases. Therefore various depths can be looked at by varying Θ.

b) As Θ approaches the grazing angle, the number of reflections, the spectral contrast and d_p decrease.

c) The area sampled increases as Θ increases.

d) Non-normal incidence of radiation requires refraction corrections.

e) d_p increases as n_{21} approaches 1.

f) By increasing n_1 of the IRE, thinner surface layers can be sampled.

g) If n_{21} decreases, the spectral contrast decreases as well as d_p. Therefore there is a balance between thinner surface layers being sampled and signal intensity.

2.3.5 CHARACTERIZATION OF PLASMA POLYMERS BY ATR-FTIR

IR spectroscopy is a useful tool for functional group identification of plasma polymers and can be performed either in the transmission or reflection modes (ATR).[1,7] The latter mode has been used in this work. IR can also complement XPS by indicating qualitative information on the presence of functional groups whilst XPS provides a semiquantitative measure of their concentrations. Broad peaks (on comparison to the monomers) may be observed in the spectra due to overlapping environments and the high crosslink densities typically found in plasma polymers.

2.3.6 EXPERIMENTAL ATR-FTIR CONFIGURATION

Infrared spectra were recorded on a FTIR Mattson Polaris instrument. The transmission analysis mode was used for obtaining a reference spectrum of TMT and bulk TiO_2 (Degussa P25) mixed with dry KBr. Coated polyethylene films were mounted onto a Specac variable angle attenuated total reflection (ATR) cell fitted with a KRS-5 crystal. Reference spectra of the clean KRS-5 crystal were acquired in air prior to each sample run. An incident beam angle of 45° resulted in 14 internal reflections.[14] Typically, 100 scans were acquired at a resolution of 4 cm^{-1}.

2.4 ATOMIC FORCE MICROSCOPY (AFM)

2.4.1 INTRODUCTION

The atomic force microscope, invented in 1986 by Binnig, Quate and Gerber,[15] can be considered a hybrid of the scanning tunnelling microscope and the stylus profilometer. Both scanning tunnelling microscopy (STM) and stylus profilometry (SP) scan a tip across a surface to generate three-dimensional images. STM can be routinely used to give atomic resolution, but its main limitation is that it requires conducting samples. The SP technique is limited by the tip size (radius of ~1 μm) and loading force (10^{-2}-10^{-5} N) resulting in possible plastic deformation of the sample.

Atomic force microscopy (AFM) has been developed to try to overcome the above such limitations. No tunnelling current is required so both conducting and non-conducting samples can be scanned. Neither light nor electrons are used to probe the surface, so the resolution of AFM is independent of the wavelength of light or the electrons. AFM overcomes the plastic deformation problems of SP by using a sharp tip giving reduced forces between itself and the sample surface, and makes possible routine force measurements of 10^{-8}-10^{-12} N.[16]

2.4.2 BASIC THEORY

As mentioned above, the atomic force microscope involves scanning a sharp tip,[15] typically made of silicon, SiO_2 or Si_3N_4,[17] across a surface and measuring indirectly the interaction force created between the proximity of the tip and the sample surface. These forces can be van der Waals, electrostatic, magnetic, capillary, ionic repulsion or frictional in nature.[17] The sharp tip is attached to a cantilever-type spring, whose deflection, Δz, is measured allowing the surface forces, F, to be determined along a scan according to Hooke's law:

$$F = k\Delta z$$

where k is the spring constant. As the sample is scanned in x and y, a z-feedback circuit connected to a sample piezoelectric ceramic can be used to control the displacement of the sample in the z direction (normal to the surface) so as to maintain a constant force against the cantilever.[18] Typical spring constants are between 0.001 to 100 Nm^{-1} and displacements from microns to ≈0.1 Å are measured by the deflection sensor[17] (see section 2.4.4). Typical forces between sample and tip lie in the range 10^{-11} to 10^{-6} N. This can be compared to the interaction between two covalently bonded atoms of

10^{-9} N at separations of ≈Å. Consequently it is possible to achieve non-destructive atomic resolution with such small forces.

2.4.3 MODES OF OPERATION

There are three modes which describe the behaviour of the tip with respect to the sample; contact mode, non-contact mode and the very new tapping mode. The first and most common imaging method is the contact mode.

2.4.3.1 Contact Mode

When the tip is at separations in the order of Å from the surface,[17] the tip is effectively in contact with the sample. Ionic repulsion forces of ~10^{-9} N between the tip and the sample surface allows high surface topographical resolution. The force is set by pushing the cantilever against the sample surface with a piezoelectric positioning element.[19] Under the best conditions,[17] atomic resolution can be achieved.

Since the relative humidity of ambient air in most laboratories is typically 30-50 %,[18] physisorbed or chemisorbed water (of thickness of ~9 nm) is commonly found on the sample surface. Consequently a meniscus forms around the tip and capillary forces strongly attract the tip to the surface. High resolution imaging can be lost since the forces in the contact region become so large that the outermost tip atoms are removed resulting in multiple tip imaging.[17] Plastic deformation can also arise on soft samples if large forces occur. Several methods have been used to avoid such sample or tip damage:

(i) Retracting the tip,[16] compensating the attractive forces by the cantilever deflection;
(ii) Immersing the sample in liquids[16,18] to minimize the capillary forces or
(iii) Running the samples in a vacuum or in a chamber of dry nitrogen where capillary forces are absent.[16,18]

2.4.3.2 Non-Contact Mode

The non-contact mode has been developed to examine soft samples where tip contact could change the topography.[19] The tip does not remain static but oscillates with a small amplitude (e.g. 5 nm) near the sample surface at a tip-surface distance of

50-150 Å. The tip-surface spacing is controlled by monitoring the resonant frequency of the cantilever which depends upon the forces between the tip and surface. As a result, information on surface topography, charge distribution, magnetic distribution and liquid film distribution can acquired.[17]

However the main disadvantage is that at small tip-surface distances, the oscillation amplitude can be affected by short range van der Waals forces and the tip becomes captured by the surface liquid layer severely degrading the image quality.[20] The tip then has to be set free to resume its oscillations. Also the tip-to-sample distance, typically 5-10 nm, defines the lateral resolution.

2.4.3.3 TappingMode™

Digital Instruments have developed the TappingMode™ to overcome the limitations of the non-contact mode.[20] The cantilever vibrates with a larger amplitude than in the non-contact mode. Cantilever damping occurs on contact of the tip with the surface water layer and sample surface, though the larger oscillation gives sufficient energy for the cantilever to overcome the surface tension of the water layer. Estimated applied forces to the surface are between 0.1-1 nN which is significantly lower than the force applied in the contact mode. The lateral resolution is comparable to the contact mode because the high vibration frequencies allow the tip to contact the sample surface many times before it translates laterally by one tip diameter.

2.4.4 DEFLECTION SENSOR

The deflection or displacement, Δz, of the cantilever allows the force, F, to be determined according to Hooke's law. Sensitive means are required therefore to measure the small deflections. One such technique is that of beam deflection which is the basis of the microscope used in this work.

A laser beam is focused onto the back of the cantilever which is usually smooth enough to reflect the light.[17] The reflected light is then reflected off a mirror and onto a position sensitive detector (PSD), a two-segmented photodiode, which is used to monitor the reflected beam. The difference between the intensity from the upper and lower halves of the diode divided by the the total intensity gives a direct measure of the lever deflection. Strong light has to be omitted so the microscope must be covered.

2.4.5 CHARACTERIZATION OF PLASMA POLYMERS BY AFM

Traditionally the surface morphologies of plasma polymers have been observed by TEM and SEM.[1,7] However wth the recent development of AFM, there is now an opportunity for a quick, non-destructive method of examining plasma polymers using the non-contact mode and/or TappingMode™. In addition, the samples do not have to be conducting as required for STM. Currently there is little recorded literature of examination of plasma polymers by AFM,[21] though there lies great potential in understanding whether gas phase or surface reactions dominate during the deposition process.

2.4.6 EXPERIMENTAL AFM CONFIGURATION

A Digital Instruments Nanoscope III atomic force microsope was used to examine the topographical nature of the deposited films. All the AFM images were acquired in air using the TappingMode™ as described above, and are presented as unfiltered data. The cantilever tip was made from silicon nitride which scanned an area of 500 x 500 nm at a scan rate of either 3.052 Hz or 5.085 Hz.

2.5 REFERENCES

1. R. d'Agostino, Ed., Plasma Deposition, Treatment, and Etching of Polymers, Academic Press, San Diego, 1990.
2. J.M. Hollas, Modern Spectroscopy, John Wiley, Chichester, 1990.
3. D. Briggs, M.P. Seah, Eds., Practical Surface Analysis, John Wiley, Chichester, 1990.
4. G. Ertl, J. Kuppers, Low Energy Electrons and Surface Chemistry, VCH, Weinheim, 1985.
5. C.D. Wagner, W.M. Riggs, L.E. Davis, J.F. Moulder, G.E. Muilenberg, Eds., Handbook of X-Ray Photoelectron Spectroscopy, Perkin-Elmer Corp., Eden Prairie, MN, 1979.
6. M. Prutton, Surface Physics, O. U. P., Oxford, 1985.
7. H. Yasuda, Plasma Polymerization, Academic Press, London, 1985.
8. G. Johansson, J. Hedman, A. Berndtsson, M. Klasson, R. Nilsson, *J. Electron Spectr.*, **2**, 1973, 295.
9. N.J. Harrick, Internal Reflection Spectroscopy, John Wiley, New York, 1967.
10. R.M. Silverstein, G.C. Bassler, T.C. Morrill, Spectrometric Identification of Organic Compounds, 4th Edn., John Wiley, New York, 1981.
11. J.R. Durig, Ed., Vibrational Spectra and Structure, A Series of Advances, Vol. 18, Elsevier, Amsterdam, 1990.
12. C.N. Banwell, Fundamentals of Molecular Spectroscopy, 3rd Edn., McGraw-Hill, London, 1983.
13. F.M. Mirabella, Jr., *Applied Spectroscopy Reviews*, **21**, 1985, 45.
14. Data obtained from the catalogue by Specac Ltd.,'Sampling Techniques for Infrared Analysis'.
15. G. Binnig, C.F. Quate, C. Gerber, *Phys. Rev. Lett.*, **56**, 1986, 930.
16. S.M. Hues, R.J. Colton, E. Meyer, H.-J. Güntherodt, *MRS Bull.*, **18**, 1993, 41.
17. E. Meyer, *Prog. Surf. Sci.*, **41**, 1992, 3.
18. N.A. Burnham, R.J. Colton, H.M. Pollock, *J. Vac. Sci. Technol.*, **A9**, 1991, 2548.
19. C.F. Quate, *Surf. Sci.*, **299/300**, 1994, 980.
20. Nanoscope Optical Viewing System Manual, Digital Instruments, Inc., Santa Barbra.
21. M. Tazaki, H. Aizawa, T. Homma, *Chem. Letts.*, 1994, 1905.

CHAPTER 3:
PLASMA ASSISTED CHEMICAL VAPOUR DEPOSITION OF TITANIUM DIOXIDE/POLYMER FILMS FROM TITANIUM TETRAISOPROPOXIDE

3.1 INTRODUCTION

Because the oxides of titanium have interesting properties (see Chapter 1) this project began by attempting to deposit thin titanium oxide/polymer composite films. This chapter focuses on the deposition of titanium dioxide (TiO_2) films, since this oxide possesses the most common oxidation state of titanium.[1]

3.1.1 REVIEW OF TITANIUM DIOXIDE FORMATION

There are a variety of techniques available for the formation of TiO_2. These include thermal oxidation of titanium,[2] sol-gel,[3] ion assisted deposition (IAD),[4] thermal hydrolysis[1,5-9], dip coating[10], reactive ion plating,[10] and reactive sputtering.[11,12] However in addition, non-plasma CVD and PACVD techniques have successfully been used to deposit TiO_2, particularly from titanium tetrachloride ($TiCl_4$) or titanium alkoxide ($Ti[OR]_4$) precursors. A survey of these two latter techniques is presented below.

3.1.1.1 $TiCl_4$ Precursor

(a) Non-Plasma Assisted CVD

Thermal studies of $TiCl_4$ in the presence of oxygen have produced rutile films at high oxygen partial pressures and at temperatures between 400 °C and 1050 °C on silicon and sapphire substrates.[13] Haas[2] examined the structural properties of TiO_2 deposited onto glass and rocksalt substrates from $TiCl_4$ and water vapour at temperatures between 200 °C and 300 °C. Below 280 °C, the films were amorphous, but post deposition annealing above 300 °C gave anatase and above 900 °C, rutile was formed.

(b) Plasma Assisted CVD

An alternative approach to thermal CVD is to use low temperature plasma enhanced/assisted chemical vapour deposition (PECVD/PACVD).[14-16] This method is

based on the low temperature breakdown of reactant species in the vicinity of an electrical glow discharge, which can subsequently lead to the deposition of desirable solid products. Such a non-isqthermal plasma may be regarded as being a partially ionized gas consisting of electrons, ions, metastables, neutrals, and photons.[17] Inherent electron temperatures are orders of magnitude greater than the corresponding temperature for any accompanying neutrals, ions, and metastables. It therefore becomes feasible for chemical reactions to proceed at near ambient temperatures whereas the analogous thermally activated reactions require far higher temperatures. For example, $TiCl_4$ and O_2 have been mainly used as the reactant gases for making TiO_2 films via this route.[18,19] It was found that below 300 °C amorphous films were deposited on glass substrates, whereas above 600 °C, rutile was formed. In addition larger crystallites were observed in contrast to those deposited by CVD under the same deposition conditions. This was thought to result from the high energy neutral species and ion bombardment from the plasma. However $TiCl_4$ is known to be corrosive, highly toxic and, in addition, the final TiO_2 film may suffer from chlorine contamination.

3.1.1.2 Alkoxide Precursors

Attempts to alleviate the problems associated with films formed from $TiCl_4$ have tended to use titanium alkoxides as the preferred alternative precursors. The alkoxides are generally non-corrosive and can be stored indefinitely in a moisture-free environment.[20] Since the Ti-O bond is already present in such compounds, lower deposition temperatures are expected.[21] Titanium tetraisopropoxide ($Ti[OCH(CH_3)_2]_4$) (TiTP) has most commonly been used since with a boiling point of 59 °C at 1 Torr, it is the most volatile of the readily available titanium alkoxides.[20] Studies using titanium tetraethoxide ($Ti[OCHCH_3]_4$) (TiTE) have however been carried out.[22-24]

(a) Non-Plasma Assisted CVD

The deposition conditions have been shown to have significant effects on the physical and chemical properties of the deposited films, as well as influencing the film growth rates. Where possible, comparisons between the different systems used are discussed, though this is not always feasible due to the great variety of deposition conditions encountered. In some cases, workers have proposed mechanisms to explain the observed decomposition byproducts and comparisons are discussed where appropriate.

Most non-plasma assisted CVD methods using TiTP have been carried out, using a carrier gas, in the presence of oxygen and/or water.[5-7,9,22,25-29] Growth rates have been improved by increasing the oxygen flow rate,[9,25] limited addition of water vapour[7,9] and elevated vapour[9] and substrate temperatures.[5,9,22,27] Carbon contamination[24] has been found in TiO_2 films deposited from TiTE at a substrate temperature of 308 °C, though the higher thermal energy supplied at 500 °C was sufficient to eliminate the carbon as gaseous CO and CO_2. Alternatively, increasing the amount of oxygen in the system gave similar results. In contrast, no significant carbon contamination[5] was found in films deposited by atomic layer epitaxy (ALE) using TiTP and water at substrate temperatures as low as 150 °C.

Deposition temperatures and post deposition annealing have been commonly shown to have important implications on the structure and crystallinity of TiO_2 deposited films. Properties such as etch rate (and hence film density), refractive index and dielectric constant have been shown to depend on the film structure. It has generally been observed by X-ray diffraction (XRD) that amorphous films are deposited below 300-400 °C.[5,7,9,26] At higher deposition temperatures, films tend to become more crystalline in form. For example, Takahashi *et al.*[22] observed anatase between 400-500 °C, but with an increasing degree of crystalline rutile content as the temperature was increased. A maximum rutile content was observed at 500°C and similarly on increasing film thickness (i.e. on increasing the deposition time). Film thicknesses greater than 10-15 μm gave only crystalline rutile films due to possible epitaxial growth of dendritic rutile crystals which completely covered the columnar anatase crystals. Similarly amorphous TiO_2 films deposited by hydrolytic CVD at 150 °C showed anatase character on annealing at 350 °C.[6] Films annealed at 700 °C consisted of an anatase-rutile mixture, whilst at 1000 °C, only rutile character was observed.

There do exist exceptions however. For example anatase films deposited between 300-350 °C were surprisingly stable since no change to rutile was observed on annealing at 900 °C for 3 hr in dry oxygen,[27] and anatase-amorphous films grown by ALE using TiTP and water at 250 °C and then annealed at 480 °C for 6 hr showed little change in the extent of crystallization.[29] This may be explained by high density films retarding further ordering.[29]

Low density films characteristically possess voids[6] into which water can diffuse.[29] The etch rate, dependent on film density,[7] can be reduced by higher deposition temperatures,[7,25] post deposition annealing,[6,27] control of added water,[7] and absence of oxygen.[25] Therefore, the increase of the refractive index,[7,25] the dielectric constant,[27] the leakage current,[27] and interface trap density[27] are generally attributed to crystallization and densification.

There are only a few reported studies devoted to the deposition of TiO_2 from TiTP (i.e. in the absence of any additional co-reactants).[21,25,30-32] Yokozawa *et al.*[25] found that the activation energy to be 150 $kJmol^{-1}$ at temperatures less than 600 °C in the absence of oxygen which decreased to approximately 27 $kJmol^{-1}$ when oxygen was added to the system (regardless of the oxygen content in the range 5-60 %). However Takahashi *et al.*[22] found that the deposition rate was independent of the oxygen content concentration over the range 0-75 % under similar pressure conditions at 500 °C. Propene and a small amount of acetone were the only organic byproducts observed.

Siefering and Griffin have proposed a three step mechanism for film growth:[21] (i) bimolecular collisional activation of TiTP in the gas phase; (ii) adsorption of the activated species on the surface and (iii) decomposition of the adsorbed species. At low TiTP vapour pressures and/or at high substrate temperatures, the growth rate was second order with respect to the TiTP with an activation energy of 35 $kJmol^{-1}$. The rate limiting step was considered to be the gas phase bimolecular collisional activation of TiTP and though the activated species were not identified, the temperature programmed desorption study indicated that loss of one or more alkoxide groups in the form of acetone may be involved. At low temperatures and with high TiTP pressures, the growth rate was zero order with respect to the TiTP with an activation energy of 150 $kJmol^{-1}$ attributed to a surface reaction limited process.

Chen and Derking also reported that the TiTP pressure and decomposition temperature were important parameters.[30] At a TiTP pressure of $2.16x10^{-3}$ mbar, the deposition rate was slow due to limited thermal activation below 325 °C. Between 325-400 °C, the growth rate rapidly increased with temperature, characteristic of 'kinetically controlled decomposition', where the surface decomposition of the precursor is rate limiting. The activation energy was calculated to be 101 ± 14 $kJmol^{-1}$. Above 400 °C, a constant growth rate was found on further increase of deposition temperature. It was proposed that the surface reaction on the substrates was so fast that the TiTP mass transfer from the gas phase to the substrate became rate limiting; this is known as 'mass-transfer-controlled' deposition. At a deposition temperature of 360 °C and low TiTP pressure ($<9x10^{-4}$ mbar), the growth rate was 1.35 with respect to TiTP and near-zero at higher TiTP pressures, giving similar results to that of Siefering and Griffin.[21]

Wu *et al.*[31] have used lower pressures (~10^{-7} Torr) to follow the surface mediated decomposition of TiTP using temperature programmed desorption studies (TPDS) and reactive scattering measurements (RSM). Film growth was initiated at approximately 180 °C in agreement with Siefering and Griffin.[21] The main decomposition products detected below 400 °C were isopropyl alcohol, acetone and propene, whereas at higher temperatures, propene and water were the dominant species. In the former case, it was

proposed that the rate limiting step was the decomposition of adsorbed intermediates and an activation energy of about 85 $kJmol^{-1}$ was determined using a first order fit with respect to the TiTP from the RSM. Above 400 °C, the surface coverage was considered to become significant. Adsorbed intermediates on the surface were reduced resulting in a greater extent of surface dehydroxylation and hence a greater decomposition to propene and water. Therefore the rate limiting step was proposed to be the replenishment of surface intermediates.

Fictorie *et al.*[32] carried out similar experiments to that of Wu *et al.*,[31] but used single rutile crystals rather than polycrystalline TiO_2 substrates. Comparable results for the activation energy from TPDS experiments were found. Two parallel pathways were proposed for the formation of TiO_2. The first pathway is favoured by higher temperatures (380-430 °C) where propene and water are formed in agreement with Wu *et al.*,[31] with lower surface coverages favouring dehydration. Such a process involves a two-step reaction via a surface hydroxyl (see Scheme 1(a)), where an adsorbed isopropoxide loses a hydrogen atom on an adjacent surface oxygen to produce propene:

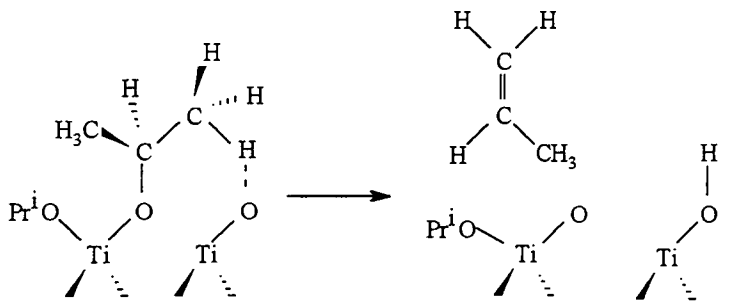

Scheme 1(a)

The hydroxyl group can then react with another isopropoxide ligand to form another propene molecule and water (see Scheme 1(b)).

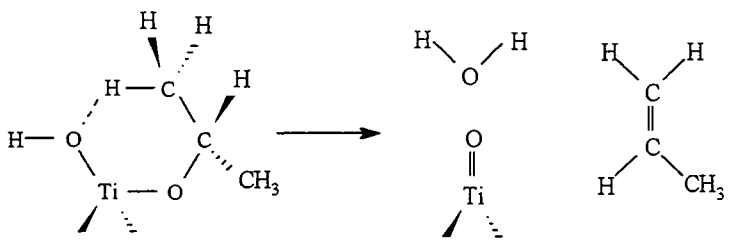

Scheme 1(b)

At lower temperatures (280-380 °C), a possible transition state consisting of a 6-membered ring (see Scheme 2) may form where a basic oxygen atom on one of the isopropoxide ligands abstracts a terminal hydrogen on another isopropoxide ligand to give propene and isopropyl alcohol:

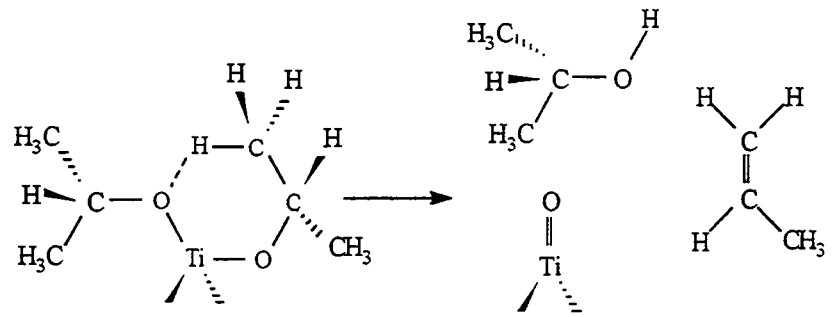

Scheme 2

In comparison to Wu *et al.*,[31] the higher temperature required to form acetone and the lower activation energy determined by RSM were explained by Fictorie *et al.* by the greater number of defects found in polycrystalline TiO_2 substrates used by Wu *et al.*[31] or by the different surface structure between rutile and anatase (since polycrystalline TiO_2 may possess rutile and anatase crystalline phases). At higher temperatures, the increased formation of surface defects was believed to aid the dehydrogenation of isopropoxide ligands to form acetone.

(b) Plasma Assisted CVD

The PACVD of titanium oxide films has only been documented in the last five years or so.[33-38] Stoichiometric, almost carbon-free TiO_2 layers have been deposited onto a heated substrate using a remote PACVD system with TiTP and inert excitation gases.[35,36] The stoichiometry was almost independent of gas parameters as well as the substrate temperature, though there was a small decrease in the carbon content. The deposition rate was affected by the power and the excitation and carrier gas flow rates. Increased substrate and post deposition annealing temperatures gave crystalline phases; etch rates decreased (the film densities increased) whilst refractive indices increased.

Deposition onto non-heated substrates has also been reported.[33,38] Amorphous films containing organic fragments were deposited, which upon annealing upto 400 °C gave the rutile structure with loss of the organic contamination.[33] Similarly films consisting of TiO_x ($0<x<2$) clusters dispersed throughout a host polymeric medium have been deposited.[38] The electrical characteristics observed were believed to originate from

variable titanium moieties belonging to the suboxides, e.g. TiO and Ti_2O_3.[39] Such TiO_x/polymeric films are potentially attractive for electrical, optical, thermal, chemical and magnetic applications.[38,40]

The next section of this chapter develops this published work and presents a detailed account of how low power plasma assisted decomposition of TiTP precursor can yield TiO_2 species embedded into a $C_xH_yO_z$ matrix.

3.2 EXPERIMENTAL

PACVD experiments were carried out in an electrodeless tubular glass reactor (5 cm internal diameter, volume 610 cm^3) which was enclosed in a Faraday cage,[41] as illustrated in Fig. 1. This was fitted with a monomer inlet, a Pirani pressure gauge, and a 47 L min^{-1} two-stage rotary pump attached to a liquid nitrogen cold trap. A 13.56 MHz radio frequency (RF) source was inductively coupled to the reaction vessel via a matching network and a copper coil (4 mm tube diameter, 9 turns) spanning 18-25 cm from the monomer inlet. Average glow discharge powers lower than 5 W could be sustained by pulsing the RF power supply.[42] The average power, <P>, absorbed by the plasma is then given by:[43]

$$< P >= P_o \times \left(\frac{T_1}{T_1 + T_2} \right)$$

where P_0 is the peak power of the pulse and T_1 and T_2 are the plasma on- and off-times respectively. For average powers less than 5 W, the peak power, P_0, was kept fixed at 5W and the duty cycles, $T_1/(T_1+T_2)$, were varied. Any further reference to power within the thesis refers to the average power, <P>, unless otherwise stated. All joints were grease-free. A fixed substrate position of 21.5 cm (i.e. in the centre of RF coils) from the precursor inlet, unless otherwise stated, was used to investigate the influence of power upon deposition characteristics.

Titanium tetraisopropoxide ($Ti[OCH(CH_3)_2]_4$) (TiTP) precursor (97% pure, Aldrich Chemicals) was transferred under a nitrogen atmosphere within a glove-box into a monomer tube, and then purified by multiple degassing freeze-pump-thaw cycles on the reactor set-up. The monomer tube and its connection to the reactor inlet were both heated to 30 ± 1 °C (as measured by a chromel-alumel thermocouple) via a heating tube (constructed inhouse) and heating tape respectively. Preliminary experiments, in the absence of monomer heating, gave non-reproducible XPS results and the volume of the plasma 'glow' frequently expanded (accompanied by a decrease in the 'glow' intensity)

into the monomer source turning it black. Such observations can be explained by a decrease in the system pressure.[44]

Two types of substrate were used in these experiments: low density polyethylene films (LDPE, Metal Box, 40 mm x 10 mm x 0.1 mm) for ATR-FTIR, and glass slides (20 mm x 7 mm x 1 mm) for XPS studies. Both were cleaned with isopropyl alcohol and left to dry in air prior to use.

A typical experimental run involved scrubbing the reactor with detergent, rinsing with isopropyl alcohol, drying in an oven, followed by a high power (50 W) air plasma treatment for 60 min. This latter step was done in the presence of glass substrates, but in the absence of polyethylene film, since oxygen glow discharges are renowned for their ability to oxidize polymer surfaces.[45] The reactor was then pumped down to a base pressure of $3x10^{-3}$ Torr with a leak rate lower than $8x10^{-11}$ kgs^{-1}. The TiTP monomer was introduced into the reaction chamber at a pressure of $8x10^{-2}$ Torr and at a flow rate of $4.6x10^{-9}$ kgs^{-1} (i.e. more than 98% of the reactants were TiTP precursor). The system was purged for 5 min before the glow discharge was ignited. After 5 min deposition time, the RF source was switched off, the monomer reservoir closed, the vacuum system let up to atmospheric pressure, and the appropriate analytical measurement undertaken.

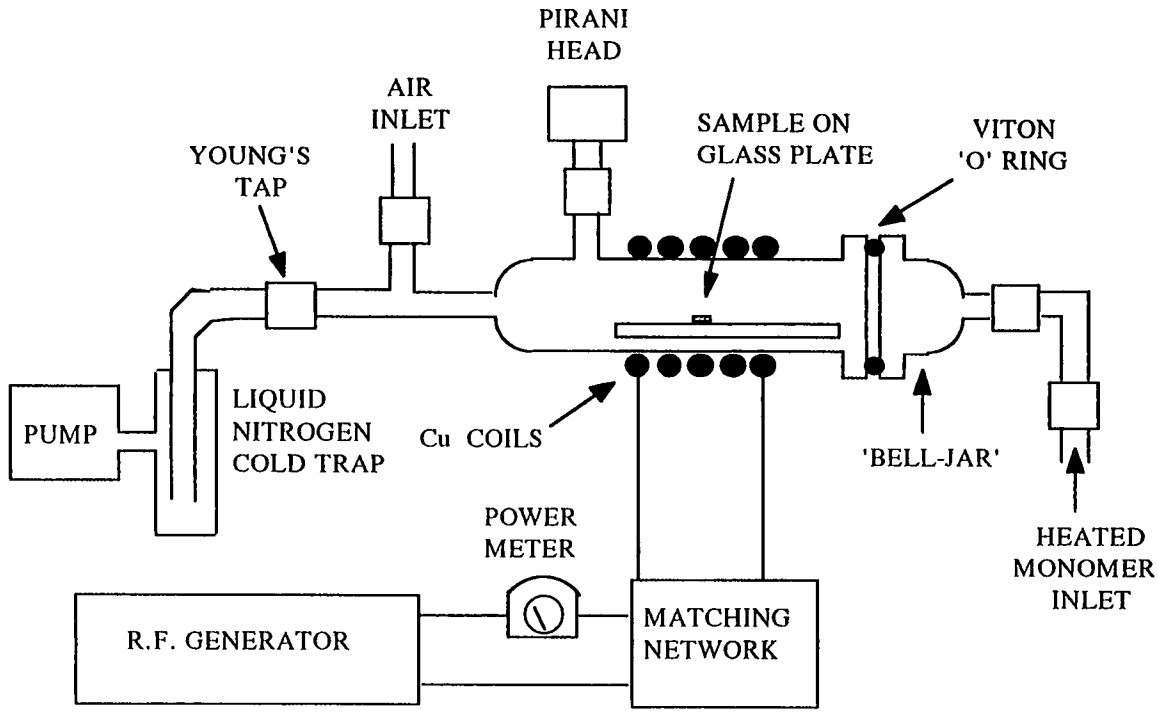

Fig. 1 Schematic diagram of the plasma reactor configuration.

3.3 RESULTS

During plasma ignition, a black film was deposited on all the surfaces exposed to the plasma i.e. on the reactor walls and substrates; the degree of darkening being greatest at higher powers, and centred on the RF coils. Exposure to air caused an instant discoloration with the deposit taking on a yellow-white appearance. This marked colour change is indicative of an increase in the oxidation state of titanium upon aerial exposure.[38] At lower powers (1-8 W) the deposited films had a slight tendency to crack, attributable to either the coatings possessing an intrinsic tensile stress,[15] or due to a chemical reaction with atmospheric gases.

3.3.1 X-RAY PHOTOELECTRON SPECTROSCOPY (XPS)

The C(1s), Ti(2p) and O(1s) XP spectra of the collected plasma deposit at 5 W are displayed in Figure 2. A range of carbon functionalities can be fitted to the C(1s) XP environment, as shown in Fig. 2(a): hydrocarbon ($\underline{C}_xH_y$ ~285.0 eV); carbon adjacent to a carboxylate group ($\underline{C}CO_2$ ~285.7 eV); carbon singly bonded to an oxygen atom ($\underline{C}$-O ~286.6 eV); carbon singly bonded to two oxygens or carbon doubly bonded to one oxygen atom (O-$\underline{C}$-O or $\underline{C}$=O ~287.9 eV); and carboxylate groups (O-$\underline{C}$=O ~289.0 eV).[46] The Ti($2p_{3/2}$) and Ti($2p_{1/2}$) XP peaks, Fig. 2(b), are centred at 459.0 ± 0.2 eV and 464.6 ± 0.2 eV respectively. These values are in close agreement with reported literature values for bulk TiO_2.[38,47-50] Precise deconvolution of the O(1s) XP spectrum, Fig. 2(c), is not possible since there are a number of likely environments that may be present to higher binding energies of the main environment at 530.6 ± 0.2 eV, associated to TiO_2.[48-50] Possible assignments for the higher binding energy environments include oxygenated carbon species,[51] substoichiometric oxide[50] or adsorbed water or OH on the surface.[52] A weak N(1s) XP signal was occasionally recorded, the most likely origin of this being reaction with atmospheric nitrogen during sample transfer to the X-ray photoelectron spectrometer.[53]

The atomic ratios, Ti/C and O/C, and elemental percentages were found to exhibit an approximate linear dependence upon glow discharge power, Figure 3. This can be attributed to there being either a greater degree of plasma polymerization of the organic moieties at higher powers, or less TiO_2 incorporation in the deposit. In the absence of a glow discharge (0 W), a small amount of monomer condensation onto the substrate was observed (see corresponding ATR-FTIR results).

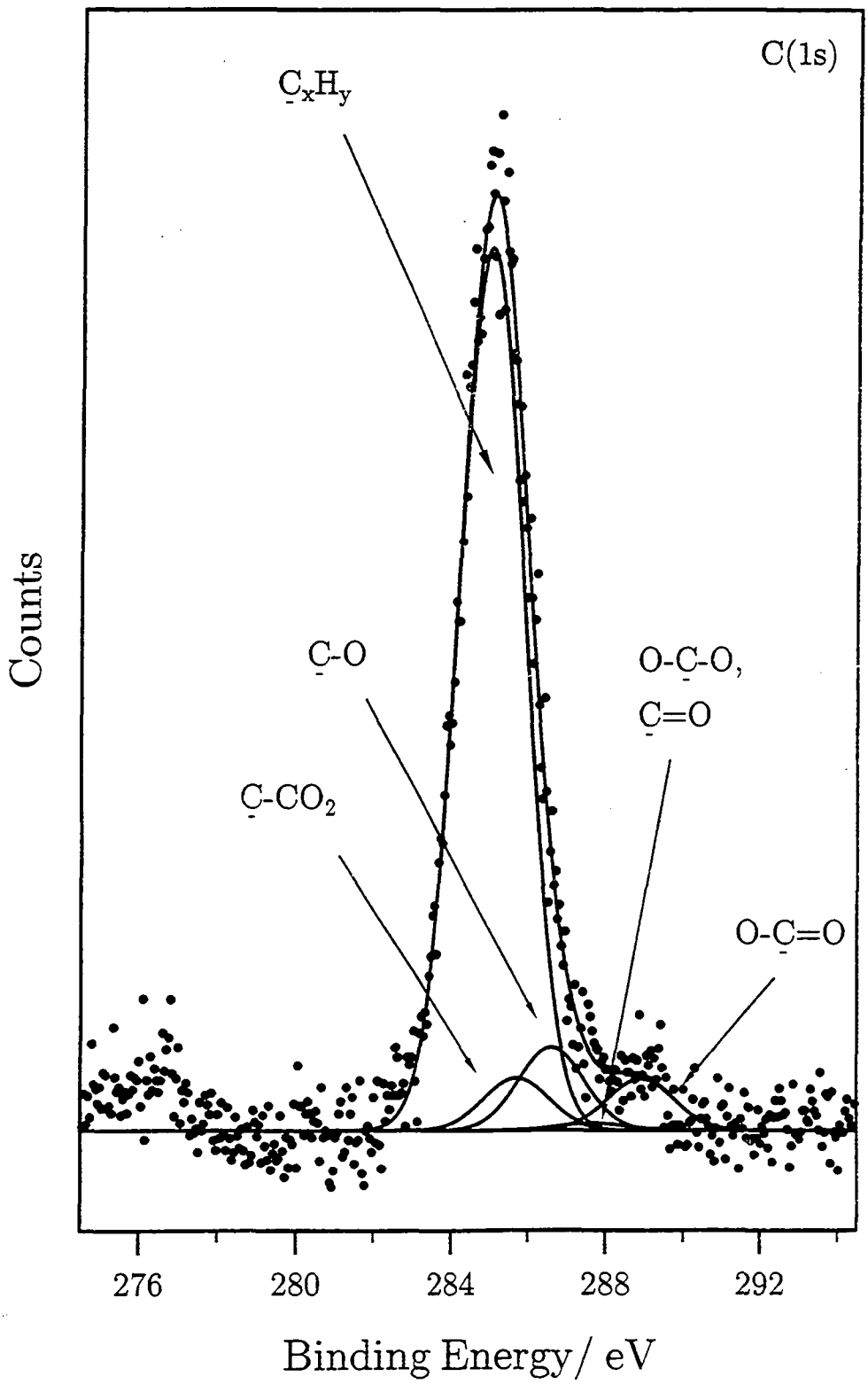

Fig. 2(a) C(1s) XP spectrum for PACVD of TiTP onto a glass substrate (5 W, 5 min, 21.5 cm).

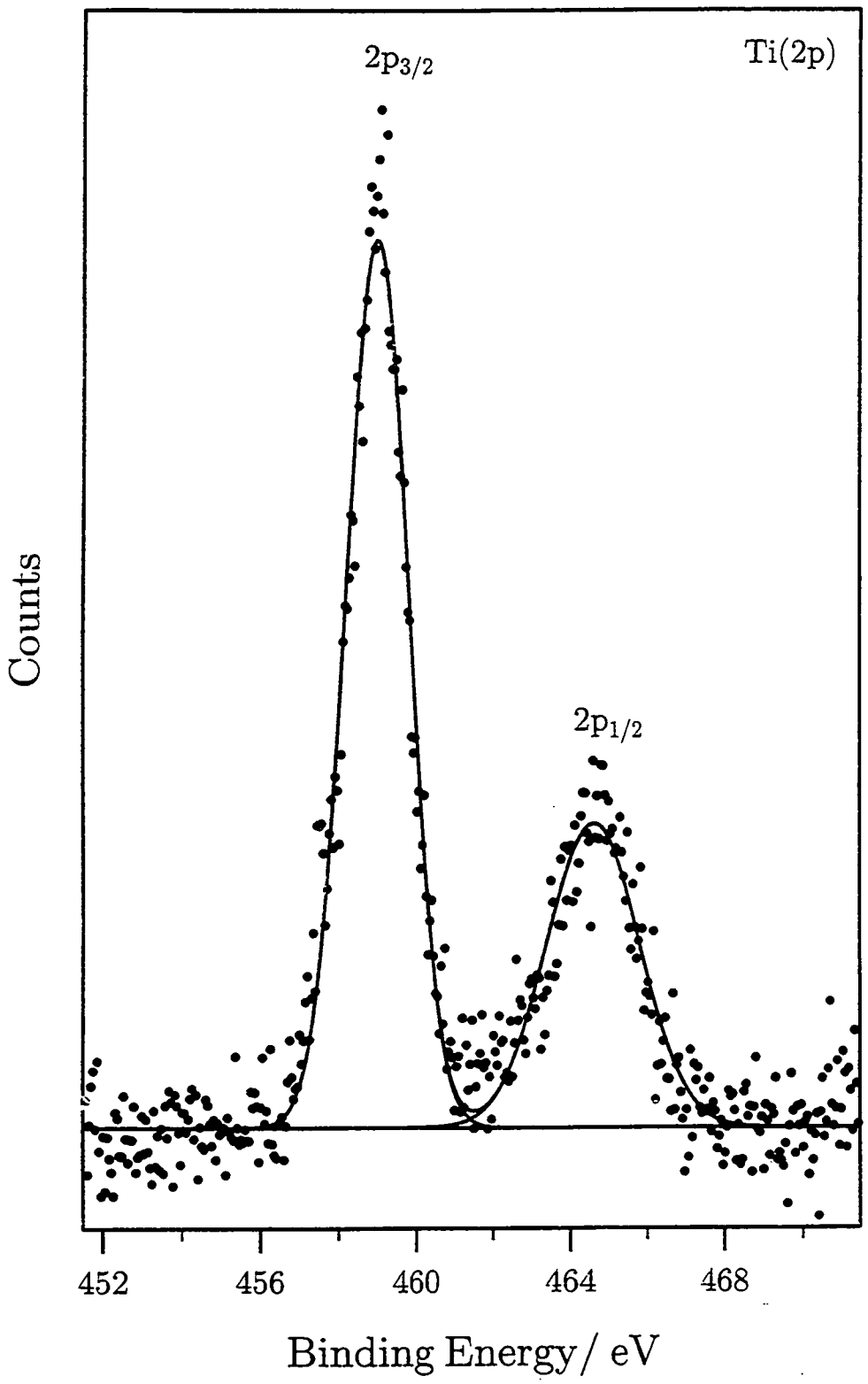

Fig. 2(b) Ti(2p) XP spectrum for PACVD of TiTP onto a glass substrate (5 W, 5 min, 21.5 cm).

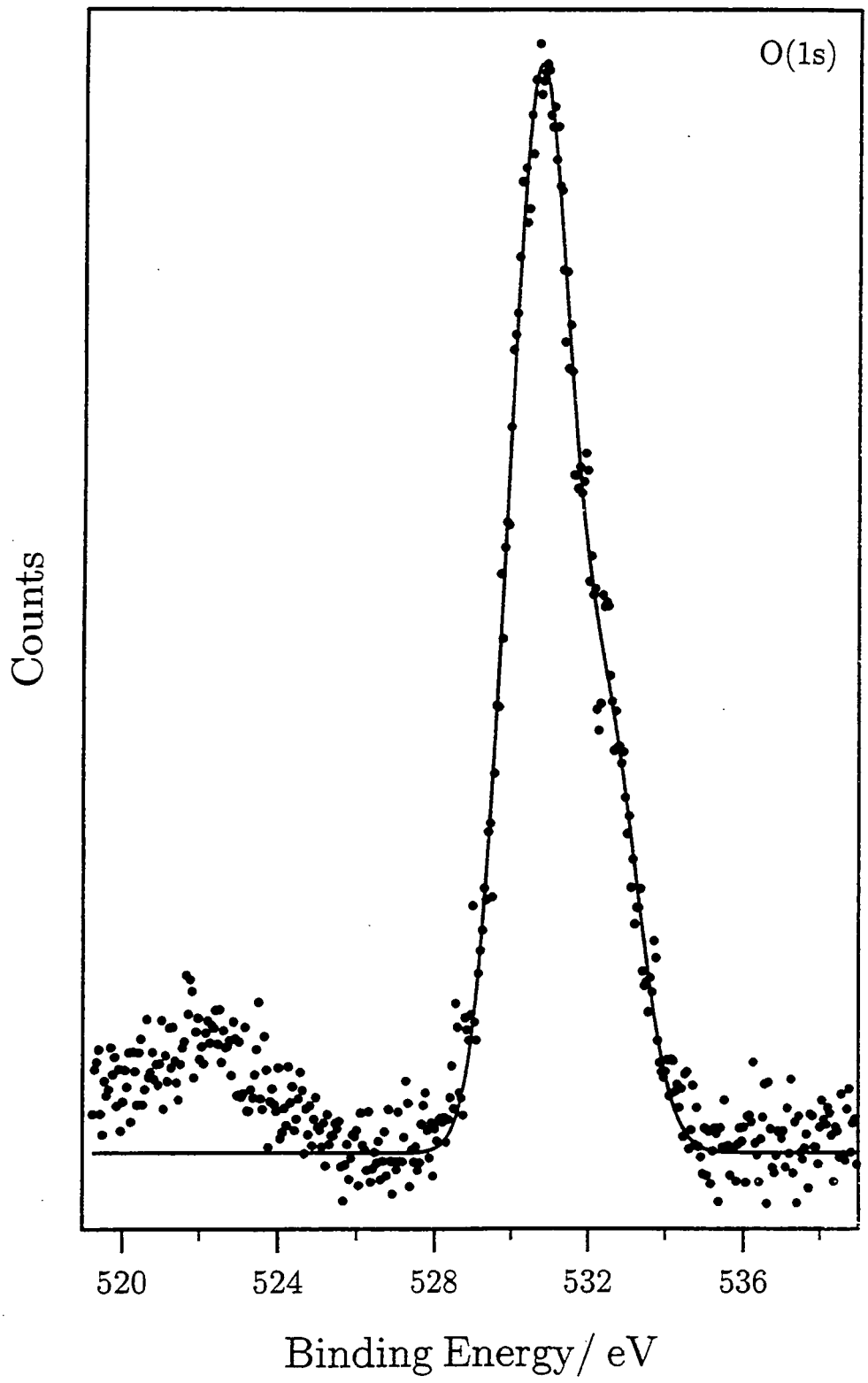

Fig. 2(c) O(1s) XP spectrum for PACVD of TiTP onto a glass substrate (5 W, 5 min, 21.5 cm).

(a)

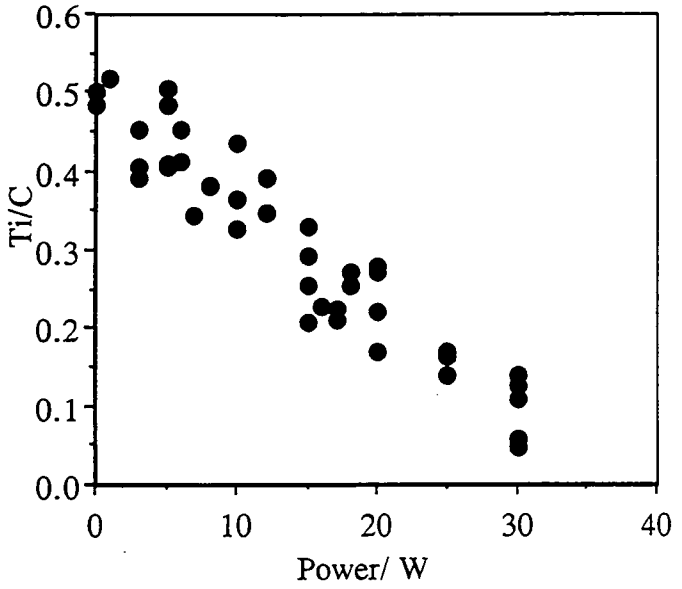

(b)

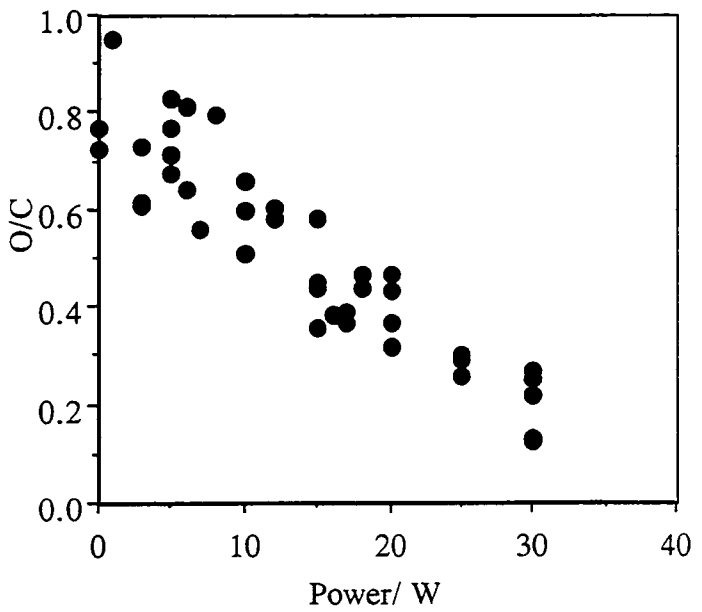

Fig. 3 Elemental atomic ratios as a function of glow discharge power (5 min, 21.5 cm): (a) Ti/C; and (b) O/C.

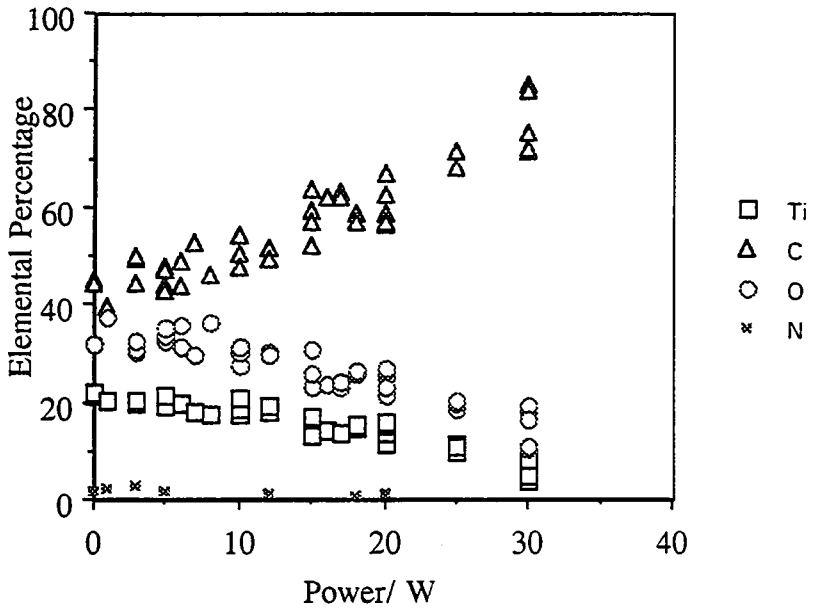

Fig. 3(c) Elemental composition as a function of glow discharge power (5 min, 21.5 cm).

Aging studies were carried out using two adjacent slides at a glow discharge power of 15 W (this being the midpower in the glow discharge power range). The aged sample was left in ambient conditions for approximately one month. The effects of oxidation on the sample can be seen in Table 1 and in the spectra in Fig. 4. The C(1s) XP region, Fig. 4(a), indicates an increase in the oxygenated carbon environments at higher binding energies to that of the hydrocarbon peak at 285.0 eV; the O(1s) XP region, Fig. 4(b), likewise shows the corresponding increase in oxygenated carbon, as well as adsorbed H_2O or OH[52] located at higher binding energies of the main oxide peak. The spectra have been normalized in order to show the qualitative peak shapes.

Table 1 Elemental composition and ratios for fresh and aged samples (15 W, 5 min, 21.5 cm).

Sample	% C	% Ti	% O	Ti/C	O/C	Ti/O
Fresh	66.8 ± 0.1	11.7 ± 0.1	21.4 ± 0.1	0.18 ± 0.01	0.32 ± 0.01	0.55 ± 0.01
Aged	65.6 ± 0.1	10.9 ± 0.1	23.5 ± 0.1	0.17 ± 0.01	0.35 ± 0.01	0.46 ± 0.01

Reactor profile studies demonstrate that film stoichiometry is fairly uniform throughout the deposition zone at low powers (5 W), Fig 5(a), but becomes position dependent at higher powers (30 W), Fig. 5(b).

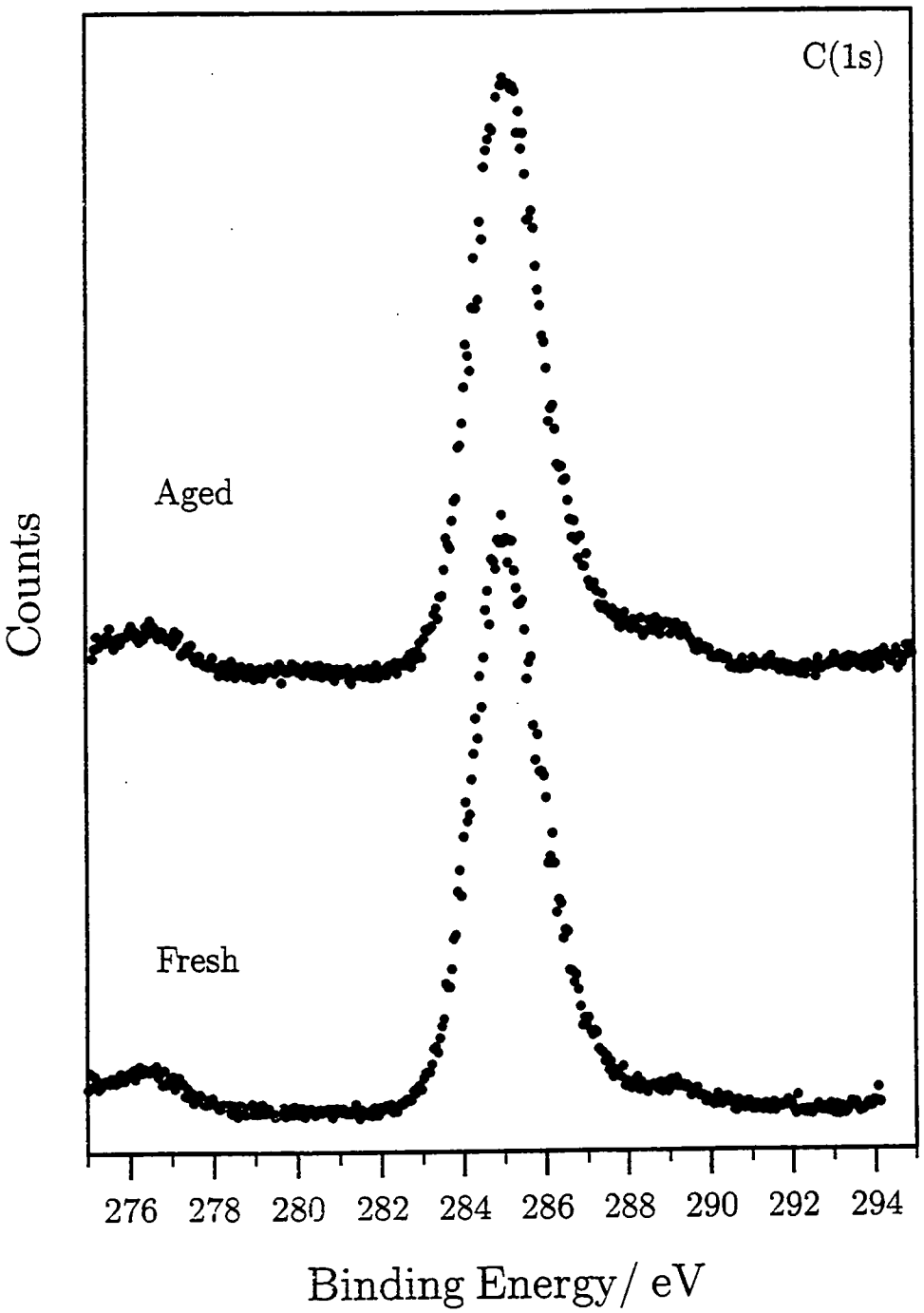

Fig. 4(a) C(1s) XP spectra for fresh and aged (approx. 1 month) PACVD samples of TiTP onto a glass substrate (15 W, 5 min, 21.5 cm).

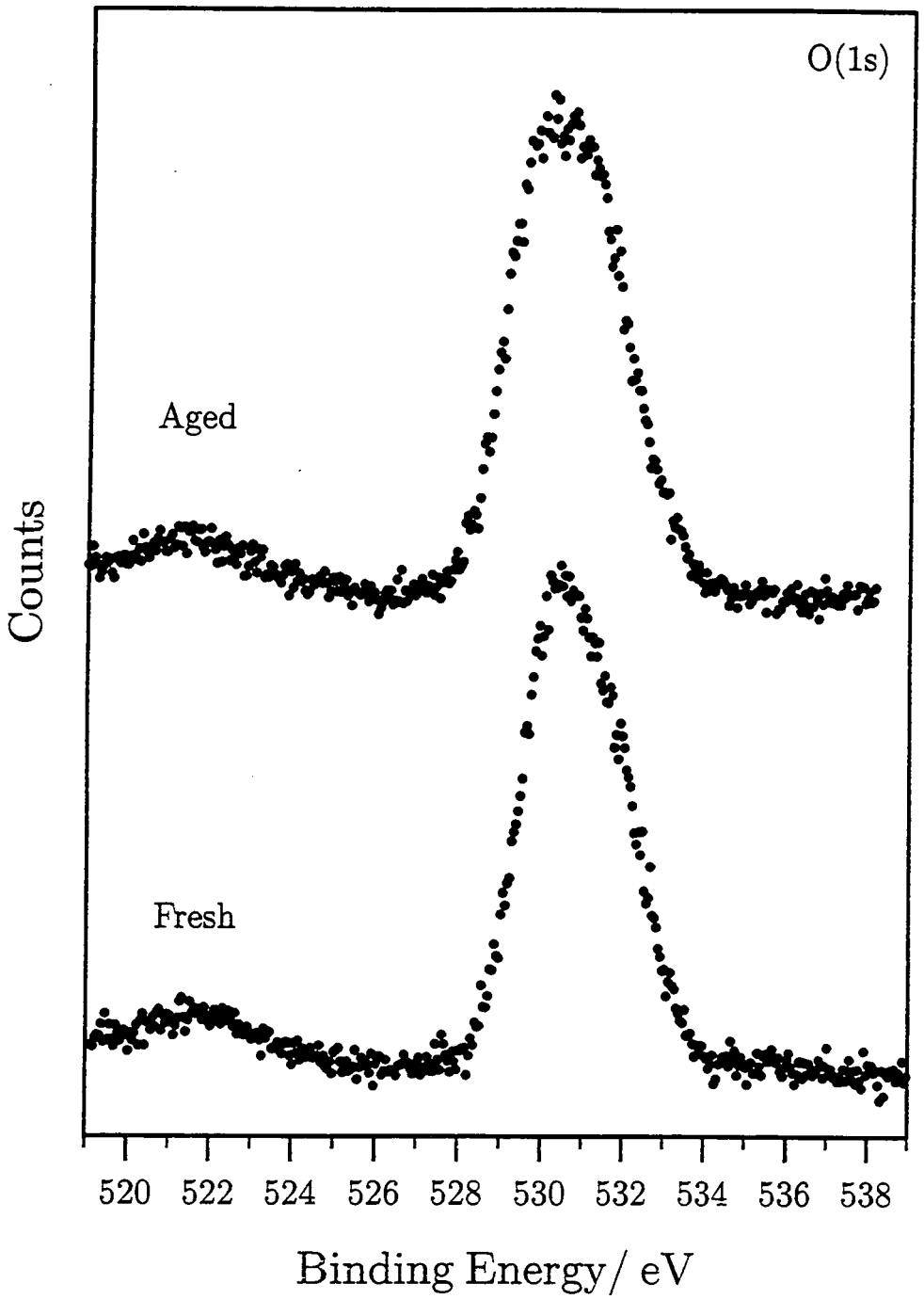

Fig. 4(b) O(1s) XP spectra for fresh and aged (approx. 1 month) PACVD samples of TiTP onto a glass substrate (15 W, 5 min, 21.5 cm).

(a)

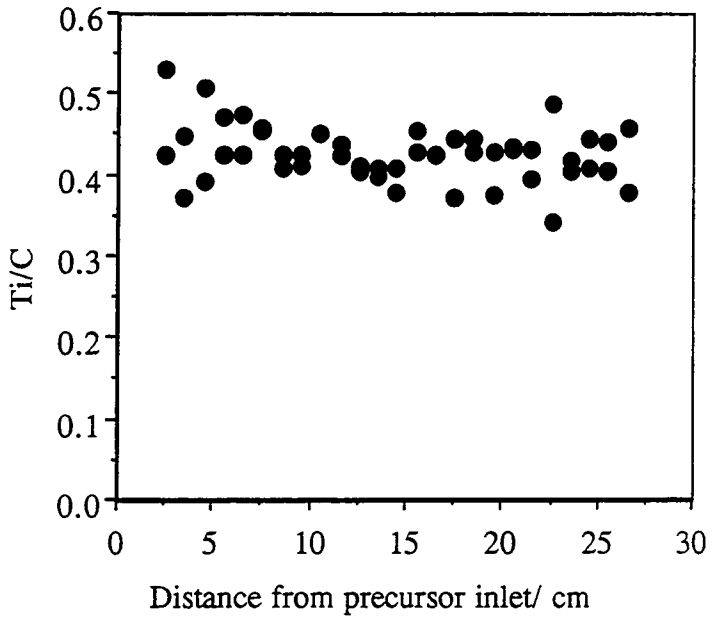

(b)

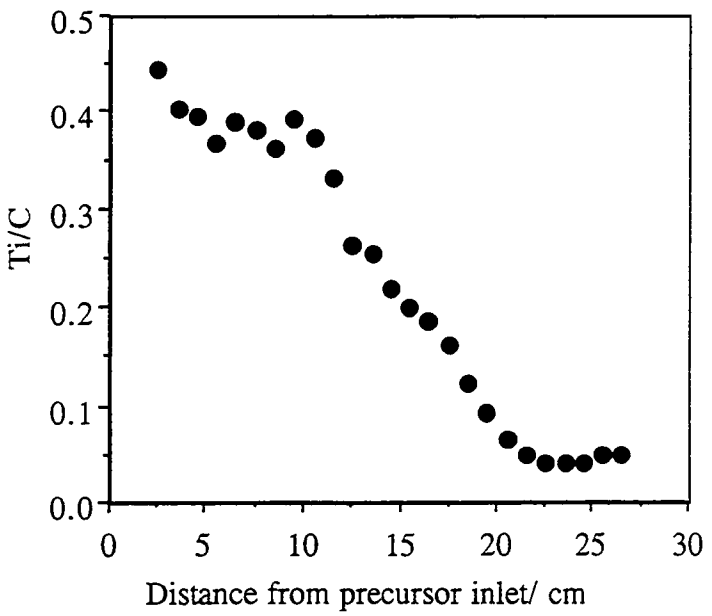

Fig. 5 XPS reactor profile for TiTP PACVD coatings (5 min): (a) 5 W; (b) 30 W.

3.3.2 XPS DEPTH PROFILING

Depth profiling was carried out on a 15 W TiTP plasma polymer sample. Figure 6 suggests that once the adventitious hydrocarbon contamination or low molecular weight hydrocarbon species are removed, the relative titanium content remains approximately constant, whilst that of oxygen decreases. In Fig. 7(a), the broadening of the Ti(2p) XP region is indicative of the different suboxide bonding states,[52] and is further supported by the shift to higher binding energies in the O(1s) XP region,[54] Fig. 7(b). However it is not clear whether this was solely due to the original status of titanium within the bulk of the film or caused by the Ar-ion bombardment resulting in the preferential sputtering of oxygen[55] or results from contributions from both.

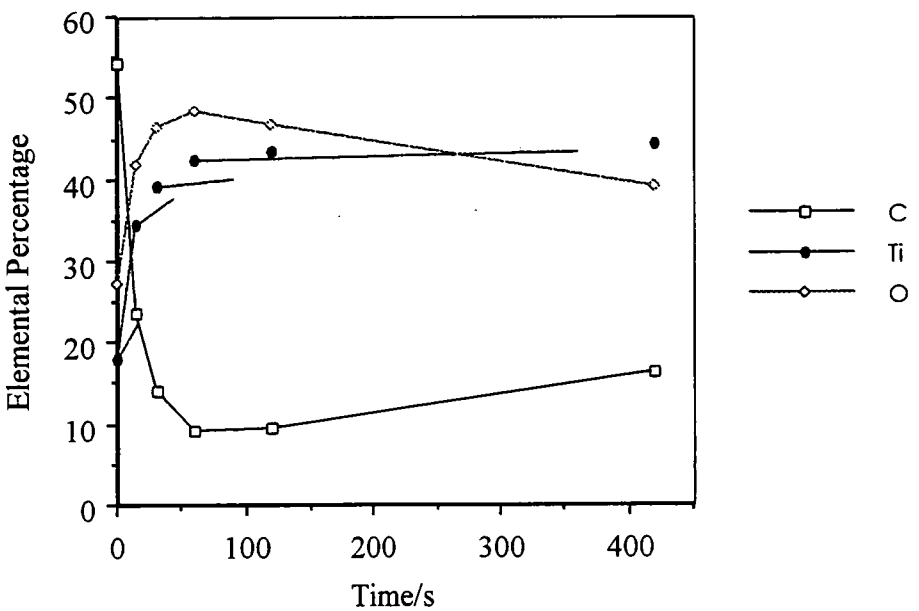

Fig. 6 XPS depth profile for PACVD of TiTP onto a glass substrate (15 W, 5 min, 21.5 cm).

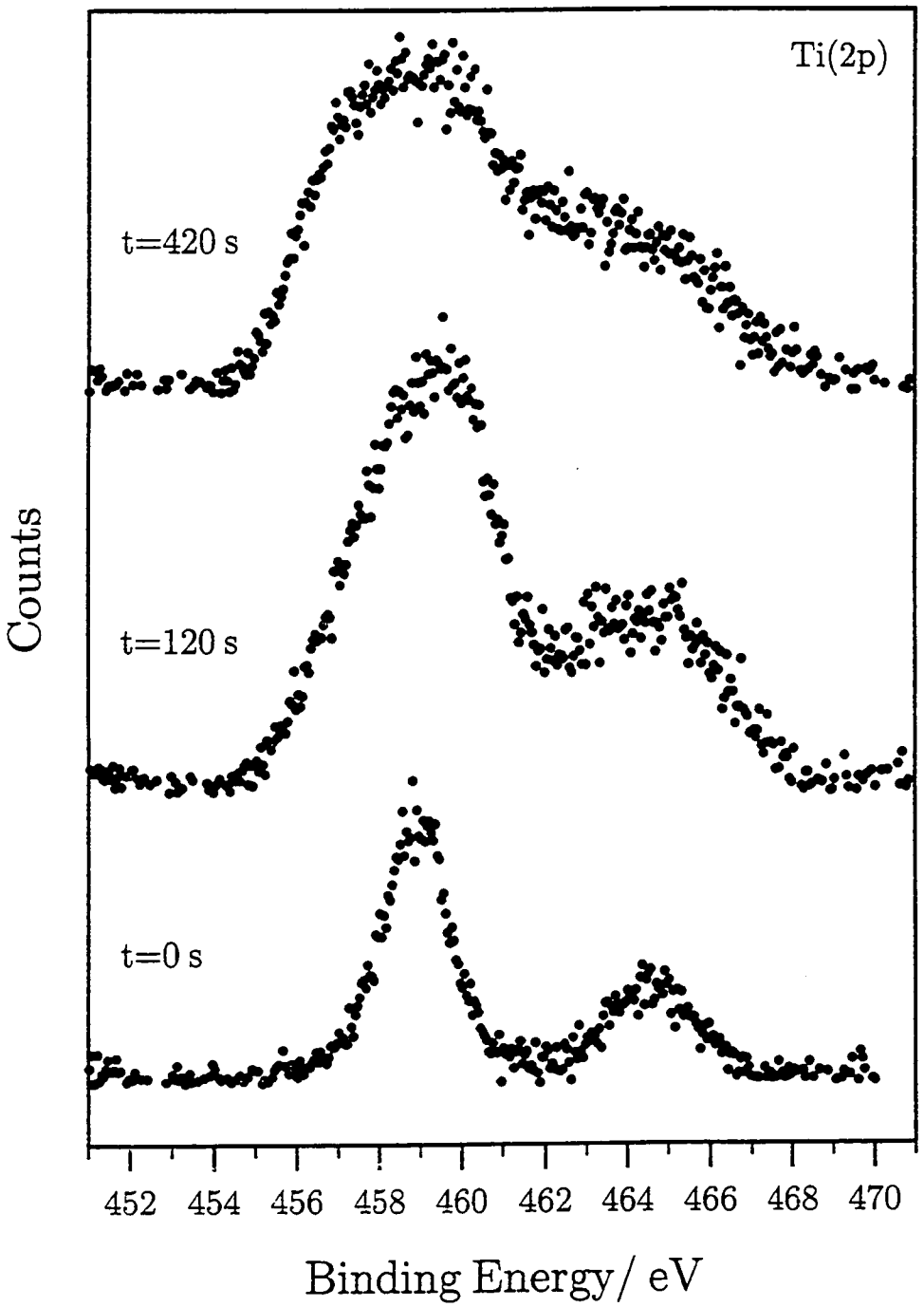

Fig. 7(a) Ti(2p) XP depth profile spectra of PACVD of TiTP onto a glass substrate (15 W, 5 min, 21.5 cm) recorded after given sputtering times.

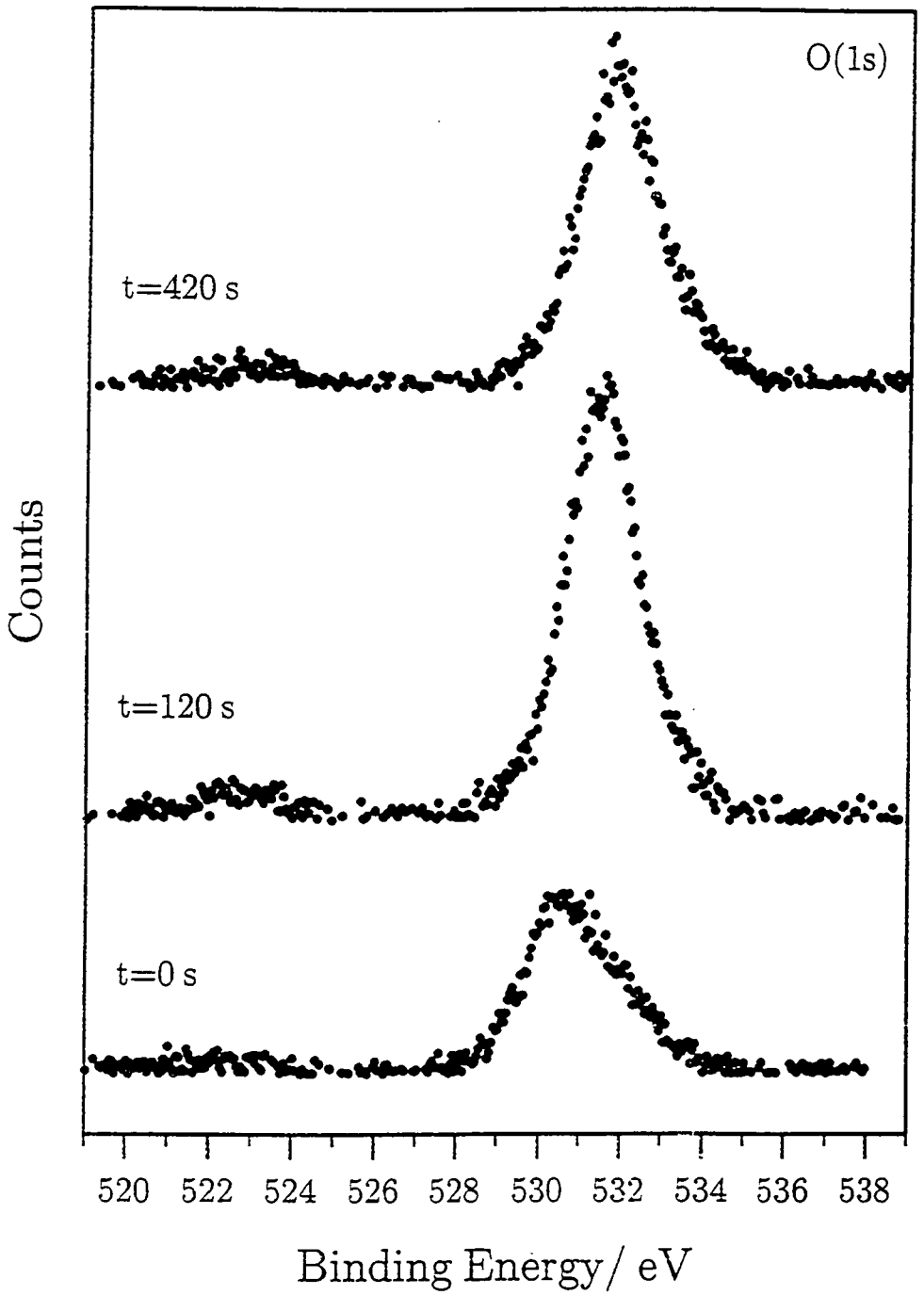

Fig. 7(b) O(1s) XP depth profile spectra of PACVD of TiTP onto a glass substrate (15 W, 5 min, 21.5 cm) recorded after given sputtering times.

3.3.3 ATTENUATED TOTAL REFLECTION FOURIER TRANSFORM INFRARED SPECTROSCOPY (ATR-FTIR)

ATR-FTIR spectra of clean, Fig. 8(a), and coated (5 W) polyethylene, Fig. 8(b), substrates are compared with the transmission FTIR spectrum of bulk TiO_2, Fig. 8(c). The characteristic absorbance bands for clean polyethylene are assigned in Table 2. A small amount of atmospheric CO_2 (antisymmetric stretch centred at 2350 cm^{-1}) was observable in some of the FTIR traces.

Lattice vibrations in bulk TiO_2 result in the broad absorbance observed below 900 cm^{-1}. The relative intensities and positions of peaks in this region are strongly influenced by TiO_2 particle shape and size.[56,57] Weak physisorbed water bands are observed at 1630-40 cm^{-1} and 3400 cm^{-1}. These originate from O-H bending and stretching respectively.[58,59]

Table 3 highlights the main literature characteristic IR absorbances for TiTP monomer.

Table 2 Infrared absorption bands for clean polyethylene film.[60-63]

Assignment	Wavenumbers/ cm^{-1}
asym C-H stretch in CH_2	2915
sym C-H stretch in CH_2	2847
CH_2 bending	1472, 1462
CH_2 wagging and/or symmetrical CH_3 movements	1366
CH_2 rocking	731, 719

Table 3 Vibrational mode assignments of TiTP.[64-66]

Assignment	Wavenumbers/ cm^{-1}
CH_3 asym stretch	2907
CH_3 sym stretch	2817
asym C-H deformation	1470
resonance split C-H	1391
sym C-H deformation	1377
resonance split C-H	1344
$(CH_3)_2CH$-skeletal	1170
C-O stretch	1131, 1006
skeletal vibrations	851
Ti-O stretch	619

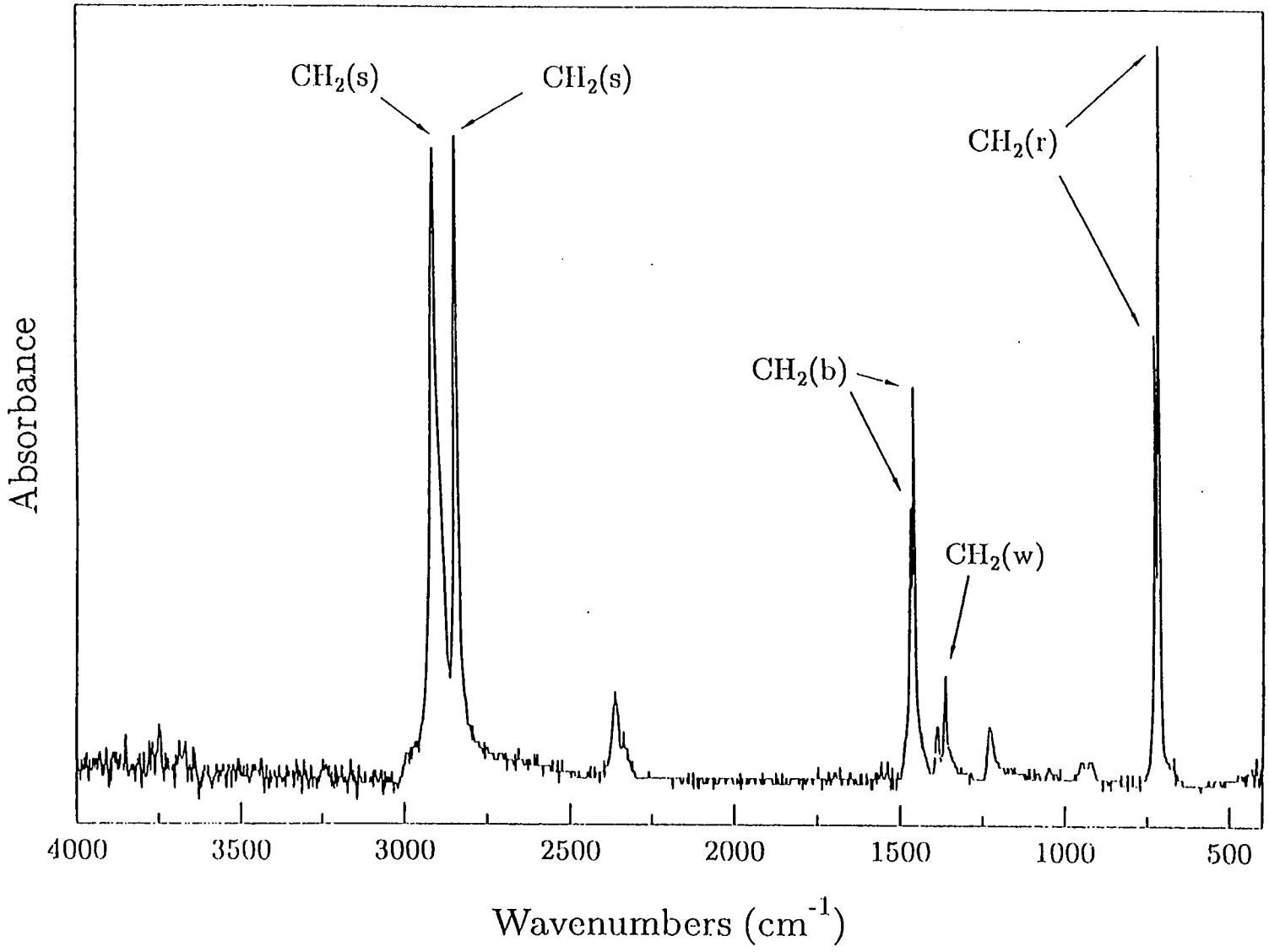

Fig. 8(a) ATR spectrum of clean polyethylene substrate.

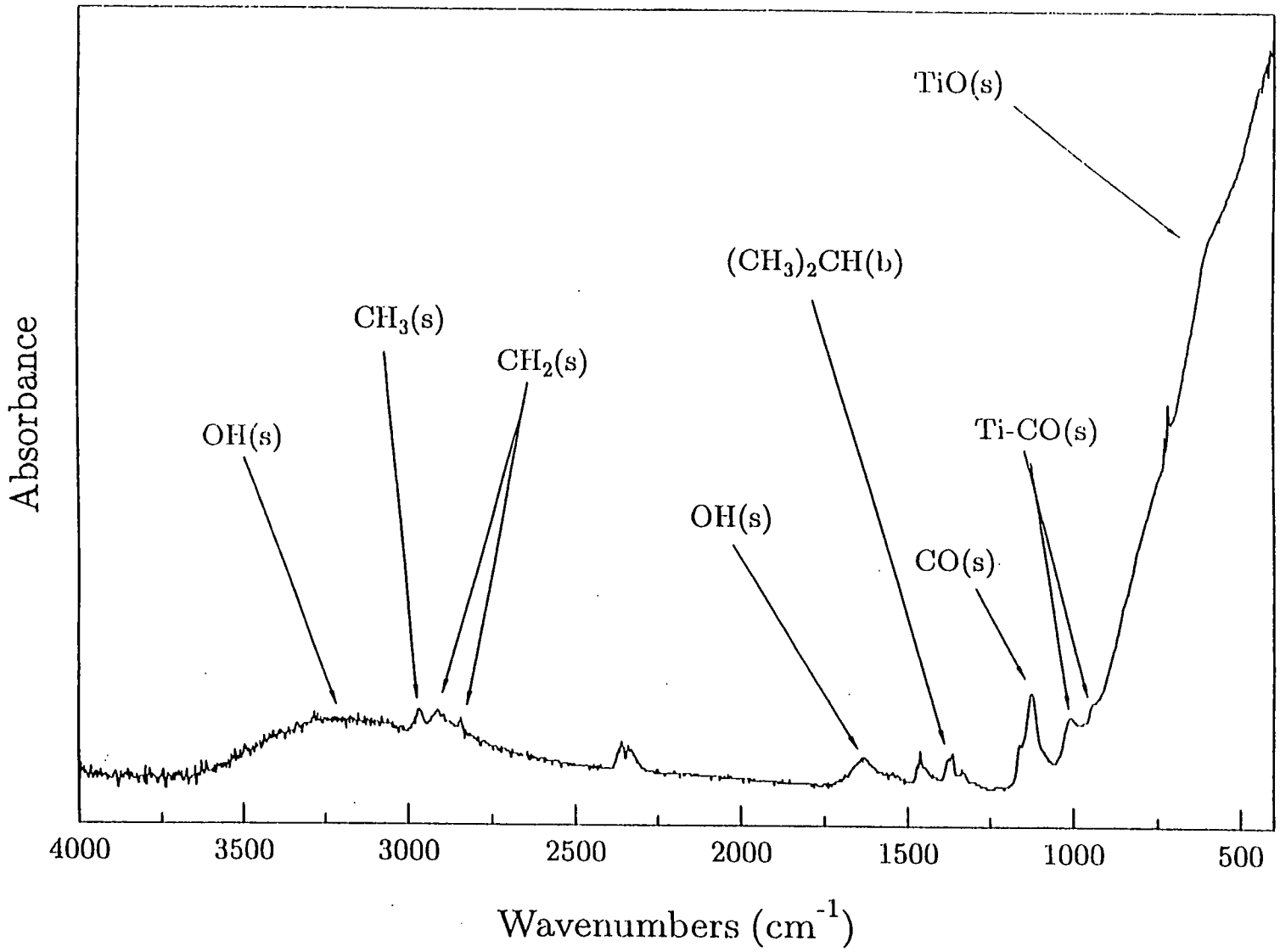

Fig. 8(b) ATR spectrum for PACVD of TiTP onto a polyethylene substrate (5 W, 5 min, 21.5 cm).

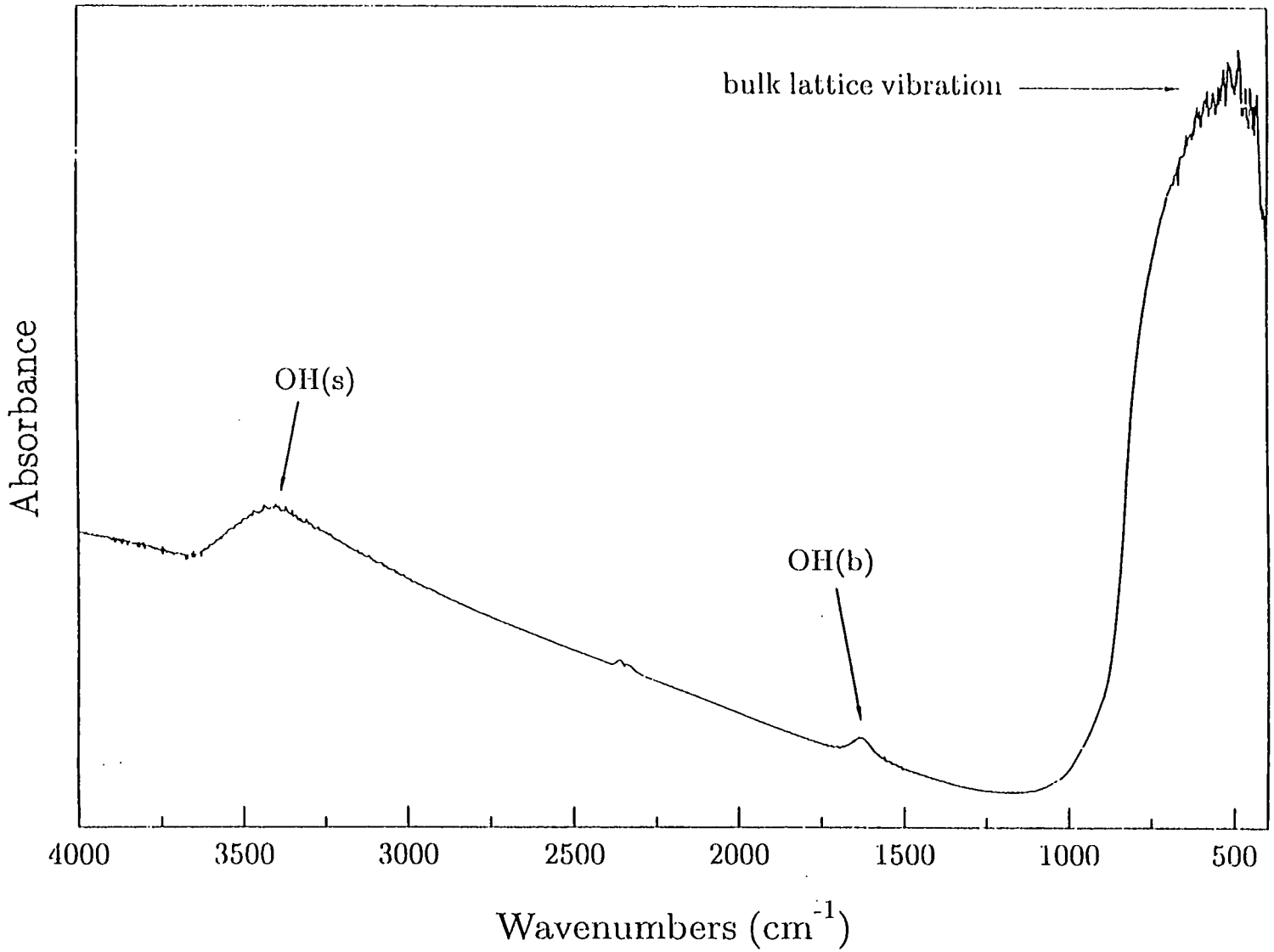

Fig. 8(c) FTIR transmission spectrum of bulk TiO_2 (Degussa, P25).

The greatest decrease in the characteristic 2915 cm^{-1} and 2847 cm^{-1} polyethylene features occurs at the lowest two glow discharge powers, Figure 9. Since the ATR-FTIR sampling depth is inversely proportional to the infrared wavenumber,[67] these bands should be more surface sensitive than the other characteristic polyethylene features at lower wavenumbers. Therefore it can be concluded that deposition of the thickest layer in the glow region occurs at approximately 5 W. The low wavenumber cut-off region associated with TiO_2 species is most intense at lower powers (2-10 W). At higher powers, this TiO_2 shoulder diminishes, and the following infrared bands become more predominant: polyethylene features, Ti(C-O) stretches at 1009 cm^{-1} and 945 cm^{-1}; a Ti-O stretch at 610 cm^{-1}; and a Ti-O absorbance[40,68] at about 470 cm^{-1}. Such variations in the infrared spectra suggest that a thinner coating is being generated in the glow region at higher powers, which may be due either to surface sputtering processes becoming predominant or to greater deposition occurring upstream towards the monomer inlet. It should be noted that only a small amount of monomer condensation is observed in the absence of any plasma (i.e. at 0 W).

ATR-FTIR reactor profiles at 5 W and 30 W are shown in Figure 10. At 5 W, the deposition rate is greatest in the centre of the coils as shown by the decrease in the characteristic polyethylene bands in Fig. 10(a), and it appears that only the relative intensities of the various incorporated species change along the reactor length. At 30 W, Fig. 10(b), two minima can be seen in the polyethylene intensities: firstly upstream, where there is a lot of TiO_2 deposition (9.5 cm from the monomer from the inlet), and secondly a build-up of polymeric species evident in the RF coils (21.5 cm from the monomer inlet). These results are consistent with the corresponding XPS measurements.

Aging effects (approximately one month) have been observed as indicated for the 30 W plasma polymer, Fig. 11. Attenuation of the bands at 1161 cm^{-1} and 1128 cm^{-1} is clearly evident, whilst the bands at 1009 cm^{-1} and 945 cm^{-1} appear to have merged under the large cut-off region below 900 cm^{-1}. The presence of the former bands in the freshly deposited film may arise from any unreacted monomer, low molecular weight hydrocarbon species and/or any alcoholic species lying on the surface or incorporated in the film. On aging, hydrolysis of any unreacted monomer will give alcoholic species. The alcohol or any low molecular weight hydrocarbon species may then either evaporate from the surface or may migrate towards the substrate in order to lower the surface energy as observed in plasma oxidized polymer surfaces.[69] Increases in the broad bands centred at 1560 cm^{-1} and 1635 cm^{-1} are evident as is the broadening in the region of 1400 cm^{-1}. The presence of trapped free radicals in plasma polymers, which tend to react with oxygen and/or water is well documented.[44] As a result, carboxylate species are formed as indicated by the increase in the 1560 cm^{-1} band and the broadening of the 1400 cm^{-1} region (asymmetric and symmetric carboxylate stretches respectively).[61] It is

possible that the increase in the 1635 cm^{-1} band is due to the presence of additional physisorbed water. This is supported by the apparent decrease in the intensity of the CH_3 environment just below 3000 cm^{-1} and the broadening of the O-H band around 3200 cm^{-1}. Alternatively, an increase in the vinylic component, consistent with trapped free radicals undergoing recombination reactions, would also give an increase in the 1635 cm^{-1} region.

3.3.4 ATOMIC FORCE MICROSCOPY (AFM)

Figure 12 shows the AFM image of a 15 W TiTP plasma polymer sample. Initially this image was ran at half the resolution (i.e. the x and y axes = 1 μm) which gave no surface information. At this higher resolution, it can be seen that the surface morphology is not smooth.

Smooth films have been deposited by CVD of TiTP at low temperatures (325-400 °C) under kinetically controlled conditions, whilst a collection of hemispheres were observed at higher temperatures under mass-transfer-controlled conditions.[30] This latter observation suggests that a gas phase reaction took place rather than a reaction at the gas/surface interface resulting in the formation of powder particles embedded in a film.[15] Evidence of particles on the surface in Fig. 12 therefore supports such a theory.

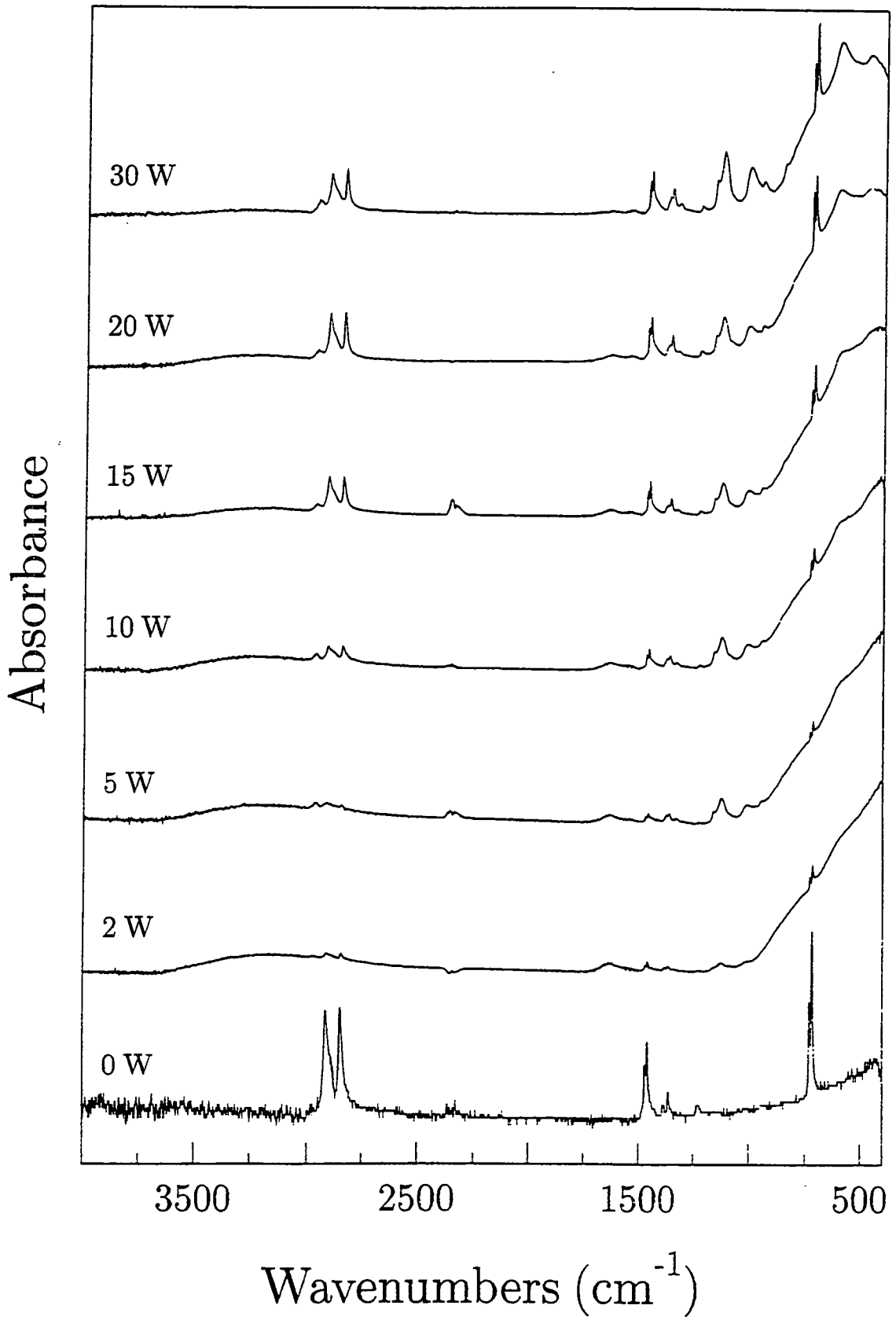

Fig. 9 ATR-FTIR spectra for PACVD of TiTP onto polyethylene film as function of glow discharge power (5 min, 21.5 cm).

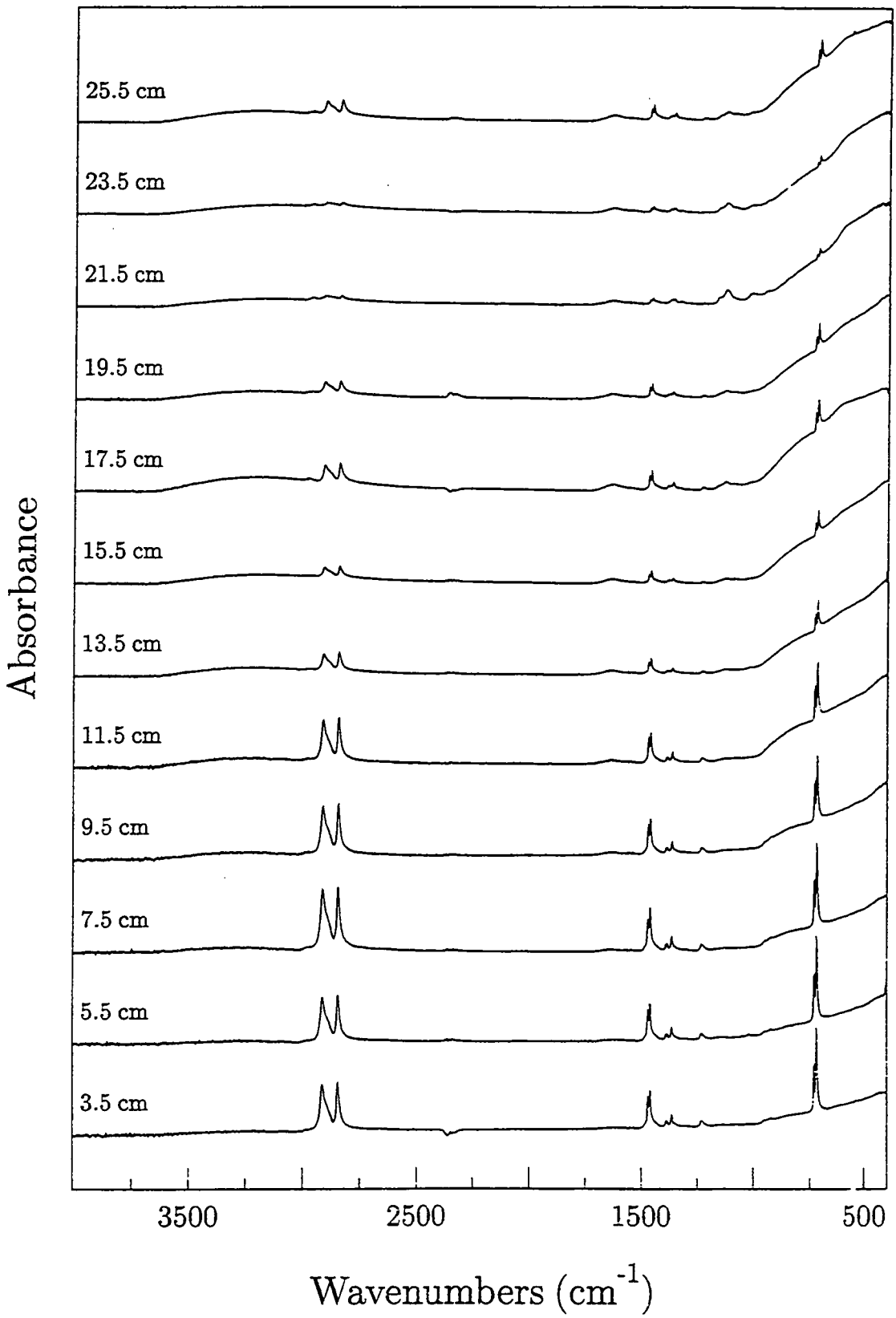

Fig. 10(a) ATR-FTIR reactor profile for TiTP of PACVD coating onto polyethylene (5 W, 5 min).

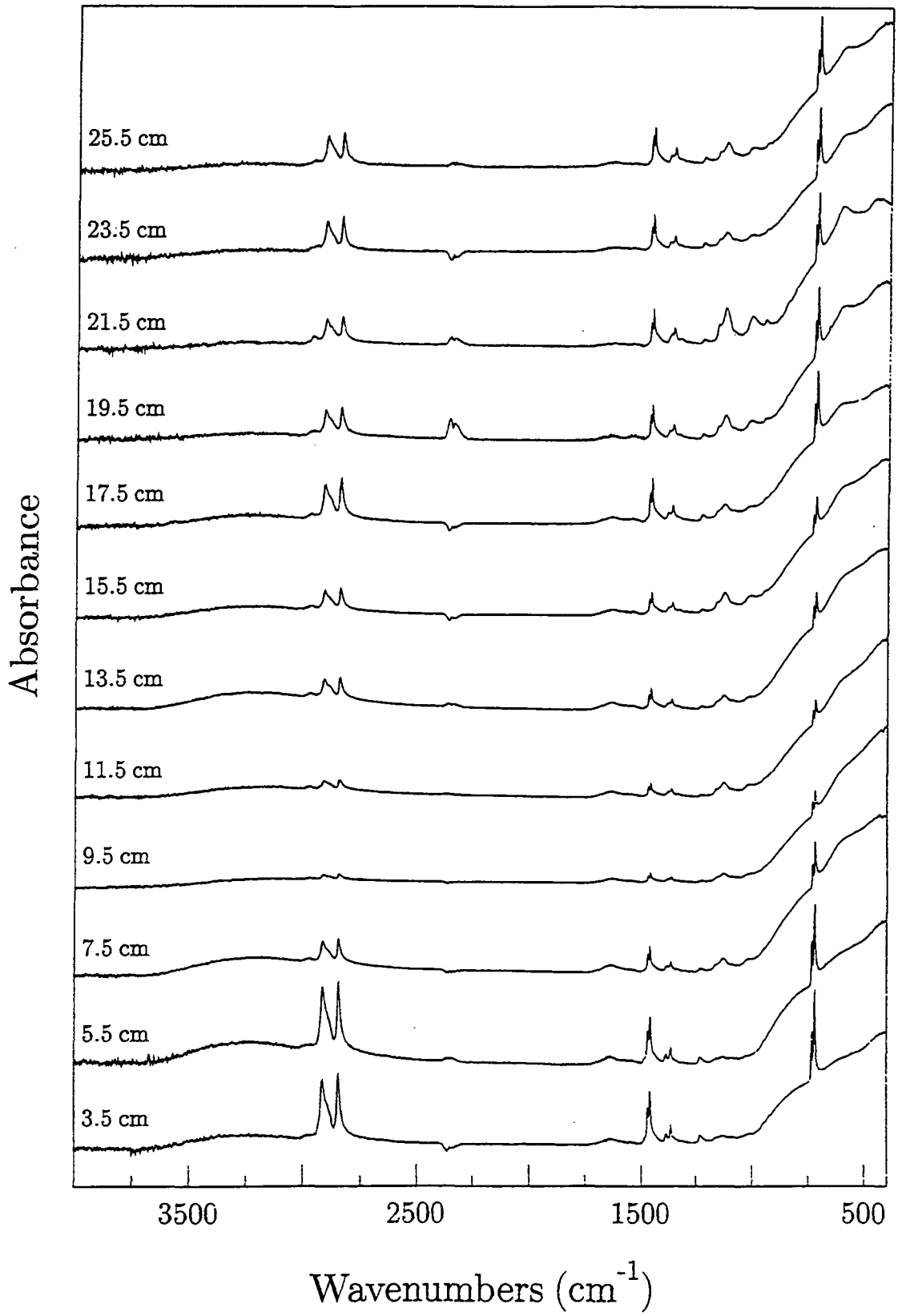

Fig. 10(b) ATR-FTIR reactor profile for TiTP of PACVD coating onto polyethylene (30 W, 5 min).

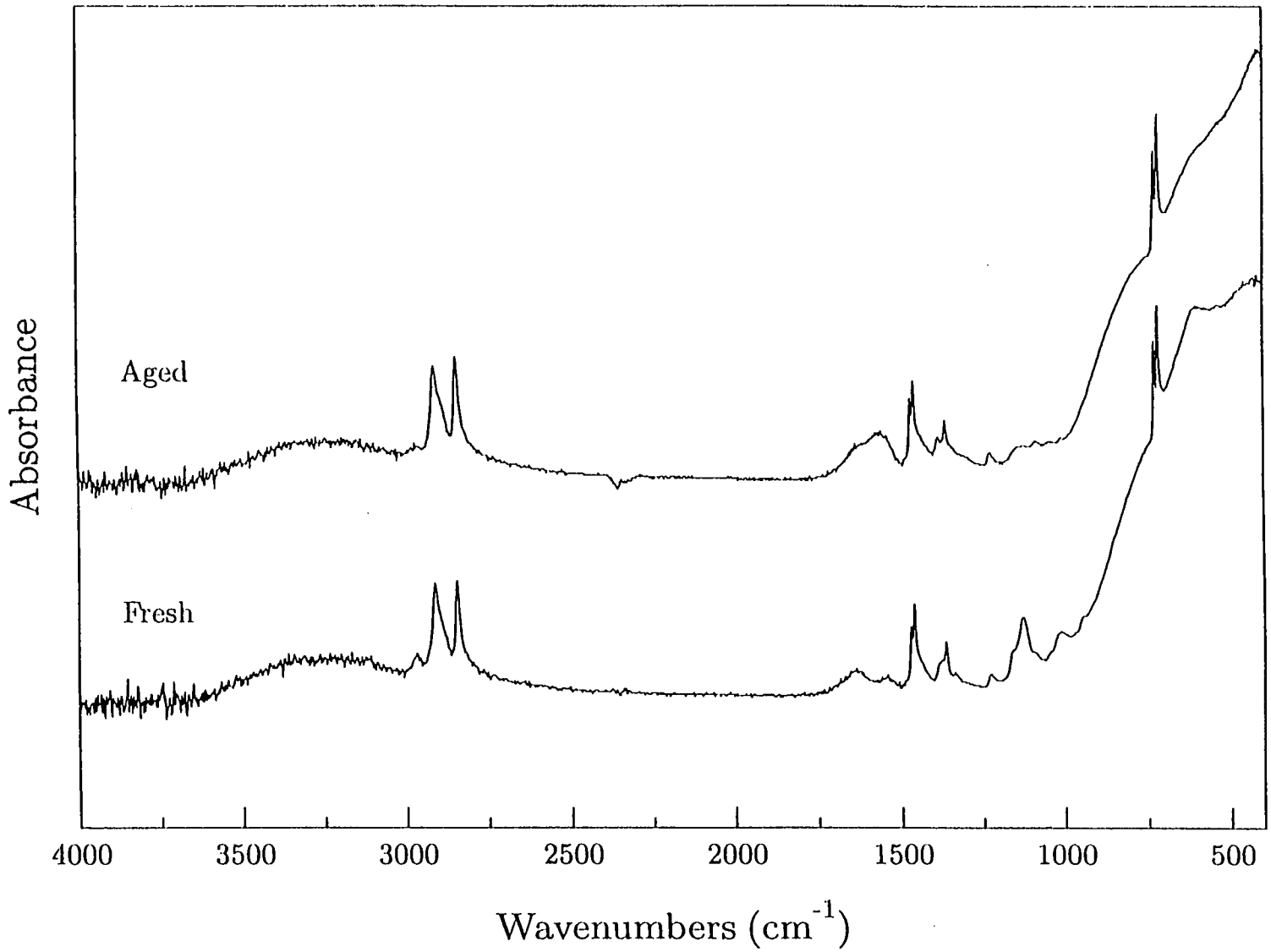

Fig. 11 ATR-FTIR spectra of PACVD of TiTP onto polyethylene substrate showing fresh and aged samples (30 W, 5 min, 21.5 cm).

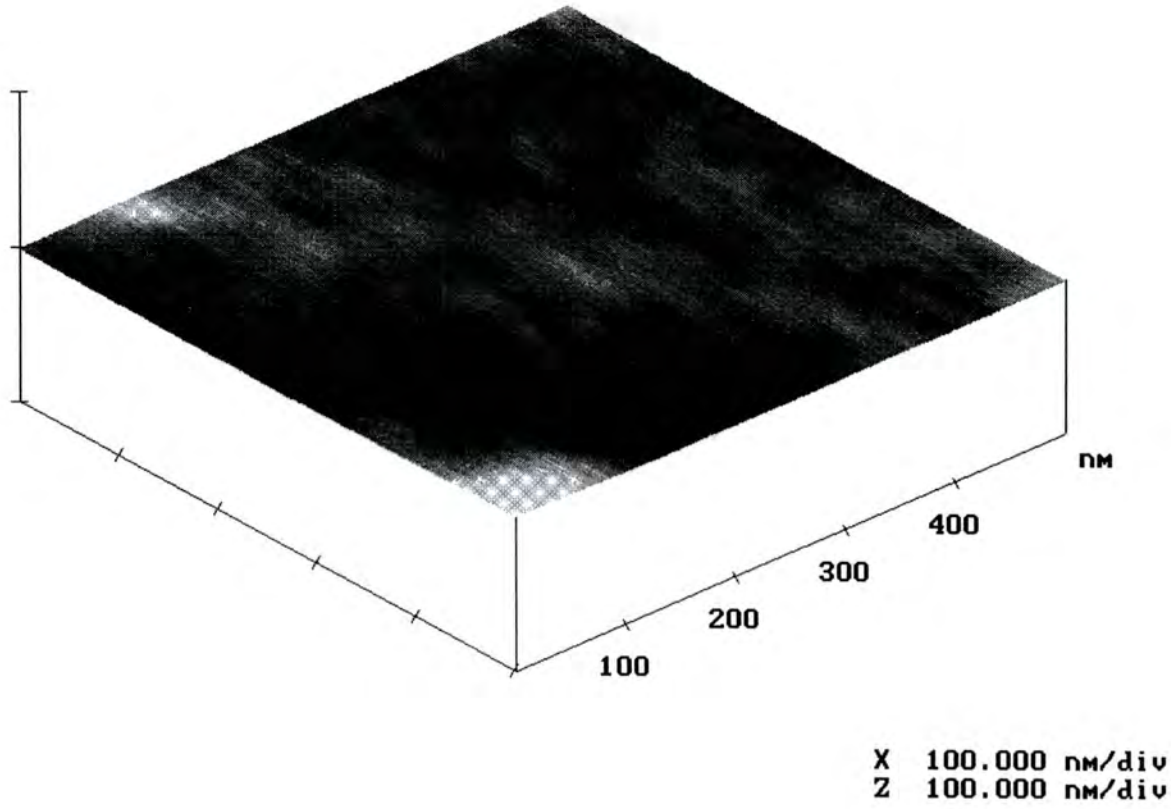

Fig. 12 AFM image for PACVD of TiTP onto a glass substrate (15 W, 5 min, 21.5 cm).

3.4 DISCUSSION

The dramatic change in colour from black to white upon exposure of the deposited coatings to air is most probably due to an increase in the titanium oxidation state from Ti^{2+} to Ti^{4+} (e.g. TiO is known to be black[38] whereas TiO_2 is white).[1] However, the XPS depth profiling data is inconclusive in supporting the existence of suboxides of titanium within the bulk of the film since Ar-ion sputtering is well known to cause preferential sputtering of oxygen,[55] resulting in the reduction of the titanium oxidation state.

The XPS and ATR-FTIR data display a strong dependency upon glow discharge power. Thermal decomposition of TiTP at a surface is reported to result in the elimination of a number of stable byproducts:[21,31,32]

$$Ti[OCH(CH_3)_2]_4 \dashrightarrow TiO_{2(s)} + \alpha H_{2(g)} + \beta(CH_3)_2C{=}O_{(g)} + \varepsilon CH_2{=}CHCH_{3(g)} + \gamma(CH_3)_2CH(OH)_{(g)}$$

In the case of PACVD, only a very small extent of TiTP monomer condensation occurs in the absence of any excitation energy (0 W). At low glow discharge powers the deposited material appears to be titanium-rich, which is consistent with most of the associated gaseous decomposition products passing through into the reactor outlet. However at higher glow discharge powers, TiO_2 deposition occurs further upstream nearer the monomer inlet, leaving any carbon containing byproducts to migrate into the glow region, where they undergo a substantially greater degree of fragmentation and thereby participate in plasma polymerization.[44] This explanation is supported by the XPS and ATR-FTIR reactor profiles: coating composition remains constant at low powers (5 W), whereas an increase in glow discharge energy (30 W) results in a higher proportion of organic species being deposited downstream in the reactor glow region.

In Park's empirical analysis of plasma assisted deposition,[70] the overall deposition rate can be described as being governed by an Arrhenius-type of activation energy, E_a:

$$D_p \propto F_M \exp[-E_a/(W/F_M)]$$

where D_p is the average deposition rate, and F_M is mass flow rate. For a given position in the reaction vessel, there will be no deposition in the absence of any electromagnetic field ($W = 0$), and also when there is a very low concentration of reactive species ($F_M = 0$). It can be assumed from thermal CVD studies[21,31,32] that the activation energy (E_a) required for TiTP decomposition to yield TiO_2 is much smaller than that needed for the plasma polymerization of any gaseous carbon containing byproducts.

Therefore TiO_2-rich layers should be formed at low powers, with most of the gaseous species passing out through the reactor outlet. However at higher glow discharge powers, TiO_2 deposition in the glow region will become limited by TiTP mass flow, F_M, and falls in magnitude on moving downstream from the monomer inlet. The remaining $C_xH_yO_z$ byproducts participate in plasma polymerization during passage through the highest energy zone of the reactor (i.e. within the RF coils). This explanation is supported the ATR-FTIR analysis of 5 W versus 30 W deposited layers. In the former case, TiO_2 rich material is mostly deposited within the RF coils, but at 30 W, TiO_2 formation occurs upstream, thereby leaving any accompanying organic species to migrate into the higher energy glow region, where they can undergo plasma polymerization.

Such a high selectivity towards TiO_2 rich films at low powers appears to have been overlooked in previous PACVD studies[38] where all the emphasis has been placed upon higher power regimes.

Aging of the deposited films results from the oxidation of titanium metal centres of suboxides, as well as from the reaction of atmospheric water and oxygen with the high density of trapped free radicals that are typically incorporated in plasma polymers.[44]

AFM has shown the formation of powder or dust particles during deposition. Such formation is thought to occur in the gas phase[15] and these particles have been shown to be suspended at the plasma/sheath boundary in low pressure plasma processes (etching, sputter and deposition plasmas).[71,72] Since the electrons are the most mobile charge carriers, the particles acquire a negative charge.[73] The formation of these particles is system dependent and not well understood.[74] They may be introduced in the discharge by plasma surface interaction or created in the volume by polymerization of the gas or its dissociation products. On extinction of the plasma, these suspended particles fall onto the film surface[71] under the influence of gravity.[15]

3.5 CONCLUSIONS

Plasma assisted decomposition of titanium tetraisopropoxide ($Ti[OCH(CH_3)_2]_4$) (TiTP) precursor can be used to generate TiO_2 species embedded into a polymeric matrix. TiO_2-rich layers are produced in the plasma glow zone at low powers and high TiTP flow rates. Higher glow discharge powers result in TiO_2 deposition occurring mainly upstream due to a much greater consumption of TiTP monomer during passage through the reactor. At low discharge powers, the majority of $C_xH_yO_z$ byproduct molecules are pumped away through the reactor outlet, whereas for higher power glow discharges

these organic species experience greater activation, leading to an increase in the rate of plasma polymerization. Aging of the plasma polymers occurs as a result of reaction of atmospheric water and oxygen with trapped free radicals and oxidation of titanium metal centres. The particulate coverage of the surface of the deposited films indicates that the gas phase reactions dominate during the deposition process.

3.6 REFERENCES

1. F.A. Cotton, G. Wilkinson, Advanced Inorganic Chemistry, 4th Edn., John Wiley, Chichester, 1980.
2. G. Haas, *Vacuum*, **2**, 1952, 331.
3. C. Sanchez, J. Livage, *New J. Chem.*, **14**, 1990, 513.
4. F.L. Williams, J.J McNally, C.A. Al-Jumaily, J.R. McNeil, *J. Vac. Sci. Technol.*, **A5**, 1987, 2159.
5. H. Döring, K. Hashimoto, A. Fujishima, *Ber. Bunsenges. Phys. Chem.*, **96**, 1992, 620.
6. E.T. Fitzgibbons, K.J. Sladek, W.H. Hartwig, *J. Electrochem. Soc.*, **119**, 1972, 735.
7. T. Fuyuki, T. Kobayashi, H. Matsunami, *J. Electrochem. Soc.*, **135,** 1988, 248.
8. F. Kirbir, H. Komiyama, *Chem. Lett.*, 1988, 791.
9. K. Kamata, K. Maruyama, S. Amano, H. Fukazawa, *J. Mater. Sci. Lett.*, **9**, 1990, 316.
10. K. Bange, C.R. Ottermann, O. Anderson, U. Jeschkowski, *Thin Solid Films*, **197**, 1991, 279.
11. S. Schiller, G. Berister, W. Sieber, *Thin Solid Films*, **83**, 1981, 239.
12. M.H. Suhail, G. Mohan Rao, S. Mohan, *J. Appl. Phys.*, **71**, 1992, 1421.
13. R.N. Ghoshtagore, A.J. Noreika, *J. Electrochem. Soc.*, **117**, 1970, 1310.
14. S. Veprek, *Plasma Chem. Plasma Process.*, *9*, 1989, 29S.
15. R. d'Agostino, Ed., Plasma Deposition, Etching of Polymers, Academic Press, London, 1990.
16. E. Kny, L.L. Levenson, W.J. James, R.A. Auerbach, *Thin Solid Films*, **85**,1981, 23.
17. H.V. Boenig, Fundamentals of Plasma Chemistry and Technology, Technomic Publ. Co. Inc., Lancaster, PA, 1988.
18. L.M. Williams, D.W. Hess, *J. Vac. Sci. Technol.*, **A1**, 1983, 1810.
19. L.M. Williams, D.W. Hess, *Thin Solid Films*, **115**, 1984, 13.
20. D.C. Bradley, *Chem. Rev.*, **89,** 1989, 1317.
21. K.L. Siefering, G.L. Griffin, *J. Electrochem. Soc.*, **137,** 1990, 814.
22. Y. Takahashi, A. Oiso, R. Tomoda, K. Sugiyama, *J. Chem. Soc. Faraday Trans. 1*, **81**, 1985, 3117.
23. S.R. Kurtz, R.G. Gordon, *Thin Solid Films*, **147**, 1987, 167.
24. T.-K. Won, S.-G .Yoon, H.-G. Kim, *J. Electrochem. Soc.*, **139**, 1992, 3284.
25. M. Yokozawa, H. Iwasu, I. Taramoto, *Jpn. J. Appl. Phys.*, 7, 1969, 96.
26. T. Fuyuki, T. Kobayashi, H. Matsunami, *Jpn. J. Appl. Phys.*, **25**, 1986, 1288.
27. N. Rausch, E.P. Burte, *J. Electrochem. Soc.*, **140,** 1993, 145.
28. H-Y. Lee, H-G. Kim, *Thin Solid Films*, **229**, 1993, 187.

29. M. Ritala, M. Leskelä, L. Liinistö, P. Haussalo. *Chem. Mater.*, **5**, 1993, 1174.
30. Z. Chen, A. Derking, *J. Mater. Sci.*, **3**, 1993, 1137.
31. Y.-M. Wu, D.C. Bradley, R.M. Nix, *Appl. Surf. Sci.*, **64**, 1993, 21.
32. C.P. Fictorie, J.F. Evans, W.L. Gladfelter, *J. Vac. Sci. Technol.*, **A12**, 1994, 1108.
33. K.S. Chen, Y.L. Juang, *Polym. Mat. Sci. Eng. ACS*, **62**, 1990, 538.
34. H. Holzschuh, H. Suhr, *Adv. Mater.*, **4**, 1992, 357.
35. H.J. Frenck, W. Kulisch, M. Kuhr, R. Kassing, *Thin Solid Films*, **201**, 1991, 327.
36. H.J. Frenck, E. Oesterschulze, R. Beckmann, W. Kulisch, R. Kassing, *Mater. Sci. Eng.*, **A139**, 1991, 394.
37 W. Kulisch, M. Witt, H.J. Frenck, R. Kassing, *Mater. Sci. Eng.*, **A140**, 1990, 715.
38. Y. Kagami, T. Yamauchi, Y. Osada, I. Yoshizaura, *J. Appl. Phys.*, **68**, 1990, 610.
39. J.B. Torrance, P. Lacorre, C. Asavaroengchai, R.M. Metzger, *Physica C*, **182**, 1991, 351.
40. N. Inagaki, S. Tasaka, Y. Nozue, *J. Appl. Polym. Sci.*, **45**, 1992, 1041.
41. A.G. Shard, H.S. Munro, J.P.S. Badyal, *Polym. Comm.*, **32**, 1991, 152.
42. D.T. Clark, D. Shuttleworth, *J. Polym. Sci. Polym. Chem. Ed.*, **18**, 1980, 27.
43. K. Nakajima, A.T. Bell, M. Shen, *J. Appl. Polym. Sci. Polym. Appl. Symp.*, **23**, 1979, 2627.
44. H. Yasuda, Plasma Polymerization, Academic Press, Orlando, FL., 1985.
45. A.G. Shard, J.P.S. Badyal, *Macromolecules*, **25**, 1992, 2053.
46. D.T. Clark, A. Dilks, *J. Polym. Sci. Polym. Chem. Edn.*, **17**, 1979, 957.
47. Handbook of X-Ray Photoelectron Spectroscopy, Ed. C.D. Wagner, W.M. Riggs, L.E. Davis, J.F. Moulder, G.E. Muilenberg, Perkin-Elmer Corp., Eden Prairie, MN, 1979.
48. M. Murata, K. Wakino, S. Ikeda, *J. Electr. Spectr. Relat. Phenom.*, **6**, 1975, 459.
49. B. Siemensmeyer, K. Bade, J.W. Schultze, *Ber. Bunsenges. Phys. Chem.*, **95**, 1991, 1461.
50. N.C. Saha, H.G. Tompkins, *J. Appl. Phys.*, **72**, 1992, 3072.
51. G. Beamson, D. Briggs, High Resolution XPS of Organic Polymers, The Scienta ESCA300 Database, John Wiley, Chichester, 1992.
52. C.N. Sayers, N.R. Armstrong, *Surf. Sci.*, **178**, 1977, 301.
53. N. Inagaki, H. Kawai, *J. Polym. Sci. Polym. Chem. Ed.*, **24**, 1986, 3381.
54. M.V. Kaznetsov, J.F. Zhuravlev, V.A Zhilyaev, V.A. Gubanov, *J. Electr. Spectr. Relat. Phenom.*, **58**, 1992, 1.
55. J.W. Coburn, *Thin Solid Films*, **64**, 1979, 371.
56. M. Ocaña, W.P. Hsu, E. Matijevic, *Langmuir*, 7, 1991, 2911.
57. J.T. Luxon, R. Summitt, *J. Chem. Phys.*, **50**, 1969, 1366.

58. D.J.C. Yates, *J. Chem. Phys.*, **65**, 1969, 746.
59. P. Jackson, G. D. Parfitt, *Trans Faraday Soc.*, **62**, 1966, 204.
60. J.L. Koenig, Chemical Microstructures of Polymer Chains, John Wiley, New York, 1980.
61. R.M. Silverstein, G.C. Bassler, T.C. Morrill, Spectrometric Identification of Organic Compounds, 4th Edn., John Wiley, New York, 1981.
62. J.P. Luongo, H. Schonhorn, *J. Polym. Sci.*, **A26**, 1968, 1619.
63. J.P. Luongo, *J. Polym. Lett.*, **2**, 1964, 75.
64. V.A. Zeitler, C.A. Brown, *J. Phys. Chem.*, **61**, 1957, 1174.
65. C.G. Barraclough, D.C. Bradley, J. Lewis, I.M. Thomas, *J. Chem. Soc.*, 1961, 2601.
66. C.T. Lynch, K.S. Mazdiyasni, J.S. Smith, W.J. Crawford, *Anal. Chem.*, **36**, 1964, 2332.
67. F.M. Mirabella, *Appl. Spec. Rev.*, **21**, 1985, 45.
68. M. Ocaña, C.J. Serna, *Spectrochim. Acta*, **47A**, 1991, 765.
69. E. Occhiello, M. Morra, P. Cinquina, F. Garbassi, *Polymer*, **33**, 1992, 3007.
70. S.Y. Park, N. Kim, *J. Appl. Polym. Sci. Polym. Appl. Symp.*, **46**, 1990, 91.
71. G.S. Selwyn, K.L. Haller, E.F. Patterson, *J. Vac. Sci. Technol.*, **A11**, 1993, 1132.
72. G.S. Selwyn, J.E. Heidenreich, K.L. Haller, *Appl. Phys. Lett.*, **57**, 1990, 1876.
73. Y. Watanabe, M. Shiratani, *Jpn. J. Appl. Phys.*, **32**, 1993, 3074.
74. J.P. Boeuf, *Phys. Rev.*, **A**, 1992, 7910.

CHAPTER 4:
PLASMA ASSISTED CHEMICAL VAPOUR DEPOSITION OF TITANIUM DIOXIDE/POLYMER FILMS FROM TITANIUM TETRAISOPROPOXIDE AND HYDROGEN

4.1 INTRODUCTION

Hydrogen is known to play an important role in the reduction process of TiO_2 when H_2O or H_2 is present, especially at high temperatures or in the presence of an electric field.[1] The suboxides, TiO and Ti_2O_3, are known to be conductors[2] and reduced or substoichiometric TiO_2 has been found to behave as an 'n'-type semiconductor.[1] There has also been interest in doping TiO_2 with hydrogen, for example to produce photochemical anodes in photoelectrochemical cells for use in a variety of photochemical reactions.[3]

Methods to reduce the density of trapped free radicals in plasma polymers, which cause the observed aging effects, include higher deposition temperatures and post deposition annealing.[4] Satisfactory results have also been achieved by adding hydrogen to the plasma discharge[5] or by subjecting the film to a hydrogen plasma immediately after deposition.[6]

This chapter describes the introduction of hydrogen gas to TiTP during PACVD in an attempt to reduce TiO_2 and to create films stable to the oxidative aging of the organic components.

4.2 EXPERIMENTAL

Modifications to the reactor configuration used for TiTP were required in order to allow the addition of a gas to the system. Various arrangements were attempted before arriving at the method illustrated Fig. 1 that gave sufficient deposition using conditions as close to those used with the previous set-up described in Chapter 3. The bell-jar was modified to include a sliding-joint with two O-rings (one Teflon and one Viton) and a gas inlet. A glass tube, the extension delivery tube, was positioned over the end of the tapered end of the sliding-joint so that the end of the extension delivery tube lay a distance of 17 cm from the sliding-joint inlet between the 2nd and 3rd coils (as counted from the right handside). The end of the extension delivery tube was fluted. The RF coils were then moved towards the monomer inlet so as to give monomer deposition

within the glow region of the RF coils such that they spanned 15.5 - 22.5 cm from the sliding-joint inlet. The fixed sample position of 19 cm from the sliding joint inlet was then chosen so that the sample lay in the middle of the reactor coils as for the original reactor configuration.

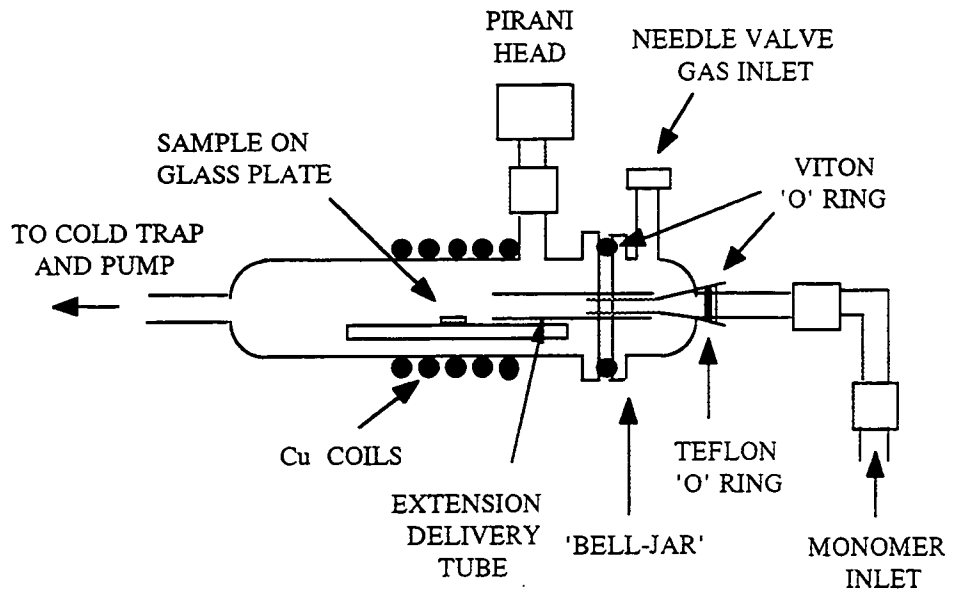

Fig. 1 Schematic diagram of the reactor with the modified monomer inlet.

The reactor was pumped down to a base pressure of 5.6×10^{-3} Torr. Hydrogen (99.992%, BOC) was purged through the reactor at an equilibrium pressure of 5.6×10^{-2} Torr for at least 10 min to give a flow rate 2.9×10^{-9} kgs^{-1}. The poorest leak rate for the system was 9.1×10^{-11} kgs^{-1}, providing at least 96.9% hydrogen gas. TiTP monomer, having been degassed by multiple-freeze-thaw cycles, was then purged through the reactor for 5 min via the sliding-joint and extension delivery tube to give a combined equilibrium pressure of 6.4×10^{-2} Torr. Plasma deposition times were dependent on the sampling depths of the analytical technique used; 5 min were adequate for XPS analysis whilst 30 min were required for ATR-FTIR analysis because thicker films were needed to give a sufficient sample signal. After extinguishing the plasma, the monomer was shut off and hydrogen was purged through at the above pressure for 5 min. The reactor was then brought up to atmosphere after valving off the hydrogen supply and samples were transferred to the relevant analytical spectrometer.

Substrates used were as described in the Chapter 3, i.e. glass for XPS analysis and polyethylene film for ATR-FTIR analysis. The reactor was scrubbed with detergent after every other 5 min deposition, rinsed with isopropyl alcohol, dried in an oven, then subjected to a high power (50 W) cleaning air plasma for 60 min. For longer depositions required for ATR-FTIR, the reactor was scrubbed after every deposition. When the

reactor was not scrubbed with detergent, it was cleaned only with a high power (50 W) air plasma. Since oxygen glow discharges are renowned for their ability to oxidize polymer surfaces,[7] polyethylene substrates were absent during the air plasma treatment.

4.3 RESULTS

During plasma ignition, a grey/black film was deposited primarily on all the surfaces within the RF coils. On exposure to air, the films tended to fade slightly in colour though this effect was much less pronounced compared with samples deposited from TiTP alone. For 30 min depositions (in the case of ATR), the polyethylene film became coated with dark localized elliptical coloured diffraction patterns which appeared to emerge from the end of the extension delivery tube. The colour intensity again tended to be darker at higher powers and faded with time. The films also had a tendency to curl, particularly at the higher powers. This has been observed with films possessing intrinsic tensile stress when deposited onto flexible substrates.[4] The presence of the grey/black colour[8,9] suggests the presence of TiO_x where $0 \leq x \leq 2$. This indicates that titanium has a lower oxidation state than +IV. (This was also observed in the absence of hydrogen-see Chapter 3 section 3.3.)

4.3.1 X-RAY PHOTOELECTRON SPECTROSCOPY (XPS)

Fig. 2 shows that the carbon content remains constant with increasing glow discharge power, whilst the titanium and oxygen contents slightly decrease and the nitrogen content slightly increases. Deposition of titanium species (i.e. the grey/black deposit) takes place predominately at the end of the extension delivery tube where TiTP enters the reactor. Since the distance between the substrate and the end of the extension delivery tube is so small (2 cm), the extent of plasma polymerization becomes limited, resulting in an almost constant composition with increasing glow discharge power.

The small presence of nitrogen on the surface, typically with values between 1-3% (though up to a maximum value of 6%) is of interest since it is present in all cases. The source of nitrogen is a matter of speculation. The possibilities include: leaks in the reactor system, nitrogen impurity in the hydrogen gas or as a result of a surface chemical reaction on exposure to air. Assuming that the hydrogen was nominally pure as stated by the manufacturer, and given the fact that nitrogen is observed for even the lowest leak rates, the most likely explanation for the appearance of nitrogen is as a result of a chemical reaction on exposure of the samples to air. The binding energies of the weak N(1s) XP spectra support this latter explanation: maxima were located at an average

binding energy of 400.5 ± 0.2 eV suggesting the formation of C-N or nitrogen bonded to oxidized carbon.[10] The most likely explanation therefore is the reaction of atmospheric nitrogen with free radicals trapped in the plasma polymer.[11] The slight increase in the nitrogen content with power then corresponds with the greater number of trapped free radicals formed at higher glow discharge powers.[12]

Other proposals, for example the dissociative chemisorption of nitrogen on metallic titanium[13-17] forming the nitride[14] or the fixation of molecular nitrogen[18] to the surface of TiO_2, can be excluded because of inappropriate binding energies observed here.

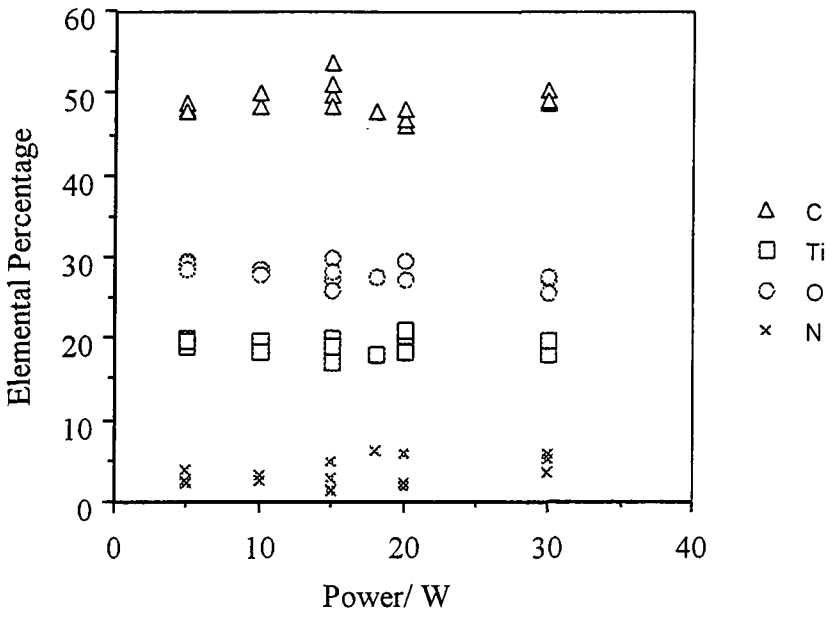

Fig. 2 Elemental composition as a function of glow discharge power (5 min, 19 cm).

Typical C(1s) and Ti(2p) spectra are shown in Fig. 3 for a 5 W, 5 min deposition. A range of carbon functionalities can be fitted to the C(1s) envelope, Fig. 3(a): hydrocarbon (C_xH_y ~285.0 eV); carbon adjacent to a carboxylate group ($\underline{C}CO_2$ ~285.7 eV); carbon singly bonded to an oxygen atom (C-O ~286.6 eV); carbon singly bonded to two oxygen atoms or carbon doubly bonded to one oxygen atom (O-C-O or C=O ~287.9 eV); carboxylate group (O-C=O ~289.0 eV) and carbonate group (O-C(=O)-O ~290.0 eV).[19] The $Ti(2p_{3/2})$ and $Ti(2p_{1/2})$ peaks, Fig. 3(b), are centred at 458.8 ± 0.2 eV and 464.4 ± 0.2 eV respectively which agree with the literature values for TiO_2.[20-22]

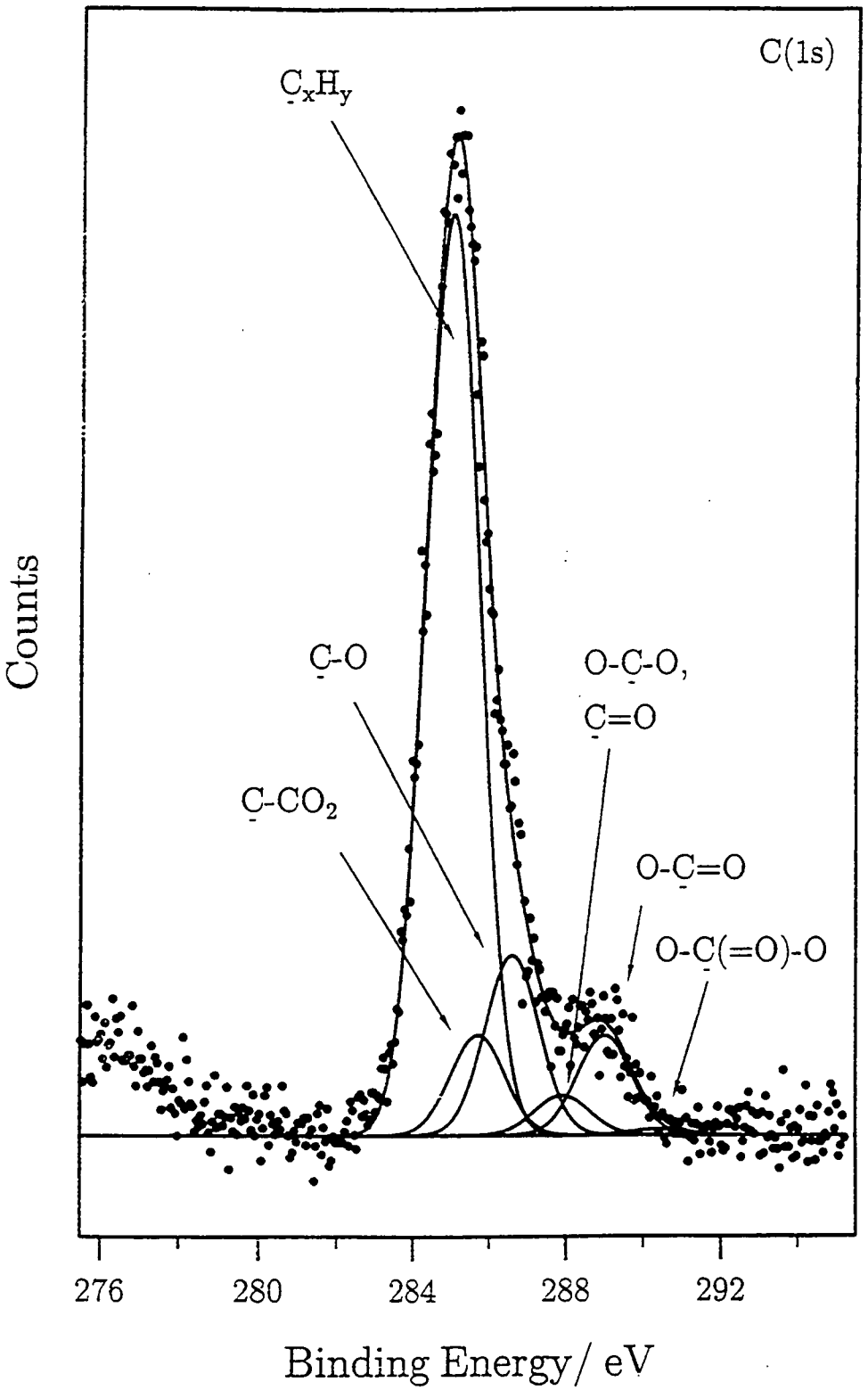

Fig. 3(a) C(1s) XP spectrum for PACVD of TiTP/H_2 onto a glass substrate (5 W, 5 min, 19 cm).

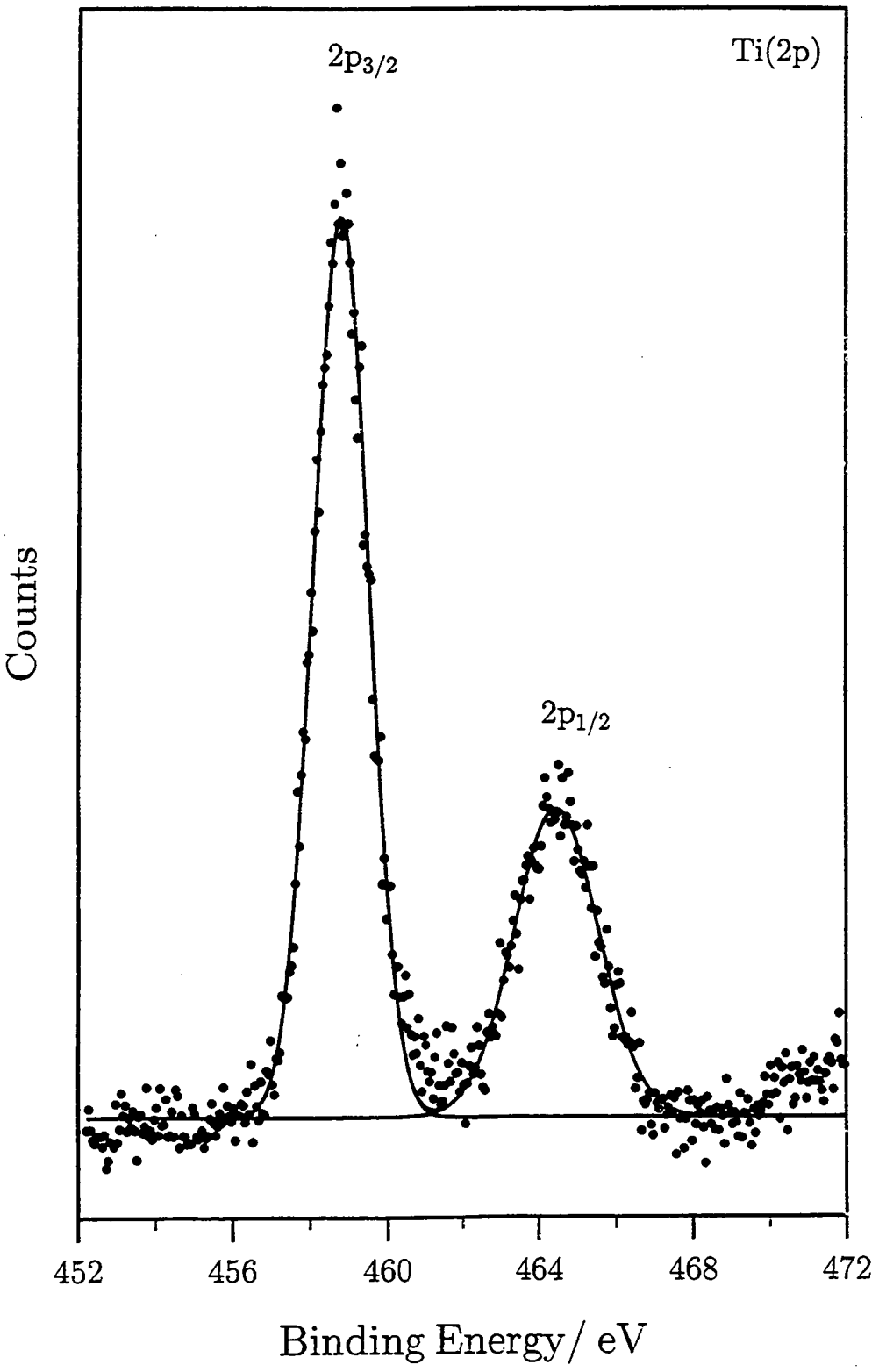

Fig. 3(b) Ti(2p) XP spectrum for PACVD of TiTP/H_2 onto a glass substrate (5 W, 5 min, 19 cm).

Deconvolution of the O(1s) spectrum, Fig. 3(c), is not possible since there are a number of likely environments that could be present at higher binding energies of the peak at 530.3 ± 0.2 eV which is associated to TiO_2.[20,23] Possible assignments for the higher binding energy environments include oxygenated carbon species,[10] substoichiometric oxide[22] or adsorbed water or OH on the surface.[24]

Further support for the localized deposition in the RF coils, particularly of the titanium species, is confirmed by samples placed downstream of the RF coils at 25.5 cm from the sliding-joint inlet. Primarily hydrocarbon was deposited with small amounts of oxygen, titanium and nitrogen. Silicon was also observed occasionally, indicating incomplete coverage of the glass substrates.

An aging study was carried out using two adjacent slides at a glow discharge power of 15 W. The aged sample was left in ambient conditions for approximately one month. Evidence of aging was not apparent since the results obtained were found to be the same within the limitations of experimental error. Aging is expected at the surface in plasma polymers due to the reaction of oxygen and/or water with trapped free radicals[12] and complete oxidation of any remaining suboxide titanium metal centres to give TiO_2.

An approximate electrical resistance measurement was carried out on a 30 W plasma polymer deposited on polyethylene using a digital multimeter (Fluke 73) where two probes were placed ~3 mm apart on the film. A value for the resistance of less than 10.5 kΩ was observed. This value is lower than that measured for uncoated polyethlene (> MΩ range). Therefore the surface conductivity for coated polyethylene is greater than that for clean polyethylene.

4.3.2 XPS DEPTH PROFILING

In Fig. 4 the carbon content rapidly decreases on removal of adventitious contamination and low molecular weight hydrocarbon species before levelling off, whilst the titanium follows an opposite trend. The oxygen content initially increases before beginning to decrease between 120-420 s. The broadening observed in the Ti(2p) XP region to lower binding energies, Fig. 5(a), indicates the presence of suboxides of titanium,[24] which is supported by the shift to higher binding energies in the O(1s) XP region, Fig. 5(b).[25] The existence of suboxides within the bulk prior to sputtering is likely, though the sputtering induced loss of oxygen to form suboxides is also highly probable.[26] The nitrogen content remains virtually constant.

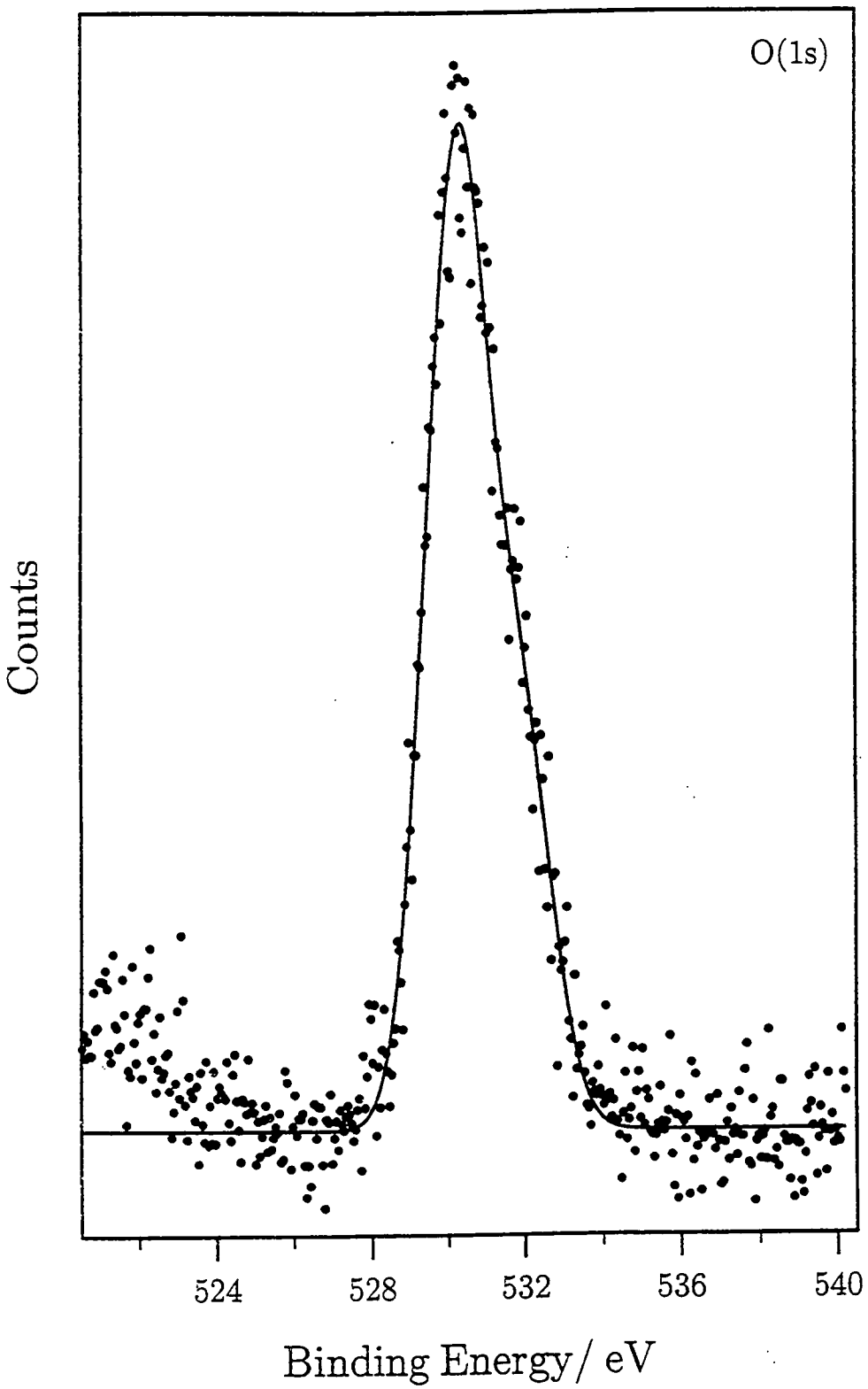

Fig. 3(c) O(1s) XP spectrum for PACVD of TiTP/H_2 onto a glass substrate (5 W, 5 min, 19 cm).

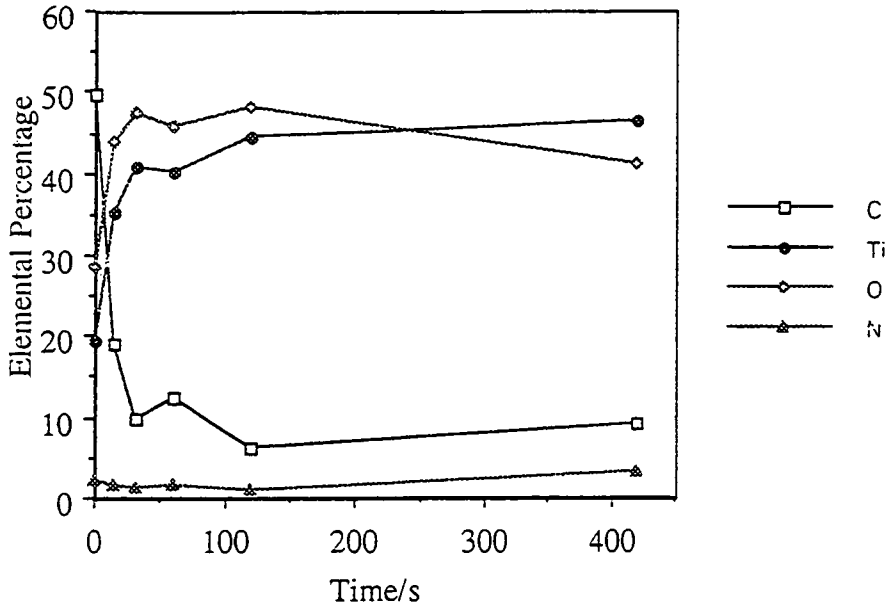

Fig. 4 XPS depth profile for PACVD of TiTP/H_2 onto a glass substrate (15 W, 5 min, 19 cm).

4.3.3 ATTENUATED TOTAL REFLECTION FOURIER TRANSFORM INFRARED SPECTROSCOPY (ATR-FTIR)

There appears to be little change in the ATR spectra with increasing power (see Fig. 6) and no significant changes are observed on aging the samples in ambient conditions for at least a month. A weak broad band above 3000 cm^{-1} suggests the presence of O-H[27] as observed in Fig. 7 for the 5 W plasma polymer. Two weak bands around 1630 cm^{-1} and 1570-1580 cm^{-1} are observed. In the former case this may be due to the presence of vinyl groups[27] or O-H bending in physisorbed water;[28] the latter case indicates the formation of the asymmetric carboxylate[27] (CO_2^-) stretch. There is little evidence of any absorbances in the 1250-1000 cm^{-1} region. On close examination, there appears to be very weak peaks at 1128 cm^{-1} and 1165 cm^{-1} which are indicative of the isopropyl group[29] or due to alcoholic C-O stretching.[27] The large absorbance region below 1000 cm^{-1} is still the main feature, and this is assignable to bulk lattice vibrations[30] seen in amorphous TiO_2.

The 5 W, 30 min reactor profile indicates a very localized deposition and only a slight attenuation of the most surface sensitive polyethylene peaks just below 3000 cm^{-1} is observed downstream, Fig. 8.

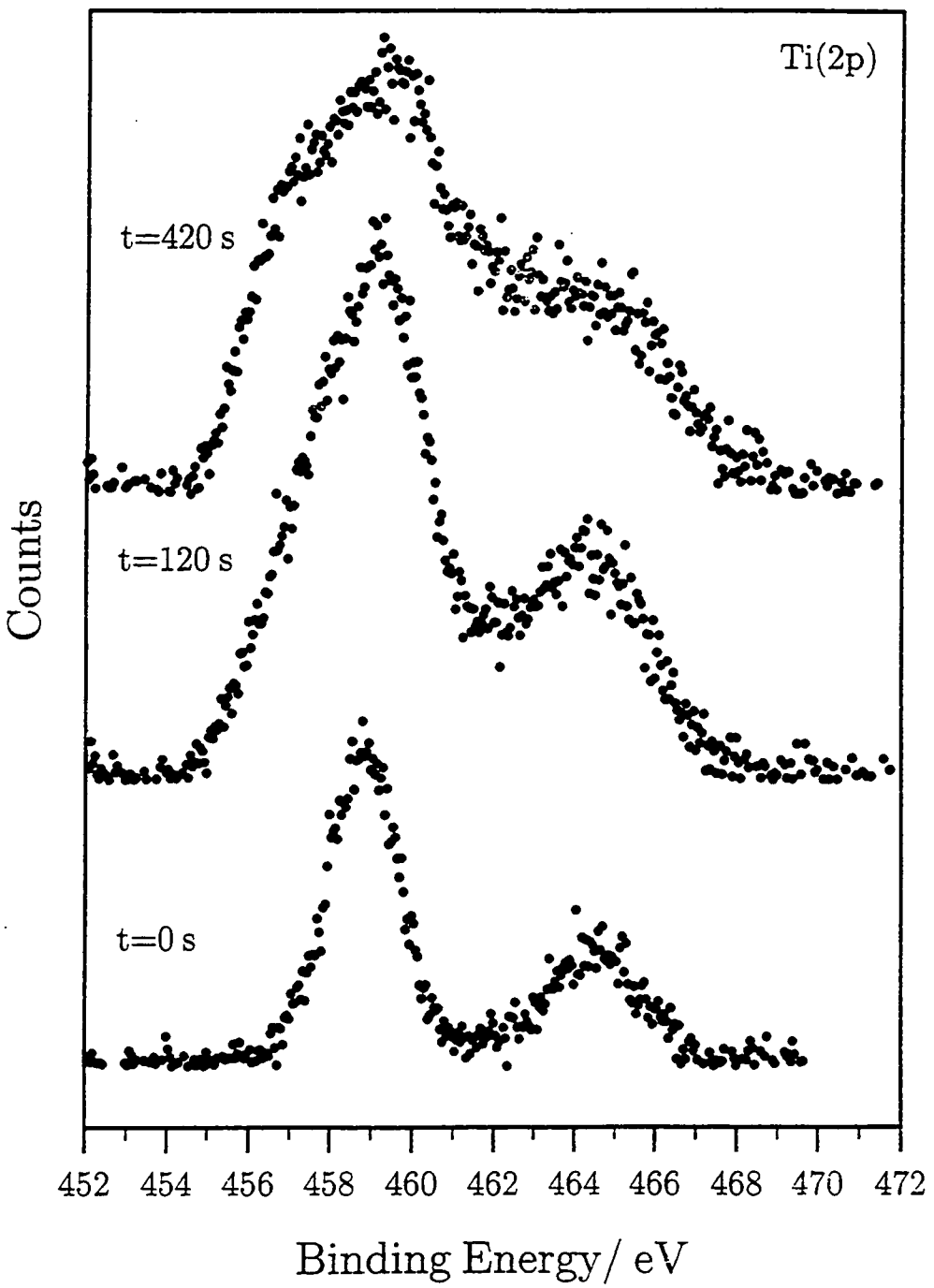

Fig. 5(a) Ti(2p) XP depth profile spectra of PACVD of TiTP/H_2 onto a glass substrate (15 W, 5 min, 21.5 cm) recorded for given sputtering times.

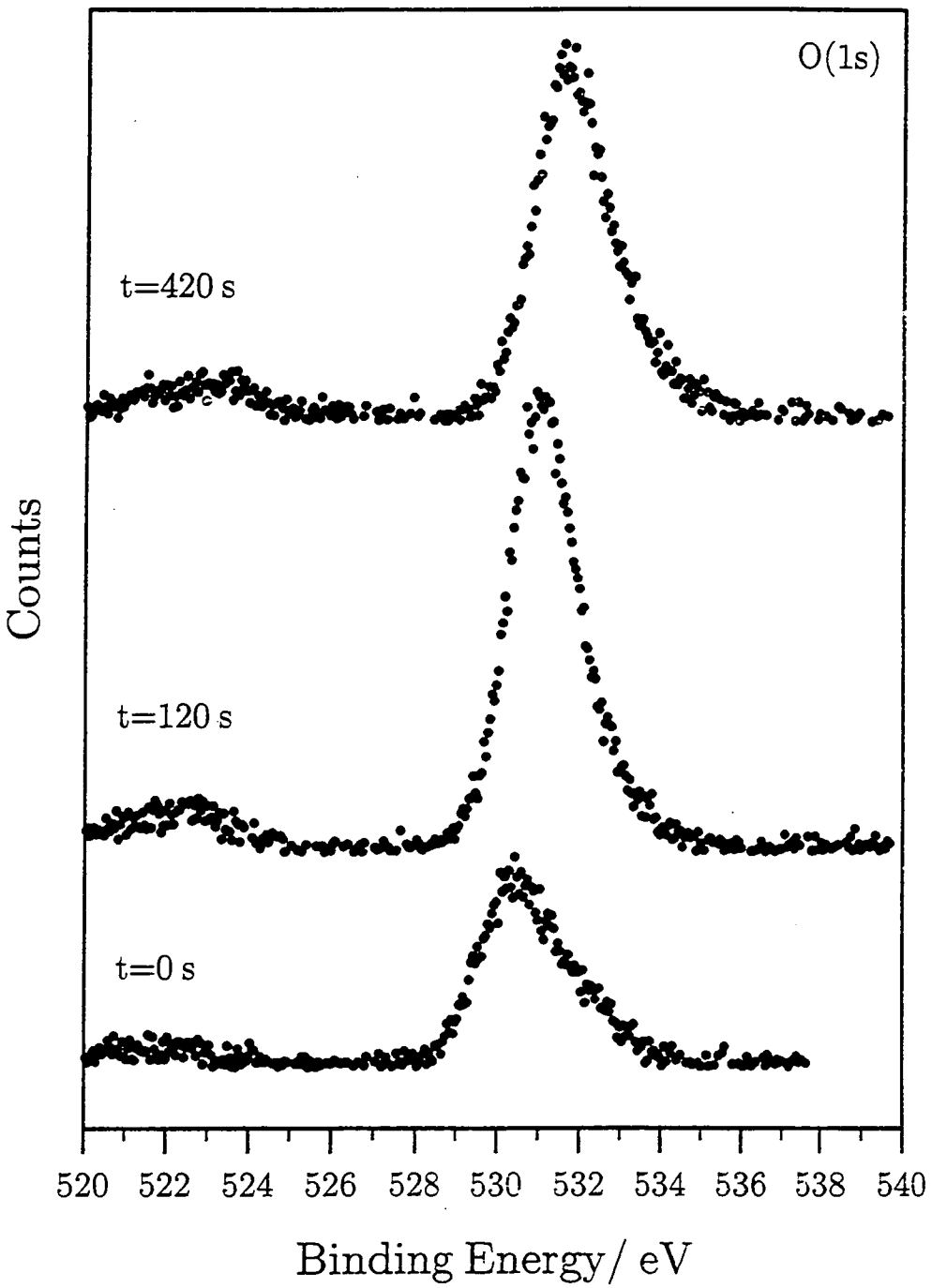

Fig. 5(b) O(1s) XP depth profile spectra of PACVD of TiTP/H_2 onto a glass substrate (15 W, 5 min, 21.5 cm) recorded for given sputtering times.

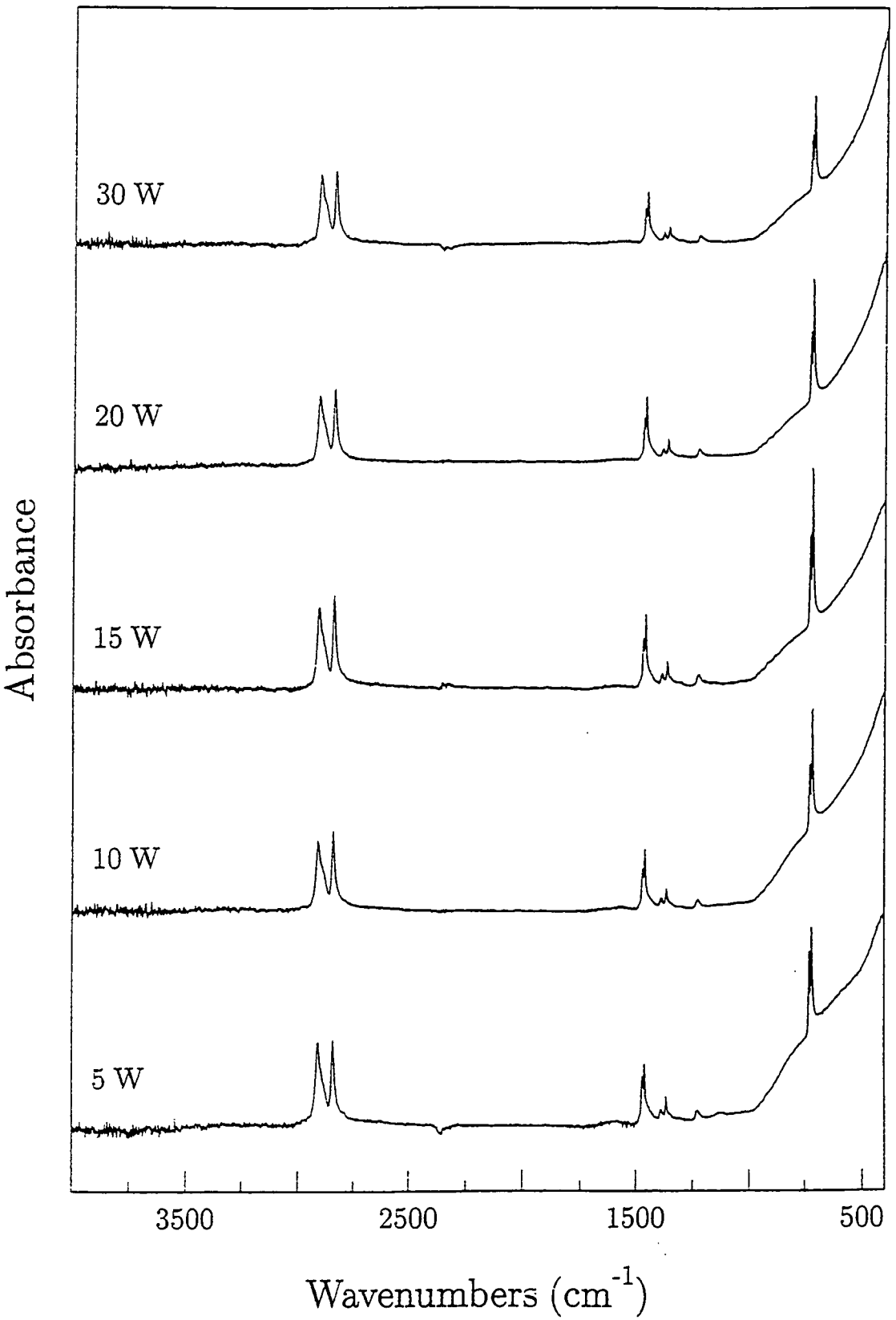

Fig. 6 ATR-FTIR spectra for PACVD of TiTP/H_2 onto polyethylene film as function of glow discharge power (30 min, 19 cm).

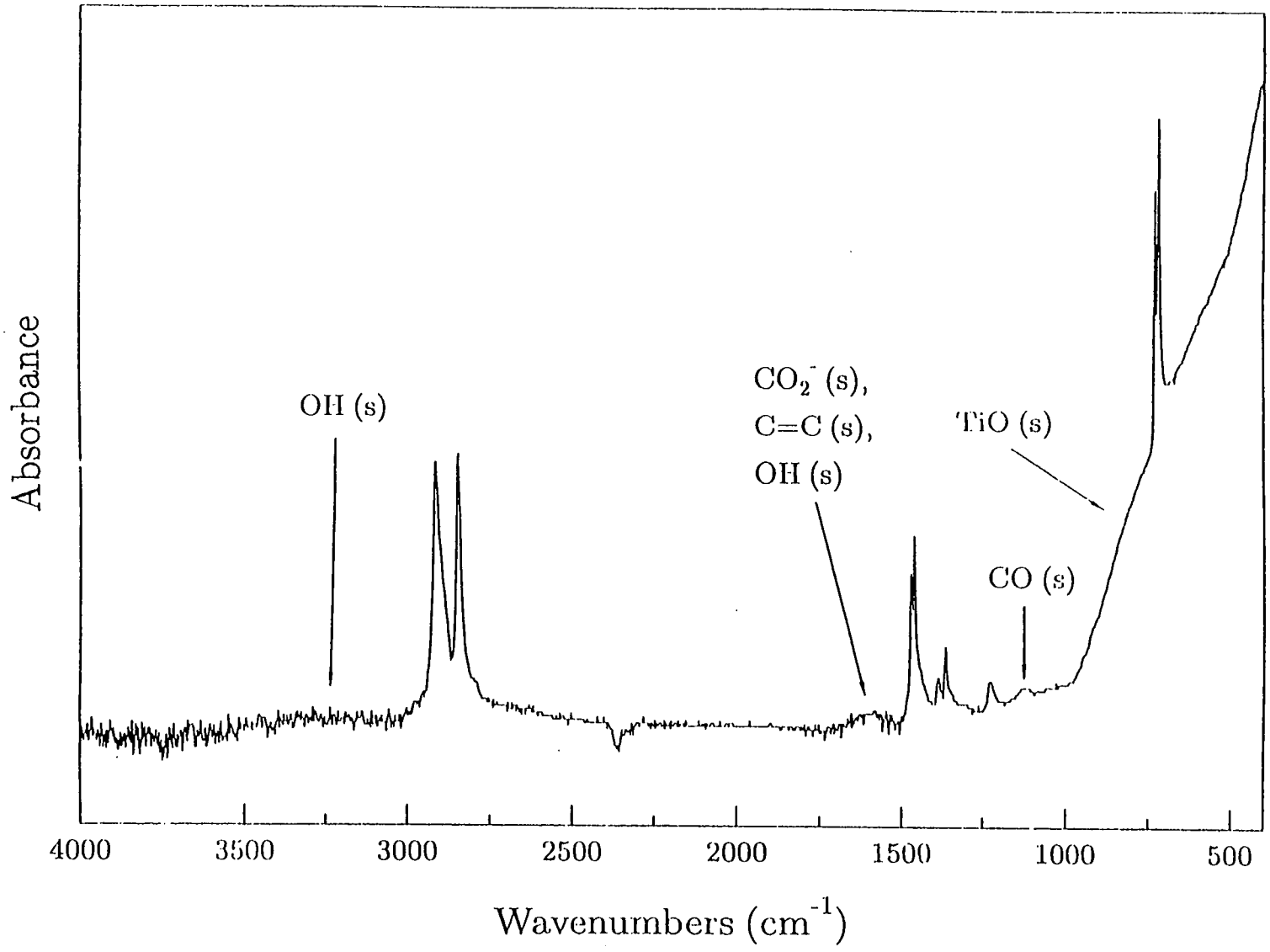

Fig. 7 ATR spectrum of the PACVD of TiTP/H_2 onto a polyethylene substrate (5 W, 30 min, 19 cm).

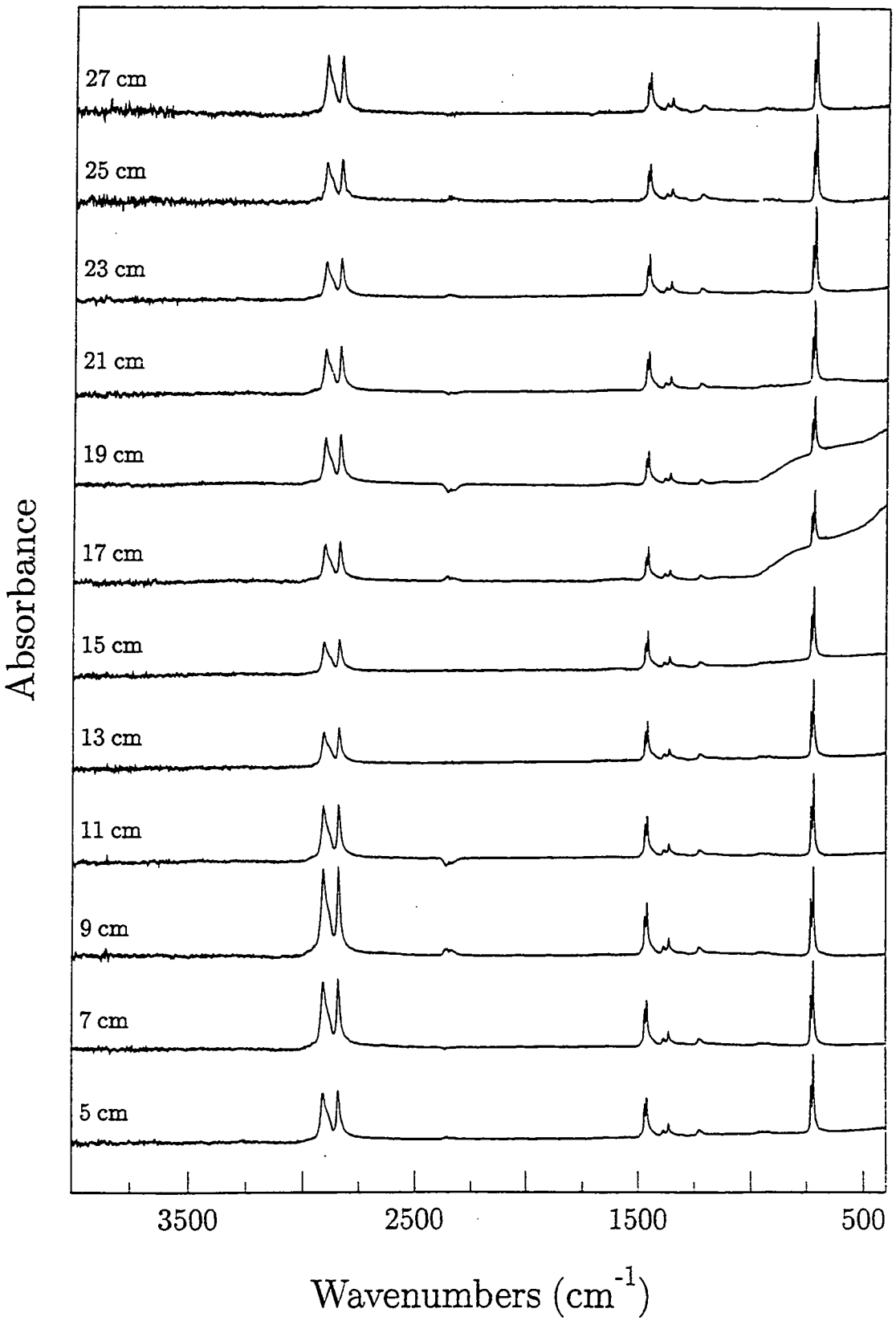

Fig. 8 ATR-FTIR reactor profile for TiTP of PACVD coating onto polyethylene (5 W, 30 min).

4.3.4 ATOMIC FORCE MICROSCOPY (AFM)

In the AFM image in Fig. 9 it can be clearly seen that the surface is covered with particles. Such powder particle or dust formation is thought to initiate in the gas phase[4] at the plasma/sheath boundary[31,32] from where particles deposit onto the film surface under the influence of gravity[4] on extinction of the plasma.[31]

4.4 DISCUSSION

The grey/black colour of the deposited films suggests the presence of suboxides of titanium.[8,9] The addition of hydrogen appears to have created a better reducing environment in comparison to those films deposited in the absence of hydrogen, since on visual inspection the oxidation to TiO_2 that takes place on exposure to air does not occur instantaneously. Note however that the presence of the corresponding binding energies for TiO_2 (in the Ti(2p) and O(1s) XP regions) confirms that oxidation on atmospheric exposure does take place.

The XPS depth profiling study indicates the presence of titanium suboxides within the bulk; such species are likely to exist within the bulk (which are oxidized on the surface) and are also created by the preferential sputtering of oxygen by Ar-ion bombardment.[26]

The redesigned reactor configuration required to allow the addition of hydrogen during plasma polymerization results in a very localized deposition region. Observation by ATR-FTIR shows that thinner films are deposited using this reactor configuration. This may be attributable to the lower monomer flow rate and reactor design.

Both the XPS and ATR-FTIR (17-19 cm from the sliding-joint inlet, Fig. 8) profile studies indicate the titanium species are deposited almost immediately after the monomer leaves the end of the extension delivery tube, whilst the organic decomposition products pass further along the reactor and undergo greater plasma polymerization. Since the distance for the monomer to travel between the end of the extension delivery tube to the substrate is small (2 cm), the fall in monomer flow rate, F_m,[33] arising from the fragmentation and hence degree of plasma polymerization, becomes almost independent of the glow discharge power. Therefore the observed elemental composition remains virtually constant on increasing the glow discharge power.

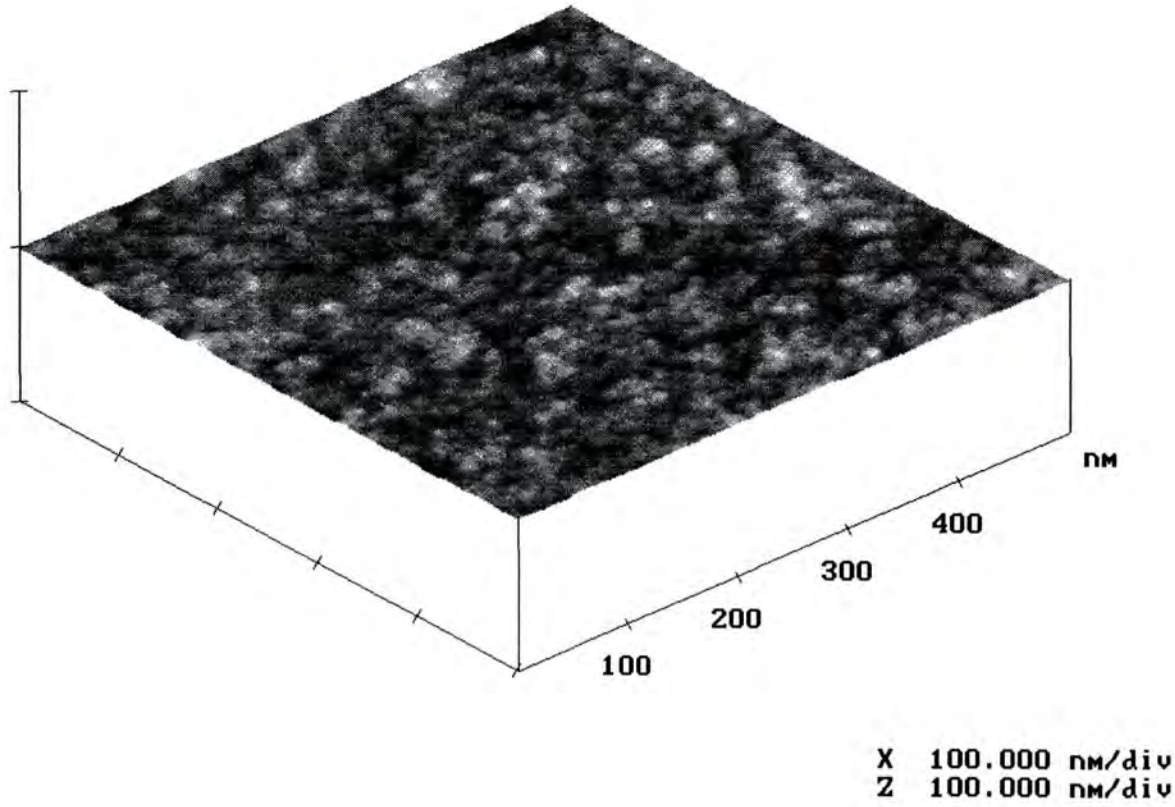

Fig. 9 AF micrograph for PACVD of TiTP/H_2 onto a glass substrate (15 W, 5 min, 19 cm).

During plasma polymerization of organic and metallorganic precursors, many new species are created in the gas phase as well as hydrogen as a major byproduct.[12] Molecular hydrogen in a plasma primarily dissociates into hydrogen radicals[34] which are able to recombine with other reactive radicals to produce stable gaseous molecular species. As a result, the addition of hydrogen increases the chances for molecular recombination:

$$R\cdot + H\cdot \rightarrow RH$$

Because the extent of plasma polymerization becomes limited using this reactor configuration, many stable organic gaseous byproducts that are formed pass harmlessly downstream. Further evidence of this is shown by the ATR-FTIR which primarily indicates Ti-O species and very little organic species (e.g. reduction of isopropyl groups) in comparison to the TiTP plasma polymers.

Long term aging is also absent, which is confirmed by both XPS and ATR-FTIR techniques. Passivation of the films to oxidation may result from the presence of excess hydrogen free radicals during deposition which 'quench' trapped free radicals via recombination reactions. This would be in agreement with stable films to oxidation deposited from hexamethyldisiloxane and hydrogen by glow discharge.[5] A similar response was observed for the plasma polymerization of styrene films that were treated with a post deposition hydrogen plasma.[6] However the incorporation of nitrogen to the films is likely to arise from the manifestation of atmospheric nitrogen reacting with trapped free radicals in the films.[11]

AFM confirms that the gas phase reactions are dominant in the film growth process.[4] Powder particles, observed on the surface, are formed in the gas phase and fall under the influence of gravity to become embedded into the growing film.

4.5 CONCLUSIONS

Localized deposition results from the redesigned reactor configuration, and the addition of hydrogen to a TiTP plasma generates films stable to aging. The increased hydrogen content in the plasma volume helps create stable volatile organic decomposition byproducts and 'quenches' any trapped free radicals. As a result of the small distance between the substrate and the delivery of monomer to the reactor, the stable organic decomposition products do not undergo plasma polymerization to any great extent. Such species pass through the reactor leaving $TiO_2/C_wH_xO_yN_z$ deposited films, and as

a result of the redesigned reactor, the compositions become almost independent of glow discharge power. The titanium species are likely to possess an oxidation state less than +IV beneath an outer TiO_2 layer. Deposition is governed by gas phase reactions with the formation of powder particles.

4.6 REFERENCES

1. S.R. Kurtz, R.G. Gordon, *Thin Solid Films*, **147**, 187, 167.
2. P.A. Cox, The Electronic Structure and Chemistry of Solids, O. U. P., Oxford, 1989.
3. D.S. Ginley, M.L. Knotek, *J. Electrochem. Soc.*, **126**, 1979, 2163.
4. R. d'Agostino, Ed., Plasma Deposition, and Etching of Polymers, Academic Press, London, 1990.
5. L.S. Tusov, V.M. Kolotyrkin, N.N. Tunitskii, *Int. Chem. Eng.*, **11**, 1971, 60.
6. G. Sawa, S. Yamanaka, S. Nakamura, S. Yamaguchi, *Jpn. J. Appl. Phys.*, **20**, 1981, L201.
7. A.G. Shard, J.P.S. Badyal, *Macromolecules*, **25**, 1992, 2053.
8. Gmelins Handbuch, Der Anorganischen Chemie, Titan, Vol. 41, Verlag Chemie, GMBH, Weinhelm/Bergstraße, 1951, p. 214.
9. H. Holzschuh, *Diploma Theses*, 1987, Eberhard-Karls-Universität, Tübingen.
10. G. Beamson, D. Briggs, High Resolution XPS of Organic Polymers, The Scienta ESCA300 Database, John Wiley, Chichester, 1992.
11. N. Inagaki, H. Kawai, *J. Polym. Sci. Polym. Chem. Ed.*, **24**, 1986, 3381.
12. H. Yasuda, Plasma Polymerization, Academic Press, Orlando, FL., 1985.
13. H.D. Shii, F. Jona, *Surf. Sci.*, **60**, 1976, 445.
14. W. Brearley, N.A. Surplice, *Surf. Sci.*, **64**, 1977, 372.
15. Y. Fukoda, F. Honda, J.W. Rabalais, *Surf. Sci.*, **91**, 1980, 165.
16. B.M. Biwer, S.L. Bernasek, *Surf. Sci.*, **167**, 1986, 207.
17. L. Soriano, M. Abbate, J.C. Fuggle, L. Jiménez, J.M. Sanz, L. Galán, C. Mythen, H.A. Padmore, *Surf. Sci.*, **281**, 1993, 120.
18. R.I. Bickley, R.K.M. Jayanty, C. Real, M. Macias, *Surf. Sci.*, **251/252**, 1991, 1052.
19. D.T. Clark, A. Dilks, *J. Polym. Sci. Polym. Chem. Edn.*, **17**, 1979, 957.
20. N.C. Saha, H.G. Tompkins, *J. Appl. Phys.*, **72**, 1992, 3072.
21. Handbook of X-Ray Photoelectron Spectroscopy, Ed. C.D. Wagner, W.M. Riggs, L.E. Davis, J.F. Moulder, G.E. Muilenberg, Perkin-Elmer Corp., Eden Prairie, MN, 1979.
22. M. Murata, K. Wakino, S. Ikeda, *J. Electr. Spectr. Relat. Phenom.*, **6**, 1975, 459.
23. B. Siemensmeyer, K. Bade, J.W. Schutze, *Ber. Bunsenges. Phys. Chem.*, **95**, 1991, 1461.
24. C.N. Sayers, N.R. Armstrong, *Surf. Sci.*, **178**, 1977, 301.
25. M.V. Kaznetsov, J.F. Zhuravlev, V.A. Zhilyaev, V.A. Gubanov, *J. Electr. Spectr. Relat. Phenom.*, **58**, 1992, 1.
26. J.W. Coburn, *Thin Solid Films*, **64**, 1979, 371.

27. R.M. Silverstein, G.C. Bassler, T.V. Morrill, Spectrometric Identification of Organic Compounds, 4th Edn., John Wiley, New York, 1981.
28. D.J.C. Yates, *J. Chem. Phys.*, **65**, 1961, 1366.
29. C.T. Lynch, K.S. Mazdiyasni, J.S. Smith, W.J. Crawford, *Anal. Chem.*, **36**, 1964, 2332.
30. M. Ocaña, W.P. Hsu, E. Matijevic, *Langmuir*, 7,1991, 2911.
31. G.S. Selwyn, K.L. Haller, E.F. Patterson, *J. Vac. Sci. Technol.*, **A11**, 1993, 1132.
32. Y. Watanabe, M. Shiratani, *Jpn. J. Appl. Phys.*, **32**, 1993, 3074.
33. S.Y. Park, N. Kim, *J. Appl. Polym. Sci. Polym. Appl. Symp.*, **46**, 1990, 91.
34. C.C. Goodyear, A. Von Engel, *Proc. Phys. Soc.*, **79**, 1962, 732.

CHAPTER 5:
PLASMA ASSISTED CHEMICAL VAPOUR DEPOSITION OF TITANIUM OXYNITRIDE/POLYMER FILMS FROM TITANIUM TETRAISOPROPOXIDE AND AMMONIA

5.1 INTRODUCTION

The introduction of nitrogen gas to organic or metallorganic/organometallic vapour usually gives rise to the formation of amine and imine groups on plasma activation.[1] However ammonia, an alternative nitrogen containing source, is more reactive than nitrogen gas since in addition to forming the above groups it may enhance the elimination of organic groups from the polymer film via the formation of nitrogen bridges between the metal atoms. Such greater reactivity arises from the lower dissociation energy[2] of ammonia (NH_3 ~391 $kJmol^{-1}$)[3] compared to nitrogen gas (N_2 ~944 $kJmol^{-1}$).[4] Because of this greater reactivity, the microelectronics industry[5] uses ammonia extensively to produce Si_3N_4 with silane, SiH_4, or silicon tetrachloride, $SiCl_4$.

Plasma polymerization of tetramethyltin and ammonia has led to Sn-N bond formation.[6] It was suggested that ammonia assists dehydrocarbonation. However films of low nitrogen content were found on hydrolysis in air of the Sn-N bond. Sadhir *et al.* produced amorphous AlN and aluminium containing polymeric films by PACVD using trimethylaluminium and nitrogen or ammonia gases at room temperature.[7] UV-VIS and IR spectroscopy indicated that the choice of nitrogen or ammonia had little effect on the plasma chemistry.

Very little PACVD work has been reported using TiTP in the presence of a nitrogen containing coreactant. Nitrogen gas has been used with TiTP in the presence of hydrogen[8,9] and also with hydrogen and argon.[10] Wierzchon *et al.* produced multicomponent Ti(O,C,N) layers[8,9] and Mayr and Stock deposited cubic titanium oxycarbonitride, Ti(O,C,N), films.[10] The latter found that the layer composition did not vary significantly between 500-700 °C and the layers were not as hard as stoichiometric TiN deposited by magnetron sputtering. However to the author's knowledge there is no evidence of PACVD using TiTP and ammonia. Such a combination may be an alternative method of producing TiN/polymer composite films, using the greater reactivity of ammonia in contrast to nitrogen gas to enhance Ti-N bond formation. The work described in this chapter set out to deposit such films using the above precursor/gas system.

5.2 EXPERIMENTAL

The reactor configuration used (with the modified monomer inlet) is described in Chapter 4. Similarly, the same reactor cleaning procedure was carried out. Before deposition, the reactor was pumped down to a base pressure of $5.6x10^{-3}$ Torr (after plasma cleaning) with a leak rate better than $8.7x10^{-11}$ kgs^{-1}, and then ammonia (Aldrich, anhydrous, 99.99+ %) was purged through the reactor for a minimum of 5 min at an equilibrium pressure at $5.6x10^{-2}$ Torr and a flow rate of $1.8x10^{-8}$ kgs^{-1}. This gave at least 99.5% ammonia gas in the system. The monomer, TiTP, was then allowed into the reactor for 5 min to give a combined pressure of about $6x10^{-2}$ Torr. The same deposition times and types of substrates for XPS and ATR-FTIR were used as described in Chapter 4. When the deposition time had elapsed the RF source was switched off and the monomer reservoir was closed. Ammonia was purged through the reactor for 2 min and the system was then pumped down for 2 min. The reactor was then brought up to atmosphere and the samples analyzed by the appropriate technique.

5.3 RESULTS

During the 5 min deposition, the glass slides turned a very pale yellow. The polyethylene strips went yellow at the lower powers and were darker yellow/green at the higher powers. Localized diffraction pattern coloured intense spots were also present which appeared to emerge at the point where the monomer left the extension delivery tube. The tendency for the polyethylene to curl was still apparent with increasing power, though to a lesser extent than with to the TiTP/H_2 system. On aging, the colours of the deposited films became less intense.

5.3.1 X-RAY PHOTOELECTRON SPECTROSCOPY (XPS)

It can be seen in Fig. 1 that the carbon and nitrogen contents initially increase before levelling off, whilst the titanium and oxygen contents follow an opposite trend. As in the process described in Chapter 4, the majority of the deposited titanium species occurs as soon as the monomer leaves the extension delivery tube, whilst the organic and ammonia species pass through the coil region and undergo a greater degree of plasma polymerization as the glow discharge power is increased.

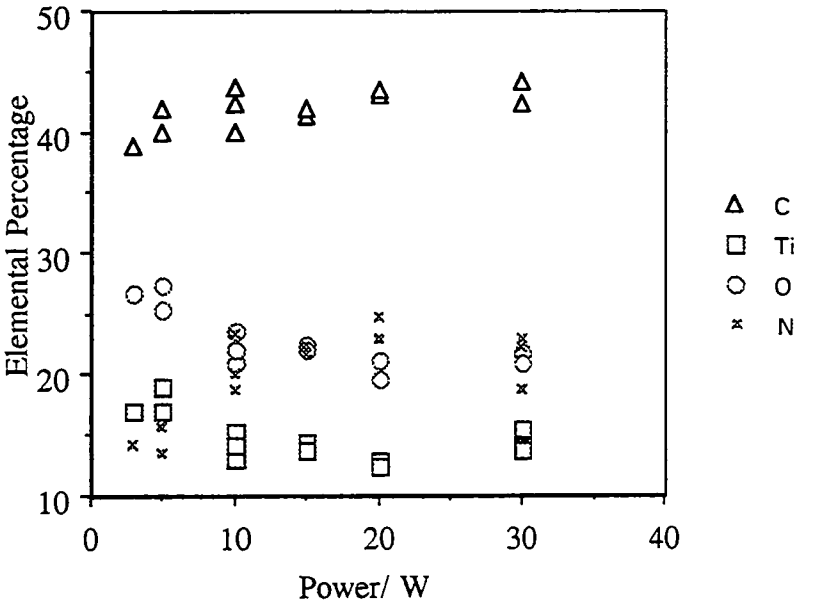

Fig. 1 Elemental composition as a function of glow discharge power (5 min, 19 cm).

The C(1s) XP spectra all have a large shoulder to higher binding energy of the hydrocarbon peak[11] at 285.0 eV as illustrated in Fig. 2(a) for the 30 W case. Due to the ambiguity of overlapping environments in this region (because, for example, the chemical shift of carbon bonded to oxygen or nitrogen depends on the nature of the substituents and amounts to 0.6, 0.7, 1.6, 1.8, 1.8, 2.9 and 4-4.5 eV for -NH_2, $\underline{C}CO_2$, $\underline{C}$-O, -NCO, -NO_2, O-$\underline{C}$-O or $\underline{C}$=O and O-$\underline{C}$=O),[11,12] it has not been possible to deconvolute the spectra with any degree of certainty. However the spectra have been fitted with four or five peaks to obtain the 'best fit' in order to determine an approximate charging offset value relative to the hydrocarbon environment at 285.0 eV.

The Ti(2p) XP spectra show peaks at 458.4 ± 0.1 eV ($2p_{3/2}$) and 464.0 ± 0.1 eV ($2p_{1/2}$), see Fig. 2(b), indicating TiO_2.[13,14] Evidence of the Ti-N environment (literature values between 455.0-455.5 eV have been assigned to the Ti($2p_{3/2}$) peak for TiN)[14-16] is not observable. The N(1s) XP spectra, see Fig. 2(c), confirm the lack of the N-Ti environment (typically found at 396.6-397.5 eV);[14-16] the maxima are located at 399.7 ± 0.2 eV with shoulders to higher binding energies. Possible assignments for the maxima correspond to amines and nitriles,[12] though deconvolution of the spectra have not been performed due to the ambiguity in the overlapping environments as discussed above.

Again, deconvolution of the O(1s) XP spectra, see Fig. 2(d), is not possible due to the different possible environments. The major environment at an average binding energy of 530.0 ± 0.2 eV closely resembles that for the oxide.[14,15] To higher binding energies, a variety of environments may exist, e.g. either oxidized carbon/oxidized carbon-nitrogen (O=C-N)[17] or substoichiometric oxide,[15] an oxynitride,[15] or adsorbed water[13,15] or OH.[13]

Two explanations may account for the absence of any nitride in the Ti(2p) and N(1s) XP regions; either no Ti-N bond formation occurred during deposition or the Ti-N surface is capped with the well known oxide layer.[15]

An aging study was carried out using two adjacent slides at a glow discharge power of 15 W. The aged sample was left in ambient conditions for approximately one month. Table 1 clearly indicates that oxidation took place. The increases at higher binding energies in the C(1s) and O(1s) XP regions shown in Fig. 3(a) and Fig. 3(b) respectively are most noticeable. The presence of trapped free radicals[18] reacting with water and/or oxygen would account for this, in addition to increased adsorbed water[15] and OH[13] on the oxide surface. Within experimental error, there was no observable change in the Ti(2p) XP spectra, because the titanium was in its fully oxidized state. The data has been normalized in order to show the qualitative peak shape changes. Loss of nitrogen is explained in the Discussion, section 5.4.

Table 1 The effect on elemental composition and ratios due to a months aging for the 15 W, 5 min TiTP/NH_3 plasma polymer.

Sample	% C ± 0.1	% Ti ± 0.1	% O ± 0.1	% N ± 0.1	Ti/C ± 0.01	O/C ± 0.01	N/C ± 0.01	Ti/O ± 0.01	Ti/N ± 0.01
Fresh	43.0	15.5	23.5	18.0	0.36	0.55	0.42	0.66	0.86
Aged	39.2	15.4	33.2	12.2	0.39	0.85	0.31	0.46	1.26

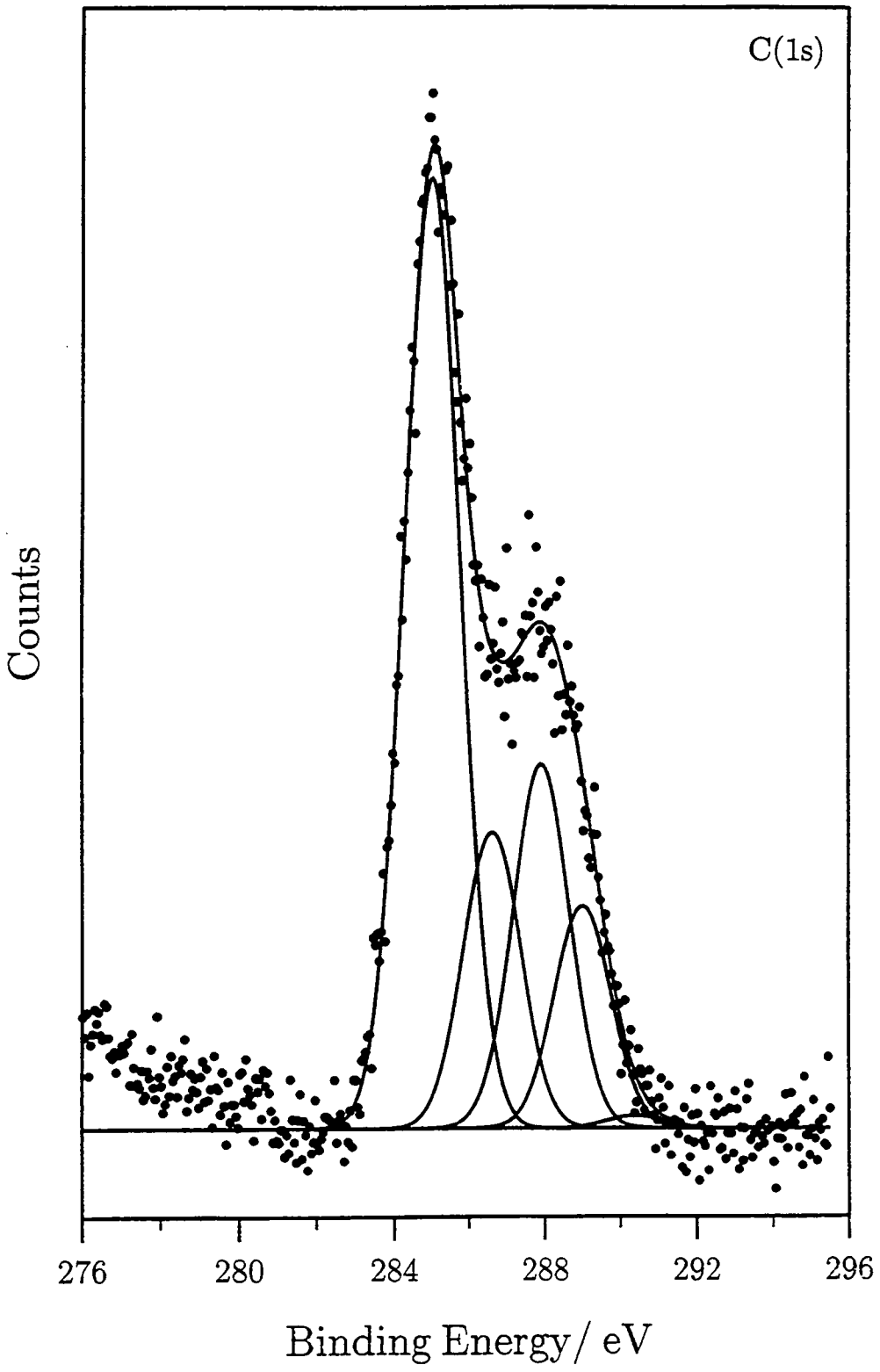

Fig. 2(a) C(1s) XP spectrum for PACVD of TiTP/NH_3 onto a glass substrate (30 W, 5 min, 19 cm).

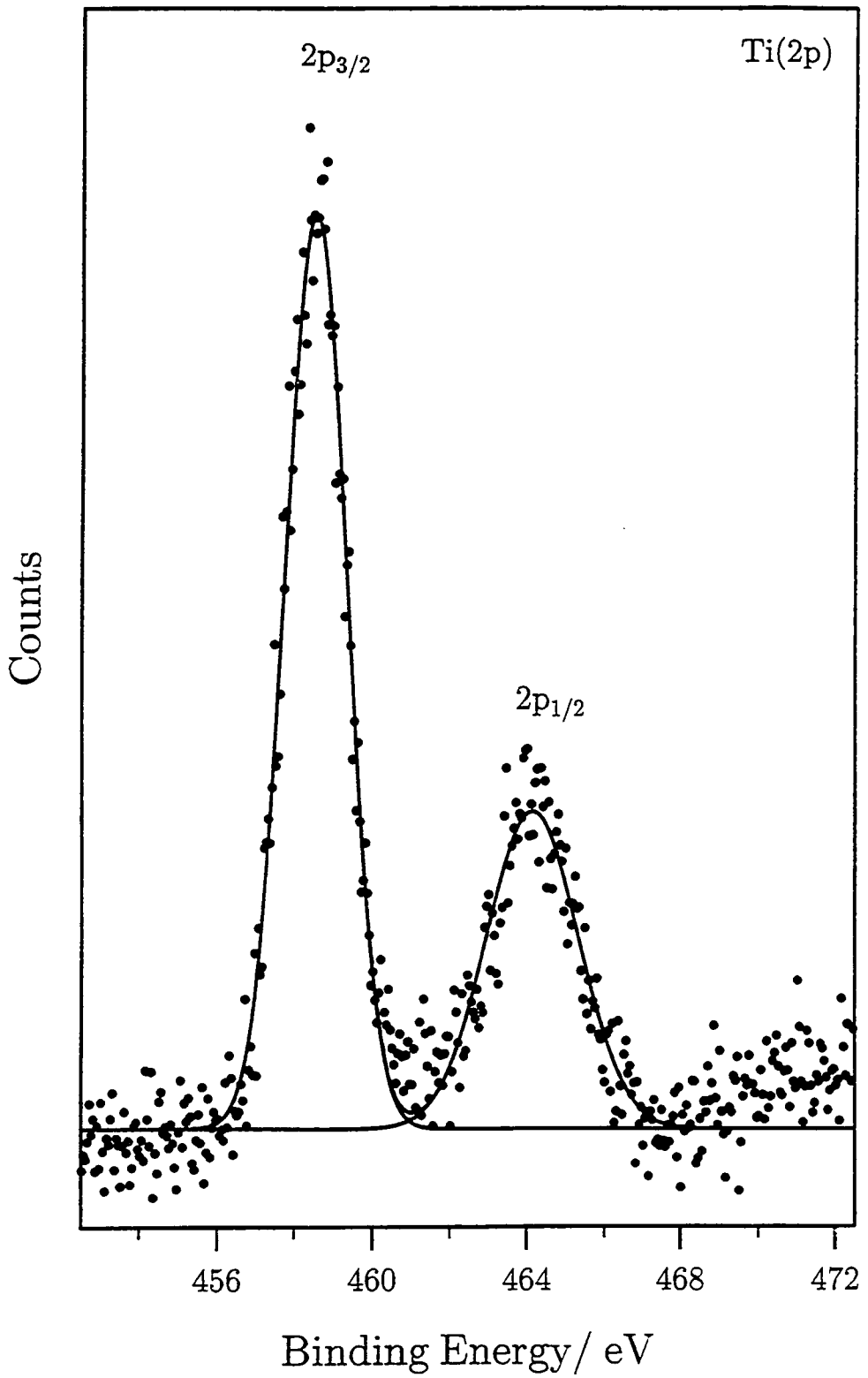

Fig. 2(b) Ti(2p) XP spectrum for PACVD of TiTP/NH_3 onto a glass substrate (30 W, 5 min, 19 cm).

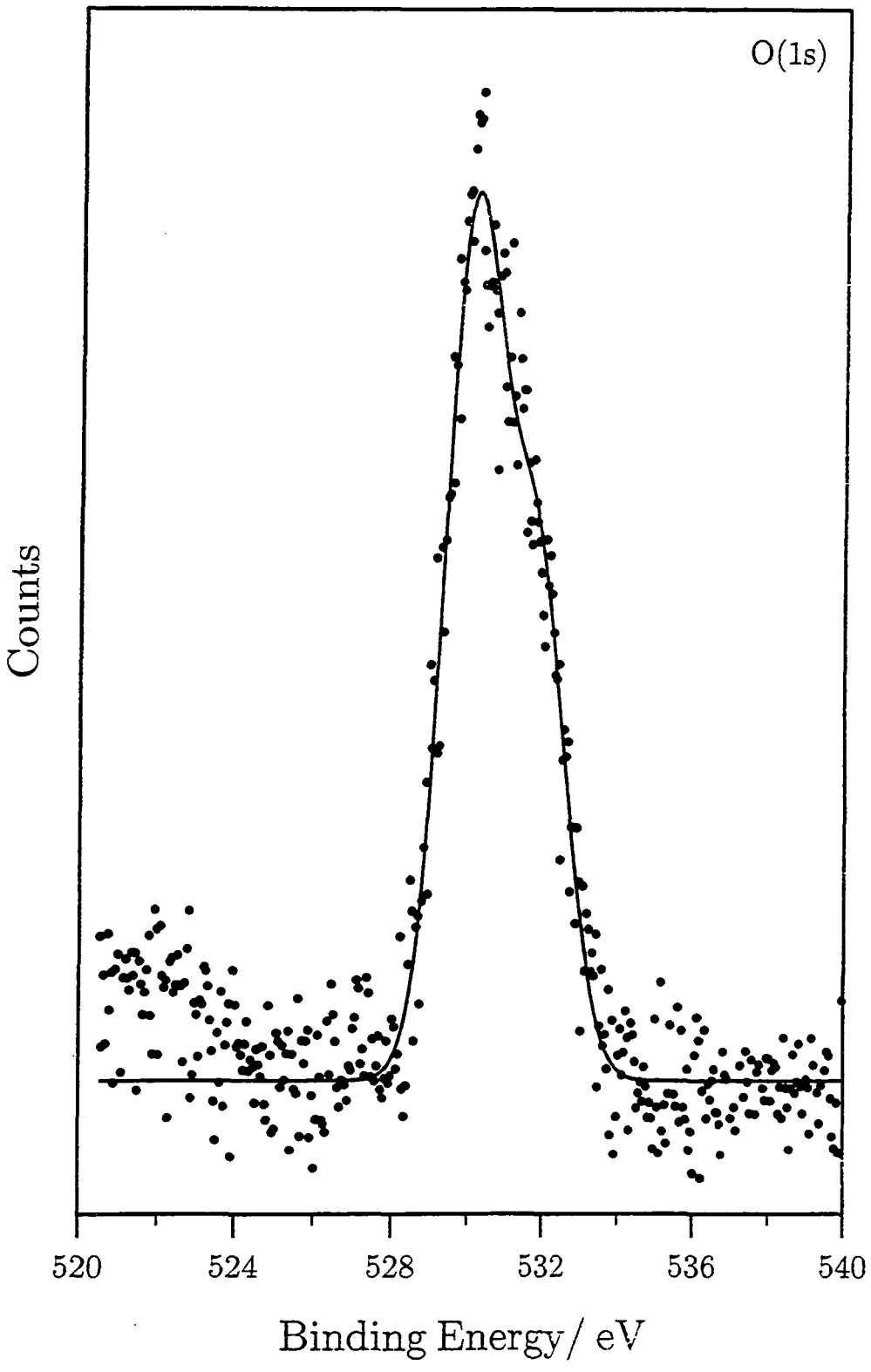

Fig. 2(c) O(1s) XP spectrum for PACVD of TiTP/NH_3 onto a glass substrate (30 W, 5 min, 19 cm).

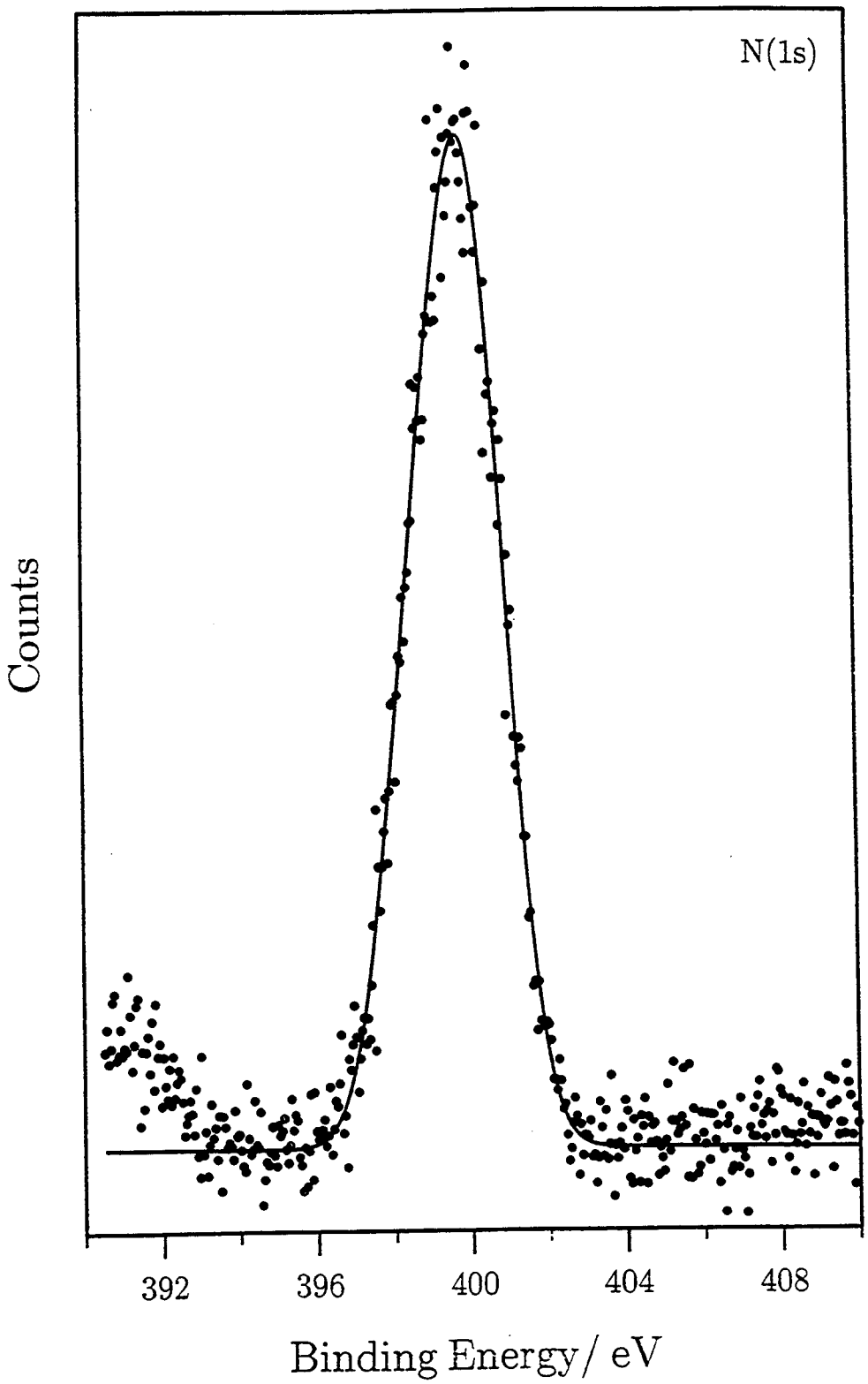

Fig. 2(d) N(1s) XP spectrum for PACVD of TiTP/NH_3 onto a glass substrate (30 W, 5 min, 19 cm).

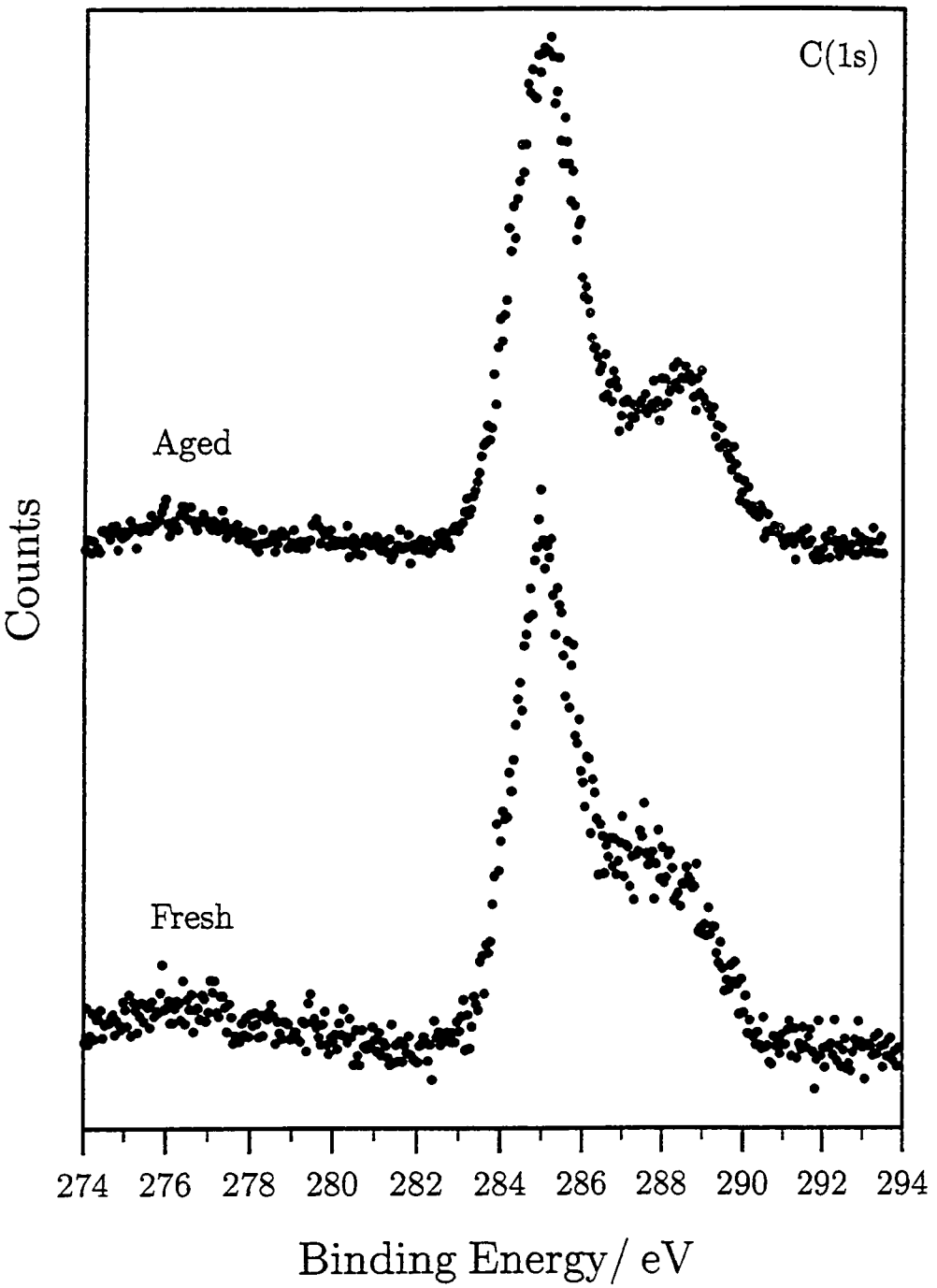

Fig. 3(a) C(1s) XP spectra for fresh and aged (approx. 1 month) PACVD samples of $TiTP/NH_3$ onto a glass substrate (15 W, 5 min, 19 cm).

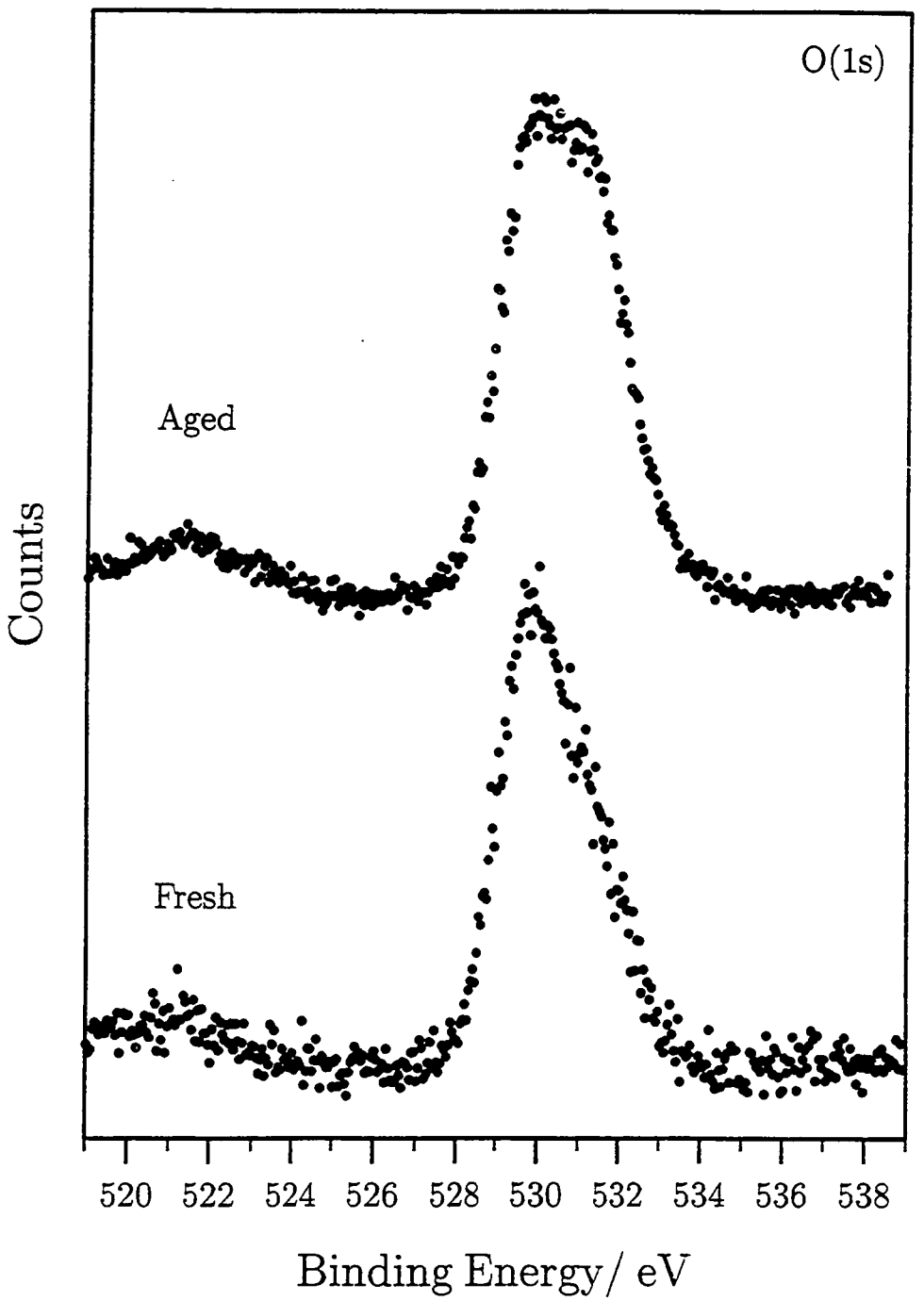

Fig. 3(b) O(1s) XP spectra for fresh and aged (approx. 1 month) PACVD samples of TiTP/NH_3 onto a glass substrate (15 W, 5 min, 19 cm).

5.3.2 XPS DEPTH PROFILING

Depth profiling was carried out on a 15 W TiTP/NH_3 plasma polymer sample. It would initially appear in Fig. 4 that the film in the bulk possesses a constant composition once adventitious carbon and low molecular weight hydrocarbon species are removed. However the amount of oxygen observed after 420 s of sputtering is deceptively high because it includes a component that arises from the substrate. (Silicon is also observed). It can also be seen in Fig. 5(a) that after 120 s of sputtering there is a shift to higher binding energies as a result of loss of oxygen in the O(1s) XP spectrum. Preferential sputtering of oxygen[19] will almost certainly have occurred and this hypothesis is supported by the broadening of the Ti (2p) XP region,[13] Fig. 5(b), that is indicative of titanium suboxides. It is also possible that this broadening to lower binding energies incorporates an intermediate[15] or oxynitride[20] component and/or a nitride component.[15]

It can be assumed that the C(1s) XP region is predominantly hydrocarbon from the plasma polymer and therefore a charging offset can be approximately determined for the sample that has been sputtered for 420 s. The corresponding N(1s) XP region shown in Fig. 5(c) indicates a new dominant peak at lower binding energy (~397.8 eV) to the environments mentioned in section 5.3.1 which is indicative of an oxynitride.[14]

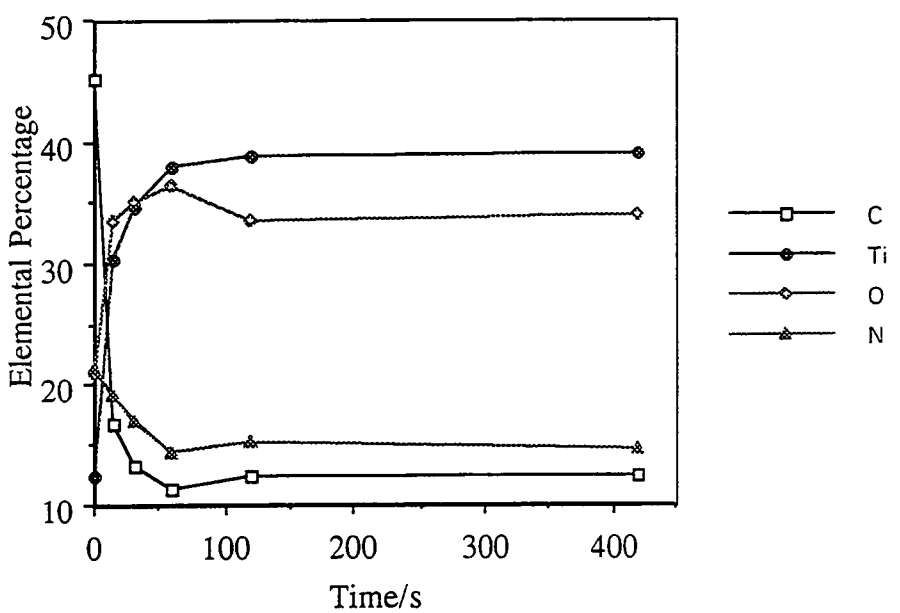

Fig. 4 XPS depth profile for PACVD of TiTP/NH_3 onto a glass substrate (15 W, 5 min, 19 cm).

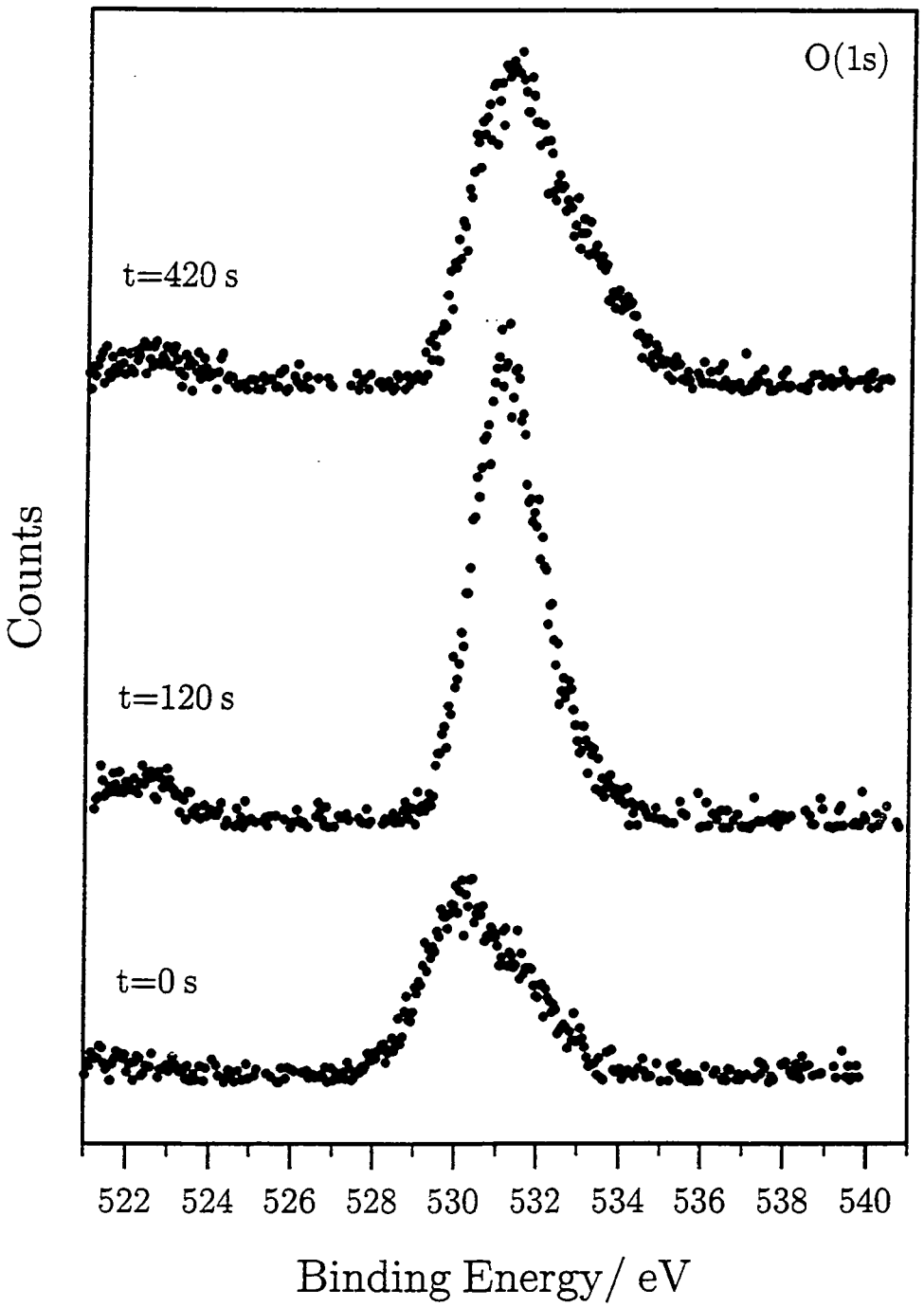

Fig. 5(a) O(1s) XP depth profile spectra of PACVD of TiTP/NH_3 onto a glass substrate (15 W, 5 min, 19 cm) recorded after given sputtering times.

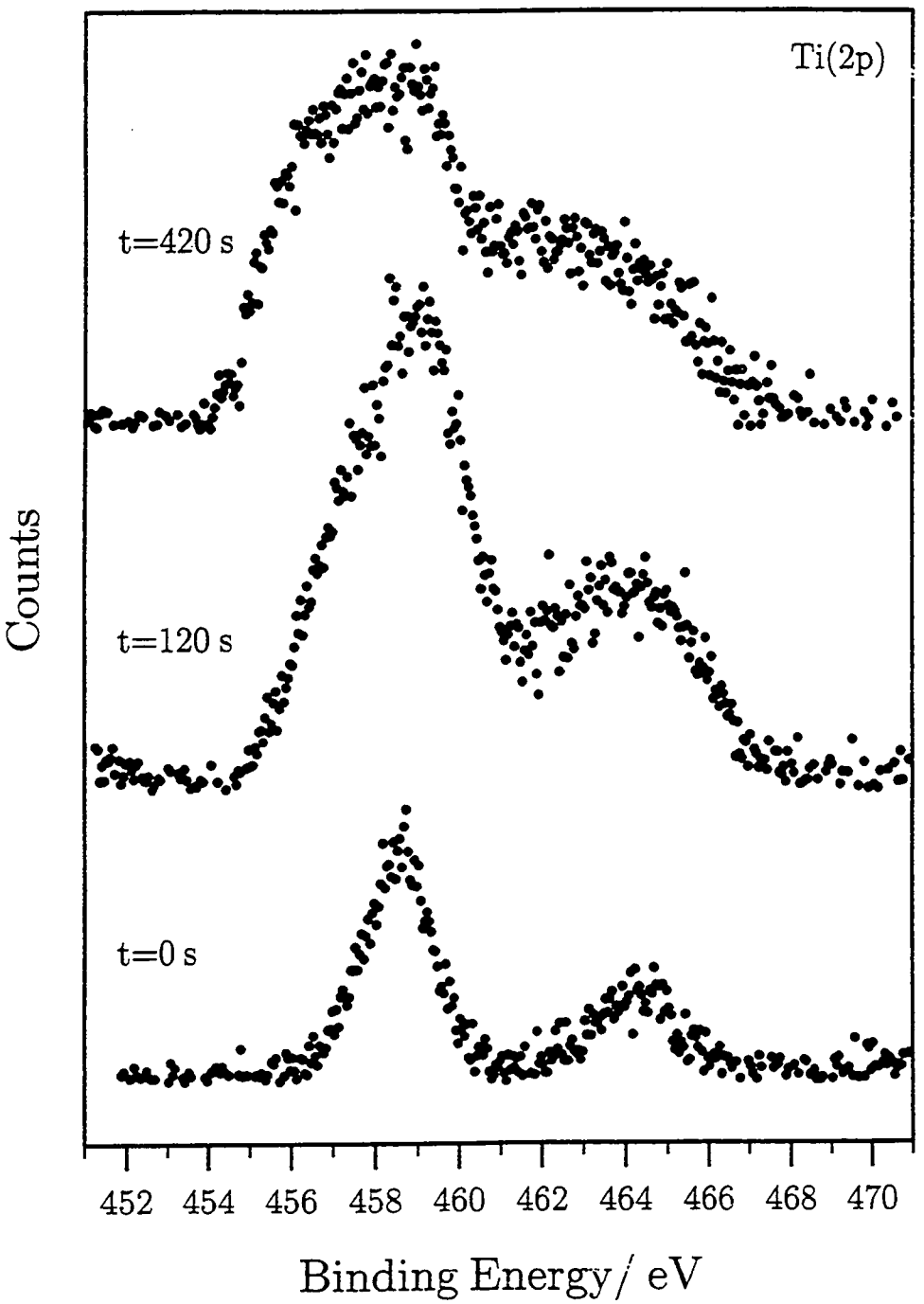

Fig. 5(b) Ti(2p) XP depth profile spectra of PACVD of TiTP/NH_3 onto a glass substrate (15 W, 5 min, 19 cm) recorded after given sputtering times.

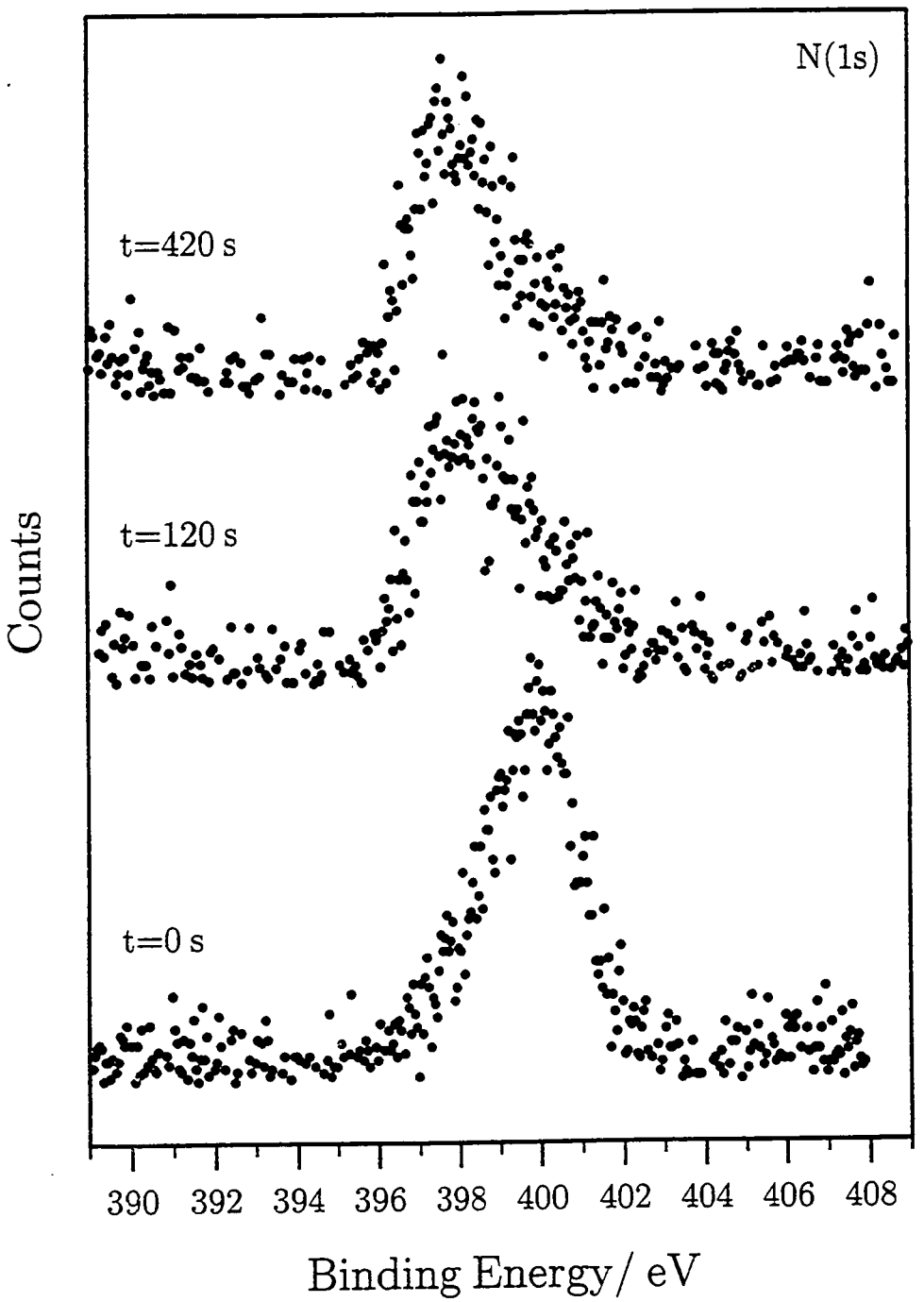

Fig. 5(c) N(1s) XP depth profile spectra of PACVD of TiTP/NH_3 onto a glass substrate (15 W, 5 min, 19 cm) recorded after given sputtering times.

5.3.3 ATTENUATED TOTAL REFLECTION FOURIER TRANSFORM INFRARED SPECTROSCOPY (ATR-FTIR)

Grafting of amino functional groups onto polymer surfaces can be achieved in the presence of an ammonia plasma.[21-23] Therefore, a control ATR experiment was carried out at the mid-range power of 15 W with only ammonia present. Evidence of new spectral features (i.e. N-H or O-H) stretches were not apparent. This would be consistent with plasma treatment of polymers[22] affecting only the top surface 20-200 Å and the ATR technique being less surface sensitive with a sampling depth of approximately a micron.[24] However, amination and oxidation products on the outermost surface layers were almost certainly present, and this is supported by the work of Mercx,[23] using XPS, the more surface sensitive technique. It can therefore be assumed that any new spectral features that arose were a consequence of PACVD alone.

In Fig. 6 it can be seen that the greatest deposition occurs at about 15 W. The most surface sensitive[24] polyethylene substrate bands at 2915 cm^{-1} and 2847 cm^{-1} are the most attenuated and the new bands are the most intense. At 30 W, the polyethylene bands are the most prominent whilst the new bands are reduced. This suggests either greater deposition occurs upstream or that sputtering takes place. The 5 W spectrum in Fig. 7 clearly shows the emergence of some interesting new bands.

The broad band centred around 3270 cm^{-1} can be assigned to O-H or N-H stretchings.[25] The broad band in the 2200-2000 cm^{-1} region (with maxima at 2193 cm^{-1}, 2150 cm^{-1} and 2037 cm^{-1}) is likely to contain multiply bonded species.[26] Precise assignment is almost impossible because there are many known titanium compounds containing different groups possessing bands between 2400-2000 cm^{-1} (e.g. cyano (nitrile) (-CN), isocyano (-NC), cyanato (-OCN), isocyanato (-NCO), fulminato (-CNO) and isofulminato (-ONC).[27-31] Also amino bands have been assigned at 2200 cm^{-1}, along with an iminonitrile (=N-CN) band at 2165 cm^{-1} for the plasma polymer of 2-vinylpyridine.[18] Typically the amino band is found at higher wavenumbers (2700-2250 cm^{-1}).[26] A nitrile band located at 2190 cm^{-1} has been assigned in the plasma polymer of methane and nitrogen.[32] In the plasma polymer of acrylonitrile (H_2C=CHCN), a C≡N stretch and a conjugated -C=N- stretch are assigned to peaks at 2250 cm^{-1} and 2200 cm^{-1}.[33] Carbodiimides[26] (-N=C=N-), ketenes[26] (>C=C=O) and isonitriles[34] (-NC) are all found near 2150 cm^{-1}, whilst ketene-imines (-C=C=N-) are observed in the 2037 cm^{-1} region.[26,33] Another possibility includes a conjugated nitrile[34] where there is an amino moiety present on the β-carbon of the double bond e.g. 3-amino crotononitrile [$(CH_3)(NH_2)$C=CH-C≡N]. Bands for the above compound were located at 2195 cm^{-1} and 2180 cm^{-1}.

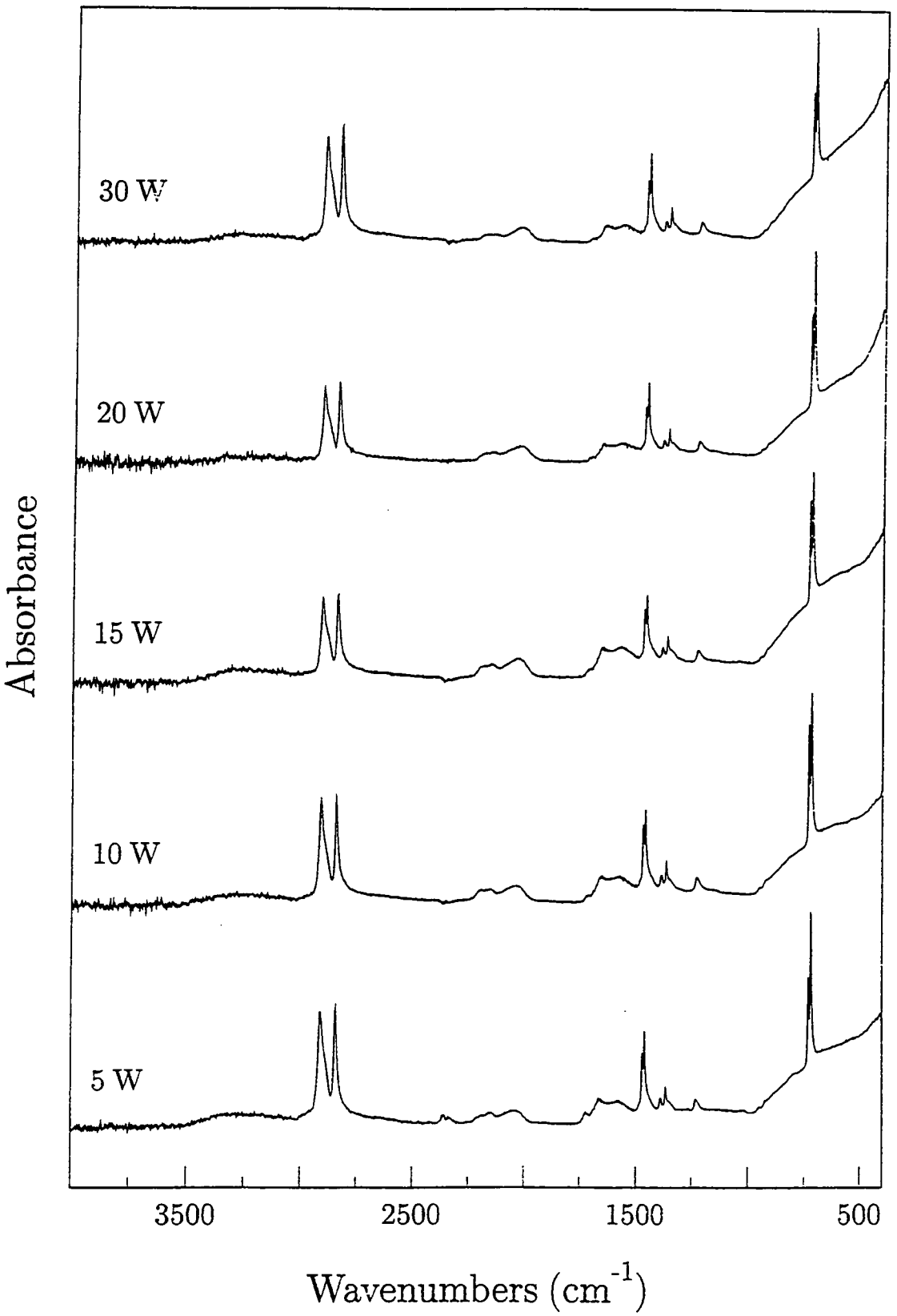

Fig. 6 ATR-FTIR spectra for PACVD of TiTP/NH_3 onto polyethylene film as function of glow discharge power (30 min, 19 cm).

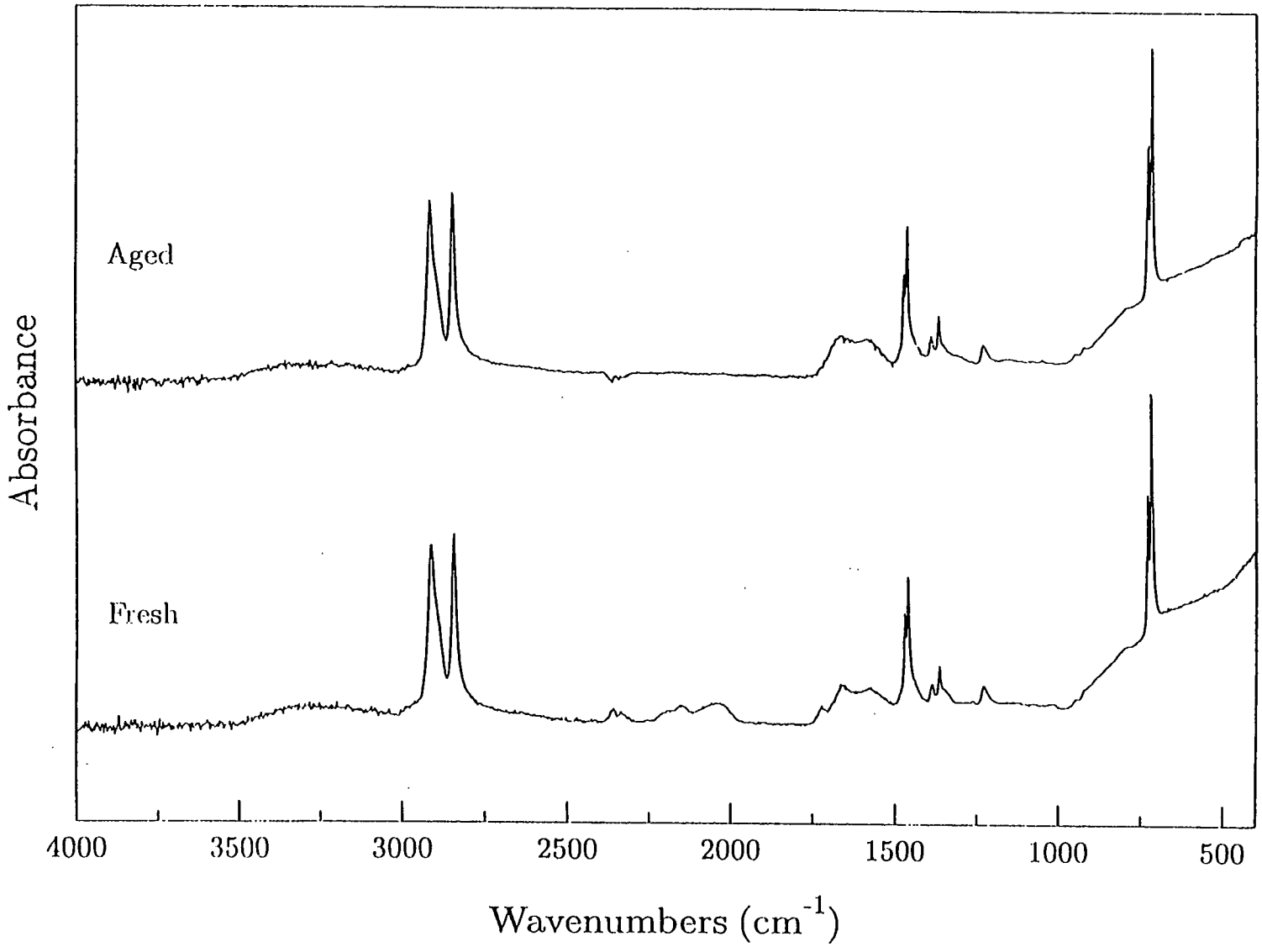

Fig. 7 ATR-FTIR spectra of PACVD of TiTP/NH_3 onto polyethylene substrate showing fresh and aged samples (5 W, 30 min, 19 cm).

A broad band between ~1750-1500 cm^{-1} appears to contain a variety of different environments with maxima located at 1723 cm^{-1}, 1661 cm^{-1} and 1582 cm^{-1}. The former band is most typical of a carbonyl stretch,[21,25] but precise assignment of the latter two bands is ambiguous because of the range of possibilities in this system. The carbonyl amide I band, the N-H bending vibration amide II band, the amine N-H bending, the vinylic stretch, the C=N stretch and the asymmetric stretches of the carboxylate and nitro (NO_2) groups are all possible assignments.[18,25] Any physisorbed water[35] on TiO_2 and vinylic[25] stretches would also be present in the above region. Imines (>C=NH), oximes and ureas (N-CO-N) are also found near 1660 cm^{-1}.[26]

The emergence of a band at ~1350 cm^{-1} may be a result from either the twist and wagging modes of CH_2 found in solid samples of long-chain acids, amides and esters[25] or from the symmetric stretches of the carboxylate or NO_2 groups.[25,26] Below 900 cm^{-1} the large absorbance arises from bulk lattice vibrations seen in amorphous TiO_2.[36] Evidence of Ti-N vibrations (as seen in $Ti(NMe_2)_4$)[37] cannot be determined since they would lie under the strong absorbance for TiO_2 discussed above.

Aging of the samples was carried out by leaving them in ambient conditions for approximately one month. The major changes, as shown in Fig. 7, include the loss of the broad band between 2200-2000 cm^{-1} and the increase in the intensity of the broad band between 1750-1500 cm^{-1}. The latter observation can be partly explained by the increased reaction of trapped free radicals with atmospheric water and/or oxygen to create more carboxylate and amide type groups.[18] More physisorbed water and an increase in the vinylic component (due to recombination of trapped free radicals) may also occur upon aging.

Explanation for the loss of the broad band between 2200-2000 cm^{-1} with aging is not straight forward, however, because the original assignments of this band are not absolutely certain. Loss of nitrile to form a carboxylic acid by hydrolysis is unlikely since acidic or basic conditions are required.[38] Since hydrolysis of isonitrile[39] to form formic acid (HCO_2H) occurs at 180 °C, hydrolysis in ambient conditions is also unfavourable. However hydrolysis of ketene and isocyanate are likely to form carboxylic acid and amine respectively[38] whilst ketene-imines are not stable. If a carbon atom adjacent to the ketene-imine group is bonded via the nitrogen atom then this bond is known to be easily broken to form a chain end radical and an unsaturated end:[33]

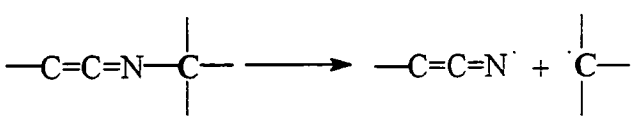

These products are likely then to react with water to form amide species. Therefore the increase in the broad band between 1750-1500 cm^{-1} would agree with loss of ketene, ketene-imine and isocyanate functionalities.

5.3.4 ATOMIC FORCE MICROSCOPY (AFM)

Little can be inferred from the AFM image shown in Fig. 8 since there appears to be no morphological relief or structure for the 15 W TiTP/NH_3 plasma polymer. It suggests either film growth at the gas/surface interface[1] and not in the gas phase giving powder formation, or that the smooth film surface is a result of the coalescence of powder particles as more polymer is deposited.[18,40]

5.4 DISCUSSION

UV emission studies of ammonia in a plasma has shown the presence of electronically excited states of stable species such as NH_3, N_2, H_2, and of radicals such as H, NH_2 and NH.[41] Nitriding of bulk titanium and titanium thin films can be achieved in such an excited environment.[42] Ammonia plasma treatments are known to form amino functional groups on the surface of polymers[21-23] and as a result, the adhesion to epoxy resins is improved.[22,23] Therefore such a plasma environment is very reactive and nitrogen incorporation is to be expected.

Depth profiling indicates the possible formation of oxynitride below an oxide capping layer, comparable to TiN which possesses an oxide layer.[15] Such Ti-N bond formation agrees with the Ti(O,C,N) films deposited by Mayr and Stock[10] and Wierzchon *et al.*[8,9] Similar metal-nitrogen bond formation were found for the plasma polymerization of tetramethyltin[6] and PACVD of trimethylaluminium,[7] both in the presence of ammonia. In the former case,[6] Sn-N bonds were detected by IR, but were found to disappear on storage in air for 0.5-1 hr as a result of hydrolysis of the Sn-N bond.

Deposition of the majority of the titanium species is near the end of the extension delivery tube within the RF coils. On increasing the glow discharge power, a higher proportion of the titanium species are deposited before they can reach the coil region. Therefore more volatile organic decomposition products, along with the ammonia species, pass through to the centre of the coil region, the highest energy zone, where they undergo a greater degree of plasma polymerization.[18]

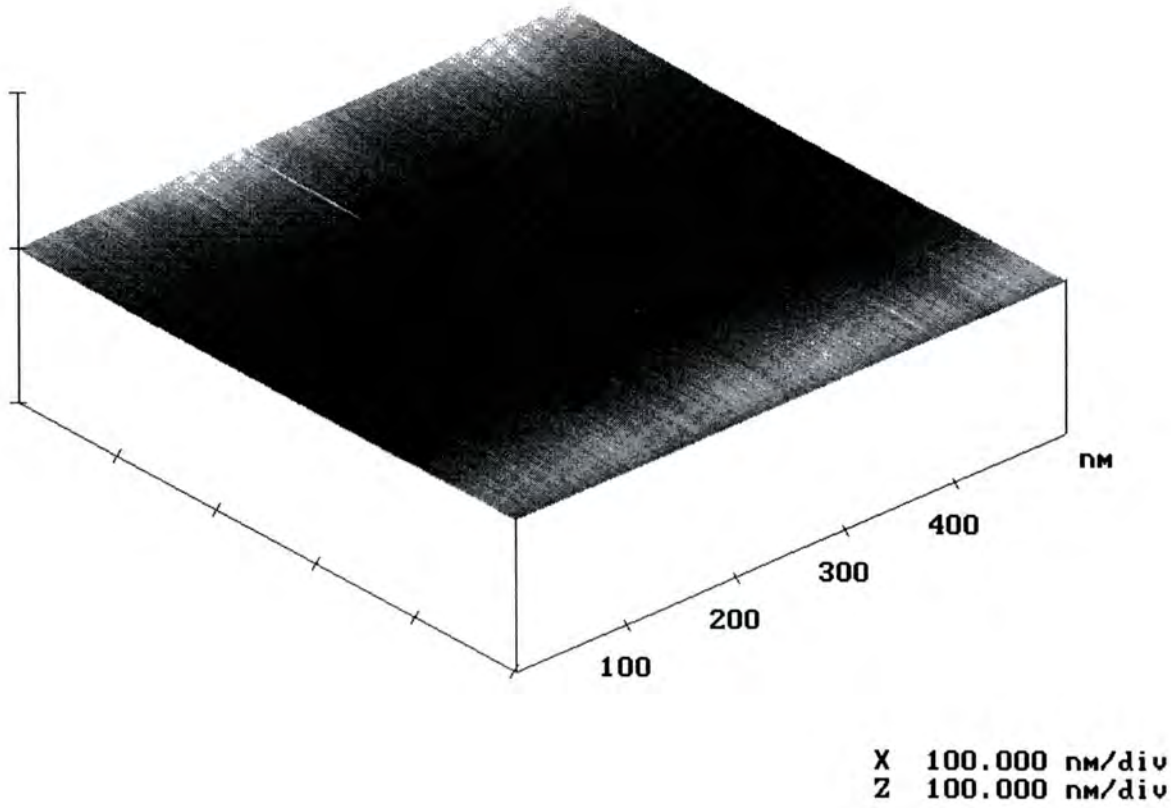

Fig. 8 AFM image for PACVD of $TiTP/NH_3$ onto a glass substrate (15 W, 5 min, 19 cm).

As a result more organo/nitroorgano species are then incorporated into the deposited films as the power is increased. Since the distance between the substrate and monomer entry into the reactor is so short (2 cm), the fall in monomer flow rate, F_m,[42] arising from the fragmentation and hence plasma polymerization, is small. As a result, only small composition changes are observed with increasing glow discharge power.

The infrared data is of limited use since complete interpretation of the broad bands is not possible. However possible routes to the formation of various functionalities can be proposed. Imine formation is known to occur under non-plasma conditions via reaction of carbonyl compounds with ammonia.[38] Acetone, a thermal decomposition product of TiTP,[43-45] may react in the gas phase with ammonia:

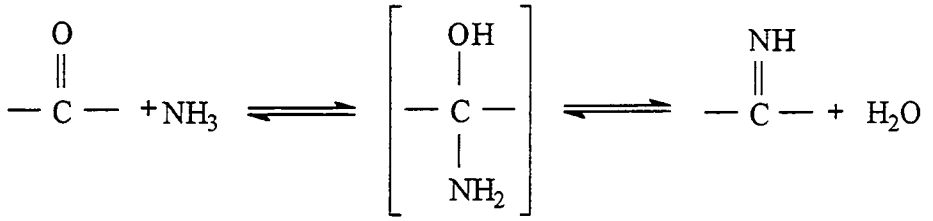

Also imine-type functionalities (>C=N-H, >C=N-R) are also known to exist on nitrogen plasma treated polymer surfaces.[46-48] It is therefore proposed that such formation may occur during the deposition.

On irradiation, imines are well known to undergo α-cleavage to form the nitrile.[49] Such a process may then occur in the plasma:

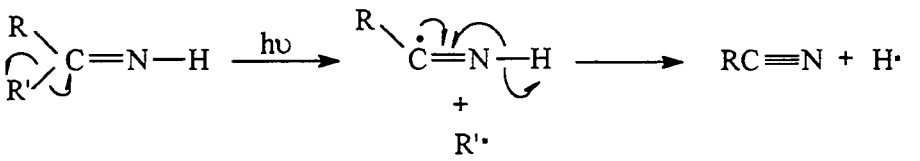

Note that imines are also unstable and rapidly hydrolyse with water to form carbonyl compounds.[38] Aging of nitrogen plasma treated polymer surfaces has been partly explained by hydrolysis of the surface imine-type functionalities:[46,47]

$$>C=N\text{-}H + H_2O \rightarrow >C=O + NH_3$$

$$>C=N\text{-}R + H_2O \rightarrow >C=O + H_2NR$$

On assumption that C≡N formation occurs, possible ketene-imine formation may then take place via two routes.[33] The first route involves a termination reaction of a radical end:

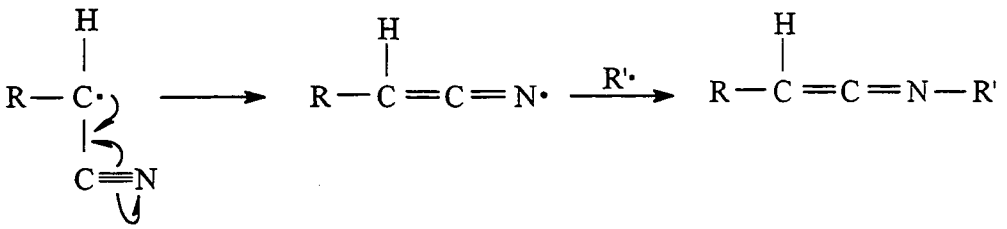

The second route involves:

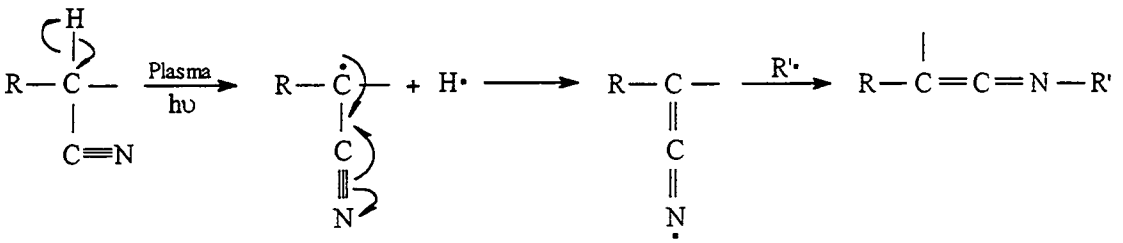

Both XPS and ATR show that aging occurs in the deposited films and is almost certainly due to the presence of trapped free radicals in the plasma polymer reacting with water and/or oxygen.[18] Hydrolysis of any unstable functional groups also accounts for the observed aging affects.

The smooth nature of the film examined by AFM results either from reactions predominantly at the gas/surface interface, or from the coalescence of powder particles on the surface which are formed in the gas phase.

5.5 CONCLUSIONS

It is proposed that the formation of Ti-N bonds has been achieved during the PACVD of a TiTP/NH_3 mixture, though their presence is only observed beneath a surface oxide capping layer. An ammonia plasma environment provides many reactive nitrogen species which are incorporated into the plasma polymer giving a composite-type, $TiO_pN_q/O_rC_sH_tN_u$ structure. Greater plasma polymerization occurs with increasing glow discharge power with less titanium species incorporated into the deposited films. Aging occurs as a result of the presence of trapped free radicals reacting with water and/or oxygen, and hydrolysis of unstable functional groups.

5.6 REFERENCES

1. R. d'Agostino, Ed., Plasma Deposition, Etching of Polymers, Academic Press, San Diego, 1990.
2. M. Gupta, V.K. Rathi, R. Thangaraj, O. P. Agnihotri, K. S. Chari, *Thin Solid Films*, **204**, 1991, 77.
3. B.S. Sywe, J. R. Schlup, J. H. Edgar, *Chem. Mater.*, **3**, 1991, 737.
4. J.G. Stark, H. G. Wallace, Chemistry Data Book, John Murray, London, 1988.
5. J.L. Vossen, W. Kern., Eds., Thin Film Processes II, Academic Press, London, 1991.
6. N. Inagaki, Y. Hashimoto, *Polym. Bull.*, **12**, 1984, 437.
7. R.K. Sadhir, H.E. Saunders, W.A. Byers, *Proc. Electr./Electron. Insul. Conf.*, 18th, 1987, 17.
8. T. Wierzchon, J. Michalski, T. Karpinski, *Proc. Plasma Surf. Eng.*, Garmisch-Partenkirchen, Vol. 1, D. G. M. Informationsges. mbH, Oberursel, 1989, p. 177.
9. T. Wierzchon, J.R. Sobiecki, *Vacuum*, **44**, 1993, 975.
10. P. Mayr, H.-R. Stock, *J. Vac. Sci. Technol.*, **A4**, 1986, 2726.
11. D.T. Clark, A. Dilks, *J. Polym. Sci. Polym. Chem. Edn.*, **17**, 1979, 957.
12. Handbook of X-Ray Photoelectron Spectroscopy, Ed. C.D. Wagner, W.M. Riggs, L.E. Davis, J.F. Moulder, G.E. Muilenberg, Perkin-Elmer Corp., Eden Prairie, MN, 1979.
13. C.N. Sayers, N.R. Armstrong, *Surf. Sci.*, **178**, 1977, 301.
14. M.V. Kaznetsov, J.F. Zhuravlev, V.A. Zhilyaev, V.A. Gubanov, *J. Electr. Spec. Relat. Phenom.*, **58**, 1992, 1.
15. N. Saha, H.G. Tompkins, *J. Appl. Phys.*, **72**, 1992, 3072.
16. B. Siemensmeyer, K. Bade, J.W. Schutze, *Ber. Bunsenges. Phys. Chem.*, **95**, 1991, 1461.
17. G. Beamson, D. Briggs, High Resolution XPS of Organic Polymers, The Scienta ESCA300 Database, John Wiley, Chichester, 1992.
18. H. Yasuda, Plasma Polymerization, Academic Press, Orlando, FL., 1985.
19. J.W. Coburn, *Thin Solid Films*, **64**, 1979, 371.
20. C. Ernsberger, J. Nickerson, T. Smith, A.E. Miller, D. Banks, *J. Vac. Sci. Technol.*, **A4**, 1986, 2784.
21. S. Gaboury, M.W. Urban, *J. Appl. Polym. Sci.*, **44**, 1992, 401.
22. E.M. Liston, *J. Adhesion*, **30**, 1989, 199.
23. F.P.M. Mercx, *Polymer*, **35**, 1994, 2098.
24. F.M. Mirabella, *Appl. Spectrosc. Rev.*, **21**, 1985, 45.
25. R.M. Silverstein, G.C. Bassler, T.V. Morrill, Spectrometric Identification of Organic Compounds, 4th Edn., John Wiley, New York, 1981.

26. D.H. Williams, I. Fleming, Spectroscopic Methods in Organic Chemistry, 3rd Edn., McGraw-Hill, London, 1987.
27. N.N. Greenwood, E.J.F. Ross, B.P. Straughan, Index of Vibrational Spectra of Inorganic and Organometallic Compounds, Vol. 1, Butterworths, London, 1972.
28. N.N. Greenwood, E.J.F. Ross, Index of Vibrational Spectra of Inorganic and Organometallic Compounds, Vol. 2, Butterworths, London, 1975.
29. N.N. Greenwood, E.J.F. Ross, Index of Vibrational Spectra of Inorganic and Organometallic Compounds, Vol. 3, Butterworths, London, 1977.
30. G. Wilkinson, F.G.A. Stone, E.A. Abel, Eds., Comprehensive Organometallic Chemistry, Vol. 3, Pergamon Press, New York, 1982.
31. A.G. Sharpe, The Chemistry of Cyano Complexes of Transition Metals, Academic Press, London, 1976.
32. H.-X. Han, B.J. Feldman, *Solid State Commun.*, **65**, 1988, 921.
33. N. Inagaki, S. Tasaka, Y. Yamada, *J. Polym. Sci. Polym. Chem. Edn.*, **30**, 1992, 2003.
34. L.J. Bellamy, The Infrared spectra of Complex Molecules, 3rd Edn., Chapman and Hall, London, 1975.
35. D.J.C. Yates, *J. Chem. Phys.*, **65**, 1961, 1366.
36. M. Ocaña, W.P. Hsu, E. Matijevic, *Langmuir*, 7,1991, 2911.
37. D.C. Bradley, M.H. Gitlitz, *J. Chem. Soc.*, **A**, 1969, 980.
38. A. Streitweiser, Jr., C.H. Heathcock, Introduction to Organic Chemistry, 3rd Edn., Macmillan, New York, 1985.
39. N.V. Sidgwick, Ed., The Organic Chemistry of Nitrogen, O.U.P., Oxford, 1966.
40. H.V. Boenig, Plasma Science and Technology, Cornell University Press, New York, 1982.
41. R. d'Agostino, F. Cramarossa, S. De Benedictis, G. Ferraro, *Plasma Chem. Plasma Proc.*, **1**, 1881, 19.
42. G. Lemperiere, J.M. Poitevin, *Thin Solid Films*, **111**,1984,339.
43. S.Y. Park, N. Kim, *J. Appl. Polym. Sci. Polym. Appl. Symp.*, **46**, 1990, 91.
44. K.L. Siefering, G.L. Griffin, *J. Electrochem. Soc.*, **137**, 1990, 814.
45. Y.-M. Wu, D.C. Bradley, R.M. Nix, *Appl. Surf. Sci.*, **64**, 1993, 21.
46. C.P. Fictorie, J.F. Evans, W.L. Gladfelter, *J. Vac. Sci. Technol.*, **A12**, 1994, 1108.
47. R. Foerch, N.S. McIntyre, R.N.S. Sodhi, D.H. Hunter, *J. Appl. Polym. Sci.*, **40**, 1990, 1903.
48. S. O'Kell, T. Henshaw, G. Farrow, M. Aindow, C. Jones, *Surf. Interface Anal.*, **23**, 1995, 319.
49. A. Gilbert, J. Baggott, Essentials of Molecular Photochemistry, Blackwell Scientific, Oxford, 1991.

CHAPTER 6:
PLASMA ASSISTED CHEMICAL VAPOUR DEPOSITION OF TITANIUM OXYCARBONITRIDE/POLYMER FILMS FROM TETRAKIS (DIMETHYLAMIDO) TITANIUM

6.1 INTRODUCTION

In Chapter 5 oxygen was found in the Ti(O,N)/polymer composite films produced by PACVD using TiTP and ammonia. Therefore the reduction of incorporated oxygen requires the use of a precursor where the titanium metal centre is directly bonded to nitrogen. This chapter describes this approach. Thin film deposition is reported using the simplest commercially available dialkylamido titanium precursor, tetrakis (dimethylamido) titanium (TMT), $Ti[N(CH_3)_2]_4$, first synthesised by Bradley and Thomas in 1960.[1]

6.1.1 REVIEW OF TITANIUM NITRIDE FORMATION

Numerous techniques have been used for making TiN films. The majority of methods use physical vapour deposition (PVD) and chemical vapour deposition (CVD) techniques, both with and without plasma assistance, though there are several other methods such as combustion synthesis[2] and pyrolysis[3] of $Ti(O\text{-}n\text{-}Bu)_4$/furfuryl alcohol mixture in the presence of ammonia.

Basic PVD techniques commonly used include evaporation and sputtering and these can be combined with or without additional chemical reactions (the reactive mode) e.g. reactive evaporation (RE) and reactive sputtering (RS).[4] Plasma assisted PVD (PAPVD) techniques discussed in Chapter 1 include activated reactive evaporation (ARE), biased activated reactive evaporation (BARE), ion plating and reactive ion plating (RIP). BARE and RIP give good adhesion due to ion bombardment during film growth.[5] RS is the most commonly used PVD technique;[6] DC, RF and magnetron sputtering are all used, with the latter being most industrially important due to high deposition rates. Magnetron sputtering can also give extremely homogeneous coatings and thermally sensitive plastics can be coated.[7] PVD processes are generally carried out at lower temperatures and vapour pressures than CVD methods,[4] though poorer step-coverage[8] usually results. For more information on PVD methods, refer to the review on the structure and properties of TiN coatings by Sundgren.[9]

The remainder of this account focuses on the CVD processes for both non-plasma and plasma assisted methods. For both methods, two common approaches have been adopted: the use of either (i) $TiCl_4$ precursor or (ii) metallorganic/organometallic precursors.

6.1.1.1 $TiCl_4$ Precursor

(a) Non-Plasma Assisted CVD

TiN coatings on metals for decorative and tribological applications have most often been made by CVD from a mixture of $TiCl_4$, N_2 and H_2. This process is thermodynamically favourable above 750 °C,[10] though significant growth rates[8] are not achieved below 900 °C. Ammonia has also been used as an alternative nitrogen source since greater deposition rates should be possible because of the much lower dissociation energy compared to nitrogen gas (NH_3 ~391 $kJmol^{-1}$ and N_2 ~944 $kJmol^{-1}$).[11] Table 1 contains examples of CVD techniques that have been used.

Oxygen and chlorine contamination are typically found in the deposited films using $TiCl_4$ which have been shown to have detrimental effects on the films' electrical resistivities and hardness. If ammonia is used as a precursor,[12] ammonium chloride and/or adducts such as $TiCl_4.(NH_3)_y$ have been formed.

Table1 Conventional CVD techniques using $TiCl_4$ precursor.

Method	Deposition Temp./ °C	Deposition Pressure/ Torr	Feed Gas*
CVD[13]	High and low temp.	?	$TiCl_4$, NH_3, (H_2, N_2)
APCVD[10]	400-700	760	$TiCl_4$, NH_3, (H_2, N_2, He, Ar)
LPCVD[14]	400-750	$1.5x10^{-3}$	$TiCl_4$, NH_3, H_2, (Ar)
LPCVD[15]	500	0.34	$TiCl_4$, NH_3
LPCVD[16]	450-700	$100\text{-}300x10^{-3}$	$TiCl_4$, H_2, (N_2)
Laser APCVD[17]	350-750	760	$TiCl_4$, N_2, (H_2)

*The brackets around the gas(es) indicate carrier gas(es).

APCVD = atmospheric pressure CVD, LPCVD = low pressure CVD

(b) Plasma Assisted CVD

If thin films of TiN are to be deposited onto thermally sensitive substrates such as carrier chips, amorphous silicon solar cells, plastics and high speed steels, then lower deposition temperatures are needed.[18] Non-plasma assisted CVD methods are therefore not suitable. One low temperature possibility being exploited is plasma assisted CVD (PACVD) (otherwise known as plasma enhanced CVD (PECVD)). This involves the formation of solid deposits by initiating chemical reactions in a gaseous discharge[19] which are not otherwise thermodynamically feasible.

Traditionally parallel plate reactors have been used to deposit TiN using $TiCl_4$ precursor where the substrate holder can be used as an electrode and can also be heated. Other variables that have been considered include the plasma power, substrate bias, deposition time, total deposition pressure, partial pressures and/or flow rates of the reactants, glow discharge excitation methods and reactor configurations. Different feedstocks have also been used (usually $TiCl_4$, N_2 and H_2 with or without Ar). Similarly, ammonia has been used as an alternative nitrogen source. Table 2 indicates some of the experimental conditions that have been used. Comparison of results between different workers is difficult because of the different experimental arrangements used. It is clear however, that film properties are dependent on the degree of contamination from chlorine and oxygen.

Table 2 Experimental details of PACVD apparatus using $TiCl_4$ precursor (continued overleaf).

Discharge	Supply	Substrate	Type of Heating	Deposition Temp./ °C	Deposition Pressure/ Torr	Feed Gas
DC[20]		Cathode	Reactor	500-800	9.8	$TiCl_4$, H_2, N_2
DC[21]		Floating	Reactor	537-777	2.3-3	$TiCl_4$, H_2, N_2
DC[22,23]	300-550 V	Cathode	None	425-600	4	$TiCl_4$, H_2, N_2, Ar
DC[24]	550-800 V	Cathode	Substrate	430-700	3.8	$TiCl_4$, H_2, N_2, Ar
DC[25,26] pulsed	550 V	Cathode	Substrate	400-700	0.4-3.8	$TiCl_4$, H_2, N_2, Ar
DC[27] pulsed	Up to 800 V	Cathode	Reactor	460	1.1-3.4	$TiCl_4$, H_2, N_2, Ar
DC[28] pulsed	400-650 V	Cathode	Reactor	450-500	0.4-3.4	$TiCl_4$, H_2, N_2, Ar
DC[29]	500 V	Cathode	Substrate	480-510	0.8-4.5	$TiCl_4$, H_2, N_2
DC[29] pulsed	500 V	Cathode	Substrate	480-510	0.8-4.5	$TiCl_4$, H_2, N_2
RF[29] capacitive	60-100 W	Floating or DC bias	Substrate	480-510	0.8-4.5	$TiCl_4$, H_2, N_2
Micro-wave[29]		Floating	Substrate	480-510	0.8-4.5	$TiCl_4$, H_2, N_2
RF[30] capacitive	Up to 50 W	Grounded	Substrate	25-500	1.1	$TiCl_4$, H_2, N_2
RF[31] capacitive	Up to 125 W	Grounded	Substrate	250-650	0.7	$TiCl_4$, H_2, N_2
RF[32] capacitive				525		$TiCl_4$, H_2, N_2, Ar

Discharge	Supply	Substrate	Type of Heating	Deposition Temp./ °C	Deposition Pressure/ Torr	Feed Gas
RF[33] capacitive	Up to 125 W	DC bias & floating	Substrate	~500	1.5	$TiCl_4$, H_2, N_2
DC[34,35]	1200 V	Cathode	None	360-770	1	$TiCl_4$, H_2, N_2
RF[34] capacitive	500 W	Grounded	Reactor	360-770	1	$TiCl_4$, H_2, N_2
Micro-wave[34]	300 W	Floating	Reactor	360-770	1	$TiCl_4$, H_2, N_2
RF[36] capacitive	500 W	Grounded	Substrate	430-770	1	$TiCl_4$, H_2, N_2
DC[37]		Cathode	Substrate	250-600	4	$TiCl_4$, H_2, N_2, Ar
RF[38,39,40] capacitive	Up to 70 W	Grounded	Substrate	Up to 450	1-4	$TiCl_4$, H_2, N_2, Ar
RF[41] capacitive	Up to 400 W	Grounded	Substrate	500	0.1-0.3	$TiCl_4$, H_2, NH_3
RF[42] capacitive	Up to 50 W	Grounded?	Substrate	400 and 500	1	$TiCl_4$, H_2, N_2, Ar
RF[42] capacitive	Up to 20 W	Grounded?	Substrate	400	0.4	$TiCl_4$, NH_3, Ar
RF[43] capacitive	Up to 25 W	Grounded	Substrate	175-400	0.2-1	$TiCl_4$, NH_3
DC[44]	Up to -1500 V	Cathode	Substrate	527	1	$TiCl_4$, H_2, NH_3
DC[44]	Up to -1500 V	Cathode	Substrate	527	1	$TiCl_4$, H_2, N_2
RF[45] capacitive	Up to 200 W	DC bias & floating	Substrate	350-500	1	$TiCl_4$, H_2, N_2
RF[46] capacitive	Up to 600 W	Grounded	Substrate	550	1	$TiCl_4$, H_2, N_2
RF[47,48] capacitive	Up to 2500 W	RF electrode DC bias & grounded	None	450-550	0.2-3.8	$TiCl_4$, H_2, N_2, Ar

6.1.1.2 Metallorganic/Organometallic Precursors

Interest in metallorganic/organometallic precursors has grown because there is increasing demand for non-toxic and non-explosive starting materials.[49] $TiCl_4$ is known to be corrosive, and films produced from this precursor have been found to contain chlorine contamination which has been shown to influence the physical and electrical properties of TiN.[24,49,50] Hardness, adhesion to substrates and electrical conductivity are all found to decrease with increasing chlorine content. Another advantage of metallorganic/organometallic precursors is that in most cases the atoms to be deposited may already be bonded directly in the starting material[51] and consequently lower deposition temperatures may be possible. Note TiN films deposited from metallorganic/organometallic precursors in the presence of ammonia are discussed in Chapter 7.

(a) Non-Plasma Assisted CVD

The volatile tetrakis (dialkylamido) titanium complexes, $Ti(NR_2)_4$ have been the most widely used metallorganic/organometallic precursors, though other nitrogen containing compounds used include the imido precursor, $[Ti(\mu N^tBu)(NMe_2)_2]_2$[18] and tris(2,2'-bipyridine)titanium(0).[52] Table 3 summarizes previous work using such precursors.

Carbon and oxygen are commonly incorporated within TiN films formed from metallorganic/organometallic precursors. The oxygen arises from oxidation in air or from the presence of absorbed oxygen and/or water on the reactor walls during deposition. However, it is the reaction pathway leading to carbon incorporation in the films that has been of interest to various workers. For instance, Sugiyama *et al.* suggested two mechanisms; one for low decomposition temperatures (LT) and another for higher decomposition temperatures (HT) using hydrogen or nitrogen atmospheres.[51] The LT mechanism (~400 °C) relies on successive elimination of amine fragments to give low valent metal amide, followed by subsequent elimination of alkyl groups to yield the nitride. However the HT mechanism (>700 °C) relies on complete degradation, with subsequent recombination of metallic species with nitrogen compounds formed and further reduction with hydrogen to yield the nitride. At high temperatures in an argon atmosphere, dilution of the nitrogen or hydrogen species may occur making nitride formation more difficult. The presence of hydrogen was thought to assist the cleavage of N-C bonds. Carbon incorporation in the grain boundaries in this case may arise from incomplete decomposition. More recently, decomposition has been shown to follow a similar loss of dialkylamine described in the LT case by Sugiyama *et al.*,[51] followed by cleavage of the N-C bond to give the alkene.[53] Since hydrogen is required to form the

dialkylamine, it has been proposed that this comes from a neighbouring alkyl group. The low valent metal centre, arising from the loss of the dialkylamine ($HNEt_2$), is suggested to act as a catalytic site and as a result, a large amount of butene, the product of dimerization of ethylene, is given off as a decomposition byproduct in the case of $Ti(NEt_2)_4$. A polymeric substance, A, thus formed, is believed to lead to the nitride or carbonitride above 400-500 °C:

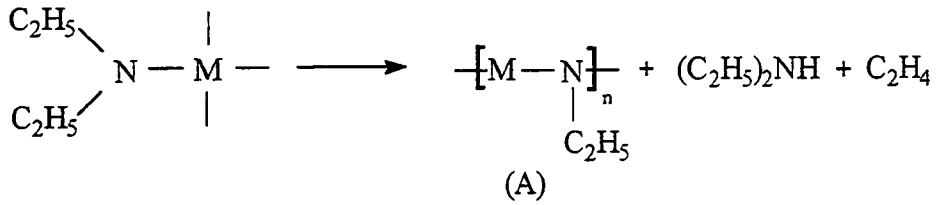

(A)

Table 3 Conventional CVD techniques using organometallic precursors.

Method	Deposition Temp./ °C	Deposition Pressure/ Torr	Feed Gas*
Thermal decomposition[51]	250	?	$Ti(NMe_2)_4$, (Ar, H_2, N_2)
Thermal decomposition[51]	350	?	$Ti(NEt_2)_4$, (Ar, H_2, N_2)
Thermal decomposition[51]	500	?	$Ti(N^nPr_2)_4$, (Ar, H_2, N_2)
Thermal decomposition[51]	600	?	$Ti(N^nBu_2)_4$, (Ar, H_2, N_2)
Thermal decomposition[53]	260-300	20-140	$Ti(NEt_2)_4$
Thermal decomposition[53]	260-300	20-140	$Ti(NPr_2)_4$
Thermal decomposition[53]	260-300	20-140	$Ti(NBu_2)_4$
APCVD[18]	350-500	760	$Ti(NMe_2)_4$, (He, N_2)
APCVD[18]	300-400	760	$Ti[(NMe_2)_3(^tBu)]$, (N_2)
APCVD[18]	400	760	$Ti(NEt_2)_4$, (He)
APCVD[18]	400	760	$Ti(NC_4H_8)_4$, (He, N_2)
APCVD[18]	400-600	760	$Ti(NC_5H_{10})_4$, (He, N_2)
APCVD[18]	400-450	760	$[Ti(\mu N^tBu)(NMe_2)_2]_2$, (He)
CVD[54]	400-650	?	$Ti(NEt_2)_4$ with/out H_2
Thermolysis[55]	>393	0.07	$Ti(NMe_2)_4$
CVD[12]	250-450	0.5-2	$Ti(NMe_2)_4$, N_2, H_2, (H_2)
Rapid-thermal LPCVD[56]	320-520	0.005-50	$Ti(NMe_2)_4$, (H_2)
CVD[57]	500-550	1.5	$CpTiC_7H_7$
CVD[57]	500-625	1.5	$Ti(^tBu\text{-}DAD)_2$
CVD[52]	370-520	$10^{-5}\rightarrow10^{-4}$	$Ti(bipy)_3$

* The brackets around the gas(es) indicate carrier gas(es).

Alternatively, there is documented electron spectroscopic evidence for the formation of titanium directly bound to carbon and nitrogen, as well as hydrocarbon incorporation.[12,18,54,55] A metal centre-mediated alkyl β-hydrogen elimination mechanism[18,54] has been proposed:

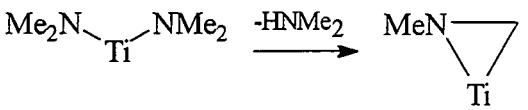

Gas phase IR studies[55] support such a mechanism since above 177 °C, the appearance of a new band at 1276 cm^{-1}, assigned to a N-C bond with partial double bond character, was observed on loss of dimethylamine:

A N=C stretch was also observed at 1590 cm^{-1}.

Reduction of titanium-bound carbon has been achieved by use of cyclic amido ligands (e.g. pyrrolidino, $-NC_4H_8$, and piperidino, $-NC_5H_{10}$) since the β-carbons are tied back in the ring preventing β-hydrogen activation.[18] As a result, heterocyclic groups are believed to be lost as radicals with the N-C bonds in the heterocyclic ligands not cleaving, leaving intact $TiNC_XH_{2X}$ fragments in the films and hence hydrocarbon incorporation. Further attempts to reduce hydrocarbon contamination by using good leaving groups on the nitrogen atom, e.g. di-tert-butylamido, failed due to the inability to synthesize such sterically hindered compounds.

(b) Plasma Assisted CVD

Plasma assisted deposition using metallorganic/organometallic precursors has been attractive, not only to eliminate chlorine contamination or formation of ammonium chloride,[23] but also to allow lower deposition temperatures. Table 4 shows some examples with metallorganic/organometallic precursors.

Table 4 Experimental details of PACVD apparatus using metallorganic/organometallic precursors.

Discharge	Supply	Substrate	Type of Heating	Deposition Temp./ °C	Deposition Pressure/ Torr	Feed Gas
RF capacitive[45]	Up to 200 W	Floating	Substrate	200-800	0.1-760	$Ti(NMe_2)_4$, N_2, Ar, He
DC pulsed[50,58]	Up to 800 W	Cathode	Reactor	280-450	0.4-3	$Ti(NMe_2)_4$, H_2, N_2, Ar
DC pulsed[50,58]	Up to 800 W	Cathode	Reactor	280-450	0.4-3	$Ti(NEt_2)_4$, H_2, N_2, Ar
DC pulsed[58]	Up to 800 W	Cathode	Reactor	280-450	0.4-3	$(Cp^*)_2Ti(Me)Cl$, H_2, N_2, Ar
MW,[59,60] ECR downstream	Up to 400 W	Floating	Substrate	350-600	$9x10^{-4}$	$Ti(NMe_2)_4$, H_2, N_2
MW,[12] ECR downstream	350 or 800 W	Floating	Substrate	350-450	0.2-5	$Ti(NMe_2)_4$, H_2, N_2
DC[61]	Up to 1000 W	Cathode	Reactor	200-500	0.8-3.8	$Ti(NMe_2)_4$, H_2, N_2, Ar
DC[61]	Up to 1000 W	Cathode	Reactor	200-500	0.8-3.8	$Ti(NEt_2)_4$, H_2, N_2, Ar
DC[19]		Cathode	Reactor	500-800	9.8	$Ti(O^iPr)_4$, H_2, N_2
DC[24]	550-800 V	Cathode	Substrate	430-700	3.8	$Ti(O^iPr)_4$, H_2, N_2, Ar

Facile Ti-C bond formation results from alkyl β-hydrogen activation[58] of tetrakis (dialkylamido) titanium precursors giving Ti(C,N) films[45,50,58,60] which also contain oxygen and hydrocarbon contamination. In the case of $(Cp^*)_2Ti(Me)Cl$, less carbon is found because the β-carbons are tied back in the Cp* ring.[58] Powder formation or flakey, poorly adhered films have been observed[45,50,58] at temperatures of 350 °C or less in the presence of a low power DC pulsed plasma. It has been suggested that this arises from gas phase nucleation due to heating required for vapour transport.[45] Similar adherence characteristics have been observed in conventional CVD[18,51] for temperatures below 350 °C. It should be noted that 350 °C has been shown to be a high enough temperature to break the C-C, C-H, C-N and Ti-N bonds.[50,58] However good adherent films can be deposited using TMT and TET $[Ti(NEt_2)_4]$ at substrate

temperatures as low as 280 °C in the presence of a high power pulsed DC plasma.[50,58] It seems likely that complete bond breaking takes place when the high power plasma is used, and that gas phase nucleation may be reduced at the lower temperature.

More recently, the use of an electron cyclotron resonance (ECR) plasma has enabled high quality, stoichiometric films to be deposited from TMT and nitrogen gas.[60,61] These films contained little carbon, oxygen and hydrogen even when deposited at temperatures as low as 100 °C. Film resistivities were comparable to those deposited by PVD methods. The explanation for these observations is as a result of using an ECR plasma which generally gives, by orders of magnitude, greater degrees of ionization, dissociation and vibrationally and electronically excited species in the molecular gases compared to RF or DC plasmas.[60,61] Consequently, a sufficiently high density of activated nitrogen species exists to react with the $Ti(NMe_2)_4$. Atomic nitrogen may replace the dimethylamido ligand to form TiN as shown by labelled $^{15}N_2$ RBS studies. As a result, any polymeric CH material produced in the coatings in RF or DC plasma processes is avoided: in which cases incomplete decomposition of TMT or lack of activated nitrogen species are likely. This work also demonstrated that the flow rate of TMT was critical to reduce the carbon and oxygen contamination and hence lower the resistivity; an excess of reactive radicals were found to be essential. Using a similar approach Intemann *et al.* demonstrated that lower deposition rates resulted from an increasing nitrogen concentration in the plasma gas because more homogeneous side reactions in the gas phase and on other hot surfaces led to a depletion of precursor over the substrate.[12] Addition of hydrogen to the plasma gas resulted in higher resistivity with the carbon content increasing[12,60,61] because of the reduction of activated nitrogen a result of nitrogen-hydrogen collisions.[60,61] Depositions in pure activated hydrogen were considered to be analogous to the thermal decomposition of TMT with activated hydrogen reacting with $*N(Me)_2$ ligands resulting in formation of dimethylamine.

In the following section, a detailed account is presented on how low pressure plasma assisted decomposition of TMT, with and without the presence of additional hydrogen gas, can yield Ti(O,C,N) species embedded in a polymeric matrix, $C_wH_xN_yO_z$.

6.2 EXPERIMENTAL

Tetrakis (dimethylamido) titanium (TMT), $Ti[N(CH_3)_2]_4$, (99% pure, Strem), being very air sensitive, was stored in the nitrogen environment of a glovebox in which it was transferred to a monomer tube. It was degassed by means of multiple freeze-pump-thaw cycles. Both low-density polyethylene films (LDPE, Metal Box) for ATR-FTIR and glass slides for XPS were used for substrates as described in Chapter 3. Both types of substrate were ultra-sonically cleaned in a bath of isopropyl alcohol for 30 s and allowed to dry in air prior to placement in the reactor at the appropriate substrate position.

Preliminary experiments with TMT at a pressure of $1.3x10^{-1}$ Torr, in the absence of monomer heating, were carried out using the same reactor configuration and substrate location as described for TiTP in Chapter 3. However the volume taken up by the pink 'glow' tended to increase into the monomer tube during the 3 min deposition due to a decrease in the system pressure.[62] The use of additional heating was not attempted since this was considered to result in lower reproducibility as experienced with the TiTP monomer. It was decided therefore to revert to the modified reactor configuration and substrate location as described for the $TiTP/H_2$ and $TiTP/NH_3$ systems in Chapters 4 and 5, since the plasma 'glow' was restricted by the sliding-joint arrangement.

The reactor was cleaned with an air plasma for 60 ± 15 min, having previously been scrubbed with detergent, rinsed with isopropyl alcohol and dried in an oven. Note polyethylene substrates were placed in the reactor after the plasma cleaning process to prevent surface oxidation as discussed in Chapter 3. Then the reactor was pumped down to a base pressure of $5.6x10^{-3}$ Torr with a leak rate better than $3x10^{-11}$ kgs^{-1}, before TMT monomer was allowed into the reactor for 2.5 min to give an equilibrium pressure of $5.6x10^{-2}$ Torr and flow rate of $2.5x10^{-8}$ kgs^{-1} (i.e. more than 99.8 % of the reactants were TMT precursor). The plasma was ignited for 3 min for XPS and 15 min for ATR, since a thicker film was required for the latter technique, before it was extinguished. The monomer source was then shut off and the reactor pumped back down for 5 min to near the base pressure (~$8.3x10^{-3}$ Torr). The reactor was then let up to atmospheric pressure and the samples transferred to the appropriate analytical instrument. Below an average power of 3 W, the pulsing mode was required to sustain a stable plasma (for $<P>$ =1 W, P_0 =3 W, T_1 =1.4 ms and T_2 =2.25 ms, see Chapter 3 for definitions).

In the case of TMT/H_2 gas mixtures, a similar procedure to that described in Chapter 4 was carried out. The reactor was pumped down to a base pressure of $5.6x10^{-3}$ Torr with a leak rate better than $3x10^{-11}$ kgs^{-1}, before hydrogen (99.993 %, BOC) was purged through the reactor for 5 min at a pressure of $5.4x10^{-2}$ Torr and flow rate of

$2.9x10^{-9}$ kgs^{-1} (i.e. more than 98.9 % of the gas was hydrogen). TMT monomer was then allowed into the reactor for 2.5 min to give a combined equilibrium pressure of $9.3x10^{-2}$ Torr. The plasma was ignited for 3 min for XPS and 15 min for ATR before it was extinguished followed by the monomer source being closed off. Hydrogen was purged through the reactor for a further 5 min before this was closed off and the reactor pumped down for 2 min to near the base pressure (~$8.3x10^{-3}$ Torr). The system was then let up to atmospheric pressure before the samples were transferred to the appropriate analytical instrument. Pulsing was still required below an average power of 3 W.

6.3 RESULTS

Both with and without the addition of hydrogen, the films that developed in the coil region of the reactor and the end of the delivery extension tube showed a brown/tan colour at powers greater than 3 W whilst for the lower powers the colour was more golden and extended back into the 'bell-jar' part of the reactor. On exposure to air, the slides appeared to be grey in colour and if they were held up and tilted towards the light, an interference diffraction pattern could be observed. The colours of both the reactor and the slides faded with time in air as above. For the longer deposition times required for ATR, the reactor was more thickly coated and darker brown in colour. On tilting towards the light, the films showed diffraction patterns. On prolonged exposure to air (~1 hr), the films had a yellow appearance prompting analysis of both freshly deposited and aged samples.

6.3.1 X-RAY PHOTOELECTRON SPECTROSCOPY (XPS)

Elemental compositions for the deposited films as a function of plasma glow discharge power are shown in Fig. 1 for both reactant gas systems in the new reactor design. In the case of TMT, Fig. 1(a), both the carbon and nitrogen contents initially increase as the power is increased and then levels off, whilst the titanium and the oxygen values follow an opposite trend. Titanium species readily oxidise on exposure to air and oxidation of the plasma polymer also occurs as clearly indicated later in the C(1s) XP spectrum, Fig. 2(a); this is most probably due to the presence of trapped free radicals[62] reacting with atmospheric water and/or oxygen. The extent of decomposition of TMT is limited because little energy is provided to the precursor molecules up to 3 W, particularly over the small distance between the end of the extension delivery tube and the substrate position through which the precursor molecules and fragments pass. Consequently the new species, created by the small amount of fragmentation/excitation of the monomer in

this low power regime, cannot undergo further substantial fragmentation/excitation/rearrangement on passing through the reactor since they rapidly reach the substrate position. Above 5 W it appears that the extent of plasma polymerization becomes independent of the glow discharge power because of the small passage of the species between entering the reactor and reaching the substrate. Therefore the composition appears to be independent of the glow discharge power.

In the case for the TMT/H_2 gas mixture, similar trends for the elemental compositions occur up to 5 W, Fig. 1(b); the carbon and nitrogen contents increase whilst those for titanium and oxygen decrease. Then above 5 W, the carbon content slightly decreases whilst the nitrogen, titanium and oxygen contents slightly increase. Therefore the main difference on introduction of hydrogen appears to be a reduction in the amount of incorporated carbon at the higher glow discharge powers.

Experimental runs for XPS analysis at glow discharge powers of 5 W and 30 W were also carried out on TMT plasma polymer films deposited at 8.5 cm, 19.0 cm and 25.5 cm from the sliding-joint inlet and the elemental compositions and ratios are shown in Table 5. The trend is the same for both powers: more organic incorporation occurs downstream and incomplete coverage occurs upstream. This indicates that once initial decomposition of TMT occurs with the condensation of titanium species, the organic byproducts undergo a greater degree of plasma polymerization as they pass through the coils (i.e. the highest energy zone). This effect is greater at 30 W. Since monomer entry to the reactor was downstream of the samples placed at 8.5 cm from the sliding joint-inlet, insufficient film coverage of the substrates was observed.

Table 5 Elemental composition and ratios obtained for TMT plasma polymers at different glow discharge powers and different substrate locations.

Power/ W	Substrate Position/ cm	% C ± 0.1	% Ti ± 0.1	% N ± 0.1	% O ± 0.1	Ti/C ± 0.01	N/C ± 0.01	O/C ± 0.01	N/Ti ± 0.01	O/Ti ± 0.01
5	8.5*	63.6	6.3	14.1	15.2	0.10	0.22	0.24	2.24	2.41
	19	58.5	10.7	12.7	18.3	0.18	0.22	0.31	1.19	1.71
	25.5	62.3	7.6	14.5	15.5	0.12	0.23	0.25	1.91	2.04
30	8.5*	80.7	0.8	10.9	4.7	0.01	0.14	0.06	13.63	0.17
	19	56.0	11.6	13.7	18.7	0.21	0.24	0.33	1.18	1.61
	25.5	80.1	2.4	13.7	3.8	0.03	0.17	0.05	5.71	1.58

* Note the remaining percentage marked by the asterix in Table 5 is made up by substrate silicon indicating insufficient coverage.

(a)

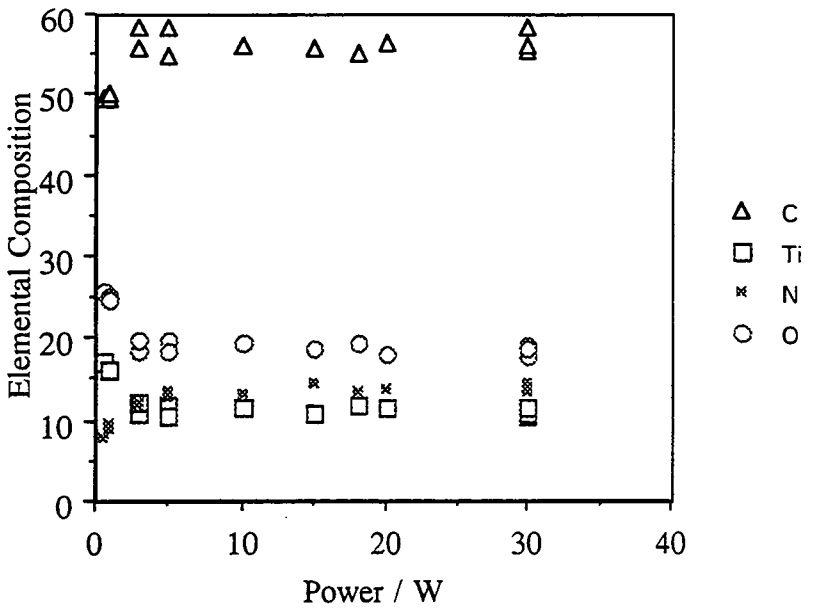

(b)

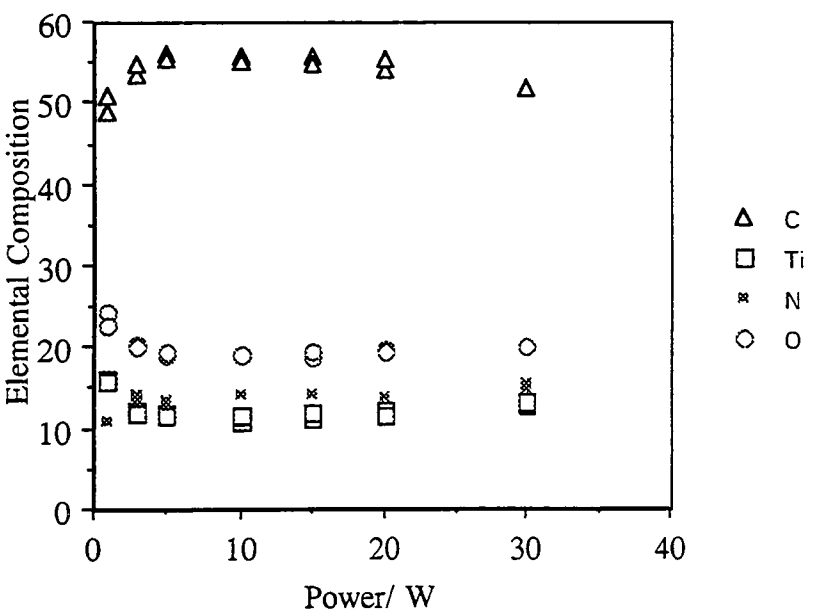

Fig. 1 Elemental percentages as a variation of glow discharge power (3 min, 19 cm): (a) TMT; and (b) TMT/H_2.

Typically in the C(1s) XP spectra as indicated in Fig. 2(a), a shoulder to higher binding energy of the hydrocarbon peak at 285.0 eV was observed. The spectra were not fully deconvoluted due to the many closely lying chemical environments that would have

given similar binding energy values (see section 5.3.1). However, in order to determine the approximate binding energies for the other elements, it was necessary to obtain the sample charging offset relative to the carbon hydrocarbon peak at 285.0 eV. This was achieved by peak fitting the carbon spectra with three peaks so as to obtain a good fit.

Figure 2 illustrates typical spectra collected for the Ti(2p), N(1s) and O(1s) respectively. Assignment of the Ti(2p) region is rather difficult since literature values given for nitrides, oxides and oxynitrides span wide ranges. The binding energy values for the XP $Ti(2p_{3/2})$ peak at 458.0 ± 0.2 eV, illustrated by a typical spectrum in Fig. 2(b), do not agree with those assigned to TiN at 455.0-455.5 eV[63-65] and are also a little low for the value quoted for that of amorphous TiO_2 at 458.8 eV.[63,66,67] A value of 458.5 eV was given for TiO_2 by Kaznetsov *et al.*[65] and for the oxide peak found in sputter cleaned, sputter deposited TiN by Strydom and Hoffman.[68] Ernsberger *et al.* proposed a model where an intermediate type species (~457 eV) occurs in the grain boundaries between the amorphous oxide cap and the nitride.[69] This has been more recently supported by Saha and Tompkins.[63] Siemensmeyer *et al.* assigned the peak at 457.5 eV found in oxidized TiN as TiN, titanium suboxides, and oxynitrides at the nitride/oxide interface.[64] It therefore seems most probable that the Ti(2p) environment consisted of some form of oxynitride with a dominant oxide component. Independent standard oxynitride samples were not characterized to confirm this assignment.

There is no evidence of the Ti-N, nitride peak, within the vicinity of 397.0-397.5 eV[63,64] in the N(1s) XP spectra, as illustrated in Fig. 2(c). The maxima were located at a binding energy of 399.5 ± 0.2 eV. Siemensmeyer *et al.* assigned the small peak at approximately 399.5 eV as the tail of the above mentioned nitride peak.[64] In the work now reported the 399.5 eV peak is the main feature in the N(1s) XP spectra and as a result, the above explanation can be discounted. Assignment to nitrogen bonded to carbon is most likely, though there may be a contribution from nitrogen bonded to oxidized carbon.[70]

Similarly the O(1s) XP spectra, see Fig. 2(d) are not easily deconvoluted, owing to the variety of possible environments. The maxima are located at 529.7 ± 0.2 eV which most closely resemble the values assigned to the oxide,[63,65] whilst at higher binding energies the variety of environments are possibly due to contributions from oxidized carbon/oxidized carbon-nitrogen (e.g. O=C-N),[70] substoichiometric oxide, an oxynitride, or adsorbed water.[63]

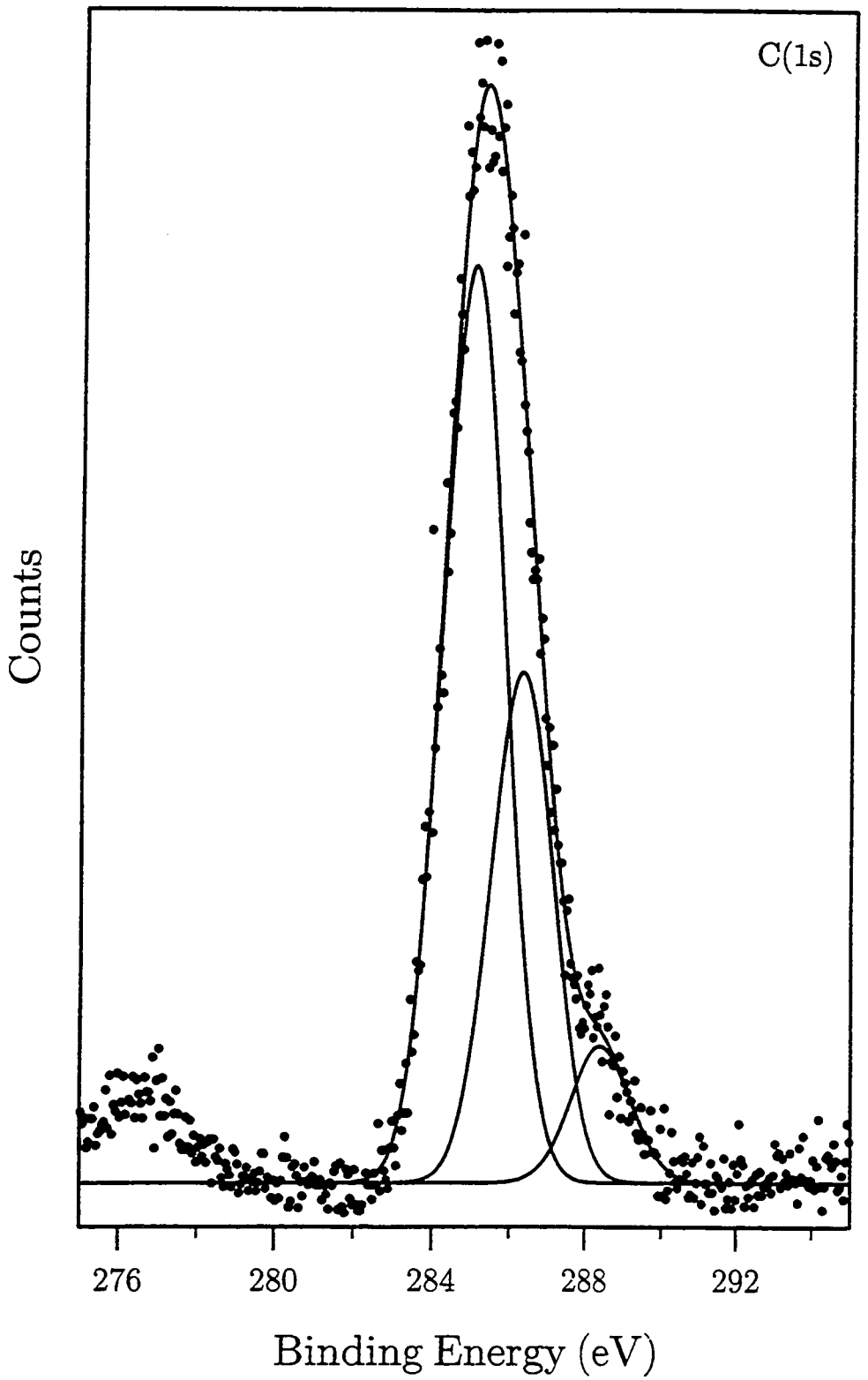

Fig. 2(a) C(1s) XP spectrum for PACVD of TMT onto a glass substrate (5 W, 3 min, 19 cm).

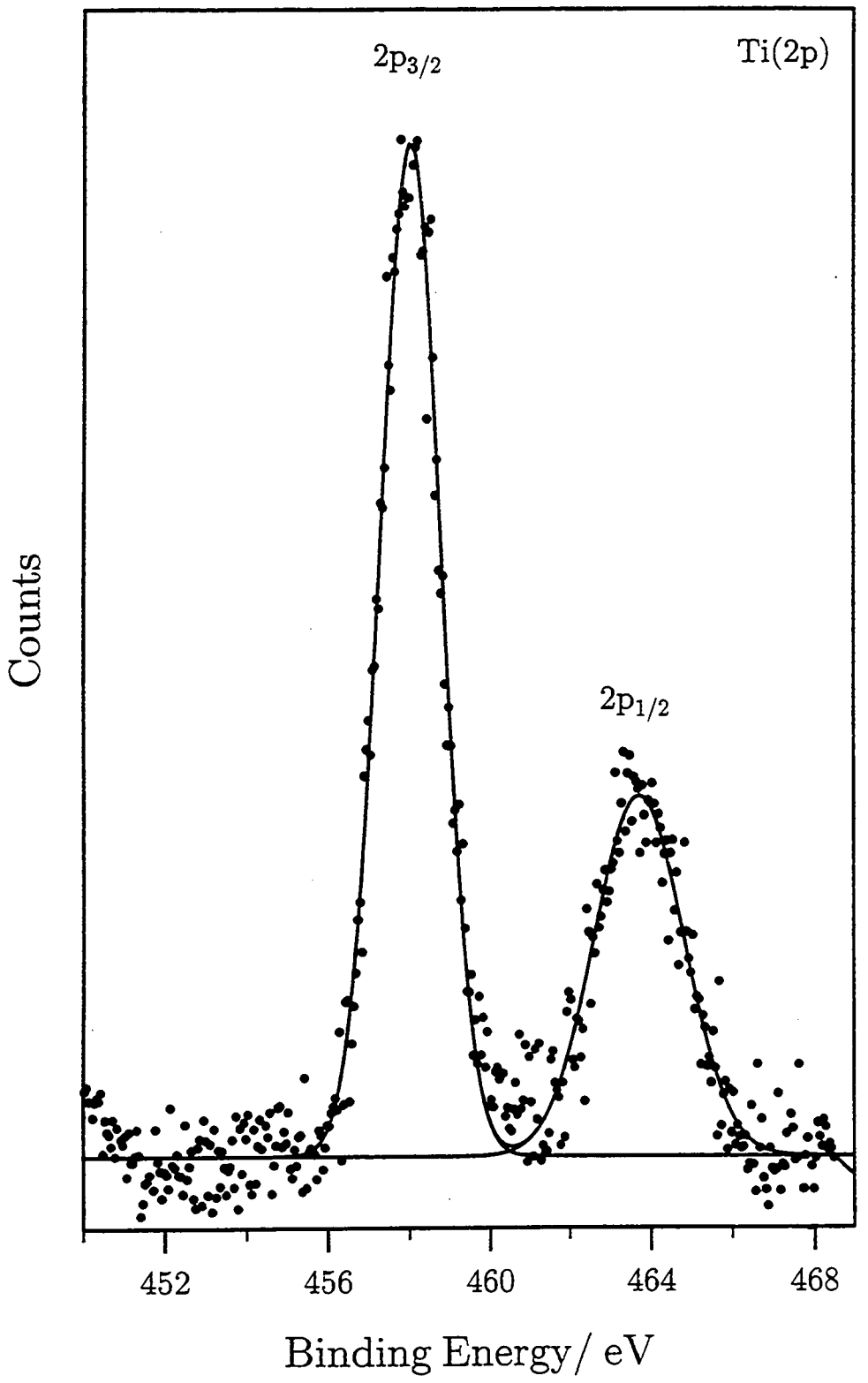

Fig. 2(b) Ti(2p) XP spectrum for PACVD of TMT onto a glass substrate (5 W, 3 min, 19 cm).

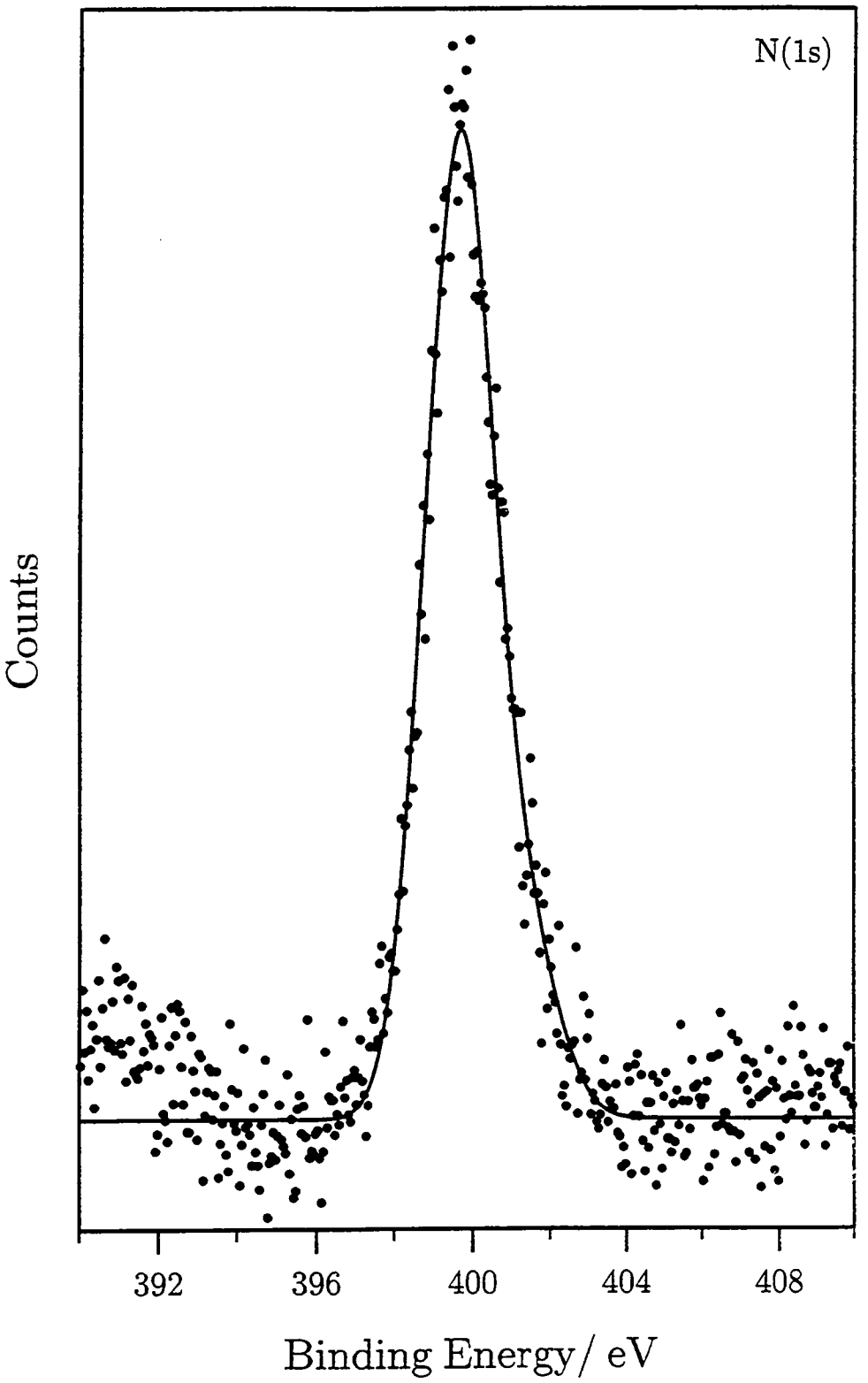

Fig. 2(c) N(1s) XP spectrum for PACVD of TMT onto a glass substrate (5 W, 3 min, 19 cm).

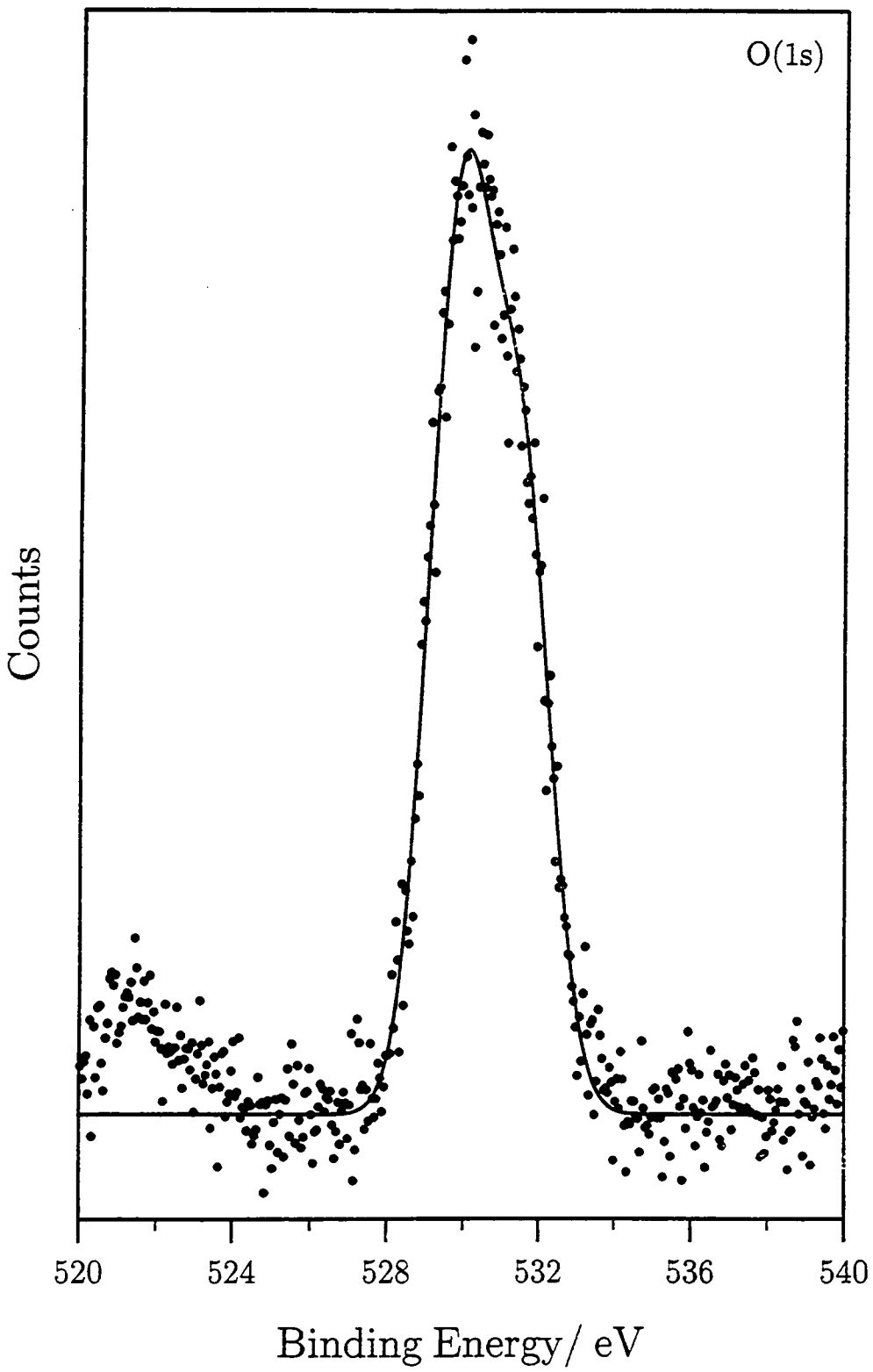

Fig. 2(d) O(1s) XP spectrum for PACVD of TMT onto a glass substrate (5 W, 3 min, 19 cm).

A 15 W TMT plasma polymer sample was left to age in ambient conditions for approximately one month. (Two samples were placed adjacent to one another at the normal substrate position of 19 cm from the sliding-joint inlet and the experiment carried out as above). The results are summarized in Table 6. The aging process reiterates the difficulty in assigning peak fits to the C(1s), N(1s) and O(1s) regions since some degree of oxidation of the fresh samples will have occurred. In Fig. 3, the aging effects are clearly illustrated by the increase in the intensities of the environments to higher binding energies of the main peaks in the aged C(1s), N(1s) and O(1s) XP spectra which is consistent with the reaction of trapped free radicals in the plasma polymer with water and/or oxygen.[62] The major peaks in the aged Ti(2p), N(1s) and O(1s) XP spectra also shift to slightly higher binding energies by about 0.3-0.5 eV; an indication of greater oxidation. The spectra have been normalized to show qualitative information from the peak shapes. Both the apparent loss of nitrogen content on aging, and the binding energy shift mentioned above are consistent with a growing capping oxide layer causing the oxynitride to move farther from the surface,[63] as well as possible loss of imine-type and amine functionalities. Loss of these latter species has been observed for nitrogen plasma treated polymer surfaces with aging.[71,72] Similar aging effects were observed for the 15 W TMT/H_2 plasma polymer and the compositional changes are given in Table 6.

Table 6 Elemental composition and ratios for fresh and aged samples (15 W, 3 min, 19 cm).

Reagents	Sample	% C ± 0.1	% Ti ± 0.1	% N ± 0.1	% O ± 0.1	Ti/C ± 0.01	N/C ± 0.01	O/C ± 0.01	N/Ti ± 0.01	O/Ti ± 0.01
TMT	Fresh	56.8	12.2	11.5	19.5	0.21	0.20	0.34	0.94	1.60
	Aged	55.9	11.6	8.6	23.8	0.22	0.15	0.42	0.74	2.05
TMT/H_2	Fresh	55.5	11.7	13.4	19.5	0.21	0.24	0.35	1.15	1.67
	Aged	54.3	10.8	10.2	24.7	0.20	0.19	0.46	0.94	2.29

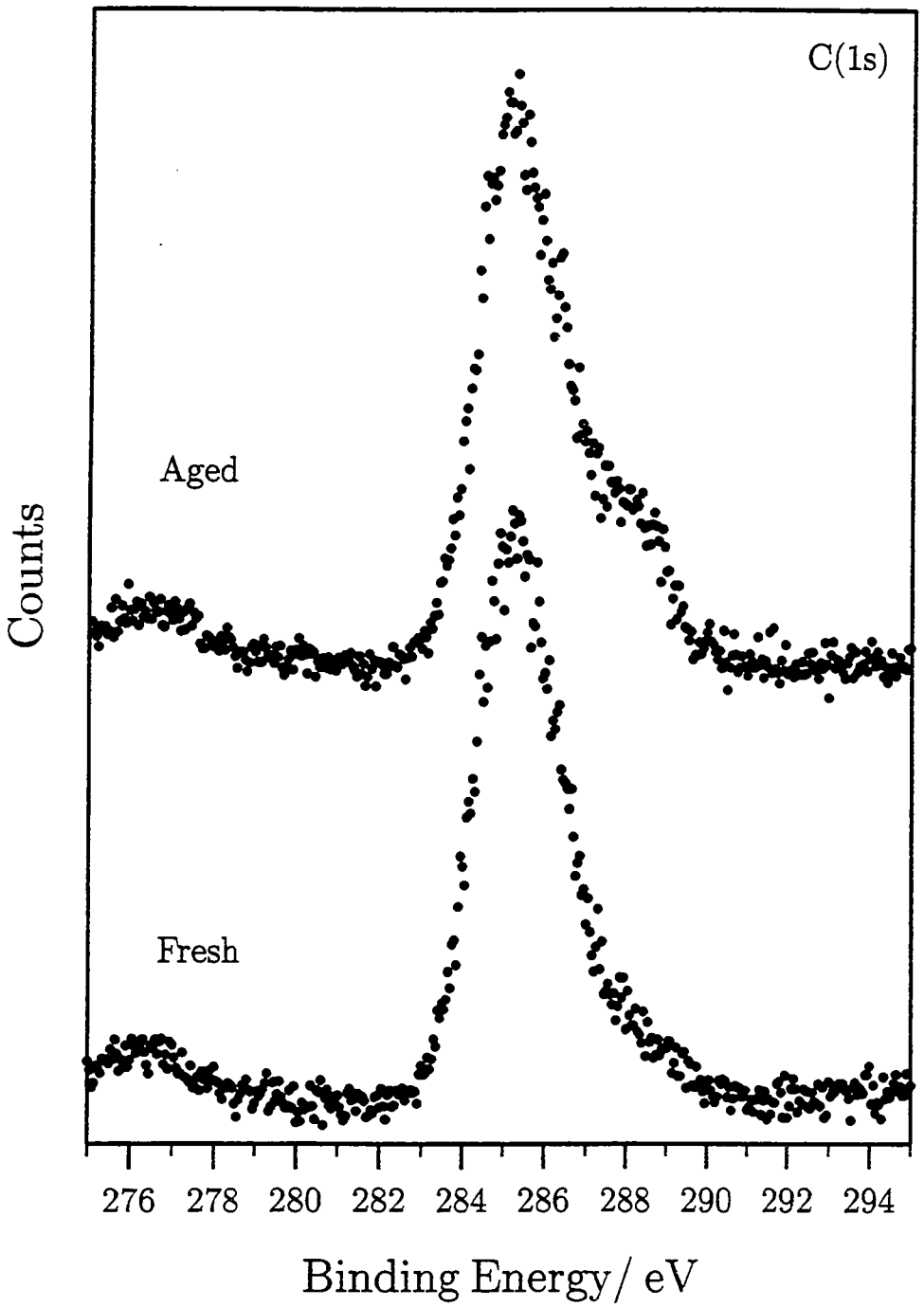

Fig. 3(a) C(1s) XP spectra for fresh and aged (approx. 1 month) PACVD samples of TMT onto a glass substrate (15 W, 3 min, 19 cm).

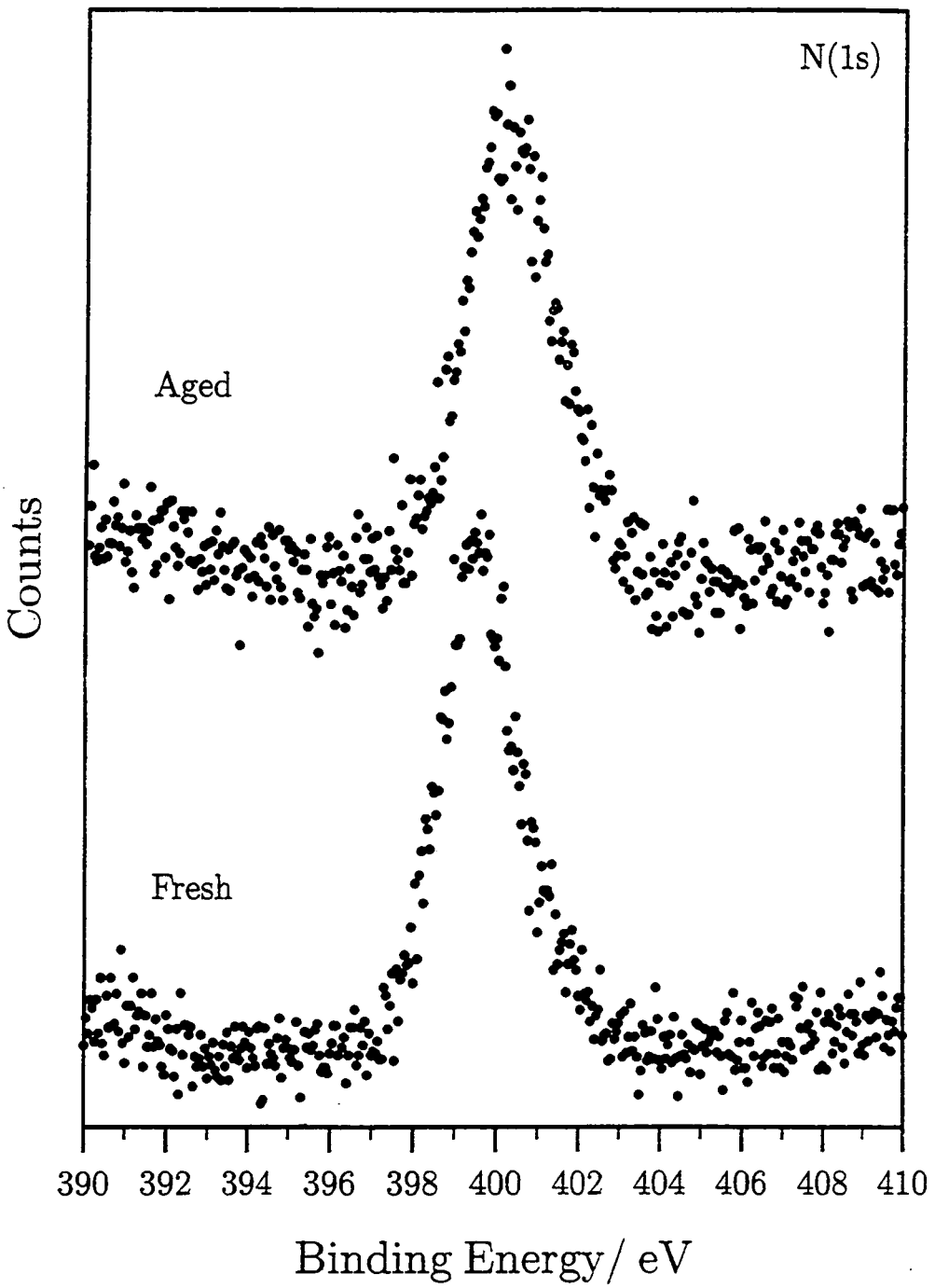

Fig. 3(b) N(1s) XP spectra for fresh and aged (approx. 1 month) PACVD samples of TMT onto a glass substrate (15 W, 3 min, 19 cm).

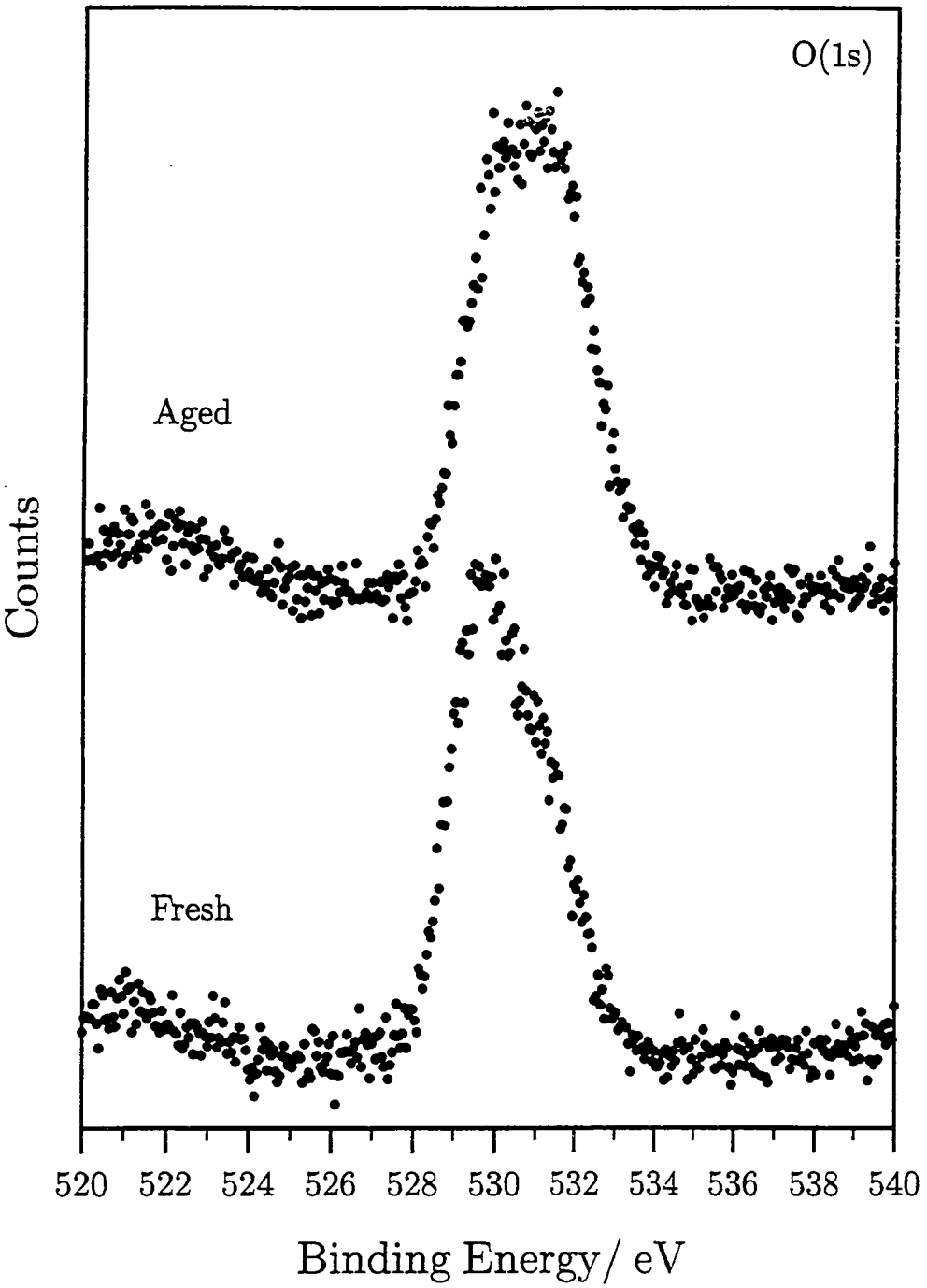

Fig. 3(c) O(1s) XP spectra for fresh and aged (approx. 1 month) PACVD samples of TMT onto a glass substrate (15 W, 3 min, 19 cm).

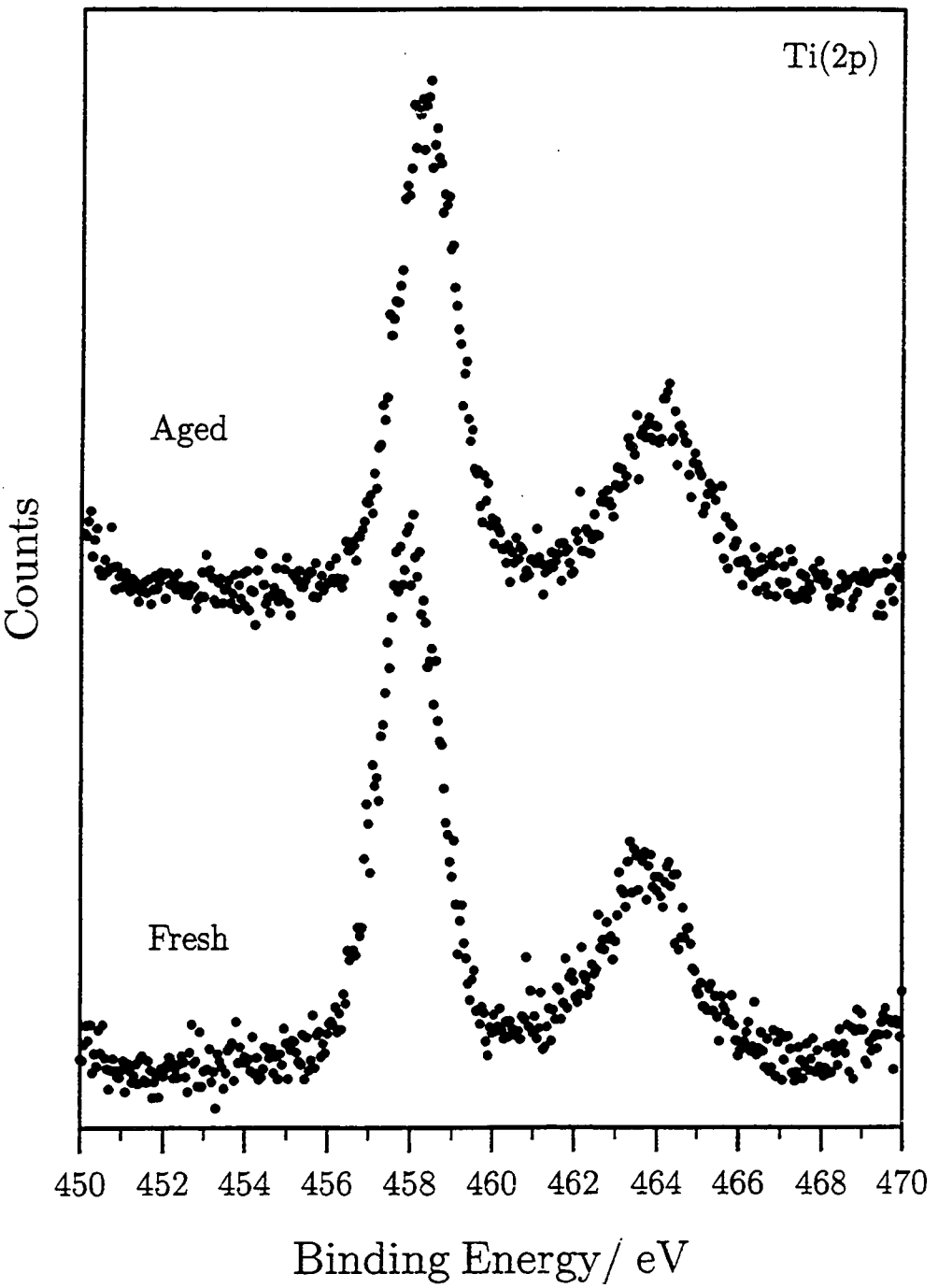

Fig. 3(d) Ti(2p) XP spectra for fresh and aged (approx. 1 month) PACVD samples of TMT onto a glass substrate (15 W, 3 min, 19 cm).

6.3.2 XPS DEPTH PROFILING

Figure 4 illustrates the elemental trends with sputtering time. For TMT, Fig. 4(a), after the initial removal of adventitious hydrocarbon contamination and low molecular hydrocarbon species (after approximately 60 s of sputtering), the carbon and titanium contents effectively remain constant, whilst the oxygen decreases and the nitrogen increases. Loss of oxygen is expected since it is typically preferentially sputtered from oxides.[73]

In the absence of any external charge compensation, the sample becomes positively charged on sputtering, as well as from X-ray bombardment. This results in an apparent increase in the peak binding energies. It can be assumed that the major environment in the C(1s) XP spectra results from plasma polymer hydrocarbon at 258.0 eV. Therefore the charge compensation offset can be approximately calculated. The presence of a weak shoulder at ~282 eV shown in Fig. 5(a) indicates the existence of titanium directly attached to carbon, as in Ti-CH_2-, Ti=CH- or TiC.[18]

Consistent with this assumption is the emergence of new dominant peak at 397.1 eV in the N(1s) XP spectrum, Fig. 5(b). Since nitrogen bonded to carbon can also be observed centred at ~399.3 eV,[70] the assignment of the 397 eV peak can be given to the form of imide (Ti=NR), imide (Ti-NR_2) or nitride (Ti-N).[18]

Broadening of the Ti(2p) XP region, Fig. 5(c), towards lower binding energies indicates a variety of low titanium oxidation states[65] which confirms the preferential sputtering of oxygen from oxides.[73] The presence of Ti-N and Ti-C environments cannot also be discounted. There is a corresponding shift to higher binding energy (~0.8 eV) in the O(1s) XP region, Fig. 5(d), again observed in reduced oxides.[65] Similar compositional trends for TMT/H_2 were found, see Fig. 4(b) and the XP spectra were almost identical.

(a)

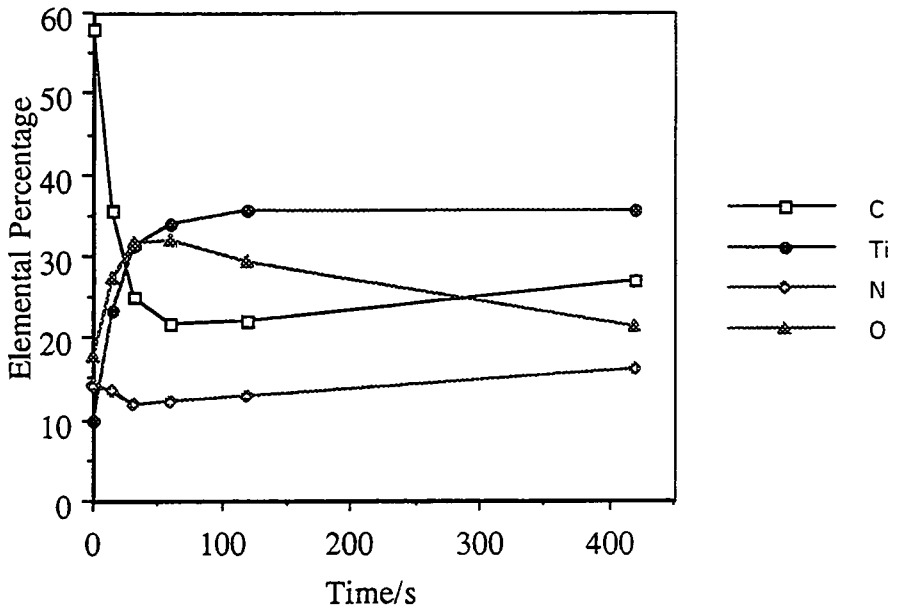

(b)

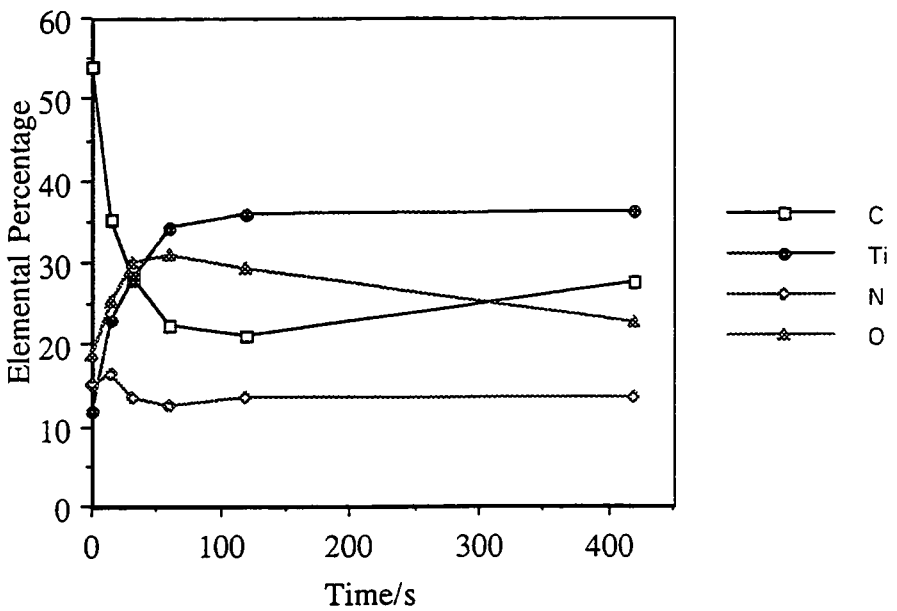

Fig. 4 XPS depth profile for PACVD films onto a glass substrate (15 W, 3 min, 19 cm): (a) TMT; and (b) TMT/H_2.

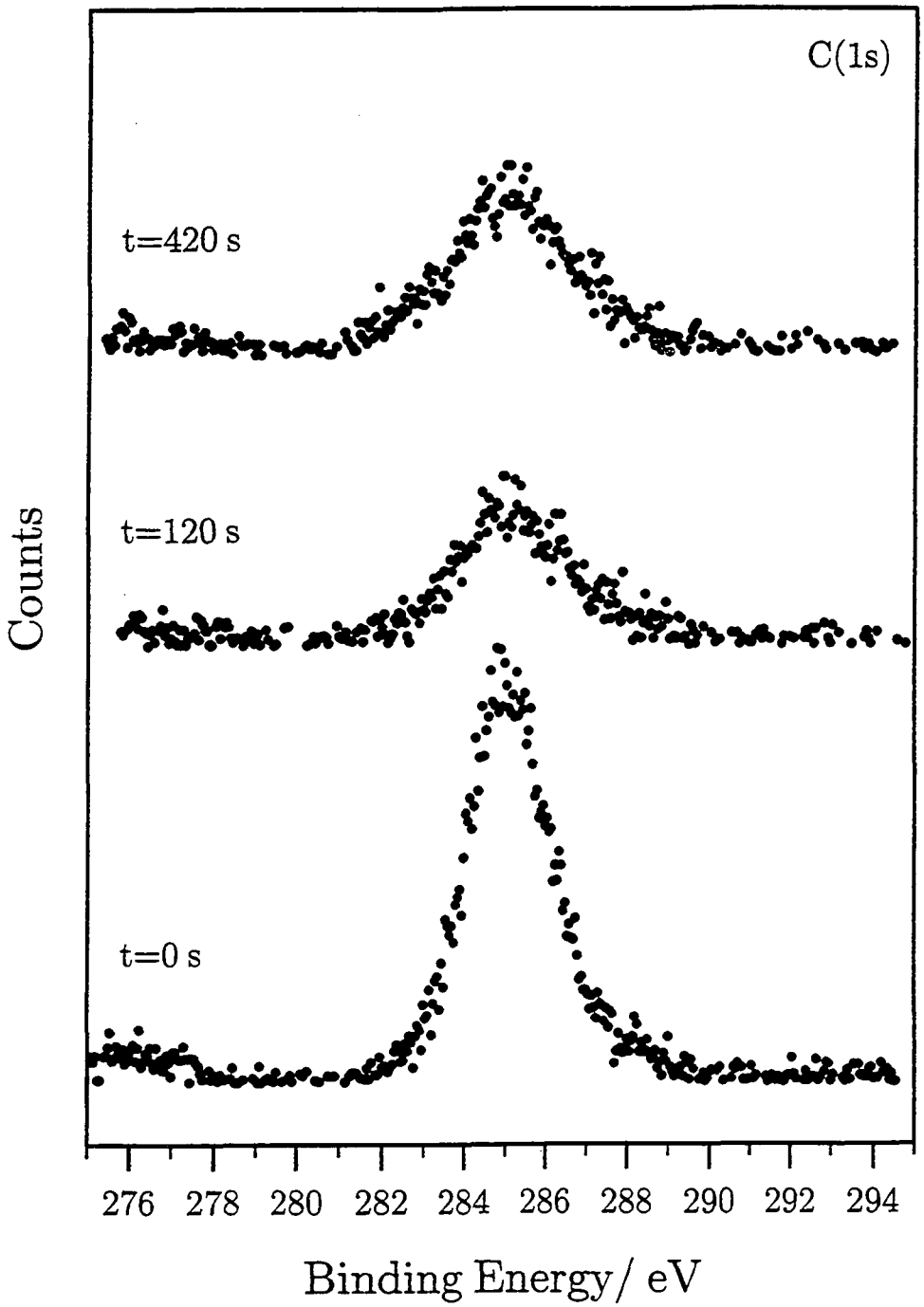

Fig. 5(a) C(1s) XP depth profile spectra of PACVD of TMT onto a glass substrate (15 W, 3 min, 19 cm) recorded after given sputtering times.

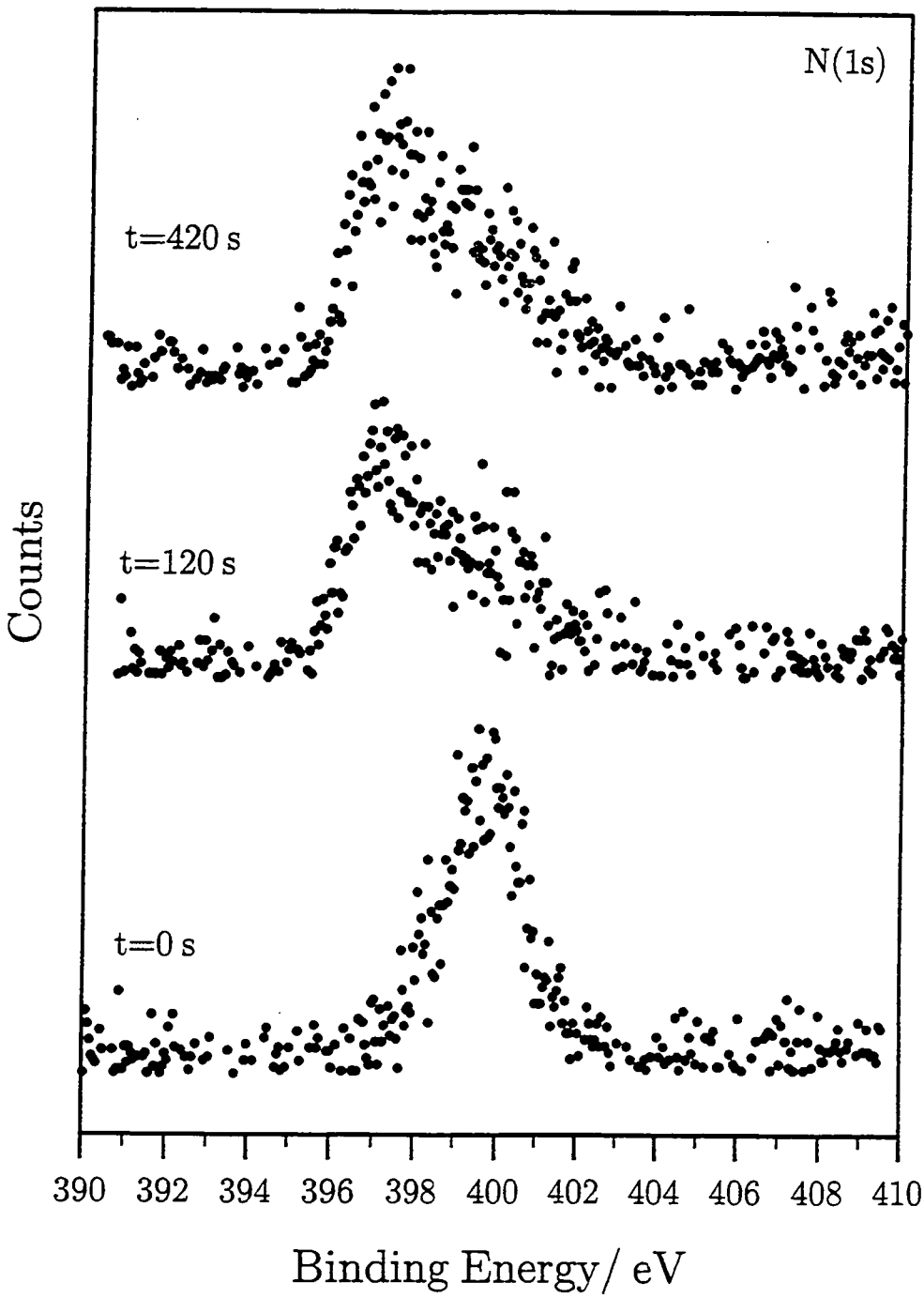

Fig. 5(b) N(1s) XP depth profile spectra of PACVD of TMT onto a glass substrate (15 W, 3 min, 19 cm) recorded after given sputtering times.

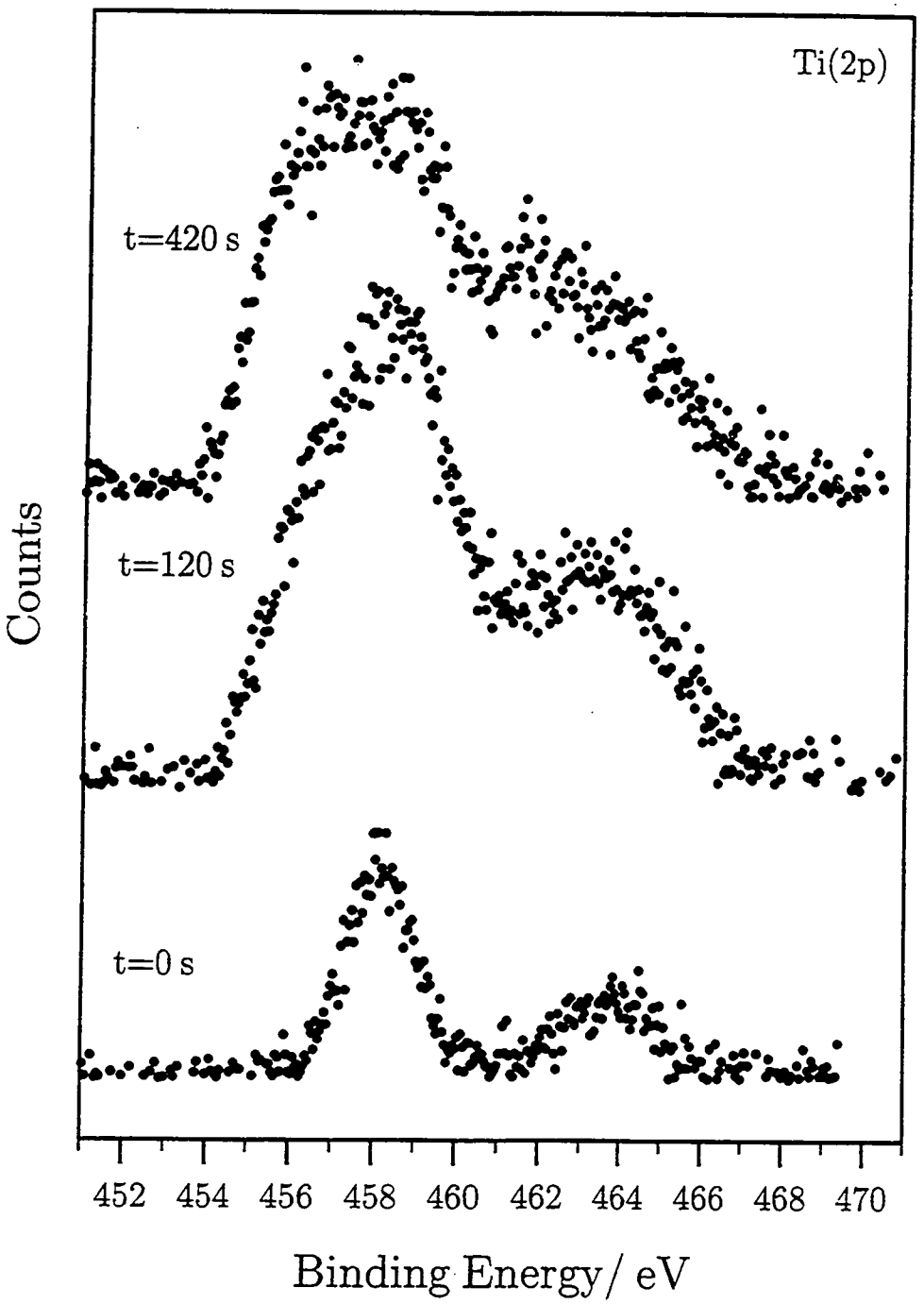

Fig. 5(c) Ti(2p) XP depth profile spectra of PACVD of TMT onto a glass substrate (15 W, 3 min, 19 cm) recorded after given sputtering times.

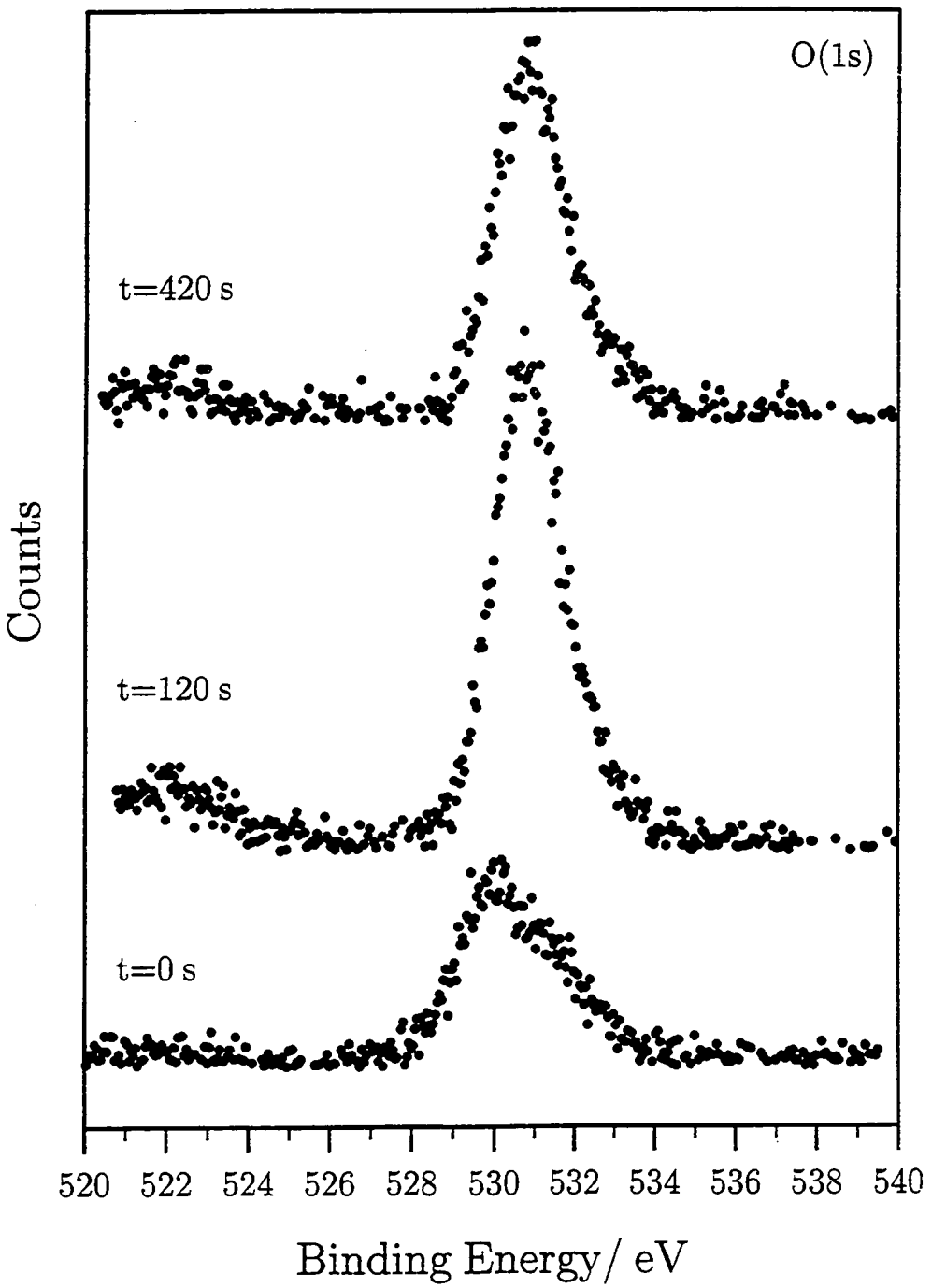

Fig. 5(d) O(1s) XP depth profile spectra of PACVD of TMT onto a glass substrate (15 W, 3 min, 19 cm) recorded after given sputtering times.

6.3.3 ATTENUATED TOTAL REFLECTION FOURIER TRANSFORM INFRARED SPECTROSCOPY (ATR-FTIR)

Figure 6 shows the infrared transmission spectrum of TMT with the main mode assignments summarized in Table 8.

Table 8 Vibrational mode assignments for TMT.[55,74,75]

Assignment	Wavenumbers/ cm^{-1}
CH_3 stretch	2907, 2850, 2768
CH_3 deform	1460, 1445, 1422, 1250
CH_3 rock	1144, 1123
NC_2 asym stretch	1055
NC_2 sym stretch	959
NH bend	787
TiN_4 asym stretch	586

It can be seen immediately in Fig. 7 that the deposited plasma polymer films of TMT and TMT/H_2 become thicker at higher powers with the attenuation of the more surface sensitive[76] polyethylene features near 2900 cm^{-1}.

The ATR spectrum of the 15 W TMT plasma polymer deposited onto polyethylene is shown in Fig. 8. Bands have been tentatively assigned since many possibilities can exist. For example, the N-H stretching and the N-H bending are found in the same general region as the hydroxyl and carbonyl stretchings.[62] Features include a broad band around 3200 cm^{-1} which could arise from O-H and/or N-H stretching.[77] A band at 2976 cm^{-1} corresponds to the asymmetric CH_3 stretching. Evidence of the broadening of the polyethylene CH_2 stretches near 2900 cm^{-1} suggests new CH_2 environments arising from the plasma polymer.

The broad band between ~1740-1500 cm^{-1} appears to include several absorbances with maxima at ~1710 cm^{-1}, ~1643 cm^{-1}, ~1607 cm^{-1} and ~1539 cm^{-1}. The 1710 cm^{-1} maximum may arise from a carbonyl stretch (e.g. from a carboxylic acid),[77] the 1643 cm^{-1} peak from the carbonyl amide I band and the N-H bending vibration amide II band at 1539 cm^{-1}.[62,63] The 1607 cm^{-1} could be an amine-like N-H bending vibration or due to the presence of vinyl groups.[62,77] The C=N stretch also falls in the above broad region as do the asymmetric stretches of the NO_2 and carboxylate groups.[77] The 1387 cm^{-1} and 1121 cm^{-1} bands are indicative of the symmetric CH_3 stretch and CH_3 rock respectively.

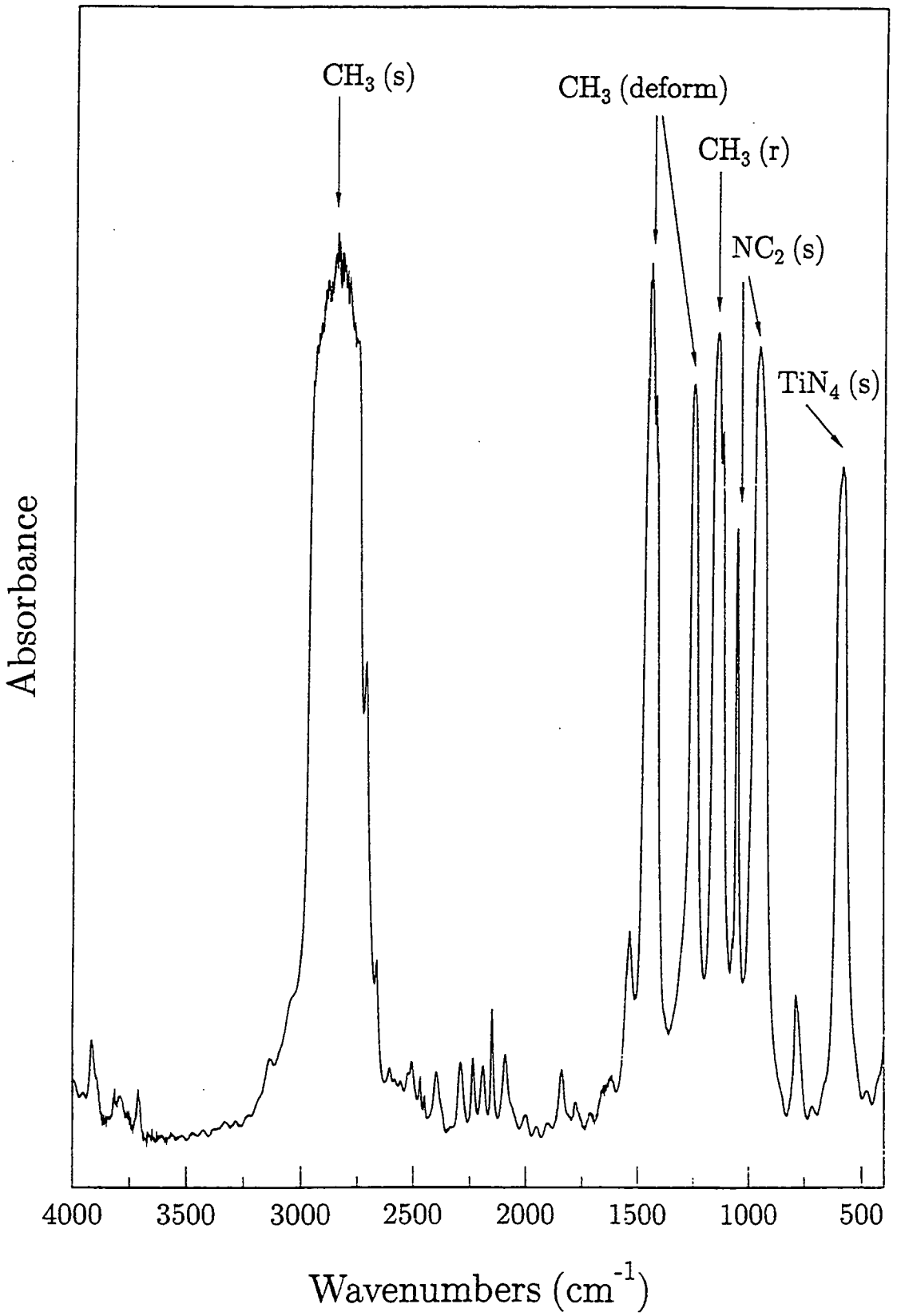

Fig. 6 Transmission IR spectrum of TMT.

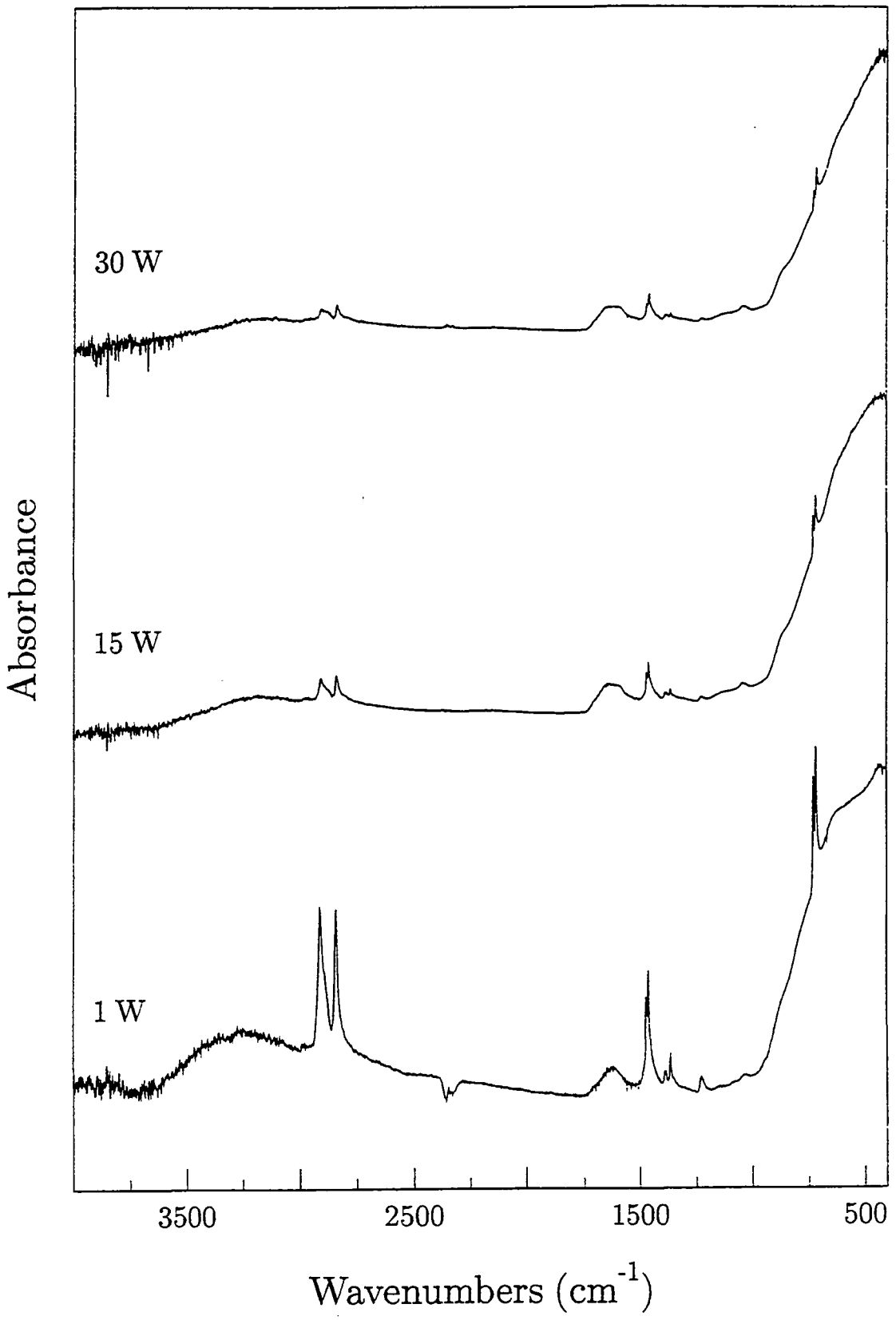

Fig. 7(a) ATR-FTIR spectra for PACVD of TMT onto polyethylene substrate as a function of glow discharge power (15 min, 19 cm).

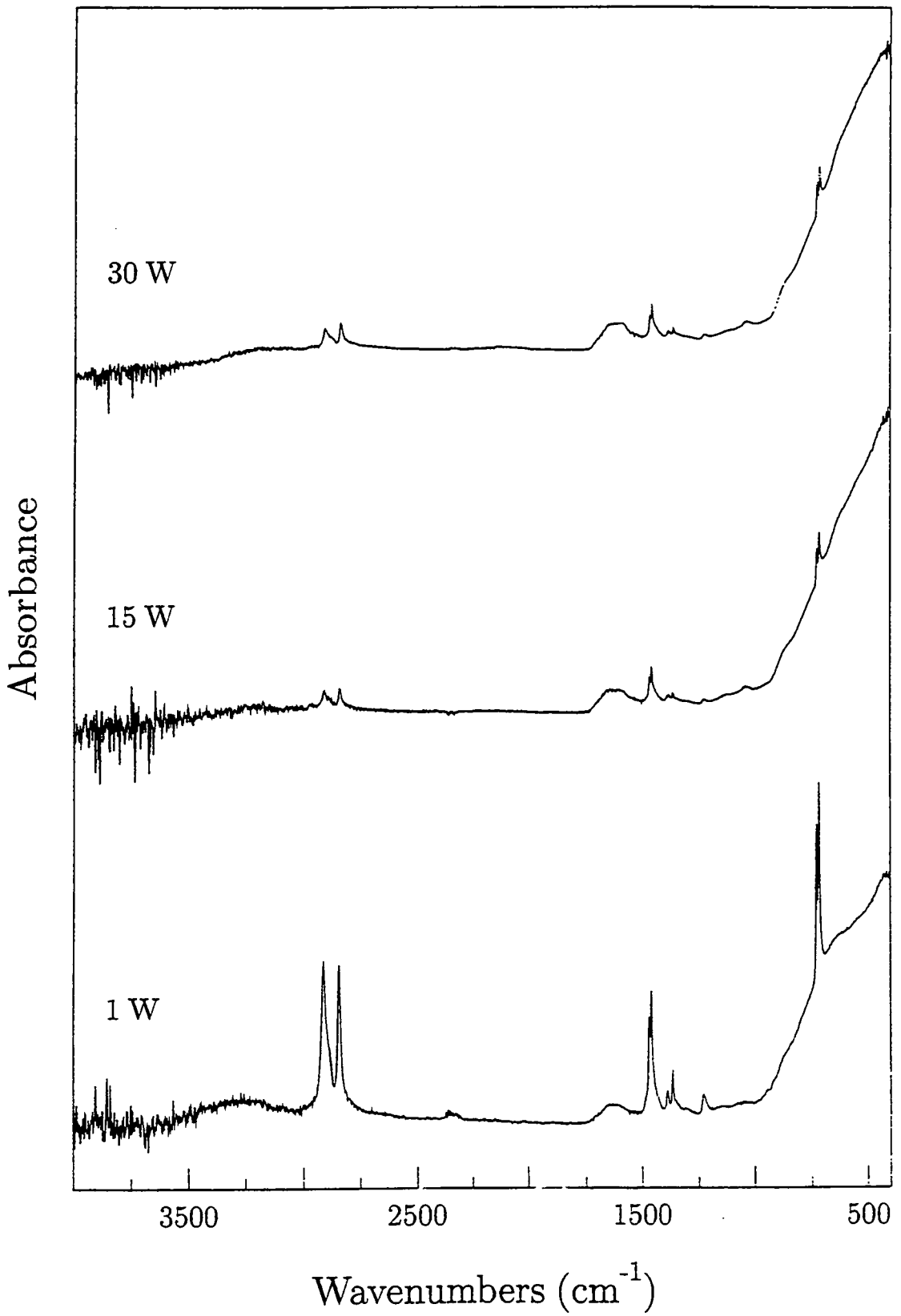

Fig. 7(b) ATR-FTIR spectra for PACVD of TMT/H_2 onto polyethylene substrate as a function of glow discharge power (15 min, 19 cm).

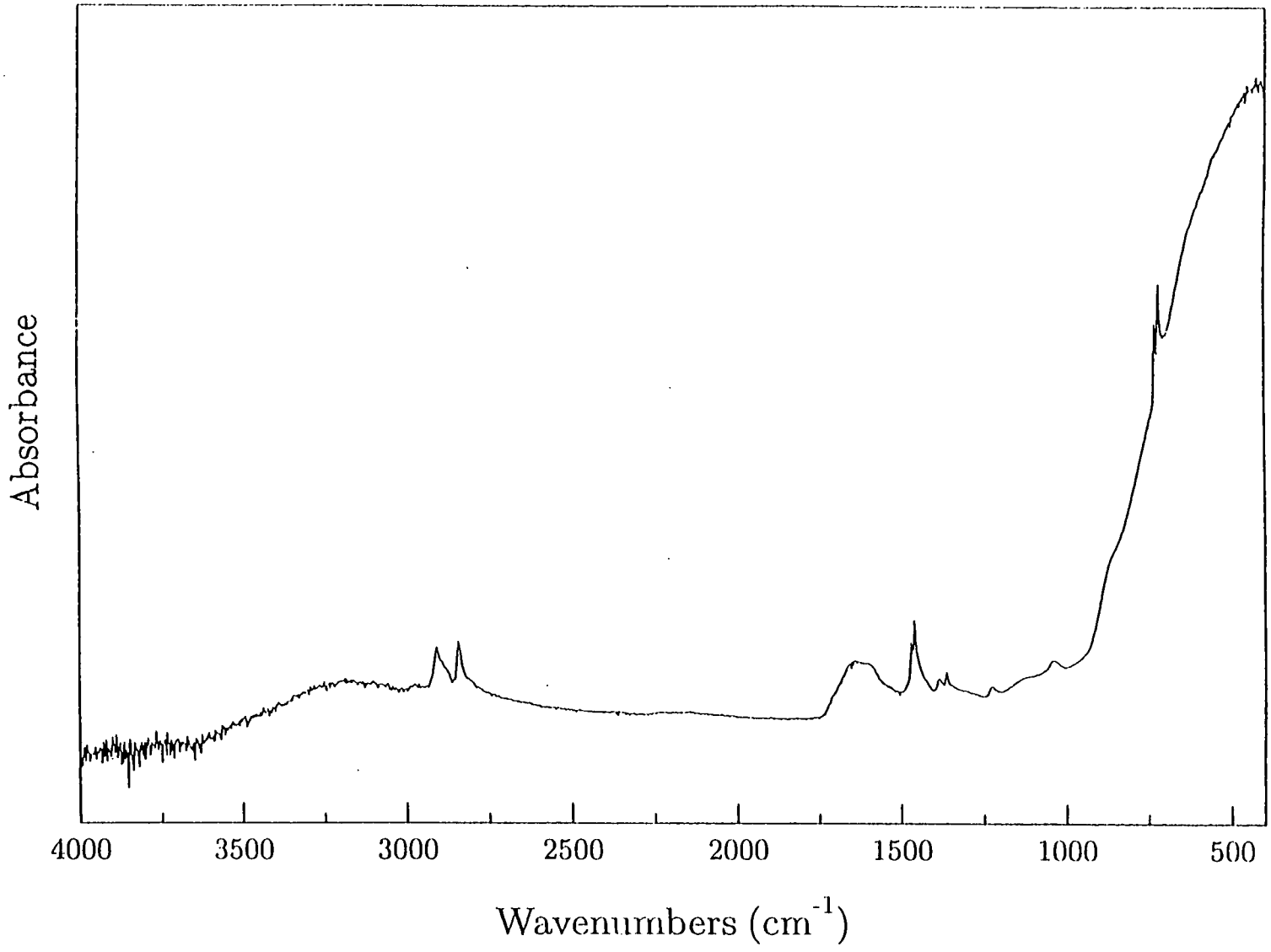

Fig. 8 ATR-FTIR spectrum for PACVD of TMT onto polyethylene substrate (15 W, 15 min, 19 cm).

The peak at 1042 cm^{-1} may indicate a C-O stretch,[77] a C-N stretch[77] or even the NC_2 asymmetric stretch seen in the TMT precursor.[55,74,75] The large cut-off region below 900 cm^{-1} is indicative of Ti-O stretchings as observed for bulk lattice vibrations[78] in TiO_2 which appears to have hidden any Ti-N stretching if at all present.

Samples placed 1 cm downstream of the normal substrate position (i.e. 20 cm from the sliding-joint inlet) gave thinner coatings as determined by the intensity of the polyethylene bands near 2900 cm^{-1}. However more intense broad bands around 3200 cm^{-1} and between 1740-1500 cm^{-1} suggest either a greater concentration of environments in this region arising from greater plasma polymerization of organic species downstream, or a greater degree of oxidation (explained in the following paragraph), since these samples were analyzed about 20 min after the 19 cm samples. The former is more probable since this agrees with the results by XPS for samples located downstream of the RF coils. Confirmation of this interpretation may be achieved by analyzing the 20 cm ATR samples first.

Samples were aged in ambient conditions for a month. The most significant changes occurred in the 1750-1000 cm^{-1} range as illustrated by Fig. 9 for the 15 W TMT/H_2 plasma polymer. The broad band between 1740-1500 cm^{-1} increases in magnitude with a maximum around 1590-95 cm^{-1}. Typically this value is indicative of the asymmetric carboxylate stretch which is commonly found in aged plasma polymers.[62] Alternatively, the increase in the broad band at ~1590 cm^{-1} may be a result of the increased presence of carbonyl, carbonyl amide I and NO_2 groups and/or an increase in the vinylic component due to the recombination of trapped free radicals.[77]

Another major feature is the emergence of the broad band with maxima around 1345 cm^{-1} and 1314 cm^{-1}. The region may include the symmetric stretch of the carboxylate[79] or NO_2 groups.[77] Alternatively this could be assigned to the twist and wagging modes of CH_2 that have been found in solid sample spectra of long-chain acids, amides and esters.[77]

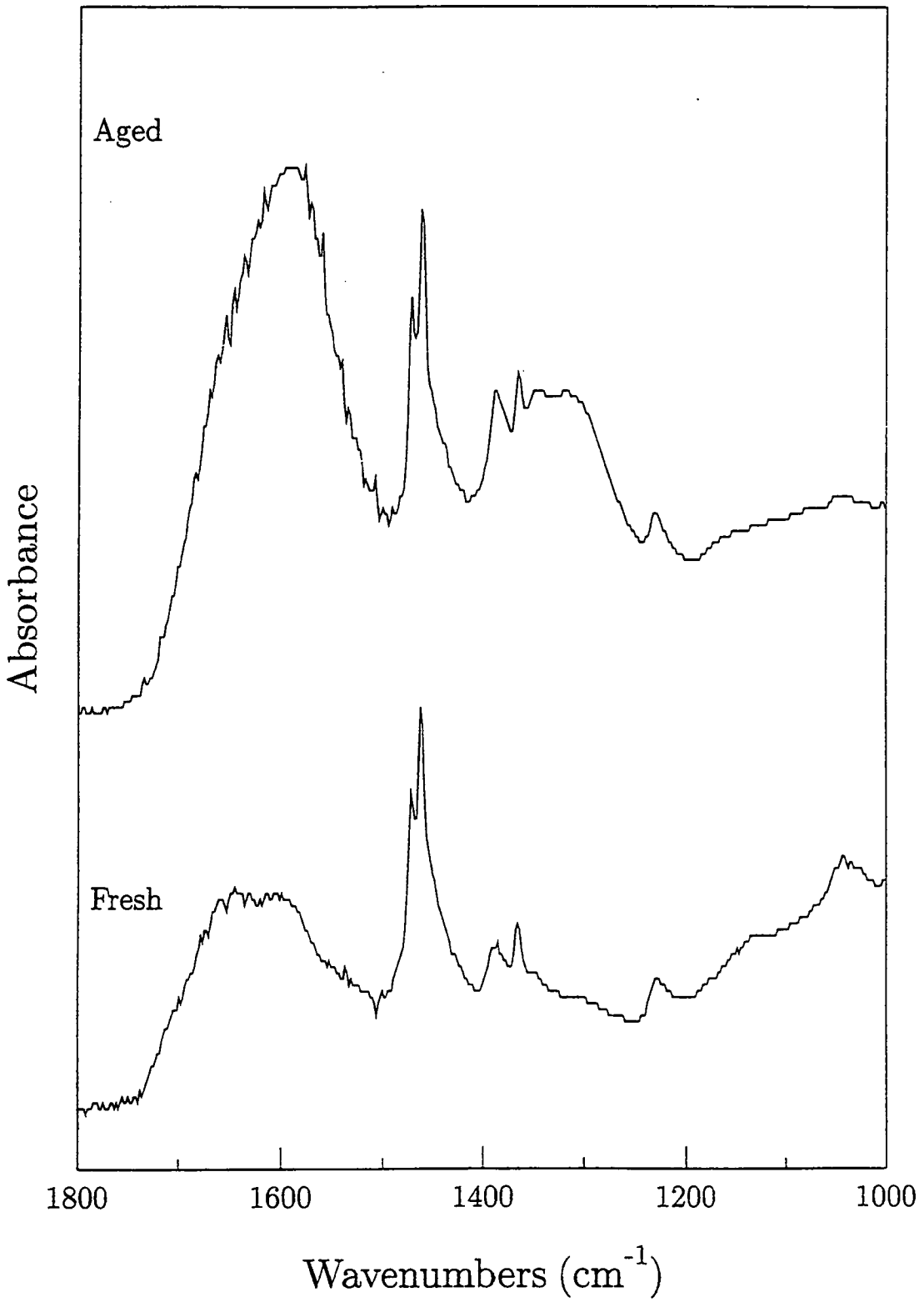

Fig. 9 ATR-FTIR spectra for PACVD of TMT/H_2 onto polyethylene substrate showing fresh and aged samples (15 W, 15 min, 19 cm).

6.3.4 ATOMIC FORCE MICROSCOPY (AFM)

In Fig. 10, the AFM image shows the surface morphology for the 15 W TMT plasma polymer sample. The presence of powder particles embedded into the polymer surface indicates that gas phase growth is dominant[80] where the particles deposit onto the growing film surface under the influence of gravity (particularly when the plasma is switched off).[81]

6.4 DISCUSSION

The origins of the grey colour of the films may result either from the carbon in the films, where carbon is directly bonded to the titanium to form Ti(C,N) by conventional thermal CVD[12] or plasma assisted CVD,[81] or from the oxygen incorporation to give Ti(O,N) or Ti(O,C,N) phases by thermal CVD.[81] The suboxides of titanium also possess this coloration.[82] Plasma films deposited by Täschner *et al.* varied from golden/bronze to grey depending on the nitrogen content in the gas phase and SIMS experiments gave evidence of hydrocarbon crack product incorporation.[81] The Ti(2p) XP spectra suggest the presence of oxynitride. The fading of the grey colour on prolonged exposure to air indicates further oxidation which is supported by the binding energy found in the Ti(2p) XP spectra and the strong IR absorbance below 900 cm^{-1}.

On the film surfaces, there is no evidence of titanium bonded directly to carbon in the C(1s) XP region. The hydrocarbon observed is in agreement with low pressure CVD studies (with substrate temperatures between 200-650 °C) where hydrocarbon IR bands were observed near 2900 cm^{-1} below a deposition temperature of 500 °C.[54] However in contrast to the results recorded here, evidence of Ti-C, Ti-N and N-Ti environments were observed in the Ti(2p) and N(1s) XP spectra by Chiu *et al.*[54]

However on XPS depth profiling, the results suggest that titanium is directly bonded to carbon and nitrogen (~282 eV and ~397 eV respectively), and hydrocarbon clearly remains present. These observations may be a manifestation of Ar^+ ion beam bombardment, or in agreement with TiN layers produced by thermal[12,18,54,56] and plasma assisted[53,58] CVD. Because all the different elemental environments were not found to broaden, it can be assumed that the interpretation given for the C(1s) XP environment is not a result of Ar^+ ion beam bombardment, but agrees with that recorded in the above literature. The evidence therefore indicates the formation of Ti(O,C,N)/polymer composite films.

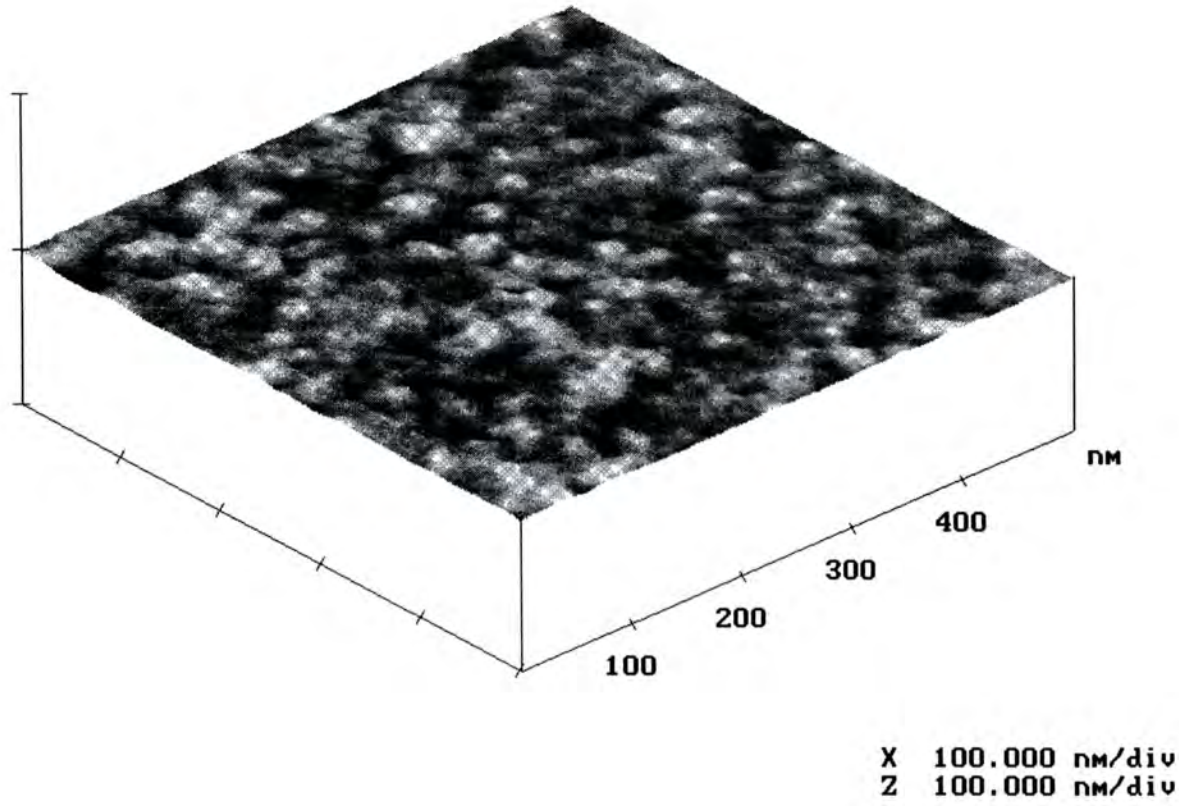

Fig. 10 AFM image for PACVD of TMT onto a glass substrate (15 W, 3 min, 19 cm).

A possible mechanism to support such observations is that of metal centre-mediated alkyl β-hydrogen elimination which was discussed in section 6.1.1.2(a) above:

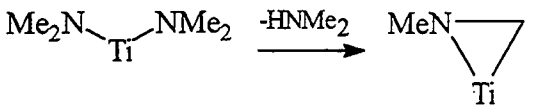

Hydrocarbon incorporation can arise from the above structure, but also from the imide (Ti=NR) or amide (Ti-NR_2) due to incomplete TMT decomposition or from plasma polymerization of organic decomposition byproducts. Exhaust byproducts from thermal decomposition of TMT include dimethylamine, methane, ethane, ethene, acetylene, ammonia, hydrogen and nitrogen; the concentrations depending on the decomposition temperature.[51] Longer chain alkene species are said to be formed on thermal decomposition since catalytic behaviour of the low valent metal centre occurs on loss of dialkylamine.[53] It has also been shown that for LPCVD using $M(NEt_2)_4$, where M=Ti or Zr, the C/M ratio decreases with increasing substrate temperature and the IR bands near 2900 cm^{-1} disappear.[54] It was proposed that the hydrocarbon is decomposed into gas phase products, leaving some carbon directly bound to titanium. Since the work here has used no external heating of the substrate, and assuming that sufficient energy is supplied to at least partially decompose TMT, a large proportion of the hydrocarbon observed is likely to arise from plasma polymerization of decomposition byproducts and from incomplete decomposition fragments of TMT. The ATR data confirms the presence of hydrocarbon, but is otherwise limited in providing information on Ti-N and Ti-C bond formation particularly since the Ti-O stretching absorbance is so strong.

For TMT alone, at low glow discharge powers (<3 W), the plasma films contained more titanium which can be explained by most of the volatile organic decomposition byproducts passing through the reactor. Above 3 W, titanium deposition occurs almost immediately on leaving the extension delivery tube, and as a consequence the organic byproducts undergo a greater degree of fragmentation and hence plasma polymerization in the centre of the coil region.[62] Since the distance between the end of the extension delivery tube and the substrate position is short (2 cm), the change in monomer flow rate is small and therefore the extent of plasma polymerization is limited. As a result, the films possess the same composition with increasing power.

For samples placed further away from the monomer inlet, the gaseous species have a longer journey through the coil region before reaching the substrate. Consequently, a higher degree of fragmentation and hence plasma polymerization occurs. This effect is greater at higher powers. The ATR data indicates that the greatest deposition occurs almost immediately that the monomer leaves the extension delivery tube and that the rate

is greatest at the higher powers. The films appear to be more organic in nature downstream, though thinner in nature, suggesting the metallic component undergoes deposition immediately, whilst the organic decomposition byproducts undergo greater plasma polymerization downstream. This agrees well with the XPS results for samples located downstream. Park's expression for the deposition rate[83] (see Chapter 3) is therefore applicable to this system with the mass flow rate of monomer, F_m, falling in magnitude on moving downstream from the monomer inlet.

Hydrogen is a major byproduct of plasma polymerization.[62] Therefore the addition of external hydrogen not only dilutes the monomer but also increases the probability for recombination reactions to occur between any organic free-radicals, R·, and the H· free radicals created:

$$R\cdot + H\cdot \rightarrow RH$$

Sugiyama *et al.* suggested that the presence of hydrogen may assist in the N-C bond cleavage[51] which would result in the formation of methyl radicals. As a consequence, methane is likely to be formed as a stable byproduct. Similarly, reactions such as the recombination of two methyl radicals will constantly occur to form stable longer chain organic byproducts. A similar decomposition pathway to that of TMT alone may occur with subsequent dimethylamine formation (i.e. H· reacts with ·$N(Me)_2$ ligands).[12] However, in order for organic components to undergo plasma polymerization, further dissociation/fragmentation reactions will need to take place requiring greater energy. Since the distance between the end of the extension delivery tube and the substrate position is small, and greater fragmentation of monomer and hydrogen is likely to occur at the higher powers, it seems feasible that more organic byproducts are created by recombination, of which most passes harmlessly to the cold trap before major plasma polymerization can take place. As a result, the carbon content decreases at the higher powers (30 W).

The instantaneous colour change of the deposited films on exposure to the atmosphere illustrates the immediate oxidation that takes place. Further oxidation takes place at the titanium metal centres (in low[53] or high valency states such as that of +IV of the monomer) and the trapped free radical centres in the plasma polymer on prolonged aging. Aging of plasma polymerized films is a common occurrence when trapped free radicals react with atmospheric oxygen and/or water.[62] XPS and ATR data clearly demonstrate this phenomenon. The XPS depth profile of the fresh sample clearly confirms that oxidation occurs into the bulk suggesting that the oxide layer formed is quite thick.

AFM indicates that gas phase processes dominant during film growth since powder particles are observed on the surface.

6.5 CONCLUSIONS

Films have been deposited on glass and polyethylene substrates using TMT and TMT/H_2. For TMT, the film composition becomes power-independent above 5 W due to the short distance over which plasma polymerization can occur. However the addition of hydrogen reduces the amount of carbon at the higher powers due to possible recombination reactions reducing the extent of plasma polymerization. Below the surface for both TMT and TMT/H_2, the presence of titanium bound to carbon and to nitrogen results from intramolecular alkyl β-hydrogen activation. This has not been previously reported for non-heated substrates in plasma assisted CVD processes. The films also contain significant amounts of oxygen due to post deposition oxidation of the titanium metal centre and reaction of atmospheric oxygen and/or water with trapped free radicals in the plasma polymers. Consequently the deposited films consist of Ti(O,C,N) in a polymeric matrix, $C_wH_xN_yO_z$.

6.6 REFERENCES

1. D.C. Bradley, I.M. Thomas, *J. Chem. Soc.*, 1960, 3857.
2. M. Eslamloo-Grami, Z.A. Munir, *J. Am. Ceram. Soc.*, **73,** 1990, 2222.
3. Z. Jiang, W.E. Rhine, *Chem. Mater.*, **3**, 1991, 1132.
4. K.-H. Habig, *J. Vac. Sci. Technol.*, **A4**, 1986, 2832.
5. B.H. Hahn, J.H. Jun, J H. Joo, *Thin Solid Films*, **153**, 1987, 115.
6. J.-E. Sundgren, B-O. Johansson, S.-E. Karlsson, *Thin Solid Films*, **105**, 1983, 353.
7. O. Knotek, F. Löffler, Metallized Plastics 2, Ed. K. L. Mittal, Plenum Press, New York, 1991, p. 141.
8. H. Suhr, *New J. Chem.*, **14**, 1990, 523.
9. J.-E. Sundgren, *Thin Solid Films*, **128**, 1985, 21.
10. S.R. Kurtz, R.G. Gordon, *Thin Solid Films*, **140**, 1986, 277.
11. M. Gupta, V.K. Rathi, R. Thangaraj, O.P. Agnihotri, K.S. Chari, *Thin Solid Films*, **204**, 1991, 77.
12. A. Intemann, H. Koerner, F. Koch, *J. Electrochem. Soc.*, **140**, 1993, 3215.
13. J. Hojo, A. Kato, *Yogo Kyokaishi*, **89**, 1981, 277.
14. M.J. Buiting, A.F. Otterloo, A.H. Montree, *J. Electrochem. Soc.*, **138**, 1991, 500.
15. N. Yokoyama, K. Hinode, Y. Homma, *J. Electrochem. Soc.*, **136**, 1989, 882.
16. A. Sherman, *J. Electrochem. Soc.*, **137**, 1990, 1892.
17. Y.H. Croonen, G. Verspui, *J. Physique IV*, C3, *J. Physique II*, **3**, 1993, 209.
18. R.M. Fix, R.G. Gordon, D.M. Hoffman, *Chem. Mater.*, **2** , 1990, 235.
19. R.F. Bunshah, *IEEE Trans. Plasma Sci.*, **18**, 1990, 846.
20. T. Wierzchon, J. Michalski, T. Karpinski, Proc. 1st. Conf. on Plasma Surface Engineering, Garmisch-Partenkirchen, Sept 1988, D.G.M. Informationsges. mbH, Oberursel, 1989, p. 177.
21. J. Michalski, T. Wierzchon, *Mater Sci. Eng.*, **A140,** 1991, 499.
22. K. Oguri, H. Fujita, T. Arai, *Thin Solid Films*, **195**, 1991, 77.
23. T. Arai, H. Fugita, K. Oguri, *Thin Solid Films*, **165**, 1988, 139.
24. P. Mayr, H.-R. Stock, *J. Vac. Sci. Technol.*, **A4**, 1986, 2726.
25. K.-T. Rie, St. Eisenberg, A. Gebauer, Proc. 1st. Conf. on Plasma Surface Engineering, Garmisch-Partenkirchen, Sept 1988, D.G.M. Informationsges. mbH, Oberursel, 1989, p. 125.
26. K.-T. Rie, J. Wöhle, *Mater Sci. Eng.*, **A139,** 1991, 37.
27. K.-T. Rie, A. Gebauer, J. Wöhle, *Plasma Chem. Plasma Proc.*, 13, 1993, 93.
28. K.-T. Rie, A. Gebauer, J. Wöhle, *Surf. Coat.Technol.*, **60**, 1993, 385.
29. H. Frellor, H.P. Lorenz, *Mater Sci. Eng.* **A140,** 1991, 534.
30. N.J. Ianno, A.U. Ahmed, D.E. Engelbert, *J. Electrochem. Soc.*, **136**, 1989, 276.

31. F.H.M. Sanders, G. Verspui, *Thin Solid Films*, **161**, 1988, L87.
32. S.J. Bull, P.R. Chalker, C.F. Ayres, D.S. Rickerby, *Mater Sci. Eng.*, **A139**, 1991, 71.
33. H.P. Lorenz, Proc. 1st. Conf. on Plasma Surface Engineering, Garmisch-Partenkirchen, Sept 1988, D.G.M. Informationsges. mbH., Oberursel, 1989, p. 163.
34. L. Shizhi, S. Yulong, X. Xiang, Y. Hongshun, Z. Cheng, Proc. 1st. Conf. on Plasma Surface Engineering, Garmisch-Partenkirchen, Sept 1988, D.G.M. Informationsges. mbH, Oberursel, 1989, p. 155.
35. L. Shizhi, H. Wu, Y. Hongshun, W. Zhongshu, *Plasma Chem. Plasma Proc.*, **4**, 1984, 147.
36. L. Shizhi, Y. Hongshun, *Proc. 7th Int. Symp. Chem. on Plasma Chemistry*, Eindhoven, Ed. C. J. Timmermans, 1985, p. 68.
37. N.J. Archer, *Thin Solid Films*, **80**, 1981, 221.
38. D.H. Jang, S.B. Kim, J.S. Chun, J.G. Kim, Proc. 1st. Conf. on Plasma Surface Engineering, Garmisch-Partenkirchen, Sept 1988, D.G.M. Informationsges. mbH, Oberursel, 1989, p. 147.
39. D.H. Jang, J.G. Chun, J.G. Kim, *Thin Solid Films*, **169**, 1989, 57.
40. D.H. Jang, J.G. Chun, J.G. Kim, *J. Vac. Sci. Technol.*, **A7**, 1989, 31.
41. R. Makanbe, S. Nakajima, O. Tabata, M. Aoki, *Thin Solid Films*, **137**, 1986, L49.
42. M.R. Hilton, M. Salmeron, G.A. Somorjai, *Thin Solid Films*, **167**, 1988, L31.
43. M.R. Hilton, L. R. Narasimhan, S. Nakamura, M. Salmeron, G.A. Somorjai, *Thin Solid Films*, **139**, 1986, 247.
44. Y. Ishii, H. Ohtsu, T. Adachi, H. Ichimura, K. Kobayashi, *Surf. Coat. Technol.*, **49**, 1991, 279.
45. M.R. Hilton, G.J. Vandentop, M. Salmeron, G.A. Somorjai, *Thin Solid Films*, **154**, 1987, 377.
46. M.C. Polo, J. Esteve, J.L. Morenza, *Surf. Coat. Technol.*, **45**, 1991, 67.
47. J. Laimer, H. Störi, R. Rödhammer, *Thin Solid Films*, **191**, 1990, 77.
48. J. Laimer, H. Störi, R. Rödhammer, *J. Vac. Sci. Technol.*, **A7**, 1989, 2952.
49. H.J. Frenck, E. Oesterschulze, R. Beckmann, W. Kulisch, R. Kassing, *Mater Sci. Eng.* **A139,** 1991, 394.
50. K.-T. Rie, A. Gebauer, *Mater Sci. Eng.*, **A139**, 1991, 61.
51. K. Sugiyama, S. Pac, Y. Takahashi, S. Motojima, *J. Electrochem. Soc.*, **122**, 1975, 1545.
52. R. Morancho, G. Constant, J.J. Ehthardt, *Thin Solid Films*, **77**, 1981, 155.
53. L.M. Dyagileva, V.V. Mar'in, E.I. Tsyganova, I.L. Gaidym, Y. A Aleksandrov, *J. Gen. Chem. USSR (Eng.)*, **54**, 1984, 538.
54. H.-T. Chiu, C.-C. Huang, *Mater. Letts.*, ***16***, 1993, 194.

55. L.H. Dubois, B.R. Zegarski, G.S. Girolami, *J. Electrochem. Soc.*, **139**, 1992, 3604
56. A. Katz, A. Feingold, S. . Pearton, S. Nakahara, M. Ellington, U.K. Chakrabarti, M. Geva, E. Lane, *J. Appl. Phys.*, **70**, 1991, 3666.
57. C.I.M.A. Spee, J.L. Linden, E.A. Van Der Zouwen-Assink, K. Timmer, F. Verbeck, H.A. Meinema, D.M. Frigo, S. Van Der Ven, *J. Physique IV*, C3, *J. Physique II*, **3**, 1993, 289.
58. K.-T. Rie, J. Wöhle, A. Gebauer, *J. Physique IV*, C2, *J. Physique II*, **1**, 1991, 397.
59. A. Weber, R. Nikulski, C.-P. Klages, *Appl. Phys. Lett.*, **63**, 1993, 325.
60. A. Weber, R. Nilulski, C.-P. Klages, M.E. Gross, W.L. Brown, E.Dons, R.M. Charatan, *J. Electrochem. Soc.*, **141**, 1994, 849.
61. H.-R. Stock, H. Berndt, P. Mayr, *Surf. Coat. Technol.*, **46**, 1991, 15.
62. H. Yasuda, Plasma Polymerization, Academic Press, Orlando, FL, 1985.
63. N.C. Saha, H.G. Tompkins, *J. Appl. Phys.*, **72**, 1992, 3072.
64. B. Siemensmeyer, K. Bade, J.W. Schultze, *Ber. Bunsenges. Phys. Chem.*, **95**, 1991, 1461.
65. M.V. Kaznetsov, J.F. Zhuravlev, V.A. Zhilyaev, V.A. Gubanov, *J. Electron. Spec. Rel. Phen.*, **58**, 1992, 1.
66. Handbook of X-Ray Photoelectron Spectroscopy, Ed. C.D. Wagner, W.M. Riggs, L.E. Davis, J.F. Moulder, G.E. Muilenberg, Perkin-Elmer Corp., Eden Prairie, MN, 1979.
67. M. Murata, K. Wakino, S. Ikeda, *J. Electr. Spectr. Relat. Phenom.*, **6**, 1975, 459.
68. I. ler. Strydom, S. Hoffmann, *J. Electron. Spec. Rel. Phen.*, **56**, 1991, 85.
69. C. Ernsberger, J. Nickerson, T. Smith, A.E. Miller, D. Banks, *J. Vac. Sci. Technol.*, **A4**, 1986, 2784.
70. G. Beamson, D. Briggs, High Resolution XPS of Organic Polymers, The Scienta ESCA300 Database, John Wiley, Chichester, 1992.
71. R. Foerch, N.S. McIntyre, R.N.S. Sodhi, D.H. Hunter, *J. Appl. Polym. Sci.*, **40**, 1990, 1903.
72. S. O'Kell, T. Henshaw, G. Farrow, M. Aindow, C. Jones, *Surf. Interface Anal.*, **23**, 1995, 319.
73. J.W. Coburn, *Thin Solid Films*, **64**, 1979, 371.
74. H. Bürger, H. Stammreich, Th. T. Sans, *Monatsch Chem.*, **97**, 1966, 1276.
75. D.C. Bradley, M.H. Gitlitz, *J. Chem. Soc.*, **A**, 1969, 980.
76. F.M. Mirabella, *Appl. Spectrosc. Rev.*, **21**, 1985, 45.
77. R.M. Silverstein, G.C. Bassler, T.C. Morrill, Spectrometric Identification of Organic Compounds, 4th Edn., Wiley, New York, 1981.
78. M. Ocaña, W.P. Hsu, E. Matijevic, *Langmuir*, 7,1991, 2911.

79. D.H. Williams, I. Fleming, Spectroscopic Methods in Organic Chemistry, 3rd Edn., McGraw-Hill, London, 1987.

80. R. d'Agostino, Ed., Plasma Deposition, Etching of Polymers, Academic Press, San Diego, 1990.

81. G.S. Selwyn, K.L. Haller, E.F. Patterson, *J. Vac. Sci. Technol.*, **A11**, 1993, 1132.

82. Ch. Täschner, K. Bartsch, A. Leonhardt, *Surf. Coat. Tech.*, **59**, 1993, 207.

83. Gmelins Handbuch, Der Anorganischen Chemie, Titan, Vol. 41, Verlag Chemie, GMBH, Weinhelm/Bergstraße, 1951, p. 214.

84. S.Y. Park, N. Kim, *J. Appl. Polym. Sci. Polym. Appl. Symp.*, **46**, 1990, 91.

CHAPTER 7:
PLASMA ASSISTED CHEMICAL VAPOUR DEPOSITION OF TITANIUM OXYCARBONITRIDE/POLYMER FILMS FROM TETRAKIS (DIMETHYLAMIDO) TITANIUM AND AMMONIA

7.1 INTRODUCTION

The desire for chlorine-free deposited TiN films by CVD methods has resulted in much research using the TMT precursor as discussed in Chapter 6. However carbon contamination, both hydrocarbon and titanium bound carbon, is commonly found due to the intramolecular alkyl β-hydrogen activation mechanism[1-5] and incomplete decomposition of TMT. Therefore a more recent approach has been based upon the solution reactivity studies carried out by Bradley and co-workers[6,7] in the early 1960's which is discussed in the following review section on transamination reactions.

7.1.1 REVIEW OF TRANSAMINATION REACTIONS

Bradley and Thomas initially reported that dialkylamido complexes underwent facile transamination reactions in solution:[6]

$$M\text{-}NR_2 + HNR'_2 \rightarrow M\text{-}NR'_2 + HNR_2$$

Primary amines led to imido-bridged oligomers[7] when the alkyl substituent was small:

$$M(NMe_2)_4 + RNH_2 \rightarrow [M(=NR)_2]_x + HNMe_2 \qquad [M=Ti, Zr]$$

and to dimer formation in the case of $^tBuNH_2$.[7] More recently, Brown and Maya found similar results where ammonolysis of the dialkylamides of titanium, zirconium and niobium gave oligomeric solid products.[8] In the case of TMT, a red solid of idealised formula $Ti_3[N(CH_3)_2](NH_2)_2(N)_3$ was formed. Pyrolysis via polymeric 'Ti_3N_4' with loss of ammonia and dimethylamine at 800 °C formed golden brown crystals of TiN. Other evidence of the displacement of NR and NR_2 groups by ammonia was shown on the pyrolysis of oligomeric titanium and nitrido compounds in a stream of ammonia.[9] Consequently, CVD studies using dialklyamides and ammonia have been reported in order to prove whether the above chemistry is applicable as a means of providing cleaner (less contaminated) TiN films, and possible mechanisms have been proposed.

One study of TMT and ammonia, using gas phase IR, showed that the only product observed was dimethylamine and the formation of a fine yellow powder resulted as the transamination product, possibly a mixed amido complex of stoichiometry $Ti(NMe_2)_{4-n}(NH_2)_n$.[4] Deuterated ammonia led to predominantly deuterated dimethylamine indicating that the ammonia provided the source of hydrogen to create the dimethylamine. Further mass spectral studies by this group,[10] have indicated that mixing TMT and ammonia in the gas phase gives a rapid transamination reaction leading to a high molecular weight polymeric intermediate which undergoes decomposition on the surface by thermal activation. Isotopic labelling of ammonia (deuterated) gave the same results as above (but observed by mass spectroscopy) and RBS studies using $^{15}NH_3$ gave predominately clean $Ti^{15}N$ films. Therefore the ammonia, provides not only the hydrogen for dimethylamine formation, but also the nitrogen for TiN formation. Similar mechanisms have been proposed by Intemann *et al.*[2] and Katz *et al.*[11] which support the above isotopic labelling experiments. Figure 1 outlines the mechanism of the former. Hydrogen and nitrogen were also found by mass spectroscopy to be present in the effluent gas.

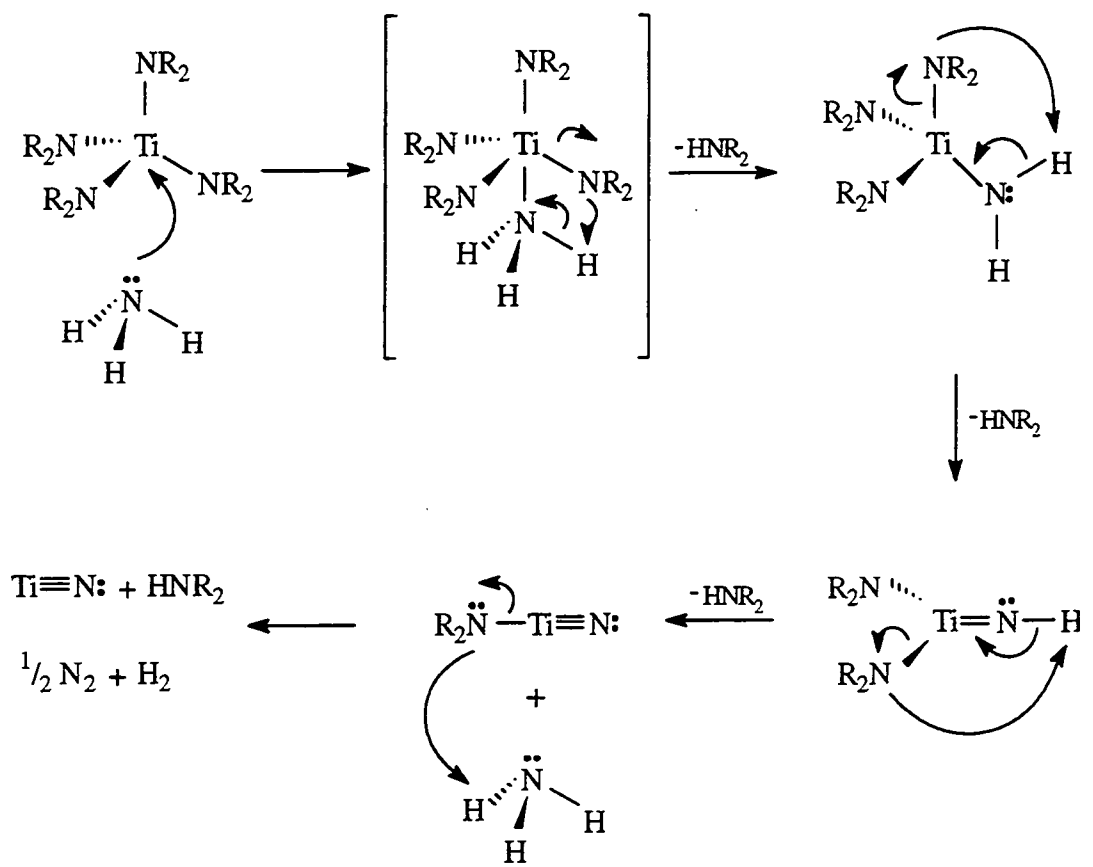

Fig. 1 The reaction mechanism for the thermal reaction of TMT and ammonia proposed by Intemann *et al.*[2]

TMT injected downstream of an ECR nitrogen or ammonia plasma[12] has been shown to form high quality TiN films at temperatures as low as 100 °C. Both species react with TMT with replacement of the dimethylamido groups to form TiN. Labelling nitrogen gave similar results as Prybyla *et al.*[10] confirming the same type of mechanism. The surface reaction is dominated by the nonthermal plasma activation of nitrogen and ammonia, the atomic nitrogen and amido radicals being the active species. Despite higher carbon, oxygen and hydrogen contamination in the films, lower resistivities were found using ammonia. This was explained by the different crystalline microstructures obtained.

It appears that the deposition temperature, total gas pressure and ammonia flow rate or ratio in the gas mixture are the most important parameters that control the film resistivities, densities and extent of contamination. Carbon contamination can be reduced by keeping the deposition temperature low (<300 °C) so as to prevent intramolecular β-hydrogen activation competing with the gas phase transamination chemistry.[3,11,13] It is interesting that in the case of $M(NEt_2)_4/NH_3$ mixtures, where M is Zr or Hf, a similar trend was not observed, possibly because ammonia has an effectively higher reactivity towards the larger metal centres, even though they possess bulkier alkyl ligands.[3] Therefore the reaction of ammonia is greater than any competing intramolecular β-hydrogen activation. In addition, higher growth rates were observed for Zr and Hf and deposition was found to occur nearer the inlet. Alternatively, the carbon content can be reduced by increasing the amount of ammonia in the gas mixture[10,11] or using higher total gas pressures.[11]

The resistivity of the films has been correlated to the presence of oxygen contamination.[14,15] The latter has been shown to depend on the density of the films,[14] which itself has been found to decrease as the total gas pressure and ammonia gas content are increased.[11,14] Sandhu *et al.* explained that cleaner films result from optimizing the conditions that promote the gas phase reactions.[14] Other groups of workers[11,16] have also seen a decrease in the resistivities with increasing ammonia flow rate, though an increase in oxygen content was observed as a result of the higher ammonia concentration in the gas mixture.[11]

There is conflicting evidence however for a resistivity dependence with deposition temperature. Fix *et al.* found that the resistivities were independent of the deposition temperature (200-400 °C) with a value of $\sim 10^3$ μΩcm.[3] Since the levels of carbon and oxygen levels were low, the high resistivity was explained by the presence of excess nitrogen and hydrogen or the small grain sizes. However an increase in the deposition temperature has been shown to reduce the resistivity.[11,12,16] Since the carbon contamination has been shown to increase with increasing temperature as mentioned

above, the lower resistivity may be explained by the formation of titanium bound carbon and greater decomposition of TMT. TiC is known to be electrically conductive.[17]

In the following sections of this chapter, the addition of ammonia to TMT has been performed as a possible route to the reduction of titanium bound carbon.

7.2 EXPERIMENTAL

The reactor configuration, samples, sample location and cleaning procedures were as described in Chapter 3. The reactor was pumped down to a base pressure of 7.5×10^{-3} Torr with a leak rate better than 7.9×10^{-11} kgs^{-1}, before ammonia (anhydrous, 99.99+ %, Aldrich) was purged through the reactor for 5 min at a pressure of 5.6×10^{-2} Torr and flow rate of 2.4×10^{-8} kgs^{-1} (i.e. more than 99.6% of the gas was ammonia). TMT monomer was then allowed into the reactor for 2.5 min to give a combined total pressure of 6.8×10^{-2} Torr. The plasma was ignited for 3 min for XPS and 15 min for ATR before it was extinguished followed by the monomer source being closed off. Ammonia was purged through the reactor for a further 2 min before this was closed off and the reactor pumped down for 2 min to a pressure of $\sim 1.1 \times 10^{-2}$ Torr. The system was then let up to atmospheric pressure before the samples were transferred to the appropriate analytical instrument. Pulsing was required below an average power of 3 W to sustain a stable plasma (for $\langle P \rangle$ =1 W, P_0 =3 W, T_1 =1.4 ms and T_2 =2.25 ms, see Chapter 3 for definitions).

7.3 RESULTS

During the 2.5 min equilibrating time of TMT/NH_3 prior to plasma deposition, formation of an orange/red deposit coated internal exposed surfaces of the reactor suggesting some kind of gas phase reaction between the two reactant gases. As a consequence, XPS and ATR samples were also run in the absence of the plasma. On activation of the plasma, a golden/brown/red film developed on the reactor walls and the extension delivery tube, which was most intense at the end of the extension delivery tube and in the coil region, and became more noticeable at the higher glow discharge powers. The slides on exposure to air tended to have a different colouration depending on the glow discharge power. At the lowest powers (0-3 W), the slides became yellow/golden. Between 5-10 W, the slides went grey and above 15 W the slides tended to be golden, more so than even the films deposited at the lowest powers. Films deposited at 15 W tended to be on the transition point between the grey and golden regimes since both grey and golden films were observed. The films tended to possess highly coloured

interference diffraction patterns similar to those mentioned in Chapter 6 and both the colour of the reactor and the slides faded with time on exposure to air.

Because longer deposition times were required for ATR, the reactor was more thickly coated and the films were darker; very dark films were observed at 30 W whilst films were yellow at 1 W. In the absence of a plasma, the colour of the films was slightly yellow/orange, which on exposure to air gradually faded back to the opaque colour of the polyethylene substrate. Again, tilting the films towards the light showed the interference patterns. On prolonged exposure to air (~1 hr), the plasma deposited films had a yellow appearance.

7.3.1 X-RAY PHOTOELECTRON SPECTROSCOPY (XPS)

Elemental composition trends for the deposited films as a function of plasma glow discharge power are shown in Fig. 2. The carbon content remains constant, whilst the titanium and oxygen contents decrease with increasing power. The nitrogen content increases with power. In the absence of a plasma activation, silicon from the substrate was also observed.

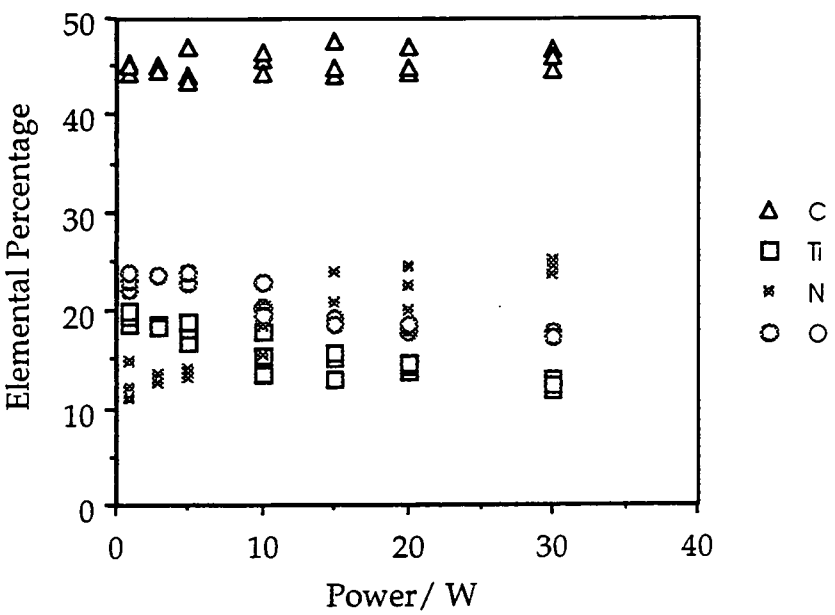

Fig. 2 Elemental composition as a function of glow discharge power (3 min, 19 cm).

Typical spectra for the C(1s), Ti(2p), N(1s) and O(1s) XP regions are shown in Fig. 3. In the C(1s) XP spectrum, Fig. 3(a), the shoulder to higher binding energies of the

hydrocarbon peak at 285.0 eV has not been fully deconvoluted, for the reasons discussed in section 5.3.1. However, in order to obtain the sample charging offset relative to the hydrocarbon peak at 285 eV, the C(1s) XP regions have been fitted with three peaks.

The Ti(2p) XP region, Fig. 3(b), in agreement with Chapter 6, suggests the formation of oxynitride with average binding energies of 458.0 ± 0.1 eV and 463.7 ± 0.1 eV for the $Ti(2p_{3/2})$ and $Ti(2p_{1/2})$ peaks respectively. Again, the N(1s) XP region, Fig. 3(c), cannot be fully deconvoluted; the maxima primarily indicate nitrogen bound to carbon[18] at 399.8 ± 0.1 eV and either nitride (Ti-N),[3,19,20] imide (Ti=NR)[3] or amide ($Ti-NR_2$)[3] at 396.8 ± 0.4 eV. Note that the peak at ~397 eV is most prominent in the absence of the plasma and gradually decreases in magnitude with increasing glow discharge power as illustrated in Fig. 4(a). At the same time, the shoulder to higher binding energies of the hydrocarbon peak at 285.0 eV in the C(1s) XP region also increases, Fig. 4(b). It should be noted however, that the change between successive powers, particularly above 10 W, is less distinct, probably due to the limited degree of plasma polymerization resulting from the small distance between the end of the extension delivery tube and the substrate. All the data in Fig. 4 has been normalized relative to the highest peak in each spectrum. It is likely that plasma-associated gas phase reactions will increasingly take place on increasing the glow discharge power.

The O(1s) XP environment, see Fig. 3(d), has not been deconvoluted; the maxima at average binding energies of 529.8 ± 0.1 eV are indicative of oxide[19,21] and at higher binding energies the variety of environments may be oxidized carbon/oxidized carbon bonded to nitrogen (O=C-N),[18] substoichiometric oxide, oxynitride or adsorbed water.[19]

A 15 W TMT/NH_3 plasma polymer sample was chosen to study any aging effects. A similar experimental routine, as mentioned in Chapter 6, was carried out with one sample analysed immediately and the other left to age in ambient conditions for approximately one month. Table 2 shows an increase in the oxygen content resulting from the presence of trapped free radicals reacting with water and/or oxygen[22] and further oxidation at the metal centre.

Table 2 Elemental composition and ratios for fresh and aged samples (15 W, 3 min, 19 cm).

Sample	% C ± 0.1	% Ti ± 0.1	% N ± 0.1	% O ± 0.1	Ti/C ± 0.01	N/C ± 0.01	O/C ± 0.01	N/Ti ± 0.01	O/Ti ± 0.01
Fresh	47.7	16.5	14.1	21.8	0.34	0.29	0.46	0.85	1.32
Aged	47.0	17.7	6.3	29.4	0.38	0.13	0.63	0.36	1.66

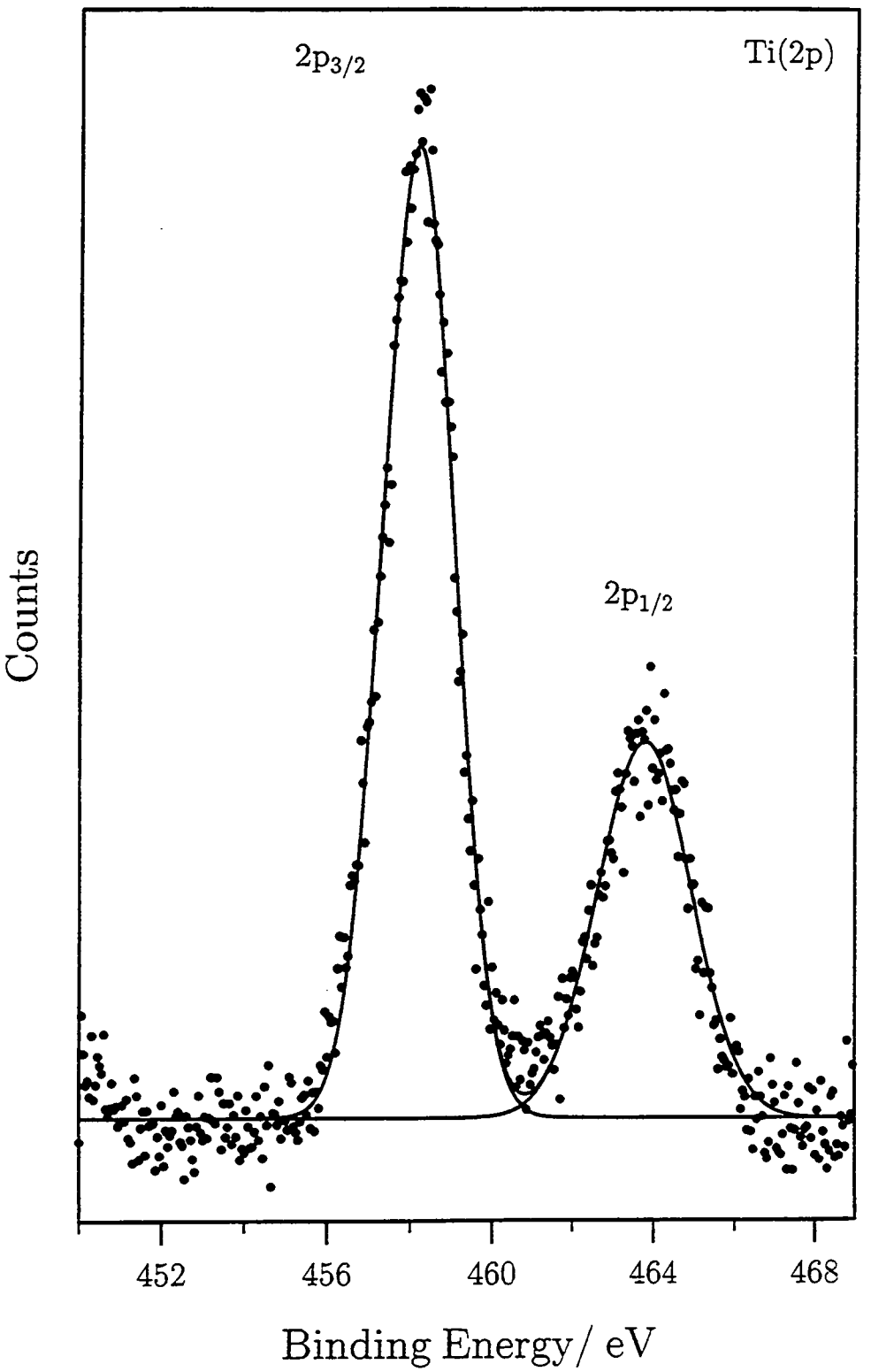

Fig. 3(b) Ti(2p) XP spectrum for PACVD of TMT/NH_3 onto a glass substrate (3 W, 3 min, 19 cm).

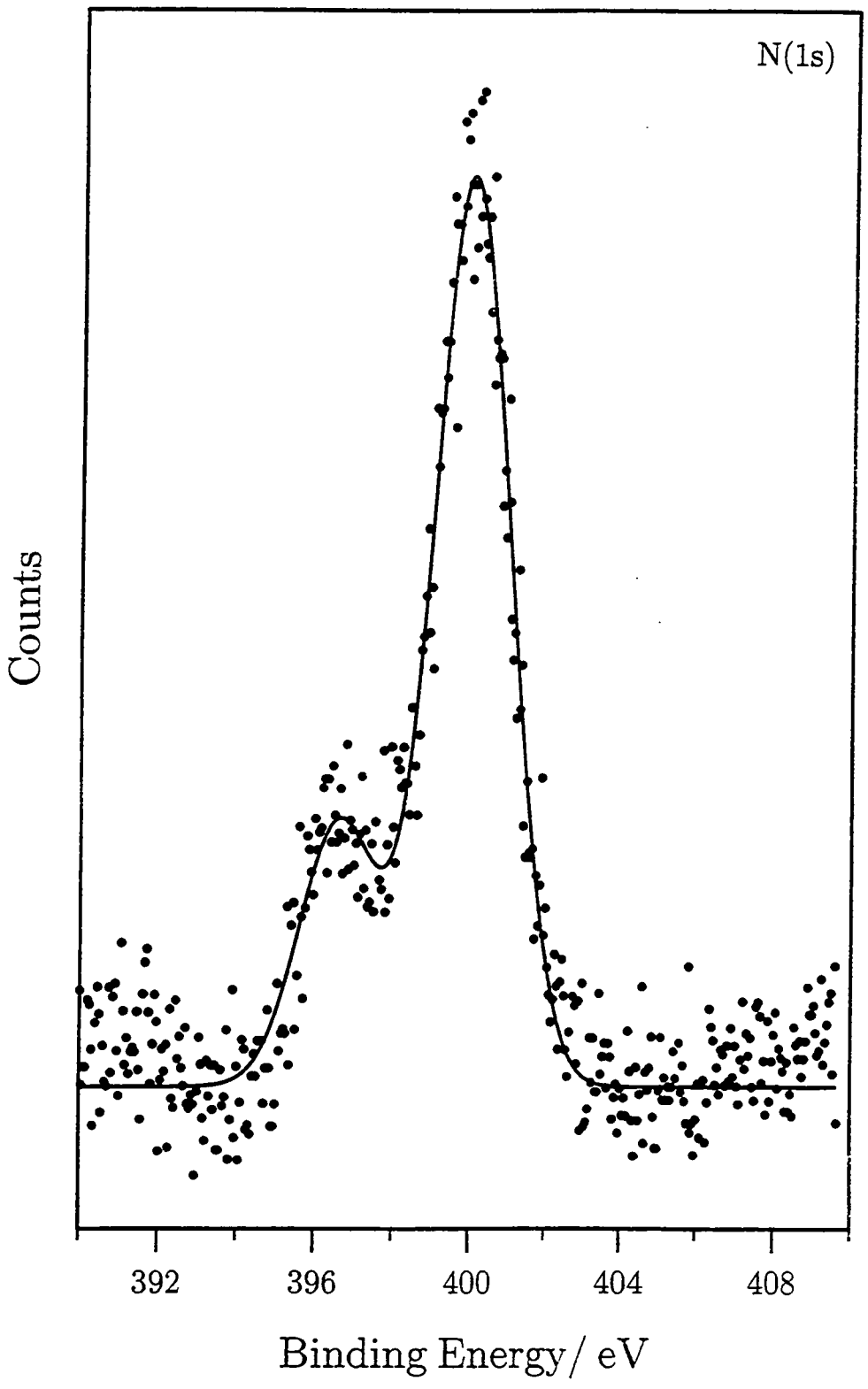

Fig. 3(c) N(1s) XP spectrum for PACVD of TMT/NH_3 onto a glass substrate (3 W, 3 min, 19 cm).

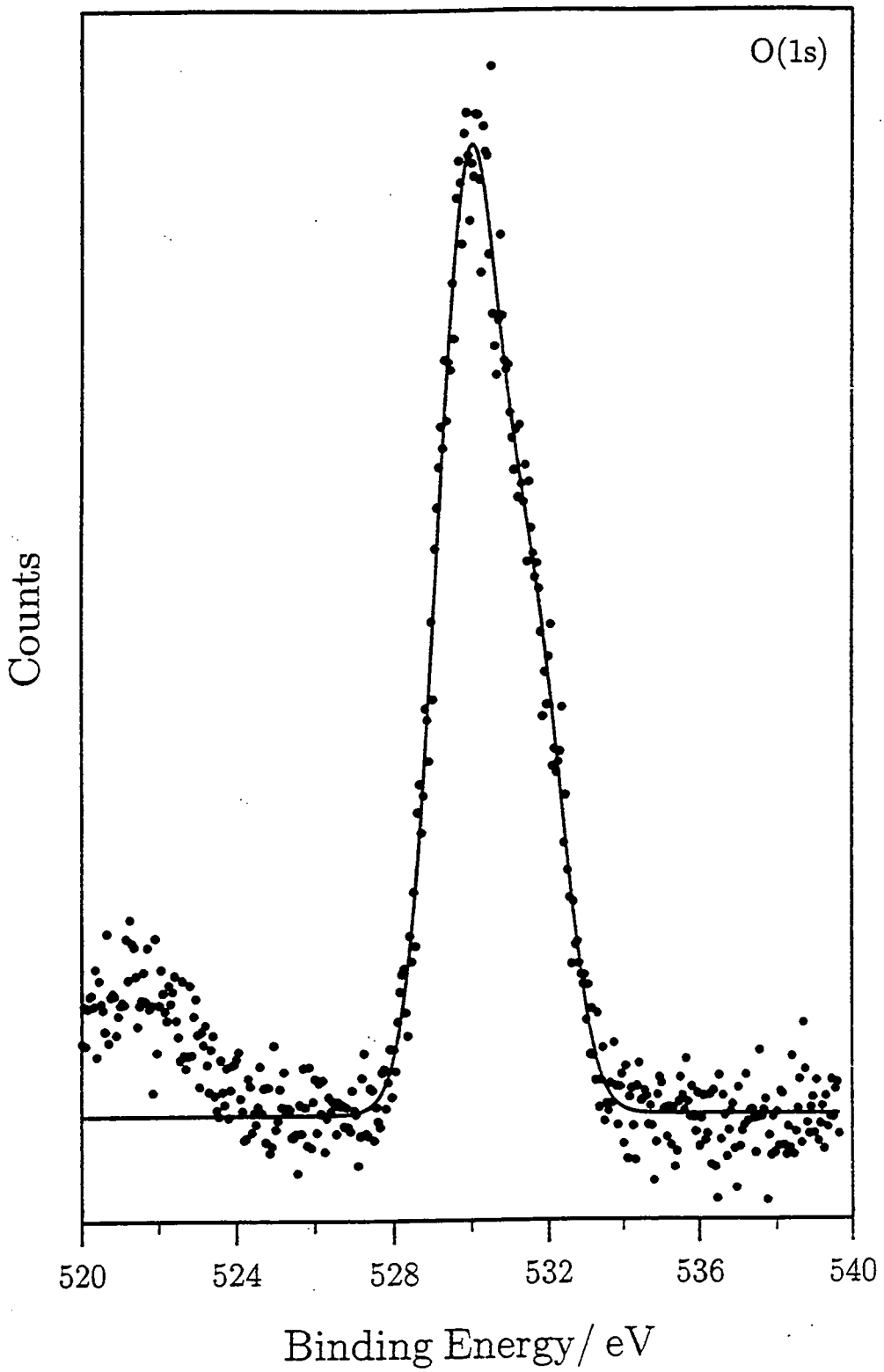

Fig. 3(d) O(1s) XP spectrum for PACVD of TMT/NH_3 onto a glass substrate (3 W, 3 min, 19 cm).

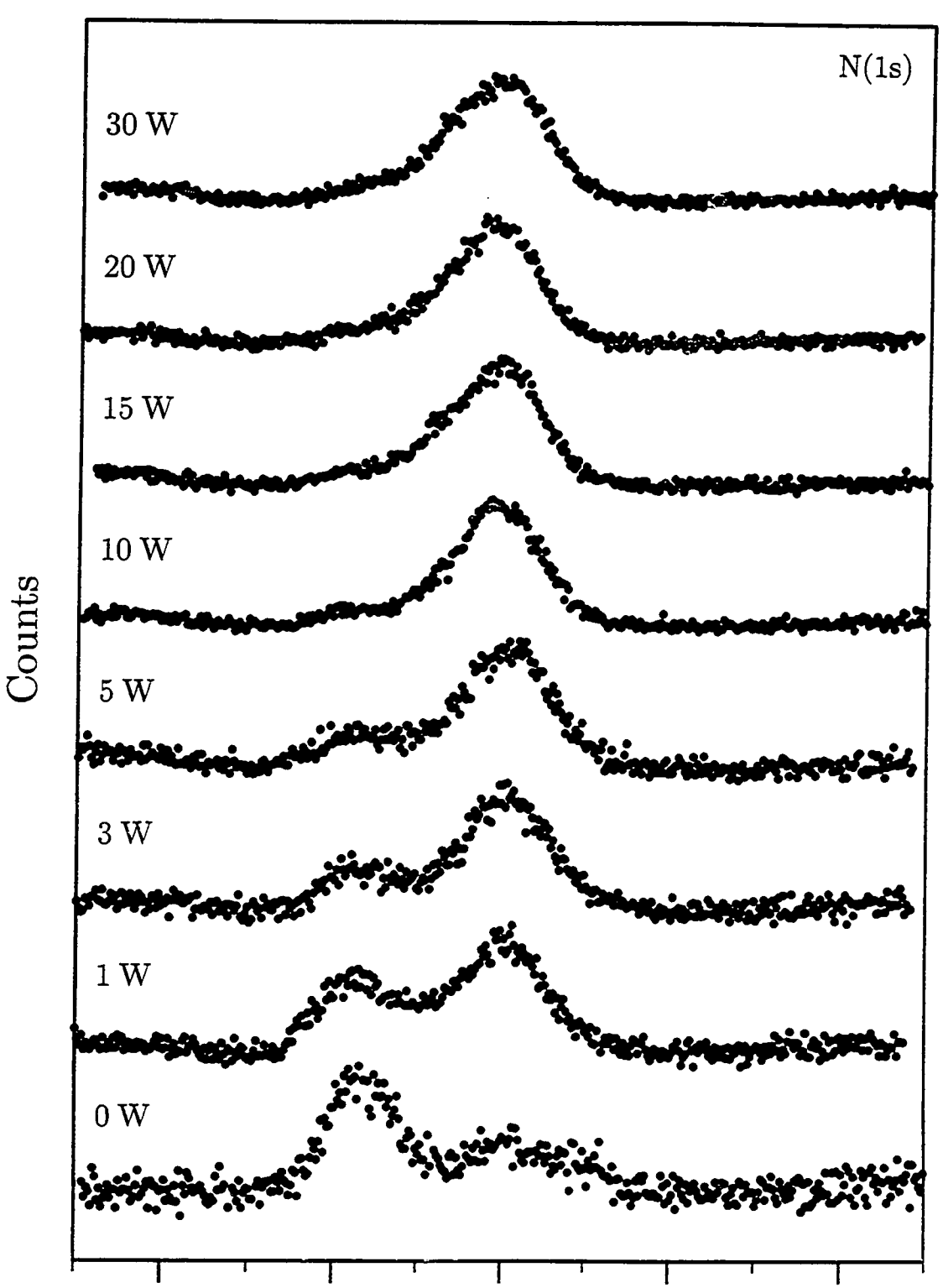

Fig. 4(a) Normalized N(1s) XP spectra for PACVD of TMT/NH_3 onto a glass substrate as a function of glow discharge power (3 min, 19 cm).

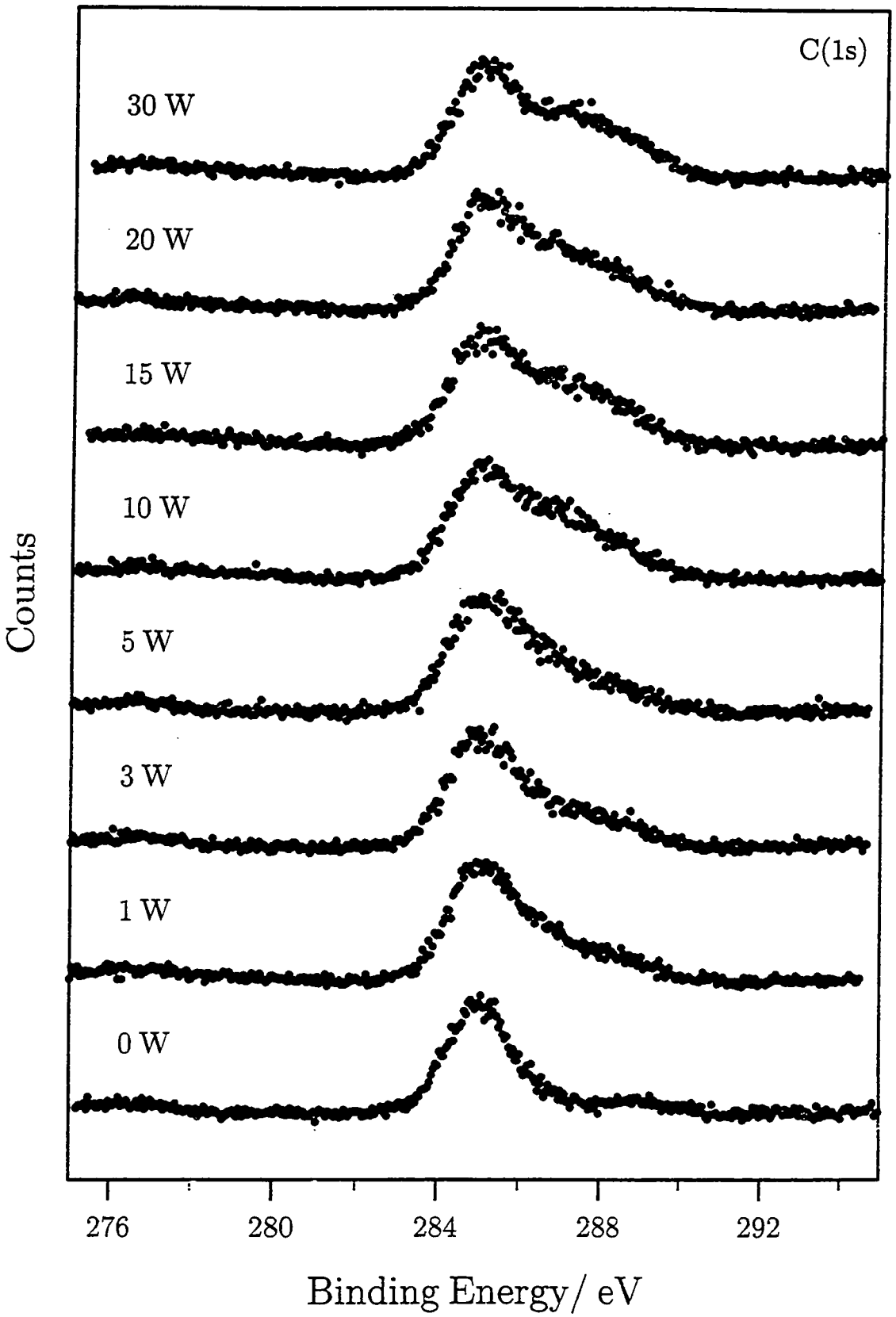

Fig. 4(b) Normalized C(1s) XP spectra for PACVD of TMT/NH_3 onto a glass substrate as a function of glow discharge power (3 min, 19 cm).

The increase in the oxidized region to higher energies of the hydrocarbon peak at 285.0 eV can be observed in Fig 5(a) in the C(1s) XP region. The N(1s) XP region, Fig. 5(b), clearly shows that the peak around 397 eV has virtually disappeared indicating oxidation of the nitride component.[19] In addition, possible loss of imine-type and amine functionalities may occur. Loss of these species has been observed for nitrogen plasma treated polymer surfaces with aging.[23,24] The O(1s) XP environment, Fig 5(c), however, shows little change in peak shape. The spectra have been normalized to show qualitative information from the peak shapes.

7.3.2 XPS DEPTH PROFILING

Fig. 6 shows the elemental composition with sputtering time. Once adventitious hydrocarbon contamination and low molecular hydrocarbon species are rapidly removed, it appears that the carbon and titanium content remains constant whilst nitrogen increases, and the oxygen decreases as a direct result of the preferential sputtering of oxygen.[25]

It can be assumed that the major environment in the C(1s) XP spectra resulted from plasma polymer hydrocarbon at 285.0 eV. Therefore the sample charging offsets can be determined. The presence of the titanium bound carbon environment at ~282 eV in the C(1s) XP region is still evident, Fig. 7(a). In the N(1s) XP region, Fig. 7(b), it can be clearly observed that there is an increase in the nitrogen bonded to titanium environment relative to the hydrocarbon content located to higher binding energies. The high presence of oxygen after the duration of sputtering suggests that the oxide layer is quite thick. Oxidation will occur on exposure to air during transfer of the sample from the reactor to the XPS chamber. The O(1s) XP spectra, Fig. 7(c), become more characteristic of that of suboxide on sputtering. The broadening of the Ti(2p) XP region, Fig. 7(d), to lower binding energies indicates the presence of suboxides[26] and the presence of Ti-N and Ti-C cannot also be discounted.

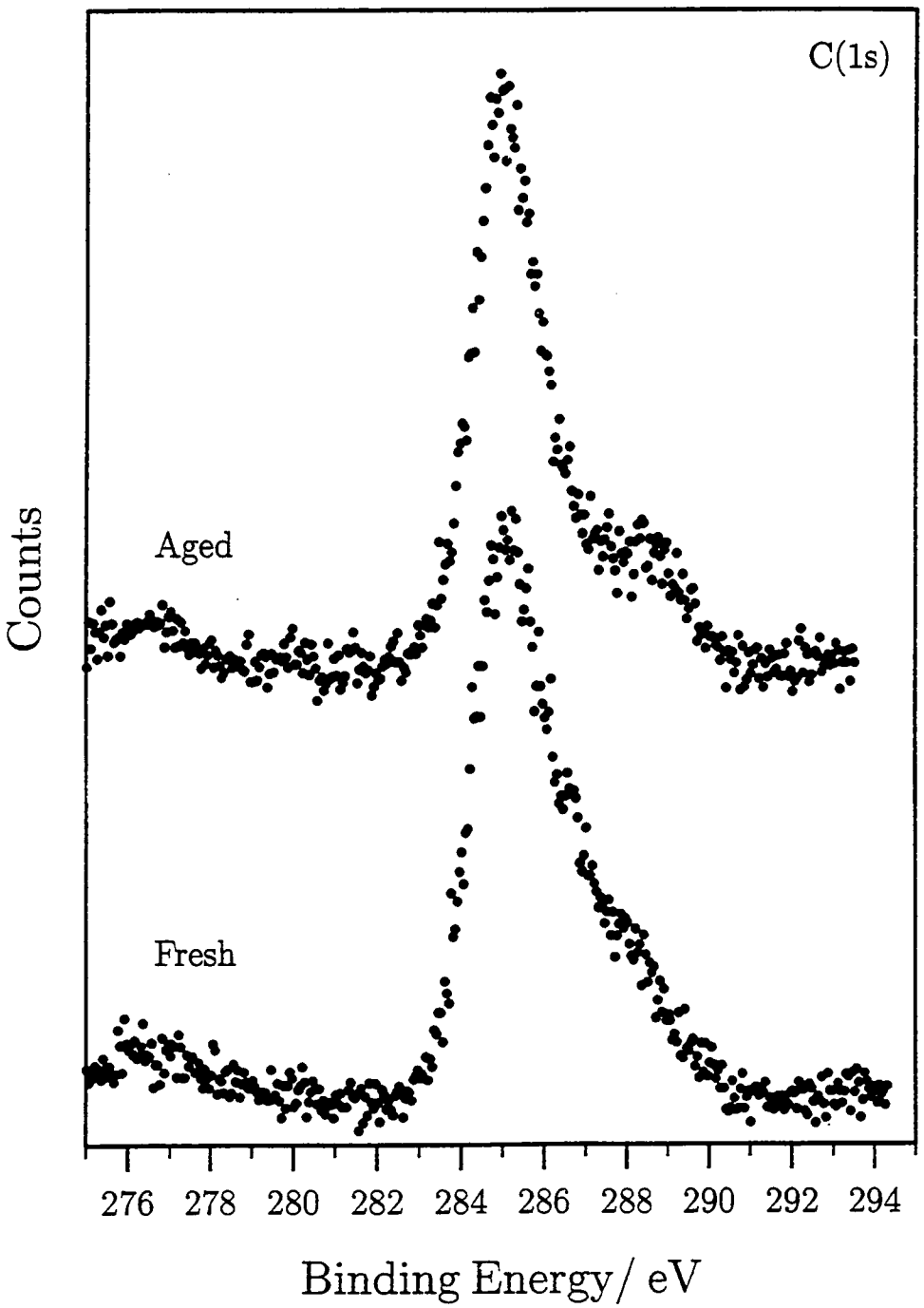

Fig. 5(a) C(1s) XP spectra for fresh and aged (approx. 1 month) PACVD samples of TMT/NH_3 onto a glass substrate (15 W, 3 min, 19 cm).

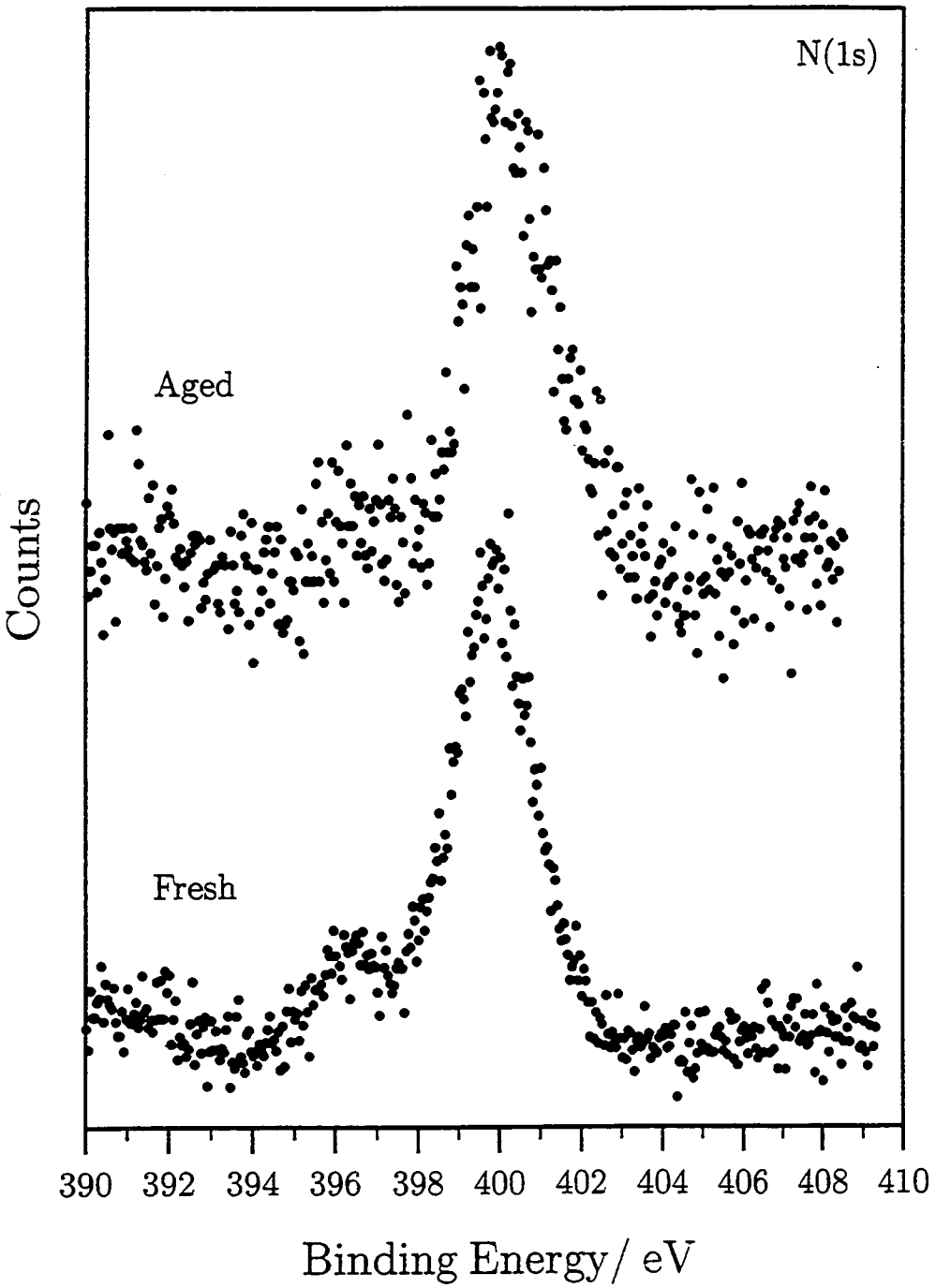

Fig. 5(b) N(1s) XP spectra for fresh and aged (approx. 1 month) PACVD samples of TMT/NH_3 onto a glass substrate (15 W, 3 min, 19 cm).

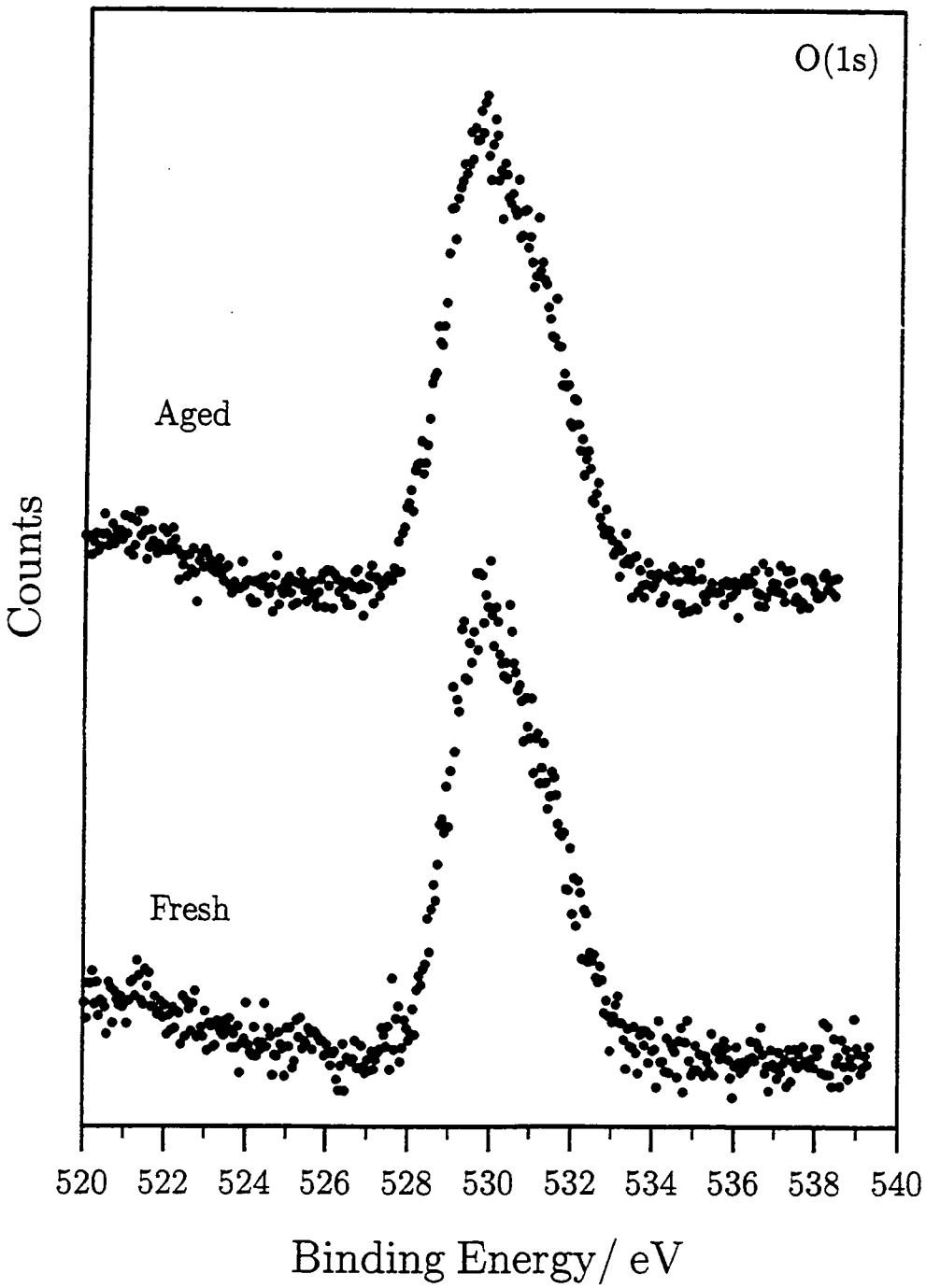

Fig. 5(c) O(1s) XP spectra for fresh and aged (approx. 1 month) PACVD samples of TMT/NH_3 onto a glass substrate (15 W, 3 min, 19 cm).

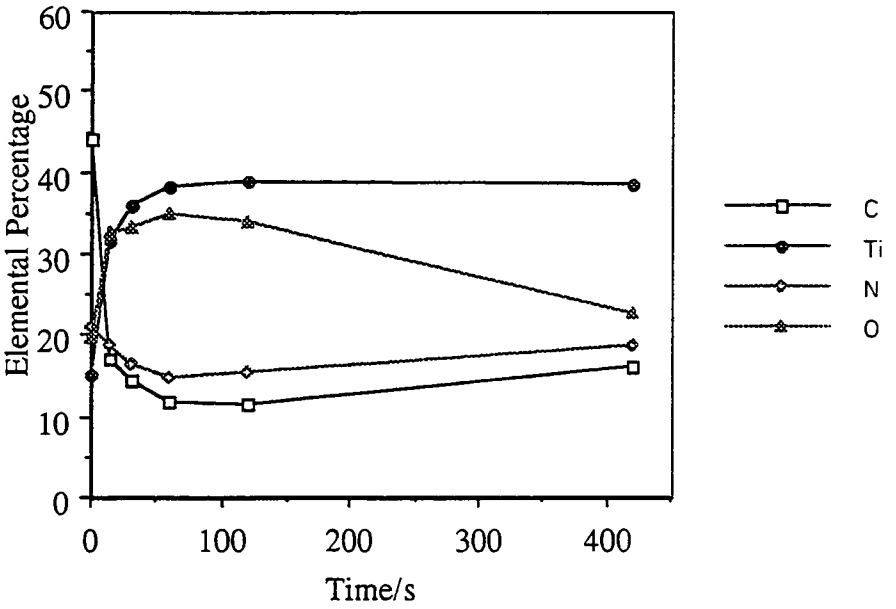

Fig. 6 XPS depth profile for PACVD of TMT/NH_3 onto a glass substrate (15 W, 3 min, 19 cm).

7.3.3 ATTENUATED TOTAL REFLECTION FOURIER TRANSFORM INFRARED SPECTROSCOPY (ATR-FTIR)

It can be seen in Fig. 8 that the deposited plasma polymer films become thicker at higher powers with the attenuation of the more surface sensitive[27] polyethylene features near 2900 cm^{-1}. Very little deposition can be seen in the absence of the plasma (0 W), though there was visible evidence of deposition with the colour change. Figure 9 shows the ATR spectrum of the 15 W TMT/NH_3 plasma polymer deposited onto polyethylene. Again, assignment of the spectral absorbances is difficult since various possibilities may be present. The broad band around 3200 cm^{-1} could arise from O-H and/or N-H stretching.[28] Evidence of the broadening of the polyethylene CH_2 stretches near 2900 cm^{-1} suggests new CH_2 environments arising from the plasma polymer.

Two weak bands at 2180 cm^{-1} and 2143 cm^{-1} are observed. This region is typically associated with multiply bonded species.[29] Though bands assigned to known titanium compounds containing different groups such as cyano (-CN), isocyano (-NC), cyanato (-OCN), isocyanato (-NCO), fulminato (-CNO) and isofulminato (-ONC) have been documented,[30-32] precise assignment is not possible since the plasma chemistry is complex and not well understood.

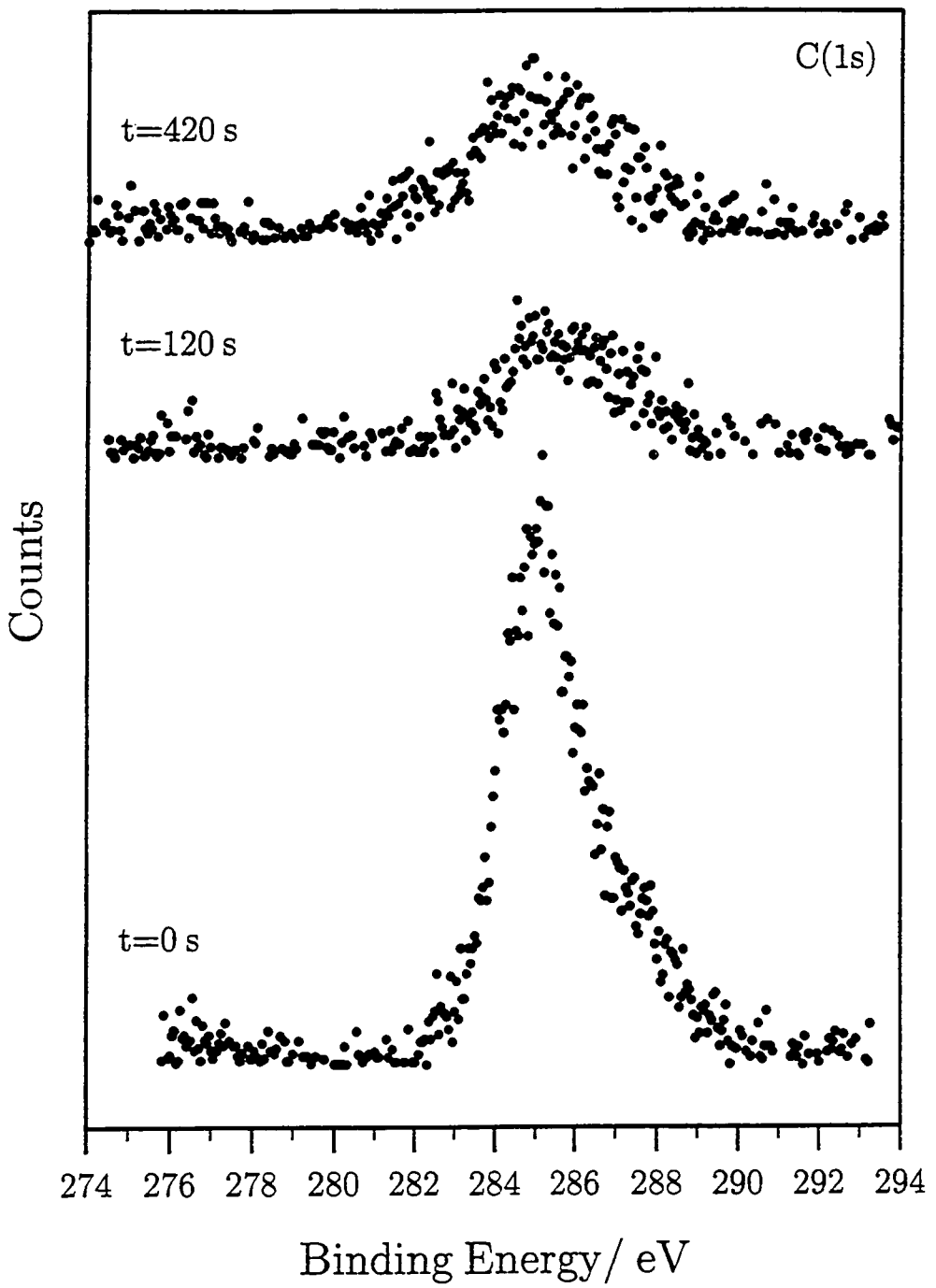

Fig. 7(a) C(1s) XP depth profile spectra for PACVD of TMT/NH_3 onto a glass substrate (15 W, 3 min, 19 cm) recorded after given sputtering times.

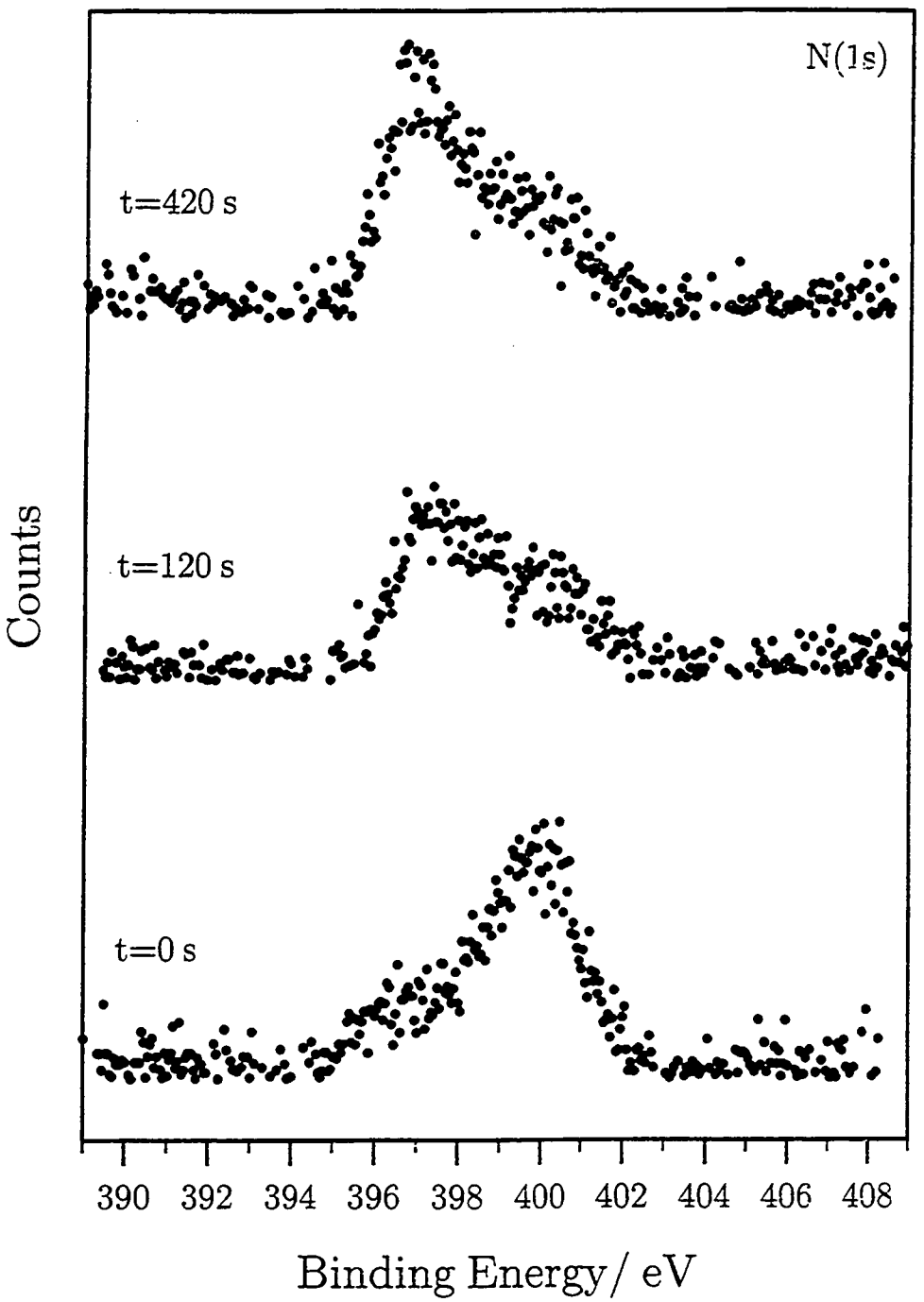

Fig. 7(b) N(1s) XP depth profile spectra for PACVD of TMT/NH_3 onto a glass substrate (15 W, 3 min, 19 cm) recorded after given sputtering times.

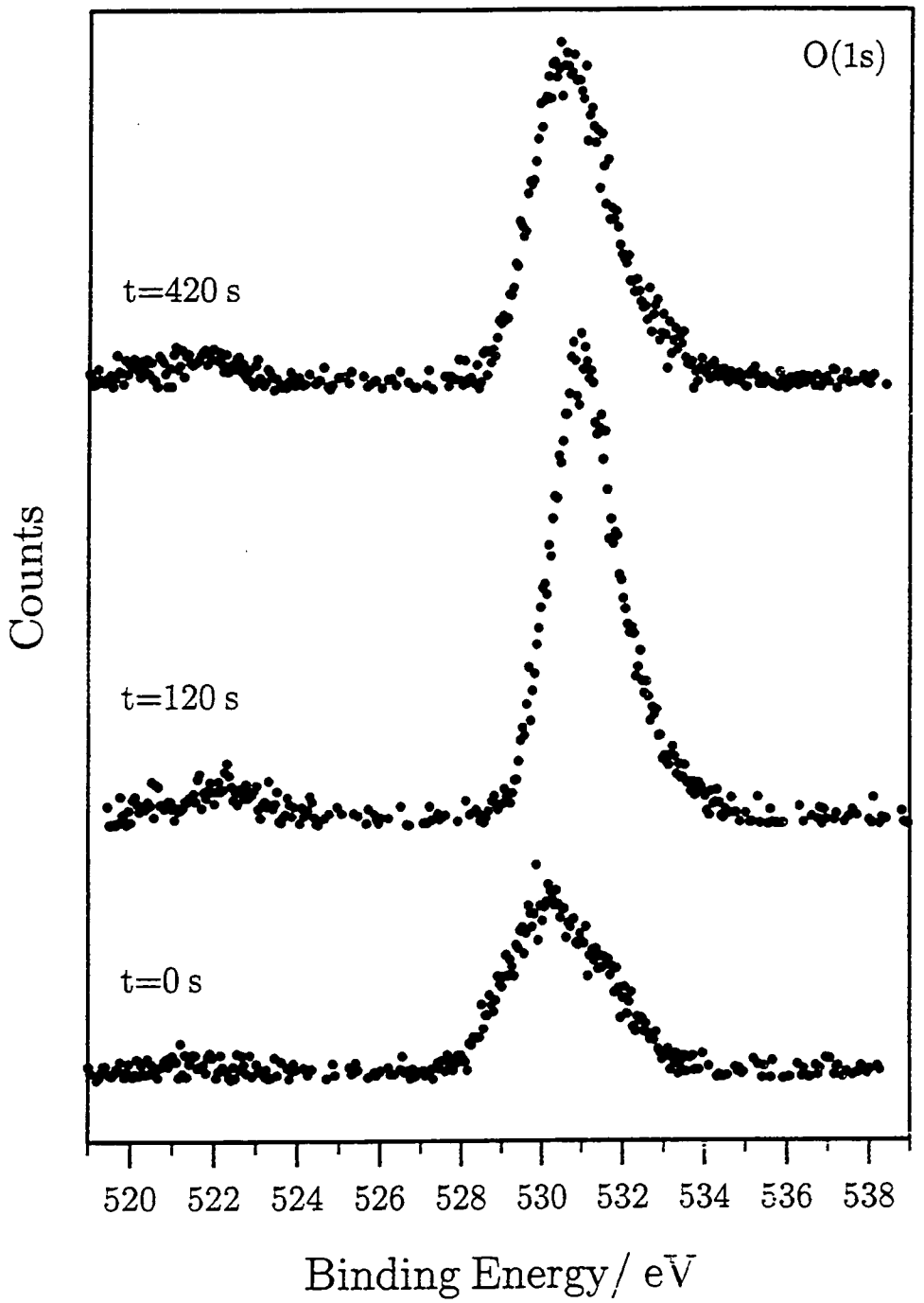

Fig. 7(c) O(1s) XP depth profile spectra for PACVD of TMT/NH_3 onto a glass substrate (15 W, 3 min, 19 cm) recorded after given sputtering times.

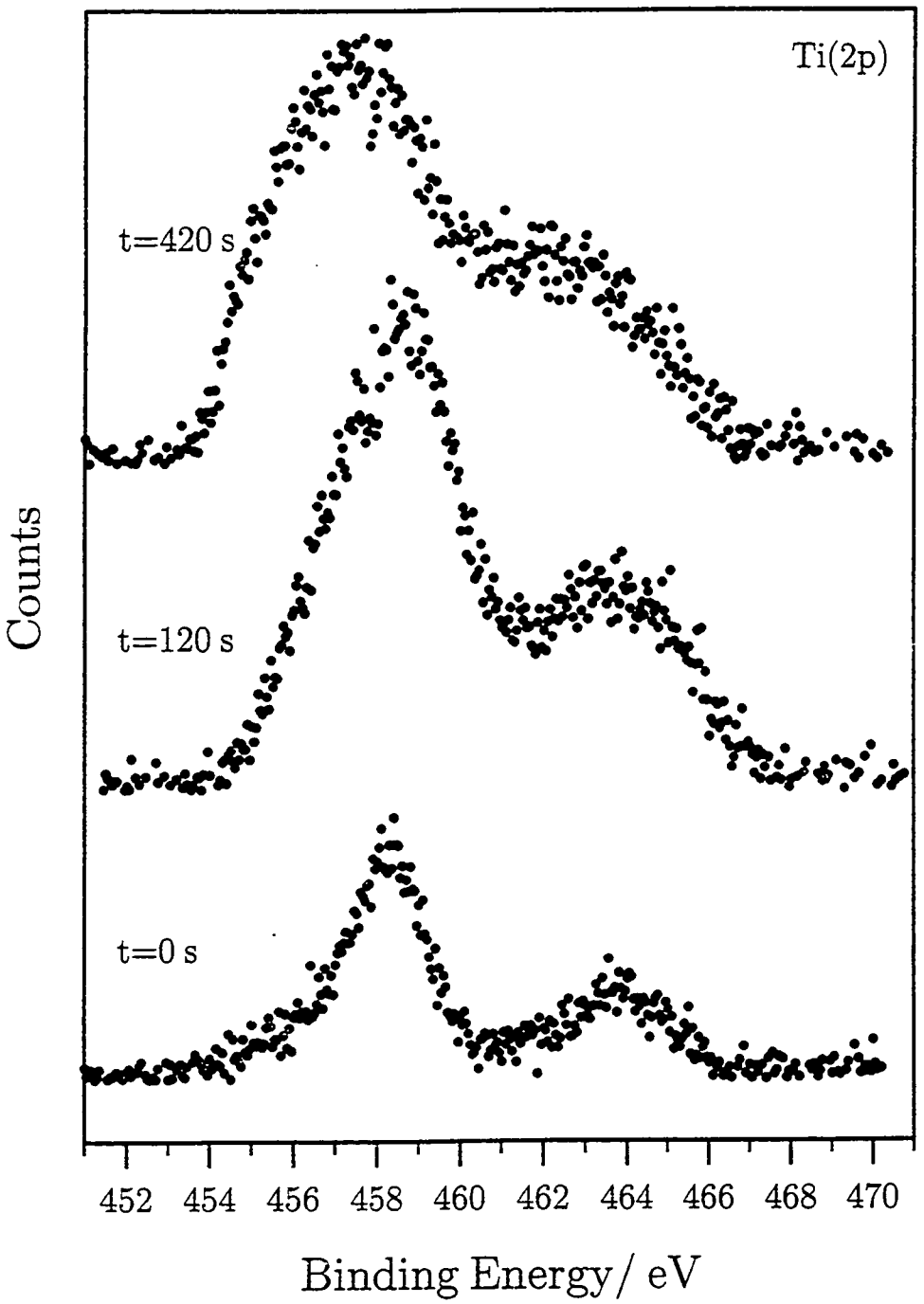

Fig. 7(d) Ti(2p) XP depth profile spectra for PACVD of TMT/NH_3 onto a glass substrate (15 W, 3 min, 19 cm) recorded after given sputtering times.

It would however be unreasonable to totally disregard such possibilities. Even amino bands at 2200 cm^{-1} have been assigned, along with an iminonitrile (=N-CN) band at 2165 cm^{-1} for the plasma polymer derived from 2-vinylpyridine.[22] Typically the amino band is found at higher wavenumbers (2700-2250 cm^{-1}).[29] A nitrile band located at 2190 cm^{-1} has been assigned in the plasma polymer of methane and nitrogen.[33] In the plasma polymer of acrylonitrile (H_2C=CHCN), a C≡N stretch and a conjugated -C=N- stretch are assigned to peaks at 2250 cm^{-1} and 2200 cm^{-1}.[34] Carbodiimides[29] (-N=C=N-), ketenes[29] (>C=C=O) and isonitriles[35] (-NC) are all found near 2150 cm^{-1}, whilst ketene-imines (-C=C=N-) are observed in the 2037 cm^{-1} region.[29,34] Azide bands at 2185 cm^{-1} and 2135 cm^{-1} have been observed in $TiCl_3N_3$.[36]

The other broad band between ~1770-1500 cm^{-1} contains a variety of different environments with maxima at ~1720 cm^{-1}, ~1661 cm^{-1}, ~1595 cm^{-1} and ~1543 cm^{-1}. The 1720 cm^{-1} environment may arise from a carbonyl stretch,[28] the 1661 cm^{-1} and 1543 cm^{-1} environments may result from the carbonyl amide I band and the N-H bending vibration amide II band respectively.[22,28] Imines (>C=NH), oximes and ureas (N-CO-N) are also found near 1660 cm^{-1}.[29] Amine N-H bending vibrations or vinylic groups fall within the region of 1595 cm^{-1}.[28] The C=N stretch and the asymmetric stretches of the carboxylate and NO_2 groups also fall in the above broad region.[28] The emergence of a band at ~1350 cm^{-1}, not seen for samples deposited in the absence of ammonia, may be a result from either the twist and wagging modes of CH_2 found in solid samples of long-chain acids, amides and esters,[28] or from the symmetric stretches of the carboxylate or NO_2 groups.[28,29] The strong absorbance below 900 cm^{-1} corresponds to Ti-O stretching as seen in bulk TiO_2.[37]

Aging of the samples for approximately one month in ambient conditions was carried out. The most significant changes occurred in the 1770-1000 cm^{-1} region which is most clearly illustrated in Fig. 10 for the 30 W plasma polymer. The broad band between 1770-1500 cm^{-1} increases in intensity with maxima at around 1660 cm^{-1} and 1600 cm^{-1}. A similar emergence of the broad band with maxima around 1350 cm^{-1}, 1339 cm^{-1} and 1320 cm^{-1} takes place. These readings correspond closely with those reported in section 5.3.3. The bands around 2100-2200 cm^{-1} almost disappear. Hydrolysis of ketene and isocyanate is likely to form carboxylic acid and amine respectively[38] whilst ketene-imines are not stable. If a carbon atom adjacent to the ketene-imine group is bonded via the nitrogen atom, then this bond is known to be easily broken to form a chain end radical and an unsaturated end.[34] These products are likely then to react with water to form amide species. Therefore the increase in the broad band between 1770-1500 cm^{-1} would agree with loss of ketene, ketene-imine and isocyanate functionalities. If azide is present, hydrolysis may take place.[36]

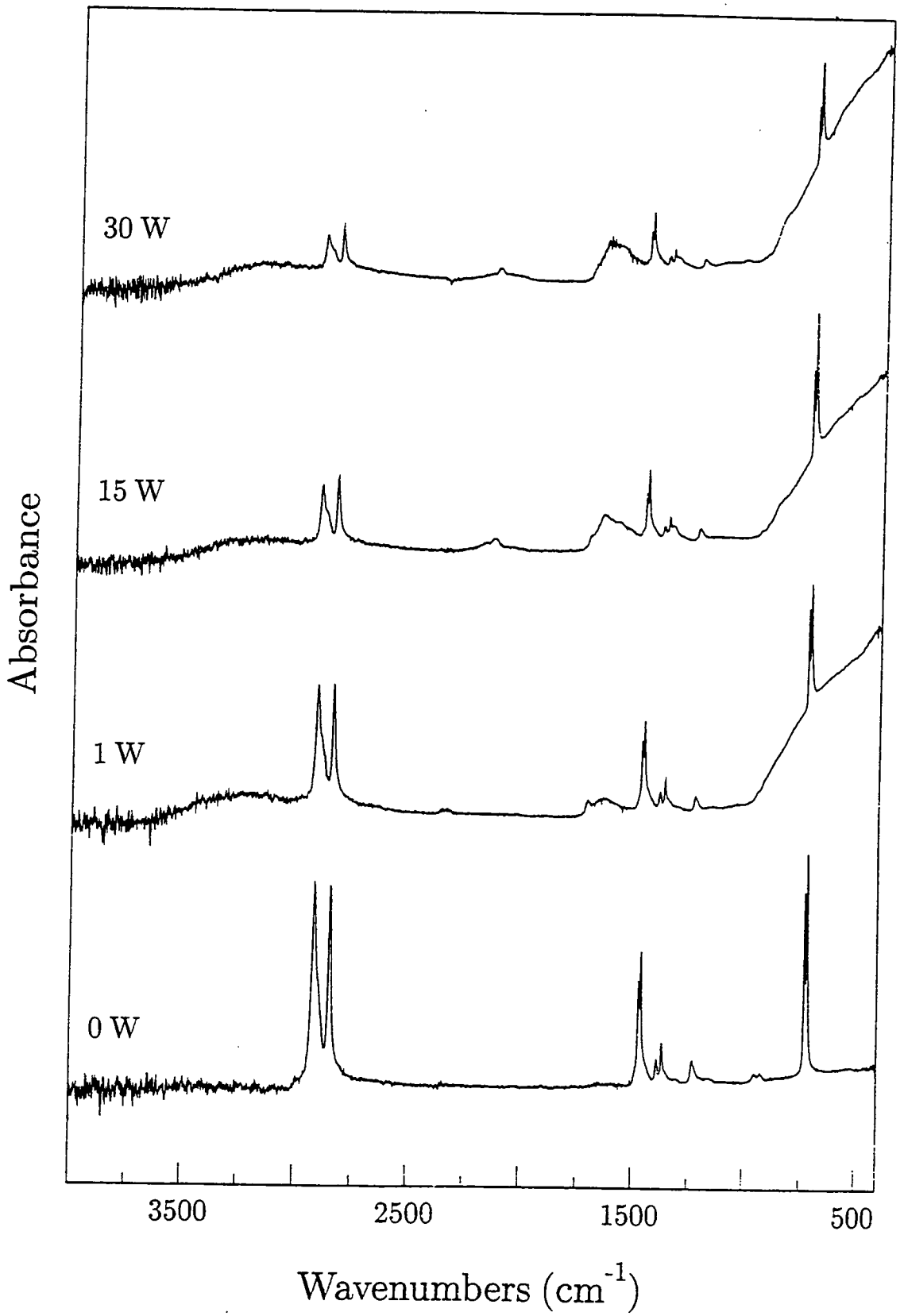

Fig. 8 ATR-FTIR spectra for PACVD of TMT/NH_3 onto polyethylene substrate as a function of glow discharge power (15 min, 19 cm).

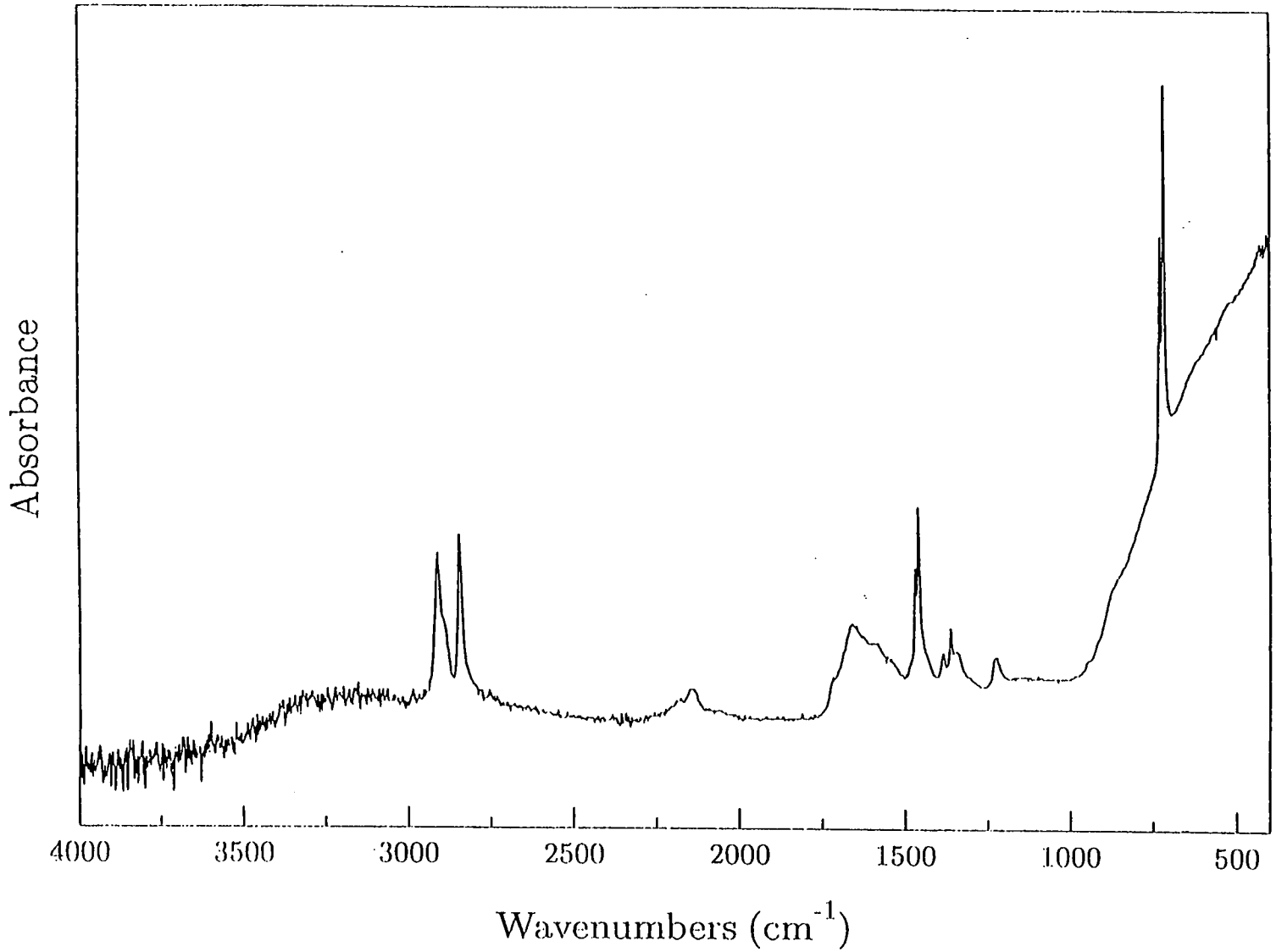

Fig. 9 ATR-FTIR spectrum for PACVD of TMT/NH_3 onto polyethylene substrate (15 W, 15 min, 19 cm).

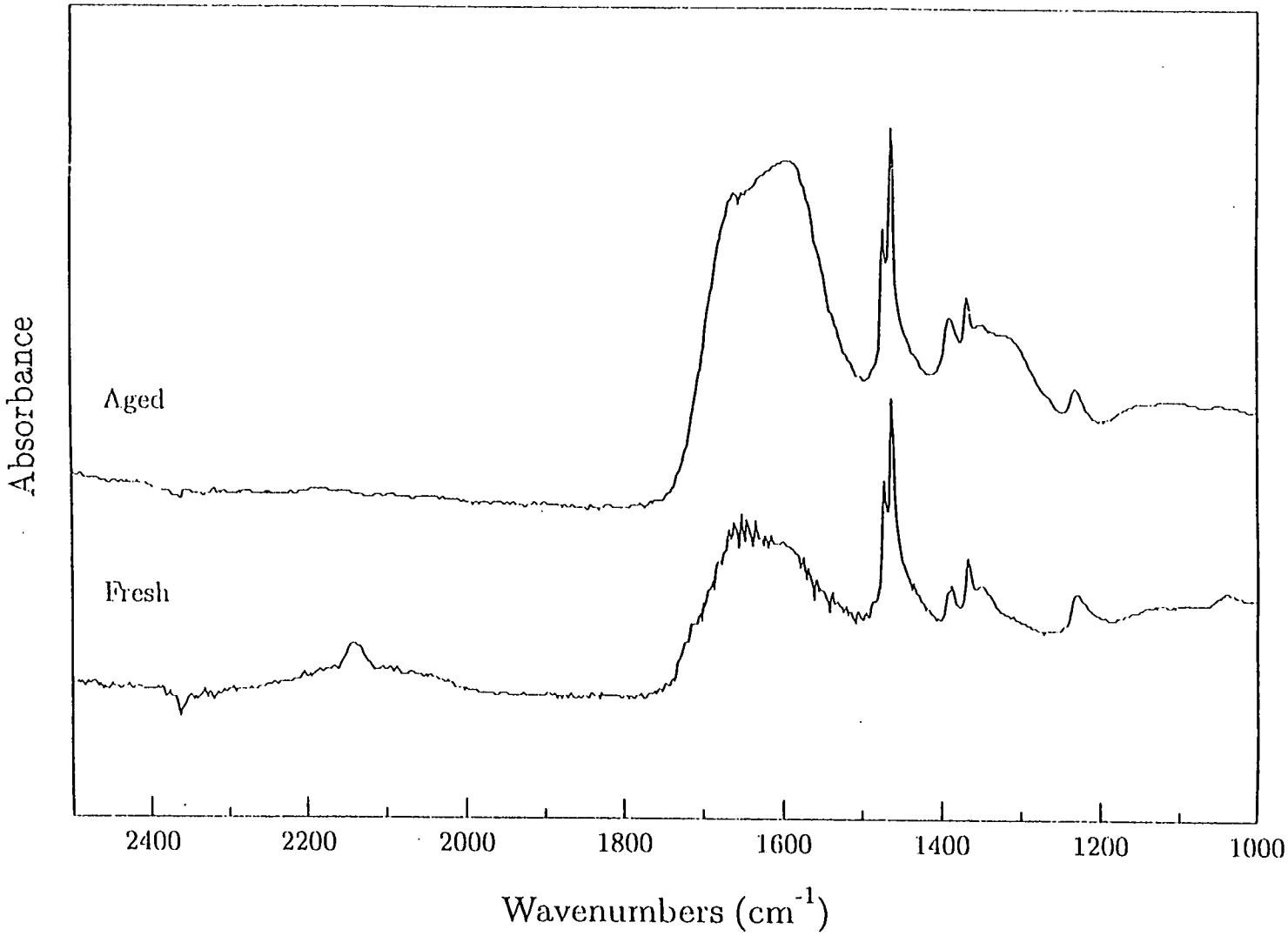

Fig. 10 ATR-FTIR spectra for PACVD of TMT/NH_3 onto polyethylene substrate showing fresh and aged samples (30 W, 15 min, 19 cm).

7.3.4 ATOMIC FORCE MICROSCOPY (AFM)

In Fig. 11, it can be clearly observed that the surface of the 15 W plasma polymer is covered with powder particles, typically associated with formation in the gas phase and not at the gas/surface interface.[39] Such particles will fall under the influence of gravity on plasma extinction.[40]

7.4 DISCUSSION

In the absence of a plasma, the colour change of films formed on the reactor walls during the mixing of the reactant gases gives clear evidence that the gas phase transamination reaction occurs.[4,8,9] The XPS results show that the main N(1s) XP environment is that due to nitrogen bound to titanium at ~397 eV. Because UV emission studies of ammonia in a plasma have shown the presence of electronically excited states of stable species such as NH_3, N_2, H_2, and radicals such as H, NH_2 and NH,[41] and since NH_2 and NH species are more reactive than ammonia,[12] it was expected that they would react more favourably with TMT via the transamination reaction, and that an increase in the nitride component in the N(1s) XP region would be observed with increasing glow discharge power. However this is not the case. More organic bound nitrogen is observed, see Fig. 4, almost certainly because other plasma induced gas phase and surface reactions also take place with increasing power. For example, dimethylamine has been shown to be a byproduct of the transamination[2,4,10] and thermal decomposition reactions of TMT.[2-5,42] It is proposed that on increasing the glow discharge power, greater fragmentation/decomposition and a greater degree of plasma polymerization of TMT and byproducts occurs, resulting in the increase in organic bound nitrogen. Such an increase is observed in the C(1s) XP region and the N(1s) XP region. (It is probable that the presence of carbon at the low powers predominantly arises from any unsubstituted dialklyamido ligands as well as a small degree of plasma polymerization of any monomer and byproducts). With increasing power however, the plasma induced reactions become increasingly important, though the extent of plasma polymerization of TMT and byproducts is limited by the short distance between the extension delivery tube and the substrate. As a result, the carbon content becomes independent of the higher glow discharge powers, consistent with the observations in Chapter 6. However the total carbon content is lower in the presence of ammonia due both to the replacement of the dialkylamido ligand with nitrogen species such as NH, NH_2 etc., and to the greater number of recombination reactions between nitrogen species and organic species which form volatile stable species that are pumped away before major plasma polymerization.

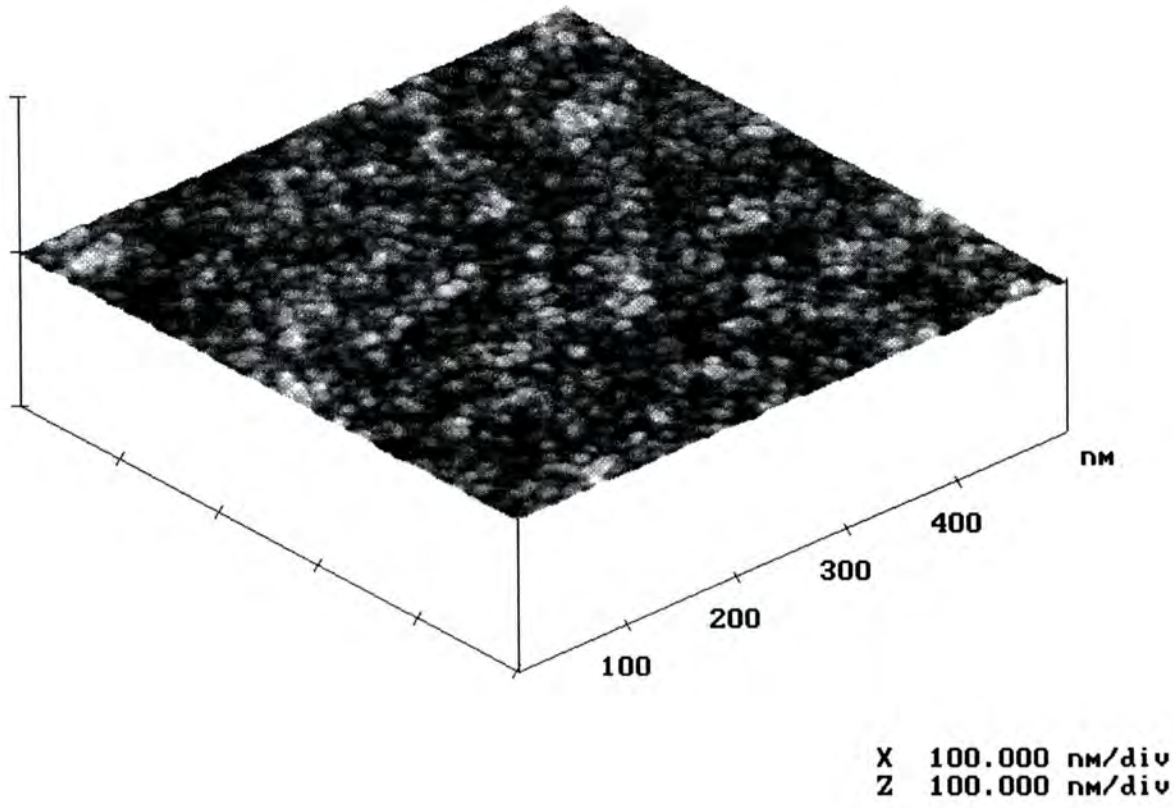

Fig. 11 AF micrograph for PACVD of TMT/NH_3 onto a glass substrate (15 W, 3 min, 19 cm).

The titanium content decreases with increasing power. This suggests that the monomer flow rate decreases as the monomer is consumed as it passes down the reactor as proposed by Park and Kim[43] and/or as a result of the gas phase transamination reaction consuming the monomer before it reaches the substrate. ATR indicates greater deposition rates at the higher powers due to the greater degree of fragmentation/decomposition of the monomer, with the deposition of the metallic species occurring immediately the monomer leaves the extension delivery tube and the organic species migrating into the heart of the glow region to undergo plasma polymerization.

The XPS depth profiling indicates the presence of titanium bound to carbon and to nitrogen. This would suggest that both the intramolecular alkyl β-hydrogen elimination reaction discussed in Chapter 6, and the transamination reaction mentioned above take place.

Oxidation on exposure to air is evident by the change in colour of the films and the XPS depth profile shows that the oxide layer is thick. Oxidation of nitrogen bound to titanium e.g. that of nitride[19] and the low valent titanium metal centre discussed by Dyagliva *et al.*[42] are likely events, as well as the reaction of trapped free radicals in the plasma polymer with atmospheric water and/or oxygen.[22] Further oxidation takes place on sustained aging in ambient conditions.

Powder particles, embedded in the surface, indicate that the gas phase reactions are dominant during the deposition process.[39]

7.5 CONCLUSIONS

The presence of ammonia with TMT results in a gas phase transamination reaction giving an orange/red deposit. On application of an RF plasma, the total carbon content is lower than in the absence of ammonia due to the transamination reaction. However the intramolecular β-hydrogen activation reaction also takes place resulting in titanium bound carbon. At the lower powers the films possess more titanium bound to nitrogen whilst the carbon content remains independent across the glow discharge power range. Oxygen incorporation occurs on oxidation in air. The films therefore deposited consist of predominantly Ti(O,C,N) in an organic polymeric matrix, $C_wH_xN_yO_z$.

7.6 REFERENCES

1. A. Katz, A. Feingold, S.J. Pearton, S. Nakahara, M. Ellington, U.K. Chakrabarti, M. Geva, E. Lane, *J. Appl. Phys.*, **70**, 1991, 3666.
2. A. Intemann, H. Koerner, F. Koch, *J. Electrochem. Soc.*, **140**, 1993, 3215.
3. R.M. Fix, R.G. Gordon, D.M. Hoffman, *Chem. Mater.*, **3** , 1991, 1138.
4. L.H. Dubois, B.R. Zegarski, G.S. Girolami, *J. Electrochem. Soc.*, **139**, 1992, 3604.
5. H.-T. Chiu, C.-C. Huang, *Mater. Letts.*, ***16***, 1993, 194.
6. D.C. Bradley, I.M. Thomas, *J.Chem. Soc.*, 1960, 3857.
7. D.C. Bradley, E.G. Torrible, *Can. J.Chem.*, **41**, 1963, 134.
8. G.M. Brown, L. Maya, *J. Am. Ceram. Soc.*, **71**, 1988, 78.
9. D. Seyforth, G. Mignani, *J. Mater. Sci. Lett.*, 7, 1988, 487.
10. J.A. Prybyla, C.-M. Chiang, L.H. Dubois, *J. Electrochem. Soc.*, **140**, 1993, 2695.
11. A. Katz, A. Feingold, S. Nakahara, S.J. Pearton, E. Lane, M. Geva, F.A. Stevie, K. Jones, *J. Appl. Phys.*, **71**, 1992, 993.
12. A. Weber, R. Nilulski, C.-P. Klages, M.E. Gross, W.L. Brown, E. Dons, R.M. Charatan, *J. Electrochem. Soc.*, **141**, 1994, 849.
13. R.M. Fix, R.G. Gordon, D.M. Hoffman, *Mater. Res. Soc. Symp, Proc.*, **168**, 1990, 357.
14. G.S. Sandhu, S.G. Meikle, T.T. Doan, *Appl. Phys. Lett.*, **62**, 1993, 240.
15. C.I.M.A. Spee, J.L. Linden, E.A. Van Der Zouwen-Assink, K. Timmer, F. Verbeck, H.A. Meinema, D.M. Frigo, S. Van Der Ven, *J. Physique IV*, C3, *J. Physique II*, **3**, 1993, 289.
16. K. Ishihara, K. Yamazaki, H. Hamada, K. Kamisako, Y. Tarui, *Jpn. J. Appl.Phys.*, **29**, 1990, 2103.
17. D.W. Fischer, *J. Appl. Phys.*, **41**, 1970, 3561.
18. G. Beamson, D. Briggs, High Resolution XPS of Organic Polymers, The Scienta ESCA300 Database, John Wiley, Chichester, 1992.
19. N.C. Saha, H.G. Tompkins, *J. Appl. Phys.*, **72**, 1992, 3072.
20. B. Siemensmeyer, K. Bade, J.W. Schultze, *Ber. Bunsenges. Phys. Chem.*, **95**, 1991, 1461.
21. M.V. Kaznetsov, J.F. Zhuravlev, V.A. Zhilyaev, V.A. Gubanov, *J. Electron. Spec. Rel. Phen.*, **58**, 1992, 1.
22. H. Yasuda, Plasma Polymerization, Academic Press, Orlando, FL, 1985.
23. R. Foerch, N.S. McIntyre, R.N.S. Sodhi, D.H. Hunter, *J. Appl. Polym. Sci.*, **40**, 1990, 1903.
24. S. O'Kell, T. Henshaw, G. Farrow, M. Aindow, C. Jones, *Surf. Interface Anal.*, **23**, 1995, 319.
25. J.W. Coburn, *Thin Solid Films*, **64**, 1979, 371.

26. C.N. Sayers, N.R. Armstrong, *Surf. Sci.*, 77, 1978, 301.
27. F.M. Mirabella, *Appl. Spectrosc. Rev.*, **21**, 1985, 45.
28. R.M. Silverstein, G.C. Bassler, T.C. Morrill, Spectrometric Identification of Organic Compounds, 4th Edn., Wiley, New York, 1981.
29. D.H. Williams, I. Fleming, Spectroscopic Methods in Organic Chemistry, 3rd Edn., McGraw-Hill, London, 1987.
30. N.N. Greenwood, E.J.F. Ross, B.P. Straughan, Index of Vibrational Spectra of Inorganic and Organometallic Compounds, Vol. 1, Butterworths, London, 1972.
31. N.N. Greenwood, E.J.F. Ross, Index of Vibrational Spectra of Inorganic and Organometallic Compounds, Vol. 2, Butterworths, London, 1975.
32. N.N. Greenwood, E.J.F. Ross, Index of Vibrational Spectra of Inorganic and Organometallic Compounds, Vol. 3, Butterworths, London, 1977.
33. H.-X. Han, B.J. Feldman, *Solid State Commun.*, **65**, 1988, 921.
34. N. Inagaki, S. Tasaka, Y. Yamada, *J. Polym. Sci. Polym. Chem. Edn.*, **30**, 1992, 2003.
35. L.J. Bellamy, The Infrared spectra of Complex Molecules, 3rd Edn., Chapman and Hall, London, 1975.
36. K. Dehnicke, *J. Inorg. Nucl. Chem.*, **27**, 1965, 809.
37. M. Ocaña, W.P. Hsu, E. Matijevic, *Langmuir*, 7, 1991, 2911.
38. A. Streitweiser, Jr., C.H. Heathcock, Introduction to Organic Chemistry, 3rd Edn., Macmillan, New York, 1985.
39. R. d'Agostino, Ed., Plasma Deposition, Etching of Polymers, Academic Press, San Diego, 1990.
40. G.S. Selwyn, K.L. Haller, E.F. Patterson, *J. Vac. Sci. Technol.*, **A11**, 1993, 1132.
41. R. d'Agostino, F. Cramarossa, S. De Benedictis, G. Ferraro, *Plasma Chem. Plasma Proc.*, **1**, 1981, 19.
42. L.M. Dyagileva, V.V. Mar'in, E I. Tsyganova, I.L. Gaidym, Y.A Aleksandrov, *J. Gen. Chem. USSR (Eng.)*, **54**, 1984, 538.
43. S.Y. Park, N. Kim, *J. Appl. Polym. Sci. Polym. Appl. Symp.*, **46**, 1990, 91.

CHAPTER 8:
CONCLUSIONS

8.1 INTRODUCTION

Injection of a precursor/gas into a low pressure glow discharge is a potentially important method of creating novel films at low temperatures. It greatly simplifies deposition onto thermally sensitive substrates and it only produces small amounts of gaseous byproducts unlike conventional wet chemical methods. This technique was adopted in this work to produce titanium ceramic/polymeric composite thin films by PACVD.

The aim was to produce nanoscale conducting/semiconducting phases dispersed in a polymeric matrix which may potentially exhibit useful electrical properties. Films, deposited onto glass and polyethylene substrates, were characterized by XPS and ATR-FTIR techniques. Surface morphology was examined by AFM. A summary of results and conclusions is reported, and possible future work is proposed.

8.2 REVIEW OF EXPERIMENTAL RESULTS AND CONCLUSIONS

8.2.1 TiTP PRECURSOR

The TiTP precursor was chosen because it is highly volatile, cheap, has already been shown to successfully produce oxides of titanium with interesting electrical properties and possesses a large organic component to provide the polymer matrix. Table 1 summarizes the deposition process conditions, as well as the analytical techniques that were used to characterize surface and bulk compositions, group functionalities and surface morphologies.

During the PACVD using TiTP, TiO_2/polymer composite films were deposited. At low powers TiO_2-rich films were produced in the plasma glow zone, whilst at higher powers deposition of TiO_2 occurred upstream, and the remaining organic byproducts underwent a greater degree of plasma polymerization as they passed into the plasma glow region.

Table 1 Summary of the TiTP/gas systems studied.

Precursor	Gas Present ($x10^{-2}$ Torr)	Power Range/ W	Total System Pressure/ $x10^{-2}$ Torr	Characterization Techniques
TiTP	-	0-30	8.0	XPS, ATR-FTIR, AFM
TiTP	H_2 (5.6)	5-30	6.4	XPS, ATR-FTIR, AFM
TiTP	NH_3 (5.6)	3-30	6.0	XPS, ATR-FTIR, AFM

Park and Kim have proposed that during plasma assisted deposition, the average deposition rate can generally be described as being governed by an Arrhenius-type of activation, E_a:

$$D_p \propto F_M \exp[-E_a/(W/F_M)]$$

where D_p is the average deposition rate, W is the glow discharge power, and F_m is the mass flow rate.[1] When the glow discharge power is zero or where the mass flow rate is zero, there is no deposition for any given reactor location. This expression has been successfully used to explain why at lower powers the deposition rates were greatest and at the higher powers, the deposition rates dropped off. Less monomer reached the RF coil region at the higher powers since much of the monomer had already been consumed upstream.

Mixing of non-polymer forming gases with the TiTP monomer required a redesigned monomer inlet configuration. The configuration adopted allowed monomer to be deposited into the highest energy zone within the RF coils. As a result of this modification, and in conjunction with a lower total monomer flow rate, the deposition was more localised within a much smaller area in the RF coils. (Little deposition was found downstream of the RF coils). Note that a small amount of deposit was produced inside the extension delivery tube configuration. In addition, the film thicknesses were lower as a result of the lower monomer flow rate.

The substrate location in the modified reactor was only 2 cm downstream of the end of the extension delivery tube, whereas in the TiTP case, the substrate location was 21.5 cm downstream from the entry of monomer to the reactor. This design meant that there was only a small decrease in the mass flow rate from leaving the extension delivery tube to reaching the substrate location. Therefore no major compositional changes were observed on increasing the glow discharge power using this monomer delivery configuration because the extent of plasma polymerization was limited over this short distance, in contrast to the initial reactor configuration. Though this reactor configuration was not used for TiTP, it is likely for the reasons given above that, if it

were used, similar results to those observed in the modified reactor would be obtained.

The addition of hydrogen gas to TiTP, intended to reduce the titanium (+IV) metal centre and aging effects suffered by the plasma polymer, appears to have been successful. The grey/blue colour of the films deposited in the presence of hydrogen suggests that TiO_x (where $0<x<2$)[2] tended to be more stable to oxidation on exposure to air since the films did not immediately lose their grey/blue colour as in the case of TiTP only, and no aging effects of the plasma polymer were observed. However in neither system (TiTP and TiTP/H_2) was it possible to determine from the XPS depth profiling whether the broadening of the Ti(2p) XP peaks[3] was solely a manifestation of the preferential sputtering of oxygen[4] resulting in suboxides of titanium, or whether the suboxides were present in any case below the outermost surface of the film, or arose from a combination of both. It is more than likely that contributions came from both sources. Nitrogen incorporation was most likely to be a manifestation of atmospheric nitrogen reacting with trapped free radicals in the plasma polymer.[5]

The addition of ammonia gas to TiTP led to the deposition of $TiO_pN_q/O_rC_sH_tN_u$ composite films within the bulk. It is proposed that the lack of the Ti-N environment at the surface in the Ti(2p) and N(1s) XP regions resulted from atmospheric oxidation.[6]

8.2.3 TMT PRECURSOR

Since TMT possesses an inherent Ti-N bond and has been successfully used to deposit conducting TiN films, it was considered a more suitable candidate for deposition of TiN/polymer composite films. Table 2 summarizes the deposition process conditions, as well as the analytical techniques that were used to characterize surface and bulk compositions, group functionalities and surface morphologies.

Table 2 Summary of the TMT/gas systems studied.

Precursor	Gas Present ($x10^{-2}$ Torr)	Power Range/ W	Total System Pressure/ $x10^{-2}$ Torr	Characterization Techniques
TMT	-	1-30	5.6	XPS, ATR-FTIR, AFM
TMT	H_2 (5.4)	1-30	9.3	XPS, ATR-FTIR, AFM
TMT	NH_3 (5.6)	0-30	6.8	XPS, ATR-FTIR, AFM

The observed binding energies of the Ti(2p) XP environments for films deposited from TMT and TMT/H_2 indicated the presence of oxynitride at the surface. This therefore supports the proposal of the formation of $TiO_pN_q/O_rC_sH_tN_u$ composite films at the

surface. However below the outermost surface, after sputtering, Ti-N and Ti-C environments were found. It is proposed that the possible alkyl β-hydrogen activation took place:[7-11]

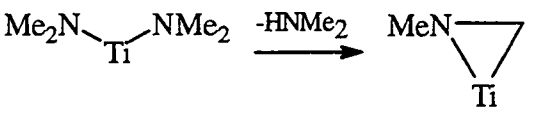

Evidence for such a mechanism has not previously been reported at ambient temperatures. The films were found to consist of $TiO_pC_qN_r/O_sC_tH_uN_v$ composite layers below the outermost surface. The addition of hydrogen to TMT resulted in a small reduction in the carbon content at higher glow discharge powers due to the formation of stable organic byproducts by recombination, which were pumped away before they could undergo major fragmentation and plasma polymerization.

The addition of ammonia gas to TMT prior to plasma activation resulted in a gas phase transamination reaction[12-14] giving an orange/red deposit. As a result, the carbon content in the deposited films was reduced in comparison to those films deposited using the TMT and TMT/H_2 systems. However the addition of ammonia failed to prevent Ti-C bond formation via the alkyl β-hydrogen activation since $TiO_pC_qN_r/O_sC_tH_uN_v$ composite films were similarly observed below the outermost surface. The N(1s) XP region at the surface indicated that the nitrogen bonded to titanium environment (either Ti-N, Ti=NR or Ti-NR_2)[9] decreased whilst the organo-nitrogen environment increased as the glow discharge power was increased. It is proposed therefore that gas phase plasma and surface reactions became increasingly important as the glow discharge power was increased.

8.3 CONCLUSIONS

The environment in a plasma is vastly complex and not well understood. Total control and optimization of the deposition process is therefore the proximate goal for great technological advancement. Traditionally much of the development work has been performed on an *ad hoc* basis or by empirical means. Until plasma diagnostic techniques and computer modelling become routine in conjunction with current methods, the rate of discovery and invention will remain limited.

Since the plasma and process parameters are strongly dependent upon one another, the systems studied were simplified by limiting the number of parameters that were varied. The key plasma variable, and the easiest to control, was the glow discharge power, though elevation of the substrate temperature, T_S, may have a similar influence upon the

structure of a given plasma polymer.[15] However the mechanisms involved are different. Pyrolysis of the growing film and surface mobility of the precursor species on the substrate influence the resulting film structure when the T_S is raised, whilst if the glow discharge power is the variable, film structure is affected by monomer fragmentation. In addition, deposition at the lowest possible temperature reduces the dangers of damaging sensitive substrates or creating diffusive broadening of existing interfaces or junctions in devices (typically encountered in conventional CVD).

It is the ability to vary and control the degree of organic/inorganic character that provides the opportunity to control the many physico-chemical properties over wide ranges. For example, the chemical composition was found to vary significantly as a function of the glow discharge power in the case of TiTP, see Table 3. Only minor chemical composition variations however were observed for the other monomer/gas systems. This was a consequence of the reactor configuration and is explained further below. As well as glow discharge power variation, substrate location also played an important role in chemical composition. For example at high powers, the metallic component was found to be predominantly deposited upstream of the RF coils for TiTP and the volatile organic component deposited in the RF coils.

Table 3 Summary of the surface elemental composition ranges observed for the precursor/gas systems for the glow discharge power range between 0-30 W.

Precursor/gas	C range/ %	Ti range/ %	N range/ %	O range/ %
TiTP	39.6-85.2	4.1-22.2	0.8-2.9	10.7-37.6
TiTP/H_2	46.1-53.7	17.2-21.1	1.2-6.3	26.1-30.0
TiTP/NH_3	38.8-44.0	12.5-19.1	13.6-24.7	19.6-27.3
TMT	49.3-56.0	10.6-16.3	8.0-14.5	17.7-25.7
TMT/H_2	48.7-56.0	11.0-16.2	13.4-15.4	18.8-24.3
TMT/NH_3	41.7-47.6	11.7-20.7	11.1-25.1	17.4-24.3

In the quest for new chemical environments within the films, a modification to the reactor was necessary in order to enable the admission of non-polymer forming gases. Flow of monomer direct into the RF coils was the result of initial attempts to achieve deposition comparable to that found in Chapter 3. Further, XPS and ATR-FTIR measurements gave more reproducible results because a more consistent monomer flow rate was achieved since no monomer heating was required. The metallic component in the new reactor configuration was almost entirely deposited within the RF coils and a greater proportion of organic species deposited downstream. As a direct result of the new reactor configuration, the chemical compositions indicated in Table 3 were found

to vary to a lower extent with glow discharge power, particularly over 5 W. Such results could be advantageous in a commercial deposition process because the requirement for an expensive high precision power supply unit could be avoided.

The highest titanium contents indicated in Table 3 were found at the lowest glow discharge powers since monomer flow rates at the substrate were near their maximum. The use of lower glow discharge powers may therefore be the best approach to encourage conduction within the films since it is the metal content that is likely to determine the conduction process.

The unique ability of a plasma to permit reactions that would normally not occur under ambient conditions was clearly demonstrated on the addition of ammonia to TiTP in Chapter 5. It would appear from the thermodynamic data that rupture of the Ti-O bond (mean bond dissociation energy of Ti-O in TiTP is 422.6 $kJmol^{-1}$)[16] would be energetically less favourable than formation of the Ti-N bond (an approximate mean bond dissociation energy of 326.3 $kJmol^{-1}$ for the Ti-N bond can be determined from the value given for TMT).[17] However plasma excitation of TiTP in the presence of ammonia overcame the thermodynamc barrier constraints and allowed Ti-N bond formation.

Films left in ambient conditions for approximately one month were found to age (except those deposited from TiTP/H_2) resulting in an increase in the oxygen content. Plasma polymers typically show oxidative aging effects due to the high density of trapped free radicals they possess.[18] These react with atmospheric oxygen and water to form hydroxyl and carbonyl groups on the surface as shown in the scheme below:

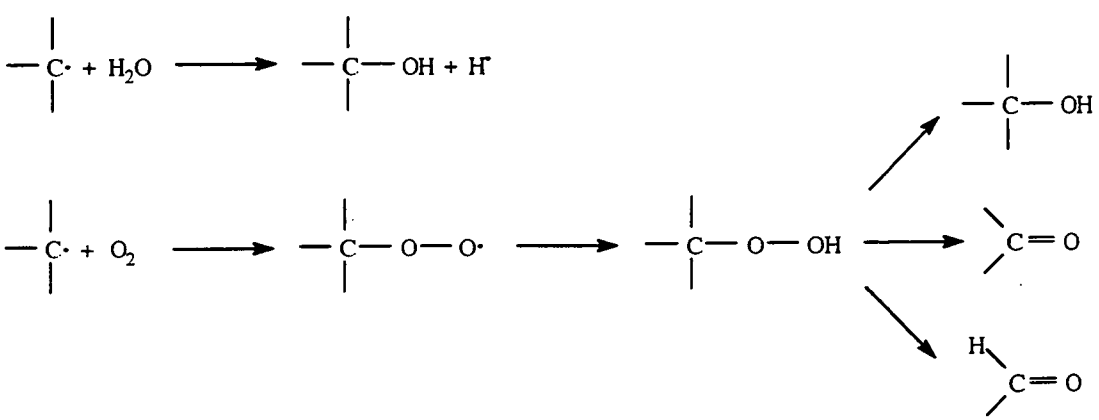

Such aging processes have been shown to have detrimental affects on the electrical properties of plasma polymers.[19] However the use of a saturated hydrogen plasma environment with TiTP was shown to be successful in preventing free radical reaction with atmospheric moisture and oxygen. This should therefore be considered as a

possible approach to eliminating the problems associated to aging. Note that whereas the introduction of hydrogen to TiTP created films stable to aging, the same did not apply to TMT and hydrogen. This may be consistent with a much greater concentration of hydrogen present with TiTP than with TMT, resulting in a much greater probability of the 'quenching' of free radicals by hydrogen radicals.

The surface morphologies of the plasma polymers were examined by the recently developed high resolution AFM technique. Such a technique is ideal because it is quick to perform with little sample preparation, and sample damage can be avoided particularly if the TappingMode™ is used. Information as to whether gas phase or surface reactions dominate during plasma assisted deposition may be inferred from the AFM images. Clear evidence of gas phase reactions was shown by the powder or dust particles present on some of the plasma polymer surfaces.[15,18,20] Alternatively AFM may become a useful tool to determine at which stage the growing film becomes smooth as the powder particles coalescence with continuing deposition.[18,20] However comparison of the individual AFM images obtained for the different precursor/gas systems remains unexplained.

The work discussed in this thesis using such reactor configurations is just the start of systematic studies. Further work is required to develop and optimize the procedures and processes to achieve the desired film physico-chemical properties. For example, clarification as to whether a conducting (nano)composite can be produced by PACVD using such precursors still has be determined. Possible future studies that might benefit the understanding of the deposition process and film properties are listed in the Future Work section below.

8.4 FUTURE WORK

(a) Determination of the variation in film composition with increasing glow discharge power using the modified reactor configuration and TiTP monomer only. This would allow comparison with current results using this reactor configuration (i.e. localized deposition and almost constant composition on increasing the glow discharge power).

(b) Determination of film composition at extremely high glow discharge powers (available from a higher power RF generator unit) resulting in a much greater decomposition of monomer molecules. A greater contrast in film compositions is likely, ranging from being almost completely inorganic to being almost completely organic, depending on substrate location. Similar results to those obtained by substrate heating may be expected.[15]

(c) Studies to examine the effects of changing other process parameters, e.g. the monomer flow rate or substrate temperature, on the film composition. This may require possible modifications to the reactor configuration and hence may invalidate direct comparison with the current results.

(d) Glow discharge power variation and substrate location studies examined by AFM in conjunction with the corresponding XPS and ATR-FTIR studies. This may lead to discovery and understanding of the different regimes within a deposition plasma where gas phase or surface reactions dominate.

(e) Studies to confirm the proposition that the deposited films are amorphous[15] using techniques such as XRD, TEM or SEM. On increasing the substrate temperature, it is expected that the introduction of crystalline phases would appear with the elimination of organic fragments.[17] Such changes in crystallinity would become evident using the above techniques.

(f) *In situ* studies by UV optical emission, gas phase infrared and mass spectroscopy of the effluent species may lead to mechanistic information[17] from the intermediate species observed in the gas phase.

(g) Having observed the possibility of improved surface conductivity for a TiTP/H_2 plasma polymer compared to clean polyethylene film, further investigation into the electrical properties of the samples needs to be performed using more rigorous techniques such as the four point probe method. As mentioned earlier, the lower glow discharge power regime may be a good starting point because a higher metal content was observed.

8.5 REFERENCES

1. S.Y. Park, N. Kim, *J. Appl. Polym. Sci. Polym. Appl. Symp.*, **46**, 1990, 91.
2. Gmelins Handbuch, Der Anorganischen Chemie, Titan, Vol. 41, Verlag Chemie, GMBH, Weinhelm/Bergstraße, 1951, p. 214.
3. C.N. Sayers, N.R. Armstrong, *Surf. Sci.*, **178**, 1977, 301.
4. J.W. Coburn, *Thin Solid Films,* **64**, 1979, 371.
5. N. Inagaki, H. Kawai, *J. Polym. Sci. Polym. Chem. Ed.*, **24**, 1986, 3381.
6. N.C. Saha, H.G. Tompkins, *J. Appl. Phys.*, **72**, 1992, 3072.
7. A. Intemann, H. Koerner, F. Koch, *J. Electrochem. Soc.*, **140**, 1993, 3215.
8. H.-T. Chiu, C.-C. Huang, *Mater. Letts.*, ***16***, 1993, 194.
9. R.M. Fix, R.G. Gordon and D.M. Hoffman, *Chem. Mater.*, **2** , 1990, 235.
10. A. Katz, A. Feingold, S.J. Pearton, S. Nakahara, M. Ellington, U.K. Chakrabarti, M. Geva, E. Lane, *J. Appl. Phys.*, **70**, 1991, 3666.
11. K.-T. Rie, A. Gebauer, *Mater Sci. Eng.*, **A139**, 1991, 61.
12. G. M. Brown, L. Maya, *J. Am. Ceram. Soc.*, **71**, 1988, 78.
13. D. Seyforth, G. Mignani, *J. Mater. Sci. Lett.*, **7**, 1988, 487.
14. L. H. Dubois, B. R. Zegarski, G. S. Girolami, *J. Electrochem. Soc.*, **139**, 1992, 3604.
15. R. d'Agostino, Ed., Plasma Deposition, Etching of Polymers, Academic Press, San Diego, 1990.
16. D.C. Bradley, R.C. Mehrotra, D.P. Gauer, Metal Alkoxides, Academic Press, London, 1978.
17. M.F. Lappert, D.S. Patil, J.B. Pedley, *J.C.S. Chem. Comm.*, 1975, 830.
18. H. Yasuda, Plasma Polymerization, Academic Press, Orlando, FL., 1985.
19. L.S. Tusov, V.M. Kolotyrkin, N.N. Tunitskii, *Int. Chem. Eng.*, **11**, 1971, 60.
20. H.V. Boenig, Plasma Science and Technology, Cornell University Press, New York, 1982.

APPENDIX

COLLOQUIA, LECTURES AND SEMINARS FROM INVITED SPEAKERS

COURSES ATTENDED

Chemistry Department induction courses;
Laboratory techniques, 6 lectures;
Basic electronics, 6 lectures.

LECTURES (* denotes attendance)

1991

Sept. 17 — Prof. R.D. Fischer, University of Hamburg, Germany
Organo-f-element Systems to Organo-Main-Group Polymers

October 17 — Dr. J.A. Salthouse, University of Manchester
Son et Lumiere - a Demonstration Lecture*

October 31 — Dr. R. Keeley, Metropolitan Police Forensic Science
Modern Forensic Science*

Nov. 6 — Prof. B.F.G. Johnson, Edinburgh University
Cluster-Surface Analogies*

Nov. 7 — Dr. A.R. Butler, University of St. Andrews
Traditional Chinese Herbal Drugs: a Different Way of Treating Disease

Nov. 13 — Prof. D. Gani, University of St. Andrews
The Chemistry of PLP-dependent Enzymes*

Nov. 20 — Dr. R.M. O'Ferral, University College, Dublin
Some Acid-catalyzed Rearrangements in Organic Chemistry*

Nov. 28 — Prof. I.M. Ward, IRC in Polymer Science, University of Leeds
The Science and Technology of Orientated Polymers*

Dec. 4 Prof. R. Grigg, Leeds University
Palladium-catalyzed Cyclization and Ion Capture Processes*

Dec. 5 Dr. W.D. Cooper, Shell Research
Colloid Science, Theory and Practice

Dec. 5 Prof. A.L. Smith, ex Unilever
Soap, Detergents and Black Puddings

1992

January 22 Dr. K.D.M. Harris, University of St. Andrews
Understanding the Properties of Solid Inclusion Compounds*

January 29 Dr. A. Holmes, Cambridge University
Cycloaddition Reactions in the Service of the Synthesis of Piperidine and Indolizidine Natural Products*

January 30 Dr. M. Anderson, Shell Research
Recent Advances in the Safe and Selective Chemical Control of Insect Pests

February 12 Prof. D. E. Fenton, Sheffield University
Polynuclear Complexes of Molecular Clefts as Models for Copper* Biosites

February 13 Dr. J. Saunders, Glaxo Group Research
Molecular Modelling in Drug Discovery

February 19 Prof. E.J. Thomas, Manchester University
Applications of Organostannanes to Organic Synthesis

February 20 Prof. E. Vogel, University of Cologne
Porphyrins, Molecules of Interdisciplinary Interest

February 25 Prof. J.F. Nixon, University of Sussex
Phosphalkynes, New Building Blocks in Inorganic and Organometallic Chemistry

March 5	Dr. N.C. Billingham, University of Sussex Degradable Plastic - Myth or Magic*
March 11	Dr. S.E. Thomas, Imperial College Recent Advances in Organoiron Chemistry*
March 12	Dr. R.A. Hann, ICI Imagedata Electronic Photography - An Image of the Future*
March 18	Dr. H. Maskill, Newcastle University Concerted or Step-wise Fragmentation in a Deamination-type Reaction*
April 7	Dr. M. Knight, University of Durham Interpreting Experiments: the Beginning of Electrochemistry*
May 6	Prof. T. Marder, University of Waterloo Metal-catalyzed Alkene Hydroboration
May 6	Dr. J.C. Gehret, Ciba-Geigy Some Aspects of Industrial Agrochemical Research
October 15	Dr. M. Glazer & Dr. S. Tarling, Oxford University & Birbeck College, London It Pays to be British! - The Chemist's Role as an Expert Witness in Patent Litigation
October 20	Dr. H.E. Bryndza, Du Pont Central Research Synthesis, Reactions and Thermochemistry of Metal (Alkyl) Cyanide Complexes and their Impact on Olefin Hydrocyanation Catalysis
October 22	Prof. A. Davies, University College London The Behaviour of Hydrogen as a Pseudometal*
October 28	Dr. J.K. Cockcroft, University of Durham Recent Developments in Powder Diffraction*
October 29	Dr. J. Emsley, Imperial College, London The Shocking History of Phosphorus*

Nov. 4 — Dr. T.P. Kee, University of Leeds
Synthesis and Co-ordination Chemistry of Silylated Phosphites

Nov. 5 — Dr. C.J. Ludman, University of Durham
Explosions - A Demonstration Lecture*

Nov. 11 — Prof. D. Robins, Glasgow University
Pyrrolizidine Alkaloids : Biological Activity, Biosynthesis and Benefits

Nov. 12 — Prof. M.R. Truter, University College, London
Luck and Logic in Host - Guest Chemistry

Nov. 18 — Dr. R. Nix, Queen Mary College, London
Characterisation of Heterogeneous Catalysts*

Nov. 25 — Prof. Y. Vallee. University of Caen
Reactive Thiocarbonyl Compounds

Nov. 25 — Prof. L.D. Quin, University of Massachusetts, Amherst
Fragmentation of Phosphorous Heterocycles as a Route to Phosphoryl Species with Uncommon Bonding

Nov. 26 — Dr. D. Humber, Glaxo, Greenford
AIDS - The Development of a Novel Series of Inhibitors of HIV

Dec. 2 — Prof. A.F. Hegarty, University College, Dublin
Highly Reactive Enols Stabilised by Steric Protection

Dec. 2 — Dr. R.A. Aitken, University of St. Andrews
The Versatile Cycloaddition Chemistry of $Bu_3P.CS_2$

Dec. 3 — Prof. P. Edwards, Birmingham University
The SCI Lecture - What is Metal?*

Dec. 9 — Dr. A.N. Burgess, ICI Runcorn
The Structure of Perfluorinated Ionomer Membranes*

1993

January 20 Dr. D.C. Clary, University of Cambridge
Energy Flow in Chemical Reactions*

January 21 Prof. L. Hall, Cambridge
NMR - Window to the Human Body*

January 27 Dr. W. Kerr, University of Strathclyde
Development of the Pauson-Khand Annulation Reaction : Organocobalt Mediated Synthesis of Natural and Unnatural Products

January 28 Prof. J. Mann, University of Reading
Murder, Magic and Medicine*

February 3 Prof. S.M. Roberts, University of Exeter
Enzymes in Organic Synthesis

February 10 Dr. D. Gillies, University of Surrey
NMR and Molecular Motion in Solution*

February 11 Prof. S. Knox, Bristol University
The Tilden Lecture Organic Chemistry at Polynuclear Metal Centres*

February 17 Dr. R.W. Kemmitt, University of Leicester
Oxatrimethylenemethane Metal Complexes

February 18 Dr. I. Fraser, ICI Wilton
Reactive Processing of Composite Materials*

February 22 Prof. D.M. Grant, University of Utah
Single Crystals, Molecular Structure, and Chemical-Shift Anisotropy

February 24 Prof. C.J.M. Stirling, University of Sheffield
Chemistry on the Flat-Reactivity of Ordered Systems*

March 10 Dr. P.K. Baker, University College of North Wales, Bangor
Chemistry of Highly Versatile 7-Coordinate Complexes

March 11	Dr. R.A.Y. Jones, University of East Anglia The Chemistry of Wine Making*
March 17	Dr. R.J.K. Taylor, University of East Anglia Adventures in Natural Product Synthesis*
March 24	Prof. I.O. Sutherland, University of Liverpool Chromogenic Reagents for Cations
May 13	Prof. J.A. Pople, Carnegie-Mellon University, Pittsburgh, USA Applications of Molecular Orbital Theory*
May 21	Prof. L. Weber, University of Bielefeld Metallo-phospha Alkenes as Synthons in Organometallic Chemistry
June 1	Prof. J.P. Konopelski, University of California, Santa Cruz Synthetic Adventures with Enantiomerically Pure Acetals
June 2	Prof. F. Ciardelli, University of Pisa Chiral Discrimination in the Stereospecific Polymerisation of Alpha Olefins*
June 7	Prof. R.S. Stein, University of Massachusetts Scattering Studies of Crystalline and Liquid Crystalline Polymers
June 16	Prof. A.K. Covington, University of Newcastle Use of Ion Selective Electrodes as Detectors in Ion Chromatography
June 17	Prof. O F. Nielsen, H.C. Ærsted Institute, University of Copenhagen Low-Frequency IR - and Raman Studies of Hydrogen Bonded Liquids
Sept. 13	Prof. Dr. A.D. Schlüter, Freie Universität Berlin, Germany Synthesis and Characterisation of Molecular Rods and Ribbons
Sept. 13	Dr. K.J. Wynne, Office of Naval Research, Washington, USA Polymer Surface Design for Minimal Adhesion*

Sept. 14 Prof. J.M. DeSimone, University of North Carolina, Chapel Hill, USA
Homogeneous and Heterogeneous Polymerisations in Environmentally Responsible Carbon Dioxide

Sept. 28 Prof. H. Ila, North Eastern Hill University, India
Synthetic Strategies for Cyclopentanoids via Oxoketene Dithioacetals

October 4 Prof. F.J. Feher, University of California, Irvine, USA
Bridging the Gap between Surfaces and Solution with Sessilquioxanes*

October 14 Dr. P. Hubberstey, University of Nottingham
Alkali Metals: Alchemist's Nightmare, Biochemist's Puzzle and Technologist's Dream*

October 20 Dr. P. Quayle, University of Manchester
Aspects of Aqueous ROMP Chemistry

October 21 Prof. R. Adams, University of South Carolina, USA
Chemistry of Metal Carbonyl Cluster Complexes : Development of Cluster Based Alkyne Hydrogenation Catalysts

October 27 Dr. R.A.L. Jones, Cavendish Laboratory, Cambridge
Perambulating Polymers*

Nov. 10 Prof. M.N.R. Ashfold, University of Bristol
High Resolution Photofragment Translational Spectroscopy : A New Way to Watch Photodissociation*

Nov. 17 Dr. A. Parker, Rutherford Appleton Laboratory, Didcot
Applications of Time Resolved Resonance Raman Spectroscopy to Chemical and Biochemical Problems*

Nov. 24 Dr. P.G. Bruce, University of St. Andrews
Structure and Properties of Inorganic Solids and Polymers*

Nov. 25 Dr. R.P. Wayne, University of Oxford
The Origin and Evolution of the Atmosphere

Dec. 1 — Prof. M.A. McKervey, Queen's University, Belfast
Synthesis and Applications of Chemically Modified Calixarenes

Dec. 8 — Prof. O. Meth-Cohn, University of Sunderland
Friedel's Folly Revisited - A Super Way to Fused Pyridines

Dec. 16 — Prof. R.F. Hudson, University of Kent
Close Encounters of the Second Kind

1994

January 26 — Prof. J. Evans, University of Southampton
Shining Light on Catalysts*

February 2 — Dr. A. Masters, University of Manchester
Modelling Water without using Pair Potentials*

February 9 — Prof. D. Young, University of Sussex
Chemical and Biological Studies on the Coenzyme Tetrahydrofolic Acid

February 16 — Prof. K.H. Theopold, University of Delaware, USA
Paramagnetic Chromium Alkyls : Synthesis and Reactivity

February 23 — Prof. P.M. Maitlis, University of Sheffield
Across the Border : From Homogeneous to Heterogeneous Catalysis*

March 2 — Dr. C. Hunter, University of Sheffield
Noncovalent Interactions between Aromatic Molecules

March 9 — Prof. F. Wilkinson, Loughborough University of Technology
Nanosecond and Picosecond Laser Flash Photolysis

March 10 — Prof. S.V. Ley, University of Cambridge
New Methods for Organic Synthesis

March 25 — Dr. J. Dilworth, University of Essex
Technetium and Rhenium Compounds with Applications as Imaging Agents

April 28 — Prof. R.J. Gillespie, McMaster University, Canada
The Molecular Structure of some Metal Fluorides and Oxofluorides: Apparent Exceptions to the VSEPR Model.

May 12 — Prof. D.A. Humphreys, McMaster University, Canada
Bringing Knowledge to Life